Higher Order Studies in Perturbative QCD

Dissertation

der Mathematisch-Naturwissenschaftlichen Fakultät
der Eberhard Karls Universität Tübingen
zur Erlangung des Grades eines
Doktors der Naturwissenschaften
(Dr. rer. nat.)

vorgelegt von
Patriz Hinderer
aus Nürtingen

Tübingen
2017

Gedruckt mit Genehmigung der Mathematisch-Naturwissenschaftlichen Fakultät der Eberhard Karls Universität Tübingen.

Tag der mündlichen Qualifikation:	24.07.2017
Dekan:	Prof. Dr. Wolfgang Rosenstiel
1. Berichterstatter:	Prof. Dr. Werner Vogelsang
2. Berichterstatter:	Prof. Dr. Thomas Gutsche

Summary

The main focus of this PhD thesis is on phenomenology of high energy particle and nuclear physics. We have performed several theoretical and phenomenological calculations aiming at a better description of collisions at hadron colliders such as the LHC or RHIC. In addition, several studies were performed relevant for lepton hadron scattering experiments carried out at JLab, HERMES, COMPASS or a future EIC.

One of the main goals of this PhD thesis are calculations of QCD threshold resummation. Threshold logarithms typically arise when the initial partons have just enough energy to produce the observed final state. In this case, the phase space available for gluon bremsstrahlung vanishes, resulting in large logarithmic corrections. This is a natural feature of QCD in higher order perturbation theory, that large corrections emerge in the edges of phase space. We obtain this behavior of QCD in all calculations discussed in this PhD thesis. If we try to get sensible answers from QCD in this area of phase space, we have to take these large logarithms into account to all orders. This procedure is known as "threshold resummation".

We investigated resummation effects beyond next-to-leading logarithmic (NLL) accuracy for di-hadron production in hadronic collisions $H_1 H_2 \to h_1 h_2 X$ at high invariant mass of the produced hadron pair. Since all particles in the underlying partonic reactions are color charged, the color structure of this process is highly non-trivial. Therefore, resummation beyond leading logarithmic accuracy may only be achieved by taking into account the color structure of the partonic process. We determined the relevant soft and hard matrices in space of color exchange operators, that appear in calculations beyond NLL accuracy. Besides these analytical calculations, we perform phenomenological studies for the di-hadron production process. We found significant improvements compared to previous studies in terms of cross section scale uncertainties.

In a related work we derived analytical approximate next-to-next-to-leading order (NNLO) results for single-inclusive jet production in hadronic collisions. Our formalism is based on threshold resummation and makes use of the fact that threshold resummation determines certain classes of threshold logarithms. Starting at NLL, we included for the first time the three leading classes of logarithms at partonic threshold. In addition, compared to previous results we also included the full dependence of the jet size

parameter R. Our results adapted also the full kinematic of jet transverse momentum p_T and rapidity η, which makes them of great phenomenological interest, for example in jet physics at hadron colliders such as the LHC, Tevatron or RHIC. Fits of parton distribution functions rely on jet data. Particularly the gluon PDF at large-x is constrained by high p_T-jets. Our approximate results are important for NNLO-PDF fits in the central rapidity and high transverse momentum region. Another important application could be the search for new physics at the LHC, where large p_T-jets are an important observable.

A very interesting field in QCD is the spin structure of the nucleon. The longitudinal spin distribution can be explored with the double spin asymmetry A_{LL} produced from longitudinally polarized hadron beams, for example at RHIC. In this thesis, we used the same methods as in the paragraph above to derive approximate NNLO results for single inclusive jet production in longitudinally polarized hadron beams. We found significant contributions, from formally subleading terms at partonic threshold. We could also perform phenomenological studies and compare them to jet production A_{LL} data from RHIC, which is a first step towards new accuracies in spin physics.

Besides the resummation studies in hadronic scattering we worked on fixed order calculations in lepton nucleon scattering processes. Particularly, we investigated the single-inclusive production of hadrons and jets in lepton nucleon scattering $lN \to hX$ and $lN \to \text{jet}X$ at next-to leading order (NLO). In contrast to the common DIS process the final state lepton remains unobserved. The treatment of the collinear divergencies from the photon propagator needs special attention in this calculation. It could either be absorbed by a photon in lepton distribution or completely avoided by a massive lepton. We could show, that in contrast to claims in the literature the almost real photon part is not the dominating contribution at NLO. The analytic results for single jet production were carried out in the "Narrow Jet Approximation" and adopt the right dependence on the jet size parameter R up to $R \sim 0.7$. Besides theoretical calculations, we do phenomenological applications of our work. Therefore, we performed numerical studies of the cross sections for present-day fixed target experiments and for a possible future electron-ion-collider (EIC).

Our unpolarized $lN \to hX$ NLO calculation is motivated by the fact, that this process attracted much theoretical and experimental interest for a transversely polarized hadron or nucleon in the initial state. In the case of polarized scattering azimuthal asymmetries were observed in experiments at JLAB and HERMES. A common approach to describe these single transverse spin asymmetries (SSA), is the so called twist-3 quark-gluon correlation function approach. So far, however, phenomenological applications for this process only have been limited to zeroth order of QCD perturbation theory. In general, for single spin asymmetries, QCD corrections to leading order are only available for more inclusive processes. The experimental data for $lN^\uparrow \to hX$ is not well described by the existing leading order studies and justifies the aim to develop a framework to go

beyond LO. Transverse spin dependent cross sections receive several contributions, the evaluation of them is highly challenging. In the present PhD thesis we focus on the so called soft-gluon-pole contribution, where the imaginary phase from the partonic hard scattering is provided from a configuration when the attached twist-3 gluon becomes soft. We developed a theoretical framework to calculate next-to-leading order QCD corrections for the soft gluon pole contribution to single-transverse spin asymmetry in $lN^{\uparrow} \to hX$. Exploring the contributions beyond leading order is crucial to determine the origin of the large asymmetries. The calculation we perform is an important step to understand how the theory of perturbative QCD is applicable to twist-3 cross sections.

In addition to the calculations concerning the transverse structure of the nucleons spin, also the longitudinal spin structure is a topic of this thesis. Therefore, we performed a study for the longitudinal double spin asymmetry in the process $\vec{l}\vec{N} \to hX$ at NLO level.

Zusammenfassung

Der Schwerpunkt der vorliegenden Doktorarbeit liegt in der Phänomenologie der hochenergie Kern- und Teilchenphysik. Mittels theoretischen Studien wurden Prozesse untersucht, die ein besseres Verständnis der Physik an Hadronbeschleunigern, wie den LHC oder RHIC liefern. Zusätzlich wurden Hadron-Lepton-Prozesse untersucht, die für Experimente wie am JLab oder bei HERMES, COMPASS und einem zukünftigen EIC relevant sind.

Einer der Schwerpunkte dieser Doktorarbeit liegt auf QCD threshold re-summations-Rechnungen. Die sogenannten threshold Logarithmen nehmen große Werte an, wenn die einlaufenden Partonen ihre gesamte Energie benötigen um den beobachteten Endzustand zu produzieren. In diesem Fall verringert sich der Phasenraum für Gluonen-Bremsstrahlung, was zu den großen Logarithmen führt. Dies ist ein immer wiederkehrendes Muster in der störungstheoretischen QCD in höheren Ordnungen, sodass sich in extremen Regionen des Phasenraums große Korrekturen ergeben. Um sinnvolle Ergebnisse in diesem Teil des Phasenraums zu bekommen, sollte man diese Logarithmen zu allen Ordnungen in der störungtheoretischen Reihe aufsummieren. Diese Prozedur nennt man "Threshold Resummation".

Wir untersuchten die Resummation solcher Logarithmen jenseits der nächst-führenden logarithmischen Ordnung (NLL) für die Dihadron-Produktion in hadronischen Kollisionen $H_1H_2 \to h_1h_2X$, wobei die invariante Paarmasse des produzierten Hadron-Paars relativ hoch ist. Da alle Teilchen in der partonischen Reaktion farbgeladen sind, ist die Farbstruktur solcher Prozesse sehr komplex und muss in Betracht gezogen werden, wenn man Genauigkeiten jenseits der führenden logarithmischen Ordnung erreichen möchte. Wir bestimmen die relevanten "weichen" und "harten" Matrizen im Raum der Farbaustauschoperatoren, welche jenseits der nächstführenden Ordnung auftauchen. Neben analytischen Rechnungen, haben wir phänomenologische Studien im Dihadron-Prozess durchgeführt. Dabei konnten signifikante Verbesserungen der Skalenungenauigkeit erzielt werden.

In einer weiteren Arbeit haben wir die "single-inclusive" Jet-Produktion in hadronischen Kollisionen näherungsweise zur nächst-zu-nächst-zu führenden Ordnung (NNLO) analytisch berechnet. Unser Formalismus basiert darauf, dass die Resummation von

threshold-Logarithmen eben diese zu allen Ordnungen vorhersagt. Ausgehend von NLL konnten wir erstmalig die ersten drei Klassen an führenden Logarithmen bestimmen und die volle Abhängigkeit des Jet-Parameters R mit einbeziehen. Desweiteren konnten wir sowohl die volle Abhängigkeit des Jets vom transversal Impulses p_T als auch dessen Abhängigkeit von der Rapitität η miteinbeziehen. Dies ist der Grund dafür, dass unsere Rechnung große Aufmerksamkeit auf sich zieht.

Ein sehr interessantes Forschungsfeld in der QCD ist die Spinstruktur des Nukleons. Die longitudinale Spin Verteilung kann anhand longitudinal polarisierter Hadron-Kollisionen untersucht werden. Die doppelte longitudinale Spin Asymmetrie A_{LL} für die "single-inclusive" Jet Produktion kann beispielsweise am RHIC gemessen werden. In der vorliegenden Doktorarbeit haben wir die selben Methoden wie im Absatz zuvor beschriebenen unpolarisierten Prozess benutzt, um näherungsweise NNLO-Ergebnisse für den polarisierten Prozess zu berechnen. Wir konnten formell an der partonischen Schwelle unterdrückte Beiträge identifizieren, welche dennoch einen signifikanten Beitrag zum Wirkungsquerschnitt liefern. Desweiteren wurden phänomenologische Studien durchgeführt und mit den aktuellen A_{LL} Jet-Daten von RHIC verglichen, dies bedeutet einen ersten Schritt zu neuen Genauigkeiten in der Spin-Physik.

Neben den Studien welche auf Resummation in hadronischen Kollisionen beruhen, wurden Berechnungen zur festen störungstheoretischen Ordnung durchgeführt. Im Detail haben wir "single-inclusive" Hadron- und Jet-Produktion in Lepton-Hadron-Streuung in nächst-zu führender Ordnung (NLO) berechnet. Im Gegensatz zum herkömmlichen DIS-Prozess wird das Lepton im Endzustand nicht beobachtet. Die kollineare Divergenz welche durch den Photon-Propagator hervorgerufen wird benötigt besondere Aufmerksamkeit. Die Divergenz kann entweder in eine Photon in Lepton Verteilung absorbiert oder durch ein massives Lepton komplett vermieden werden. Wir konnten zeigen, dass im Gegensatz zur bisherigen Literatur der Wirkungsquerschnitt nicht durch beinahe reelle Photonen dominiert wird. Die analytischen Ergebnisse der Jet-Produktion wurden in der sogenannten "Narrow Jet Approximation" durchgeführt und nehmen die annähernd korrekte Abhängigkeit des Jet-Parameters R bis zu $R \sim 0.7$ an. Desweiteren wurden phänomenologische Studien für aktuelle und zukünftige Experimente, wie den Electron-Ion-Collider (EIC) durchgeführt.

Die unpolarisierte $lN \to hX$ NLO Rechnung wurde dadurch motiviert, dass der Prozess, bei dem das einlaufende Hadron oder Nukleon transversal polarisiert ist, viel Aufmerksamkeit, im Experiment als auch in der Theorie auf sich zog. Im transversal polarisierten Streuprozess bei Experimenten am JLab und HERMES wurden azimuthale Asymmetrien beobachtet. Ein Zugang um diese einfach transversalen Spin Asymmetrien (SSA) zu beschreiben bietet der sogenannte Twist-3 Quark-Gluon Korrelationsfunktionsansatz. Bisher gelang es nur diesen Prozess zur führenden Ordnung zu berechnen. Im Allgemeinen wurden SSA-Observablen nur in stärker inklusiven Prozessen jenseits der führenden Ordnung bestimmt. Die experimentellen Daten für den Prozess $lN^{\uparrow} \to hX$

werden durch die existierenden LO Ergebnissen nur sehr schlecht beschrieben. Eines der Ziele der vorliegenden Doktorarbeit war es Methoden zu entwickeln um diesen Prozess zur nächst führenden Ordnung zu berechnen. Der polarisierte Wirkungsquerschnitt besteht aus einigen Beiträgen, wobei deren Berechnung außerordentlich schwierig ist. In der vorliegenden Arbeit beschäftigen wir uns mit dem sogenannten Soft-Gluon-Pol-Beitrag, welcher von Konfigurationen hervorgerufen wird, indem das zusätzliche Twist-3 Gluon weich wird. Wir entwickelten Methoden um NLO Korrekturen für den Soft-Gluon-Pol-Beitrag im Prozess $lN^{\uparrow} \to hX$ zu berechnen. Um die Herkunft der Asymmetrien zu bestimmen, ist es unumgehbar den Prozess jenseits der führenden Ordnung zu verstehen. Deswegen ist unsere Rechnung ein wichtiger Schritt um die störungstheoretische QCD auf komplizierte Twist-3-Prozesse anzuwenden.

Zusätzlich zu der Rechnung welche sich mit der transversalen Spin-Struktur des Nukleons beschäftigt, haben wir den Prozess für ein longitudinal polarisiertes Nukleon berechnet. Wir haben dafür die doppelte longitudinale Spin Asymmetrie in NLO für den Prozess $\vec{l}\vec{N} \to hX$ bestimmt.

List of Publications

Journal Articles

1. D. de Florian, P. Hinderer, A. Mukherjee, F. Ringer, and W. Vogelsang, "Approximate Next-to-Next-to-Leading Order Corrections to Hadronic Jet Production", Physical Review Letters **112**, 082001 (2014) 10.1103/PhysRevLett.112.082001

2. P. Hinderer, F. Ringer, G. F. Sterman, and W. Vogelsang, "Toward NNLL threshold resummation for hadron pair production in hadronic collisions", Physical Review D **91**, 014016 (2015) 10.1103/PhysRevD.91.014016, arXiv:1411.3149

3. P. Hinderer, M. Schlegel, and W. Vogelsang, "Single-inclusive production of hadrons and jets in lepton-nucleon scattering at NLO", Physical Review D **92**, 014001 (2015) 10.1103/PhysRevD.92.014001

4. P. Hinderer, M. Schlegel, and W. Vogelsang, "Double-Longitudinal Spin Asymmetry in Single-Inclusive Lepton Scattering at NLO", Phys. Rev. **D96**, 014002 (2017) 10.1103/PhysRevD.96.014002, arXiv:1703.10872 [hep-ph]

5. Y. Koike, P. Hinderer, and W. Vogelsang, "NLO Correction to Single Spin Asymmetry in $lp^{\uparrow} \to hX$", in preparation

Conference Proceedings

1. M. Schlegel, P. Hinderer, and W. Vogelsang, "NLO K-factors for Single-Inclusive Leptoproduction of Hadrons", (2015), arXiv:1510.07421

2. P. Hinderer, F. Ringer, G. F. Sterman, and W. Vogelsang, "Toward NNLL Resummation for Hadron Production in Hadronic Collisions", (2015), arXiv:1510.08037

Contents

Chapter 1.

Introduction

The theory of strong interactions - quantum chromodynamics (QCD) - was developed more than four decades ago [8, 9]. Since that time, it continues its triumph by explaining the nature of hadrons and thus the building blocks of nature. But, unlike the quantized theory of electro-magnetic fields, - quantum electrodynamics (QED) -, many phenomena are not accessible by direct weak coupling perturbation theory. On the other hand, through its complexity QCD offers a very rich phenomenology, that is in many cases very tough to describe theoretically to high accuracies. Therefore, QCD is even more than 40 years after its invention in the spotlight of ongoing research.

The experimental progress that has been achieved, produces an ever growing need for theoretical predictions to very high accuracies. The most precise predictions from QCD are achieved by utilizing the ansatz of perturbation theory. The spectrum where perturbative QCD (pQCD) is faced with experimental setups is enormously large. From the search of new physics at the LHC on the TeV scale, down to scattering experiments aiming to a better understanding of the nucleons spin structure on the lower and mid GeV scale, for example at HERA, RHIC and COMPASS. The theoretical success relies on a few enormously prosperous concepts established in QCD. The most fundamental one, that justifies in general the pQCD ansatz, is asymptotic freedom, a key feature of QCD. It states that the effective coupling of QCD goes to zero at zero distance, i.e. at high energies [10, 11]. Therefore, scattering processes of strongly interacting particles at high energies, can be described by using the methods of Feynman perturbation Theory.

But, unlike in QED we cannot get high precision predictions from pure Feynman perturbation Theory. The reason is another key feature of QCD, confinement. It states, that there are no free color charged particles, i.e they are bound in colorless hadrons. Therefore, all physical processes do not only involve the strongly interacting color charged particles, but also colorless hadrons far away from the hard scattering point. The proton for example, has a mass around ~ 938 MeV, that must include the binding energy

of the internal quarks and gluons. Therefore, the binding energy for a single quark or gluon inside a proton is relatively small. Small in a sense, that at these energy scales the coupling is far to big to exploit perturbative QCD. This leads unavoidable to a two scale problem in QCD. We have on the one hand the hadronic energy scale and on the other hand the scale of the hard scattering process in the perturbative regime. Now we are facing the problem, that we can solve the hard scattering part by using perturbative methods, but we are not able to describe the external hadrons with this theory. The factorization theorem of QCD helps to get along with exactly this problem.

Factorization is the central theorem in perturbative QCD. The theorem states that one can factor the hard scattering part from the non perturbative hadronic part of the cross section. We will explain the basic properties of the factorization theorem in section 1.3 in this thesis. Since factorization was introduced into the theory, the parton structure of hadrons is determined by high energy scattering experiments, i.e. one can extract the parton distribution functions (PDF) from experimental data. The PDFs are universal functions, in a sense that they are independent of the actual hard process. In fact, these properties of the theory allow us to face pQCD to experimental data.

This thesis is structured as follows. In the subsequent sections of this introductory chapter we outline the basic concepts of perturbative QCD. We give a general overview on QCD, concerning its Lagrangian and renormalization. We thematize the running of the QCD gauge coupling and discuss the perturbative treatment of a hard scattering process. Further, we show how to define infrared safe observables, which is crucial to obtain well defined answers from QCD. We give an introduction to the factorization theorem and hence the evolution property of parton distribution functions. In the end we complete this chapter with a brief introduction to threshold resummation.

The subsequent chapters are structured mainly along the papers listed on page xi.

In chapter 2 we present a NLO calculation in single hadron and jet production in a lepton nucleon induced process. This chapter is based on publications [3, 6] and is the basis for chapters 3 and 4, where we perform NLO calculations to the single transverse and the double longitudinal spin asymmetries [4, 5].

In the second part of this thesis, we investigate the resummation of threshold logarithms in pp induced processes. In chapter 5 we perform a calculation beyond next-to-leading logarithm accuracy for di-hadron production [2]. Based on this chapter, we present approximate next-to-next-to leading order results for single jet production in unpolarized- and longitudinally polarized pp scattering in chapters 6 and 7 based on publication [1].

1.1. Quantum Chromo Dynamics

1.1.1. QCD Lagrangian

In a quantum field theory the behavior of a set of particles should follow from the Lagrangian density. In the case of QCD the Lagrangian density connects quarks with mass m represented by spin one half matter fields Ψ_{kjf}, with the massless spin one gluon field A^a_μ. The quark fields are specified by the Dirac index k, a color index j and the flavor index f. The color index has three values, which has been shown experimentally. As far is known, the flavor index has six values "up", "down", "strange", "charm", "bottom" and "top". The gluon field has a color index a taking on eight values representing the eight generating matrices of SU(3). On the gluon field, the index μ is a Lorentz vector index. In the following discussion we assume the sum on flavor, color and Dirac indices on quark fields as implicit. Then we can express the classical Lagrangian density as

$$\mathcal{L}_{\text{class.}} = \bar{\Psi}(\mathrm{i}\not{D} - m)\Psi - \frac{1}{4}G^a_{\mu\nu}G^{\mu\nu}_a \ , \tag{1.1}$$

where the covariant derivative is given by

$$D_\mu\Psi = (\partial_\mu + \mathrm{i}gT^aA^a_\mu)\Psi \ . \tag{1.2}$$

Here, T^a are the generating matrices of the SU(3) colour gauge group and the factor g is the coupling strength in QCD. $G^{\mu\nu}_a$ is the gluon field strength tensor which is given by

$$G^{\mu\nu}_a = \partial_\mu A^a_\nu - \partial_\nu A^a_\mu - g f_{abc}A^b_\mu A^a_\nu; . \tag{1.3}$$

In contrast to QED which is an abelian gauge theory we have an additional term in equation (1.3) proportional to f_{abc}, the structure constant of the SU(3) gauge group. The structure constant is defined by the commutator $[T_a, T_b] = if_{abc}T_c$. Considering these definitions, we see that the classical Lagrangian density in equation (1.1) is invariant under local (i.e. space time dependent) SU(3) gauge transformations:

$$\begin{aligned} \Psi_{kjf}(x) &\to \left[e^{-\mathrm{i}g\omega_b(x)T^b}\right]_{ji}\Psi_{kif}(x) \\ A^b_\mu(x)T^b &\to \frac{1}{\mathrm{i}g}\, e^{-\mathrm{i}g\omega_b(x)T^b}\, D_\mu\, e^{\mathrm{i}g\omega_b(x)T^\beta} \end{aligned} \tag{1.4}$$

A novel way to quantize the theory is the path integral formalism [12]. Here, the Feynman rules for perturbation theory are derived from a functional integral by using the Faddeev - Popov method for gauge fixing [13]. For covariant gauge fixing we include the term

$$\mathcal{L}_{\text{gf}} = -\frac{1}{2\xi}(\partial \cdot A_a)^2 \ , \tag{1.5}$$

into the Lagrangian. The parameter ξ is the gauge parameter that cancels in a physical observable. The most common choices are Feynman $\xi \to 1$ and Landau gauge $\xi \to 0$. If we fix the gauge like in equation (1.5), we must take special care of unphysical polarizations of the gluon propagator. To fix that issue, we include an anti-commuting complex scalar Faddeev-Popov "ghost" field η into the Lagrangian [13]. This "gauge compensating" contribution is given by

$$\mathcal{L}_{\text{gc}} = \partial_\mu \bar{\eta}_a \, \partial^\mu \eta^a + g \, \partial_\mu \bar{\eta}_c \, f_{abc} \, A^b_\mu \eta_a \, . \tag{1.6}$$

Therefore, we can rewrite the Lagrangian as

$$\begin{aligned} \mathcal{L} &= \mathcal{L}_{\text{class.}} + \mathcal{L}_{\text{gf}} + \mathcal{L}_{\text{gc}} \\ &= \bar{\Psi}(\mathrm{i}\not{D} - m)\Psi - \frac{1}{4} G^a_{\mu\nu} G^{\mu\nu}_a - \frac{1}{2\xi}(\partial \cdot A_a)^2 + \partial_\mu \bar{\eta}_a \, \partial^\mu \eta^a \\ &\quad + g \, \partial_\mu \bar{\eta}_c \, f_{abc} \, A^b_\mu \eta_a \, , \end{aligned} \tag{1.7}$$

from where we can derive Feynman rules for Green functions. So far, in equation (1.7) all quantities are bare functions and parameters.

Another common gauge in particle physics is the axial gauge which is non-covariant. In that gauge, we implement the condition $n \cdot A_a = 0$ into the Lagrangian by using the gauge fixing term

$$\mathcal{L}_{\text{gf}} = -\frac{1}{2\xi} \, (n \cdot A_a)^2 \, . \tag{1.8}$$

In axial gauge are no gauge compensating ghost fields required. But, the gluon propagator gets more complicated instead. We can choose the gauge four vector n_μ differently. Where $n^2 = 0$ is called "light like", $n^2 > 0$ "temporal" and $n^2 < 0$ "purely axial" gauge.

1.1.2. Renormalization

As most relativistic field theories QCD is ultra-violet (UV) divergent. It is important to mention, that these divergences are property of the exact theory [14] and appear when the continuum limit is taken. In perturbation theory these divergences are caused by large loop momenta and can be removed order by order by a modification of the bare parameters in the Lagrangian density $\mathcal{L}$. Before we renormalize the theory we have to make the UV divergences manifest, in a sense, that we have to define the theory with a regulator, that takes care of the UV divergences. The most common regulators are dimensional regularization and non zero lattice spacing. In context of analytical perturbative calculations dimensional regularization is of special interest, where a generalization of space time to non integer values regulates the divergent part. In $4 - 2\varepsilon$ space time dimensions UV divergences from loop amplitudes appear as poles in ε when $\varepsilon \to 0$.

When we renormalize the theory to obtain finite Green functions, we use the freedom to change the normalization of the parameters m and g and the normalization of the fields, i.e.

$$\begin{aligned} \Psi &\to Z_2^{1/2}\Psi \\ A_\mu^a &\to Z_3^{1/2} A_\mu^a \\ \eta &\to Z_g \eta \end{aligned} \tag{1.9}$$

If we implement renormalization into the theory we can use a counterterm approach. That means by introducing (1.9) into (1.7) we can split the Lagrangian into three parts

$$\mathcal{L} = \mathcal{L}_{\text{free}} + \mathcal{L}_{\text{int.}} + \mathcal{L}_{\text{c.t.}} \tag{1.10}$$

The free Lagrangian $\mathcal{L}_{\text{free}}$ contains the kinetic terms of the theory. It is the origin of the free propagators.

$$\mathcal{L}_{\text{free}} = \bar{\Psi}(\mathrm{i}\not{D} - m)\Psi - \frac{1}{4}\left(\partial_\mu A_\nu^a - \partial_\nu A_\mu^a\right)^2 - \frac{1}{2\xi}(\partial \cdot A_a)^2 + \partial_\mu \bar{\eta}_a \, \partial^\mu \eta^a \tag{1.11}$$

In contrast to equation (1.7) m is now the finite renormalized mass. The interaction Lagrangian $\mathcal{L}_{\text{int.}}$ contains terms that describe the interaction between the different fields and in case of the gluonic part self interactions.

$$\begin{aligned} \mathcal{L}_{\text{int.}} = &-g\mu^\varepsilon \bar{\Psi} T^a \not{A}^a \Psi + g\mu^\varepsilon f_{abc} A^{b\mu} A^{c\nu} \partial_\mu A_\nu^a - \frac{g^2 \mu^{2\varepsilon}}{4}(f_{abc} A_\mu^b A_\nu^c)^2 \\ &+ g\mu^\varepsilon f_{abc} \partial_\mu \bar{\eta}^c A_\mu^b \eta^a \end{aligned} \tag{1.12}$$

Where μ is the unit mass, it ensures that the renormalized coupling g remains dimensionless for all values for ε in dimensional regularization. The appearance of the unit mass is an artifact of the regularization scheme. The counter term Lagrangian is the remaining part of equation (1.7) after using the replacements (1.9). In perturbative QCD this part of the Lagrangian is treated as part of the interaction and gives rise to an additional set of vertices and propagators. They have the same structure as the vertices emerging from equation (1.7) but with different coefficients. In a perturbative calculation these coefficient are adjusted in a way that the UV divergences are canceled order by order in the perturbative expansion.

1.1.3. Renormalization group and asymptotic freedom

If we compute a physical observable the appearance of an arbitrary mass scale μ introduced in the previous section seems to reduce the predictive power of the theory. But in reality, the freedom of choosing μ is used to optimize the accuracy of any fixed order calculation. It exploits the fact, that the full theory must be invariant under changing

the renormalization prescription. Therefore, the full theory is also invariant under variation of μ and its dependent renormalized parameters. This is called renormalization group invariance.

Let $\mathcal{S}(\alpha_s, m/Q, Q^2/\mu^2)$ be an arbitrary physical observable that depends on a large energy scale Q, the renormalized coupling α_s, renormalized mass m and on the renormalization scale itself. Here we define in analogy to Quantum Electro Dynamics (QED) $\alpha_s = g^2/4\pi$. Then, the renormalization group invariance states

$$\mu^2 \frac{\mathrm{d}}{\mathrm{d}\mu^2} \mathcal{S}(\alpha_s, m/Q, Q^2/\mu^2) = 0 \,, \tag{1.13}$$

using the chain rule we obtain

$$\left[\mu^2 \frac{\partial}{\partial \mu^2} + \beta(\alpha_s) \frac{\partial}{\partial \alpha_s} - \gamma_m(\alpha_s) m \frac{\partial}{\partial m} \right] \mathcal{S}(\alpha_s, m/Q, Q^2/\mu^2) = 0 \,. \tag{1.14}$$

The introduced functions β and γ_m are defined by [15]

$$\begin{aligned} \beta(\alpha_s) &= \mu^2 \frac{\partial}{\partial \mu^2} \alpha_s \,, \\ \gamma_m(g, m) &= \frac{-\mu^2}{m} \frac{\partial}{\partial \mu^2} m \,, \end{aligned} \tag{1.15}$$

where β is the so called QCD beta function and γ_m the anomalous dimension. They are both perturbative and can be expanded as

$$\beta(\alpha_s) = -\alpha_s^2 \left(b_1 + b_2 \alpha_s + b_3 \alpha_s^2 + \mathcal{O}(\alpha_s^3)\right);, \tag{1.16}$$

$$\gamma_m(\alpha_s) = \alpha_s \left(c_1 + c_2 \alpha_s + \mathcal{O}(\alpha_s^2)\right) \,. \tag{1.17}$$

As a consequence of the RG equation (1.14), the masses of the quarks and the coupling have not fixed values at all energy scales. This becomes clear by looking at equation (1.14), to solve it we have to introduce a running coupling $\alpha_s(\mu^2)$ and a running mass $m(\mu)$. This running of $\alpha_s(\mu^2)$ is in the end the justification for perturbation theory at high energies using α_s as the expansion parameter.

We now investigate the running of α_s in more detail. In this discussion we neglect the quark masses as it is often done in the perturbative regime of the theory. This is justified by the fact that for any observable the anomalous dimension leads to a change of mass with Q with a power of $\log(Q)$ which is accompanied by an inverse power of Q from the expansion. Therefore, the logarithm never overcomes the Q for large Q and justifies the ansatz to neglect quark masses at high energies.

To investigate the behavior of α_s at high energies, we take the zero mass limit of our observable $\mathcal{S}$.

$$\mathcal{S}(\alpha_s, 0, Q^2/\mu^2) \equiv \tilde{\mathcal{S}}(\alpha_s, Q^2/\mu^2) \tag{1.18}$$

This simplifies equation (1.14) to

$$\left[\mu^2 \frac{\partial}{\partial \mu^2} + \beta(\alpha_s) \frac{\partial}{\partial \alpha_s}\right] \tilde{\mathcal{S}}(\alpha_s, Q^2/\mu^2) = 0 \; . \tag{1.19}$$

We can rewrite this equation in a simpler form

$$\left[-\frac{\partial}{\partial t} + \beta(\alpha_s) \frac{\partial}{\partial \alpha_s}\right] \tilde{\mathcal{S}}(\alpha_s, e^t) = 0 \; , \tag{1.20}$$

where we introduced a new variable $t = \log(Q^2/\mu^2)$. Equation (1.20) is a first order partial differential equation that we can solve by introducing an implicit definition for the strong coupling

$$t = \int_{\alpha_s(\mu^2)}^{\alpha_s(Q^2)} \frac{\mathrm{d}\chi}{\beta(\chi)} \; . \tag{1.21}$$

Using this definition, by differentiation we get

$$\frac{\partial \alpha_s(Q^2)}{\partial t} = \beta(\alpha_s(Q^2)) \; , \tag{1.22}$$

$$\frac{\partial \alpha_s(Q^2)}{\partial \alpha_s(\mu^2)} = \frac{\beta(\alpha_s(Q^2))}{\beta(\alpha_s(\mu^2))} \; . \tag{1.23}$$

It follows that $\tilde{\mathcal{S}}(\alpha_s(Q^2), 1)$ is a solution of equation (1.20). Therefore, all the scale dependence in our physical observable $\tilde{\mathcal{S}}$ enters through the running coupling constant $\alpha_s(Q^2)$. The scale dependence of the coupling constant is determined by the renormalization group equation for α_s (1.22).

$$Q^2 \frac{\partial \alpha_s}{\partial Q^2} = \beta(\alpha_s) \tag{1.24}$$

We now investigate the behaviour of α_s in more detail. To do so, we need the coefficients of the QCD β-function equation (1.16) [16, 17]

$$b_0 = \frac{1}{12\pi}(11 C_A - 2 N_f) \; , \tag{1.25a}$$

$$b_1 = \frac{1}{24\pi^2}(17 C_A^2 - 5 C_A N_f - 3 C_F N_f) \; , \tag{1.25b}$$

$$b_2 = \frac{1}{64\pi^3}\left(\frac{2857}{54} C_A^3 - \frac{1415}{54} C_A^2 N_f - \frac{205}{18} C_A C_F N_f + \frac{78}{54} C_A N_f^2 + \frac{11}{9} C_F N_f^2\right) \; , \tag{1.25c}$$

where N_f is the number of active flavors The coefficients of the QCD β-function can be extracted order by order from the loop corrections to the bare vertices. The sign of the

β-function determines the behavior of the coupling as a function of the energy scale. In other words, a negative β-function implies that the coupling decreases for higher energy scales. We conclude that QCD is asymptotically free for $b_0 > 0 \Leftrightarrow \ N_f \leq 16$. At leading order (LO) in perturbation theory we can solve equation (1.16) exactly

$$\alpha_s(Q^2) = \frac{\alpha_s(\mu^2)}{1 + b_0 \alpha_s(\mu^2) \log\left(Q^2/\mu^2\right)} \tag{1.26}$$

This relation between $\alpha_s(\mu^2)$ and $\alpha_s(Q^2)$ is valid if both energy scales are in the perturbative region. Since one of the main topic of this thesis is resummation, we have a closer look at equation (1.26). We can expand it as

$$\alpha_s(Q^2) = \sum_{i=0}^{\infty} \alpha_s(\mu^2)^{i+1} \left(-b_0 \log\left(Q^2/\mu^2\right)\right)^i \ . \tag{1.27}$$

This is a first example of a resummation of logarithms of a certain type. Here we sum logarithms of the type $\alpha_s(\mu^2)^{i+1} \left(-b_0 \log\left(Q^2/\mu^2\right)\right)^i$ to all orders in the strong coupling. Although we have only the one loop result (b_0) in our calculation, RG invariance allows us to make all order predictions for this kind of logarithms. This approach is very similar to other resummation techniques, where we exploit RG invariance of the theory to sum up classes of logarithms and it is examplarely how this could increase the accuracy of a calculation.

In the main body of this thesis we need the strong coupling at NNLO accuracy. For completeness we give the result

$$\begin{aligned} \alpha_s(Q^2) = \frac{\alpha_s(\mu^2)}{X} \Bigg[& 1 - \frac{b_1}{b_0} \alpha_s(\mu^2) \frac{\log X}{X} \\ & + \alpha_s(\mu^2)^2 \left(\frac{b_2}{b_0} \frac{1 - X}{X^2} + \frac{b_1^2}{b_0^2} \frac{\log^2 X - \log X + X - 1}{X^2} \right) \Bigg] \ , \end{aligned} \tag{1.28}$$

where

$$X = 1 + b_0 \alpha_s(\mu^2) \log(Q^2/\mu^2) \ . \tag{1.29}$$

With equation (1.26) at LO and (1.28) at NNLO it is possible to compute α_s at a scale Q in case that it is known at some reference scale μ. Therefore, perturbative QCD predicts only the variation of α_s the non perturbative initial α_s at a certain scale is taken from global fits to experimental data [18]. In figure (1.1) the QCD prediction and experimental data from various experiments spanning a large range of the evaluation scale Q for α_s are shown. In the high energy regime, i.e. large Q, the strong coupling becomes small and we conclude that perturbative QCD is an useful tool to solve the theory in that particular region. On the other hand, figure (1.1) shows that the strong coupling has a steep rise towards smaller energies. In that regime, the quarks and

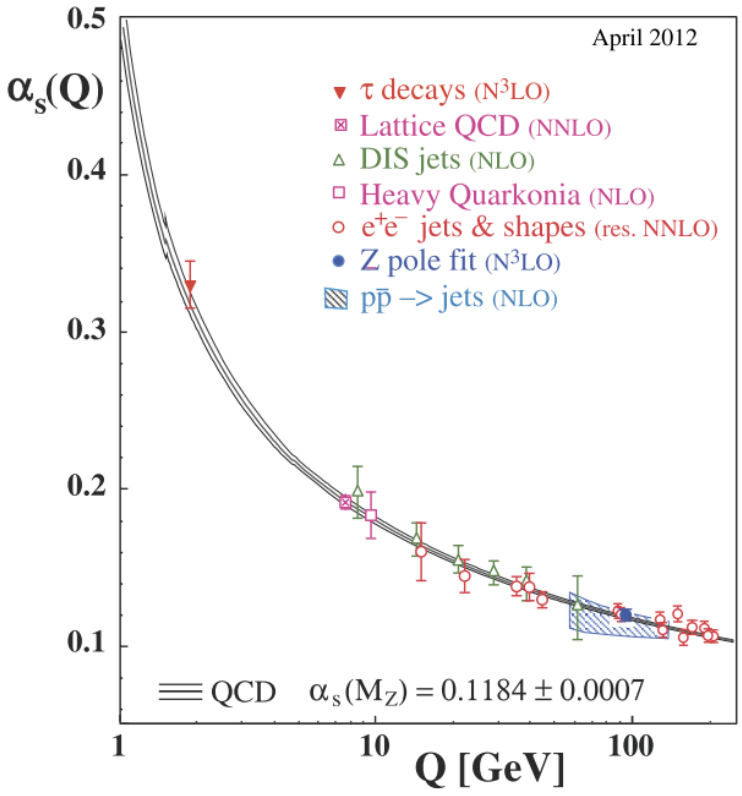

Figure 1.1.: Scale dependence of α_s as a function of Q. The data shown here is used to evaluate the strong coupling at the Z-boson mass. Figure taken from [19].

gluons interact strongly with each other. This is the regions where the quarks and gluons are confined to colorless hadrons. This steep unbound rise of $\alpha_s(\mu^2)$ towards small scales gives rise to so called Landau poles in the numerical treatment of threshold resummation that is a main topic of this thesis. We will keep that in mind when we come to threshold resummation.

1.2. Infrared safety

To illustrate the fundamental concept of infrared safety, we examine in this section the simplest measurable observable which can be computed in pure perturbative QCD: The total cross section for the $e^+e^- \to$ hadrons annihilation process at high energies. Although this paragraph is included for pedagogical reasons, i.e. to scrutinize the appearing divergences and how to handle them, this process was very important in the history of particle physics. We start with the inclusive cross section, in a sense that we

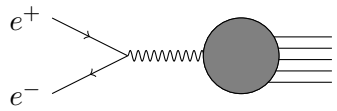

Figure 1.2.: Amplitude for $e^+e^- \to$ hadrons

do not extract any information of our hadronic final state and we do not include any non perturbative dynamics in the present calculation.

1.2.1. e^+e^- total cross section

We consider the process $e^+e^- \to$ hadrons to lowest order in electromagnetism α^2. The present calculation shows the derivation of the first order correction in the strong coupling α_s for this process. To justify this perturbative ansatz, the energy transfer in the s-channel diagram figure (1.2) $Q^2 = q^2 = (l_1 + l_2)^2$ must be in the perturbative regime. l_1 and l_2 denotes the electron and positron momenta. At lowest order in terms of the electromagnetic coupling hadronic and the leptonic parts in the cross section factorize

$$\sigma = \frac{8\pi^2\alpha^2}{Q^6} L_{\mu\nu} W^{\mu\nu} \,, \tag{1.30}$$

where the most general tensor structure for unpolarized lepton beams is given by

$$L^{\mu\nu} = l_1^\mu l_2^\nu + l_1^\nu l_2^\mu - g^{\mu\nu} l_1 \cdot l_2 \,. \tag{1.31}$$

The hadronic tensor must satisfy the ward identity $q_\mu W^{\mu\nu} = 0$ that determines its tensor structure. This tensor structure is accompanied by a scalar function R, dependent on the center of mass energy Q^2. Thus we have

$$W^{\mu\nu} = \left(-g^{\mu\nu} q^2 + q^\mu q^\nu\right) \frac{1}{6\pi} R(Q^2) \,. \tag{1.32}$$

As mentioned above, for sufficient large Q^2 we can address the perturbative expansion to $R(Q^2)$. In other words, with pQCD we can resolve the small distance dynamics of the order $\propto 1/Q$ in the gray blob in figure (1.2). We have to keep that always in mind when we apply pQCD to get physical answers. Surely, in higher orders the gray blob can include long distance physics, that can not be handled by the pQCD ansatz. But, we ignore that for the moment and assume all vertices dominantly in the perturbative region. In fact, this is a valid assumption for this process.

The leading order (LO) contribution to the inclusive cross section has only one contribution shown in figure (1.3). Calculating the trace we end up with

$$R^0 = N_c \sum_f e_f^2 \,, \tag{1.33}$$

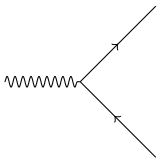

Figure 1.3.: LO contribution to the hadronic tensor

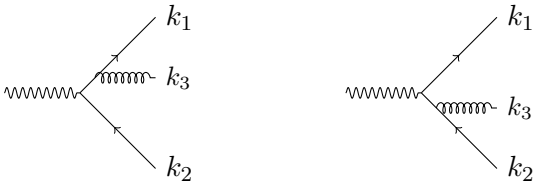

Figure 1.4.: NLO real emission contribution to the hadronic tensor.

where $N_c = 3$ is the number of quark colors. The leading order cross section is then given by,

$$\sigma = \frac{4\pi\alpha}{3Q^2} N_c \sum_f e_f \ . \tag{1.34}$$

The next-to-leading order (NLO) cross section receives contributions from virtual gluon figure (1.5) and real gluon corrections figure (1.4).We start with the computation of the real gluon emission part.

NLO real gluon

The real NLO correction to the hadronic tensor shown in figure (1.4) provides an additional gluon in the final state. Therefore we have to integrate over all additional phase space configuration for the additional gluon. Performing this phase space integration provides several divergences that we have to handle in a well defined way. The differential three particle phase space for this process is evaluated as [20],

$$\mathrm{d}\Phi_3 = \frac{1}{(2\pi)^2} \frac{Q^2}{32} \mathrm{d}\alpha \ \mathrm{d}\cos\beta \ \mathrm{d}\gamma \ \mathrm{d}x_1 \ \mathrm{d}x_2 \ , \tag{1.35}$$

where α,β and γ are the Euler angles and $x_i = 2E_{k_i}/Q$. By using standard Feynman rules the partonic function can be evaluated and integrated over phases pace. Finally, after integrating over all Euler angles we end up with

$$\sigma^{(1)} = \sigma^{(0)} \int \mathrm{d}x_1 \ \mathrm{d}x_2 \ C_F \frac{\alpha_s}{2\pi} \frac{x_1^2 + x_2^2}{(1-x_1)(1-x_2)} \ , \tag{1.36}$$

where the integration region is given by the constrains $0 \leq x_1, x_2 \leq 1$ and $x_1 + x_2 \geq 1$. From these constraint one can easily see that equation (1.36) has singularities at different phase space regions. The singularities arise for configurations where the gluon is either collinear to the quark $x_1 = 1$ or antiquark $x_2 = 1$, or when it became soft $x_1 = x_2 = 1$. These singularities in equation (1.36) are not physical. They appear as a remnant of our treatment of QCD as a perturbative series and the assumption that our final state partons are massless and "on-shell". Here we have to distinguish clearly from the UV-singularities, which are a property of the fundamental quantum field theory, whereas the IR-singularities are artificial singularities, coming from the treatment of external particles. For a well defined (-or infrared save) observable these divergencies cancel, if we include the complete perturbative order. In the case of e^+e^- annihilation they must completely cancel among real and virtual NLO corrections. To make this divergence manifest, we have to regulate the integral in a way, that we can observe a temporarily finite result. There are several regulators given in the literature, that follow different strategies. A very sophisticated and widespread ansatz in high energy physics is the dimensional regularization approach. In dimensional regularization the IR divergences are regulated by assuming non integer values for the space time dimension, i.e. $d > 4$. The deviation from $d = 4$ is expressed as $d = 4 - 2\varepsilon$ and affects both the Dirac traces and the phase space integral. The epsilon dependent real NLO correction is given by

$$\sigma^{(1)}_{\text{real}} = \sigma^{(0)} \frac{(1-\varepsilon)^2}{(3-2\varepsilon)\Gamma[2(1-\varepsilon)]} \int \mathrm{d}x_1 \, \mathrm{d}x_2 \, C_F \frac{2\alpha_s}{\pi} \times \frac{x_1^2 + x_2^2 - \varepsilon(2 - x_1 - x_2)}{(1-x_1)^{(1+\varepsilon)}(1-x_2)^{(1+\varepsilon)}} \,, \tag{1.37}$$

where $\varepsilon < 0$ provides a finite result for the integral.

$$\sigma^{(1)}_{\text{real}} = \sigma^{(0)} \frac{(1-\varepsilon)^2}{(3-2\varepsilon)\Gamma[2(1-\varepsilon)]} C_F \frac{2\alpha_s}{\pi} \left[\frac{2}{\varepsilon^2} + \frac{2}{\varepsilon} + \frac{19}{2} + \mathcal{O}(\varepsilon) \right] \tag{1.38}$$

Equation (1.38) shows that dimensional regularization converts the soft and collinear gluon configurations of equation (1.4) into poles around $\varepsilon \to 0$. In this quantifiable representation we can compare the appearing poles in the real part to its counterpart coming from virtual gluon exchange.

NLO virtual gluon

The virtual correction has three contributions shown in figure 1.5. These diagrams have to be integrated over all virtual gluon momenta k and interfere them with the leading order diagram of figure 1.3. The virtual part has another hidden divergency coming from infinite virtual gluon momenta k. These UV divergencies are present in each of the diagrams shown in figure 1.5 and are regulated by dimensional regularization similar

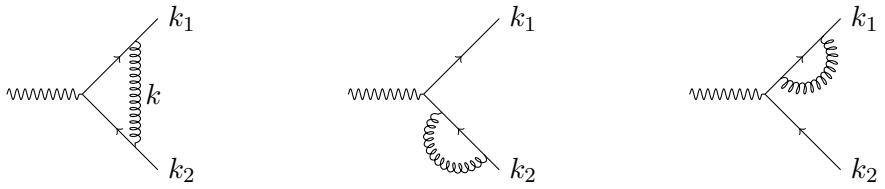

Figure 1.5.: NLO virtual contribution to the hadronic tensor.

to the IR part but with $d < 4$. Since, there is no QCD vertex in the leading order of our process, the three contributing diagrams shown in figure 1.5 must be UV-finite. Therefore, the UV-divergencies we find in each of the diagrams must cancel in their sum. After the UV poles are canceled we can switch to $d > 4$ to regulate the IR part of the diagrams. We end up with

$$\sigma^{(1)}_{\text{virtual}} = \sigma^{(0)} \frac{(1-\varepsilon)^2}{(3-2\varepsilon)\Gamma[2(1-\varepsilon)]} C_F \frac{2\alpha_s}{\pi} \left[-\frac{2}{\varepsilon^2} - \frac{2}{\varepsilon} - 8 + \mathcal{O}(\varepsilon) \right] . \tag{1.39}$$

Final result

Now after calculating all contributions that appear at NLO we confirm that the pole structure in the real (1.38) and in the virtual (1.39) cancel each other. We remain with a final result where the physical limit $\varepsilon \to 0$ is well defined. We end up with the result up to NLO

$$R(Q^2) = R^0 \left(1 + \frac{3\alpha_s}{4\pi} C_F \right) \tag{1.40}$$

We can conclude that the total inclusive cross section is actual infrared safe observable. This also generalizes to all order in pQCD as was shown by Kinoshita, Lee and Nauenberg [21, 22]. In fact the total inclusive cross section is the easiest definition of an infrared safe cross section.

1.2.2. Infrared safety for complicated final states

In the previous section we conclude that for the total inclusive cross section all divergencies in $e^+e^- \to$ hadrons coming from soft or collinear parton configurations cancel. Therefore, we have shown that this particular cross section at NLO is infrared save. In fact, there are other methods to show this behavior of the cross section, i.e. one can show from unitarity that the long time evolution of a hadronic final state cancels out in this cross section. Therefore, the total cross section is independent of long time physics and thus infrared save. Admittedly, in order to learn more about the dynamics in a scattering process, we have to extract more information from the final state. Because

of this the problem of infrared safety gets more delicate and attracts more attention. The main problem is that a detector is a long distance away from the interaction and implicates long time physics living on small energy scales. Unfortunately, this is the region where QCD perturbation theory is out of control. We see that an infrared save observable in high energy scattering processes must be insensitive to these kind of interactions. Otherwise, it is impossible to extract reliable predictions from a QCD process.

To understand the fundamental concept of infrared safety we construct a physical observable from the cross section

$$\frac{\mathrm{d}\sigma[n]}{\mathrm{d}\Omega_2 \prod\limits_{\substack{i=3 \\ i\leq n}}^{n} \mathrm{d}E_i \, \mathrm{d}\Omega_i} \,, \tag{1.41}$$

representing a n-hadron final state. Here we follow closely [23, 24]. If we measure a physical quantity $\mathcal{I}$ we can specify it through symmetric functions $\mathcal{S}_n$ describing the observable for the n particle final state.

$$\mathcal{I} = \sum_{n=2} \frac{1}{n!} \int \mathrm{d}\Omega_2 \prod_{\substack{j=3 \\ j\leq n}}^{n} \mathrm{d}E_j \, \mathrm{d}\Omega_j \frac{\mathrm{d}\sigma[n]}{\mathrm{d}\Omega_2 \prod\limits_{\substack{i=3 \\ i\leq n}}^{n} \mathrm{d}E_i \, \mathrm{d}\Omega_i} \, \mathcal{S}_n(p_1^\mu, ..., p_n^\mu) \tag{1.42}$$

In order for the observable to be infrared save, we need

$$\mathcal{S}_{n-1}(p_1^\mu, ..., (1-\lambda)p_n^\mu, \lambda p_n^\mu) = \mathcal{S}_{n-1}(p_1^\mu, ..., p_n^\mu) \,, \tag{1.43}$$

where $0 \leq \lambda \leq 1$. Equation (1.43) implicates an infrared save observable should not depend whether a particle splits into two collinear particles or not. It also shows no sensitivity weather a particle splits into a particle carrying approximately all momenta in the initial particles direction and an approximately zero momentum particle in any direction. Of course the cross section is also insensitive to a recombination process of particles having the momentum configurations described above.

One way to construct an infrared save observable, i.e. eliminate the sensitivity to the long distance physics, is to introduce a function that takes care of the long time evolution. Consider the cross section

$$\frac{\mathrm{d}\sigma(e^+e^- \to \text{hadron} + X)}{\mathrm{d}E_{\text{hadron}}} \,. \tag{1.44}$$

It can be written as a convolution between a hard scattering function describing the process $e^+e^- \to \text{quark} + X$ or $e^+e^- \to \text{gluon} + X$ and a fragmentation function quark $\to$ hadron $+ X$ or gluon $\to$ hadron $+ X$. The functions describing the long time evolution of our final state are in the non perturbative region and hence not accessible by the

pQCD ansatz. Nowadays, these functions are obtained by fitting to experimental data. However, these functions are universal in a sense that they are the same for all processes. This factorization of the final state long time evolution is similar to factorization in the initial state. We will discuss the initial state factorization in the next section.

1.3. Factorization and Evolution

So far we considered only simple initial states, i.e. electron positron annihilation, whereas in the main body of this thesis we mostly consider hadronic initial states. Therefore, we need a systematic treatment of scattering processes, that are given by a hadronic initial state. As an example we examine the most simple process in hadron hadron scattering, the Drell-Yan process, i.e. lepton anti-lepton pair production. Hadrons are extended objects made up of constituents, the partons, that are bound by field interactions. We know that these partons are quarks and gluons described by QCD in the non perturbative regime. This is exactly the difficulty here. Therefore, a high energy hadron scattering process is always a two scale problem, the perturbative scale occurring in the inner hard scattering part and the non-perturbative scale describing the hadron itself. Exactly this interplay of these two scales is the topic of this section.

1.3.1. The Drell-Yan process

We start with the description of the Drell-Yan process and its kinematics. The Drell-Yan process is lepton pair production with two initial state hadrons A and B. We have

$$H_A + H_B \to l + \bar{l} + X \tag{1.45}$$

where X denotes a possible additional unobserved final sate. We consider the differential cross section

$$\frac{\mathrm{d}\sigma}{\mathrm{d}Q^2 \mathrm{d}\eta} \tag{1.46}$$

where Q^2 is the square of the lepton pair mass and η its rapidity defined by

$$\eta = \frac{1}{2} \ln \left(\frac{q \cdot P_A}{q \cdot P_B} \right) . \tag{1.47}$$

P_A and P_B are the momenta of the incoming hadrons and q of the virtual photon that produce the lepton pair. We can describe the cross section up to corrections suppressed

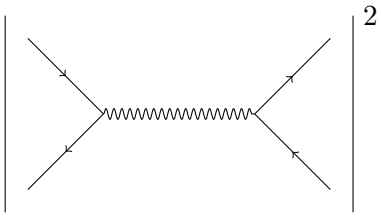

Figure 1.6.: Leading order contribution to the partonic function G_{ab}.

by $\propto 1/Q^2$ as [25]

$$\frac{\mathrm{d}\sigma}{\mathrm{d}Q^2\mathrm{d}\eta} = \sum_{a,b} \int_{x_A}^{1} \mathrm{d}\xi_A \int_{x_B}^{1} \mathrm{d}\xi_B f_{a/A}(\xi_A,\mu)\; H_{ab}\left(\frac{x_A}{\xi_A},\frac{x_B}{\xi_B},Q,\frac{Q}{\mu},\alpha_s(\mu^2)\right)\; f_{b/B}(\xi_B,\mu)\;. \tag{1.48}$$

The sum runs over all parton types a, b and

$$x_A = \mathrm{e}^{\eta}\sqrt{\frac{Q^2}{s}}\;, \quad x_B = \mathrm{e}^{-\eta}\sqrt{\frac{Q^2}{s}}\;. \tag{1.49}$$

H_{ab} represents the hard scattering that is dominated by ultraviolet contributions. This hard function is given by the partonic cross section which is computable in QCD perturbation theory. The function f, representing the parton distribution inside the incoming hadron, includes phenomena living on the hadronic mass scale. Therefore, it is not accessible by the perturbative ansatz [1]. This parton distribution function (PDF) $f_{a/A}(\xi_A,\mu)$ gives the longitudinal distribution of finding a parton a inside hadron A with longitudinal or collinear momentum fraction ξ_A and evaluated by a mass scale μ. We will show later how this factorization mass scale is inserted in the function f by dimensional transmutation. The cross section formula (1.48) is a Drell-Yan generalization of Feynman's parton model [28] including higher order effects in the strong coupling.

The hard scattering part

Factorization ensures that the hard scattering part is insensitive to the species of the mother hadron. Therefore, the simplest choice for the external hadron in equation (1.48) is an incoming parton. We assume the partons a and b to have a vanishing transverse momentum and zero mass. The appearing mass singularities are regulated by dimensional regularization in $4-2\varepsilon$ dimensions. We call this cross section G_{ab}

$$\frac{\mathrm{d}\sigma(ab\to l\bar{l}X)}{\mathrm{d}Q^2\mathrm{d}\eta} = G_{ab}\left(x_A,x_B,Q,\frac{Q}{\mu},\alpha_s,\varepsilon\right)\;. \tag{1.50}$$

[1] A theoretical approach to calculate PDFs from first principles are lattice calculations, where recent developments allow to include factorization properties within this formalism [26, 27].

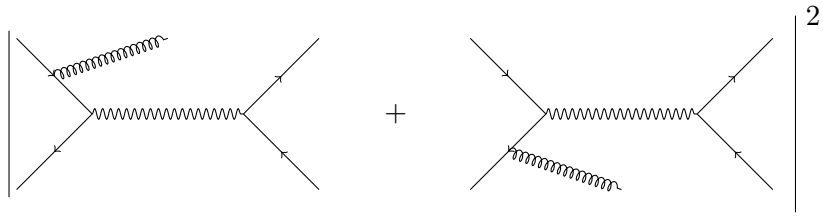

Figure 1.7.: Real next-to leading order correction to the partonic function G_{ab}.

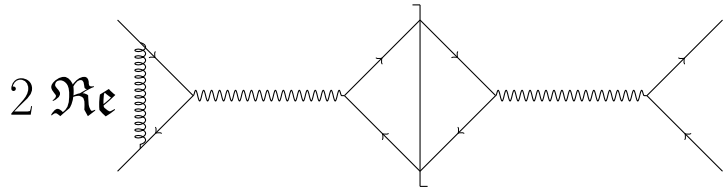

Figure 1.8.: One loop next-to leading order correction to the partonic function G_{ab}.

The factorization formula (1.48) applied to initial state partons turns into

$$G_{ab}\left(x_A, x_B, Q, \frac{Q}{\mu}, \alpha_s, \varepsilon\right) = \tag{1.51}$$
$$\int_{x_A}^{1} \mathrm{d}\xi_A \int_{x_B}^{1} \mathrm{d}\xi_B \; \tilde{f}_{c/a}(\xi_A, \varepsilon)\; H_{cd}\left(\frac{x_A}{\xi_A}, \frac{x_B}{\xi_B}, Q, \frac{Q}{\mu}, \alpha_s, \varepsilon\right)\; \tilde{f}_{d/b}(\xi_B, \varepsilon)\;,$$

where now the entirely perturbative function $\tilde{f}_{c/a}(\xi_A, \varepsilon)$ represent a distribution for a parton c in parton a with momentum fraction ξ_A. We see that both equations (1.48) and (1.51) depend on an arbitrary mass scale μ. This scale is introduced in dimensional regularization to keep the mass dimension at integer values by replacing the four dimensional integrals appearing in H_{ab} by

$$\int \mathrm{d}^4 k \to \left(\frac{\mu^2}{4\pi}\mathrm{e}^{\gamma_E}\right)^{\varepsilon} \int \mathrm{d}^{4-2\varepsilon} k\;. \tag{1.52}$$

Obviously, this replacement leaves the mass dimensionality independent from ε. The divergencies that are regularized by dimensional regularization are reflected by poles for $\varepsilon \to 0$ and can be subtracted. For a well presented summary see [29]. In principle these subtraction can differ in finite pieces, where the minimal subtraction (MS) scheme does not subtract any finite contributions. Here, by using the factor $(\mathrm{e}^{\gamma_E}/(4\pi))^{\varepsilon}$ we subtract ε-poles accompanied by this combination, which is well known as the ($\overline{\mathrm{MS}}$) scheme, γ_E is the Euler constant.

Owed to the fact that we assume partons as the initial state particles in G_{ab} at high

energy scales this function is perturbative and has the expansion

$$G_{ab} = G_{ab}^{(0)} + \frac{\alpha_s}{\pi} G_{ab}^{(1)} + \mathcal{O}(\alpha_s^2) \,. \tag{1.53}$$

Similarly to G_{ab} the function H_{ab} of equation (1.48) has an expansion in the strong coupling

$$H_{ab} = H_{ab}^{(0)} + \frac{\alpha_s}{\pi} H_{ab}^{(1)} + \mathcal{O}(\alpha_s^2) \,. \tag{1.54}$$

It is clear that both one loop corrections $G_{ab}^{(1)}$ and $H_{ab}^{(1)}$ have ultraviolet divergencies coming from large momenta in virtual graphs, appearing as $1/\varepsilon$ poles. Those UV-poles can be subtracted using the standard ($\overline{\text{MS}}$) scheme. We mention, that similarly to the virtual graphs in e^+e^- scattering in the previous section, the sum of all virtual graphs is UV finite. After this rearrangement of the UV-poles, $1/\varepsilon$ infrared-poles still remain in G. These IR poles are a remainder from the fact that we assume the incoming partons as on-shell massless particles. The object of the factorization theorem is to quantify these poles and give descriptions how to shift them into the definition of the PDF. To do so, we have to find a relation between H and G order by order in perturbation theory. Considering that, we have to specify the functions $\tilde{f}_{a/b}$. Due to the factorization theorem these functions absorb the sensitivity to small momenta in G_{ab}. After UV renormalization in the ($\overline{\text{MS}}$) scheme we have

$$\tilde{f}_{a/b}(\xi, \varepsilon) = \delta_{ab}\delta(1-\xi) - \frac{1}{2\varepsilon}\frac{\alpha_s}{\pi} P_{a/b}^{(0)}(\xi) + \mathcal{O}(\alpha_s^2) \tag{1.55}$$

where $P_{a/b}^{(0)}$ is the Altarelli-Parisi splitting kernel [30]. The first term reflects that in the leading order process is no additional splitting. The second order term includes the IR-divergent part that turns up as a $1/\varepsilon$ here. We motivate equation (1.55) in the next section by a calculation using the operator definition for $\tilde{f}$.

Using equation (1.55) in equation (1.51) and perform an one loop expansion we obtain

$$\begin{aligned} & G_{ab}^{(0)}\left(x_A, x_B, Q, \frac{Q}{\mu}, \alpha_s, \varepsilon\right) + \frac{\alpha_s}{\pi} G_{ab}^{(1)}\left(x_A, x_B, Q, \frac{Q}{\mu}, \alpha_s, \varepsilon\right) \qquad (1.56) \\ &= H_{ab}^{(0)}\left(\frac{x_A}{\xi_A}, \frac{x_B}{\xi_B}, Q, \frac{Q}{\mu}, \varepsilon\right) + \frac{\alpha_s}{\pi} H_{ab}^{(1)}\left(\frac{x_A}{\xi_A}, \frac{x_B}{\xi_B}, Q, \frac{Q}{\mu}, \varepsilon\right) \\ &\quad - \frac{1}{2\varepsilon}\frac{\alpha_s}{\pi} \sum_c \int_{x_A}^1 \mathrm{d}\xi_A P_{c/a}^{(0)}(\xi_A) H_{cb}^{(0)}\left(\frac{x_A}{\xi_A}, x_B, Q, \frac{Q}{\mu}, \varepsilon\right) \\ &\quad - \frac{1}{2\varepsilon}\frac{\alpha_s}{\pi} \sum_d \int_{x_B}^1 \mathrm{d}\xi_B P_{d/b}^{(0)}(\xi_B) H_{ad}^{(0)}\left(x_A, \frac{x_B}{\xi_B}, Q, \frac{Q}{\mu}, \varepsilon\right) \\ &\quad + \mathcal{O}(\alpha_s^2) \,. \qquad (1.57) \end{aligned}$$

At lowest order we get

$$G_{ab}^{(0)}\left(x_A, x_B, Q, \frac{Q}{\mu}, \alpha_s, \varepsilon\right) = H_{ab}^{(0)}\left(\frac{x_A}{\xi_A}, \frac{x_B}{\xi_B}, Q, \frac{Q}{\mu}, \varepsilon\right) , \tag{1.58}$$

and at one loop order

$$\begin{aligned} H_{ab}^{(1)}\left(x_A, x_B, Q, \frac{Q}{\mu}, \alpha_s, \varepsilon\right) &= G_{ab}^{(1)}\left(\frac{x_A}{\xi_A}, \frac{x_B}{\xi_B}, Q, \frac{Q}{\mu}, \varepsilon\right) \\ &+\frac{1}{2\varepsilon}\sum_c \int_{x_A}^1 \mathrm{d}\xi_A P_{c/a}^{(0)}(\xi_A) G_{cb}^{(0)}\left(\frac{x_A}{\xi_A}, x_B, Q, \frac{Q}{\mu}, \varepsilon\right) \\ &+\frac{1}{2\varepsilon}\sum_d \int_{x_B}^1 \mathrm{d}\xi_B P_{d/b}^{(0)}(\xi_B) G_{ad}^{(0)}\left(x_A, \frac{x_B}{\xi_B}, Q, \frac{Q}{\mu}, \varepsilon\right) . \end{aligned} \tag{1.59}$$

The equations above shows how we can calculate the hard scattering part in the factorized cross section formula (1.48). The procedure is to calculate the partonic cross section equation (1.51) assuming on-shell massless partons and subtract the divergent $1/\varepsilon$ terms from equation (1.59). The result is then finite for $\varepsilon \to 0$. Now that we know how to calculate the hard scattering part in the factorized cross section, we have to give a clear definition of the parton distribution function that take care of the long distance physics.

We want to mention that the factorized cross section given in equation (1.48) is an approximation. In a sense that only one particle per initial state parton is involved and we do not allow any further interactions between the hard scattering part and the non perturbative hadronic part. Nevertheless, such interactions are conceivable, where the hard scattering part further interacts with the soft part of the cross section. It comes out that such contributions, often called higher twist contributions, are suppressed by powers of $1/Q^2$. Therefore, equation (1.48) receives $\mathcal{O}(1/Q^2)$ corrections that are suppressed in the discussed cross section. In chapter 4 we are faced with a physical quantity, - a single transverse spin asymmetry -, where the leading twist contribution cancels out. Therefore, to describe this asymmetry we have to take these higher twist contributions into account.

1.3.2. Parton distribution functions and evolution

The parton distribution functions are an essential component of the factorization formula equation (1.48). They take care of all the long distance physics that live below the perturbative scale. Despite a clear definition in terms of operators the theoretical access to the distribution of partons in a hadron is very limited. The problem relies in the fact, that we can not use standard pQCD techniques to give a prediction for

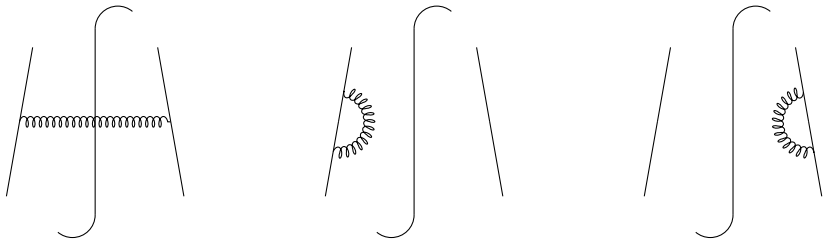

Figure 1.9.: One loop correction to the quark distribution eq. (1.60) in light cone gauge $\mathcal{G} = 1$.

the PDFs by only using the QCD Lagrangian as an input. Considerable efforts have been achieved by performing lattice calculations [26, 27]. To this day, high precision predictions for collider or fixed target experiments are performed with PDFs extracted from experimental data [31–33].

We follow in our formal definition of the parton distribution functions the one given in [29, 34]. If we describe a hadron with momentum P which has a large component P^+, i.e. $P^- = P_\perp = 0$, in arbitrary gauge the quark distribution with momentum ξP in hadron A carrying momenta P is given by

$$f_{q/A}(\xi) = \frac{1}{4\pi} \int \mathrm{d}x^- \, \mathrm{e}^{-\mathrm{i}\xi P^+ x^-} \, \langle P| \, \overline{\Psi}(x^-)\gamma^+ \mathcal{G} \Psi(0) \, |P\rangle \ . \tag{1.60}$$

The operator $\mathcal{G}$ ensures gauge invariance and is given by path ordered exponentiated gluon fields

$$\mathcal{G} = \mathcal{P} \exp\left[\mathrm{i}g \int_0^{x^-} \mathrm{d}y^- A_c^+(y^-) T_c\right] \tag{1.61}$$

where $\mathcal{P}$ is the path ordering operator. Consequently, in light cone gauge, i.e. $A_c^+ = 0$, the operator $\mathcal{G}$ is equal unity. Besides the distribution of quarks in a hadron we need the definition of the gluon distribution

$$f_{g/A}(\xi) = \frac{1}{4\pi} \int \mathrm{d}x^- \, \mathrm{e}^{-\mathrm{i}\xi P^+ x^-} \, \langle P| \, F_a^{+\,\nu}(x^-) \mathcal{G}_{ab} F_{b\,\nu}^+(0) \, |P\rangle \ , \tag{1.62}$$

where $F_a^{\mu\nu}$ is the gluon field strength tensor and the operator $\mathcal{G}_{ab}$ is given by equation (1.61) by using the octet representation for the generating matrices.

The operator products in (1.60) and (1.62) require renormalization as they are UV divergent. Obviously this renormalization procedure inserts a mass scale μ into the PDF, from which we can derive a renormalization group equation for the distributions

that leads to the Dokshitzer-Gribov-Lipatov-Altarelli-Parisi (DGLAP) equations

$$\frac{\mathrm{d}}{\mathrm{d}\mu} f_{a/A}(\xi,\mu) = \sum_b \int_\xi^1 \frac{\mathrm{d}\zeta}{\zeta}\, P_{a/b}(\zeta,\alpha_s(\mu^2))\; f_{b/A}(\xi/\zeta,\mu)\;. \tag{1.63}$$

$P_{a/b}$ is the splitting-kernel that can be calculated in perturbative QCD from the parton in parton distribution. The splitting function represents that a parton b splits in a parton a carrying momentum fraction ζ. The splitting function has the perturbative expansion

$$P_{a/b}(\zeta,\alpha_s(\mu^2)) = \frac{\alpha_s(\mu^2)}{\pi} P^{(0)}_{a/b}(\zeta) + \left(\frac{\alpha_s(\mu^2)}{\pi}\right)^2 P^{(1)}_{a/b}(\zeta) + \mathcal{O}(\alpha_s^3) \tag{1.64}$$

The splitting functions are calculated up to three loop order for the spin averaged [35] and the helicity dependent case [36]. It is convenient to rewrite the evolution equation in three pieces. The quark singlet (q^s) and non-singlet (q^{ns}) part as well as the gluon contribution (g). With

$$q^s = \sum_q (q+\bar{q}), \quad \text{and} \quad q^{ns} = q - \bar{q}\;, \tag{1.65}$$

where the sum runs over all quark flavors. We rewrite equation (1.63) as

$$\begin{aligned}
\frac{\partial q^{ns}}{\partial \ln \mu^2} &= \frac{\alpha_s(\mu^2)}{\pi} P^{(0)}_{qq} \otimes q^{ns}\;, \\
\frac{\partial q^{ns}}{\partial \ln \mu^2} \begin{pmatrix} q^s \\ g \end{pmatrix} &= \frac{\alpha_s(\mu^2)}{\pi} \begin{pmatrix} P^{(0)}_{qq} & 2N_f P^{(0)}_{qg} \\ P^{(0)}_{gq} & P^{(0)}_{gg} \end{pmatrix} \otimes \begin{pmatrix} q^s \\ g \end{pmatrix}\;,
\end{aligned} \tag{1.66}$$

where the $\otimes$ indicates appropriate convolution as in equation (1.63). As indicated in equation (1.55) one method to extract the LO splitting kernel is to calculate the renormalized parton in parton distribution $\tilde{f}_{a/b}$ at one loop and extract the IR-pole contribution. For example to extract the splitting kernel $P^{(0)}_{qq}$ we have to calculate the one-loop contribution to $\tilde{f}_{q/q}$ shown in figure (1.9). To do so we can use the operator definition of equation (1.60) in light cone gauge with the hadronic- replaced by a quark-state

$$f_{q/q}(\xi) = \frac{1}{4\pi} \int \mathrm{d}x^-\; \mathrm{e}^{-\mathrm{i}\xi p^+ x^-}\; \langle q(p)|\, \overline{\Psi}(x^-)\gamma^+\Psi(0)\,|q(p)\rangle\;. \tag{1.67}$$

To understand the pole structure we do not have to go through the complete calculation. At one loop order one has simple diagrams shown in figure (1.9) that contain IR divergencies that arise because we assume on-shell massless partons as well as UV divergencies coming from large momenta in the operator product. The overall transverse

integral is zero for the diagrams, this is due to the fact that the integrals cancels out among the UV and the IR singular parts, i.e.

$$\left(\frac{\mu^2}{4\pi}\mathrm{e}^{\gamma_E}\right)^{\varepsilon}\int\frac{\mathrm{d}^{2-2\varepsilon}k_\perp}{(2\pi)^{2-2\varepsilon}}\frac{1}{k_\perp^2}=\frac{1}{4\pi}\left(\frac{1}{\varepsilon_{\mathrm{UV}}}-\frac{1}{\varepsilon_{\mathrm{IR}}}\right)\,. \tag{1.68}$$

Using that we get after a lengthy calculation

$$\tilde{f}_{q/q}(\xi,\varepsilon)=\delta_{aa}\delta(1-\xi)+\left(\frac{1}{\varepsilon_{\mathrm{UV}}}-\frac{1}{\varepsilon_{\mathrm{IR}}}\right)\frac{\alpha_s}{2\pi}P_{qq}^{(0)}(\xi)+\text{c.t.}\,, \tag{1.69}$$

where c.t. includes the appropriate $\overline{\mathrm{MS}}$ counter terms to cancel the UV pole. From that we get the LO qq splitting kernel

$$P_{qq}^{(0)}(\xi)=C_F\left(\frac{1+\xi^2}{(1-\xi)_+}+\frac{3}{2}\delta(1-\xi)\right)\,. \tag{1.70}$$

For completeness we give the other LO splitting kernels that can be obtained by similar calculations

$$\begin{aligned}
P_{qg}^{(0)}(\xi)&=\frac{1}{2}\left(\xi^2+(1-\xi)^2\right)\,,\\
P_{gq}^{(0)}(\xi)&=C_F\left(\frac{1+(1-\xi)^2}{\xi}\right)\,,\\
P_{gg}^{(0)}(\xi)&=2C_A\left(\frac{1-\xi}{\xi}+\xi(1-\xi)+\frac{\xi}{(1-\xi)_+}\right)\\
&\quad+\left(\frac{11}{6}C_A-\frac{1}{3}N_f\right)\delta(1-\xi)\,.
\end{aligned} \tag{1.71}$$

With the knowledge of these splittig kernels we can evolve the PDF from one scale to another without any further non perturbative input. The procedure is non trivial and requires Mellin-space techniques as shown in [37]. Evidently, this scale evolution is a milestone in pQCD and increase the predictive power of the theory enormously.

1.4. Resummation

In this section we introduce the basic concepts of resummation using the Drell-Yan process as an example. In the following parts, we show briefly how resummation follows from strong factorization properties.

1.4.1. Resummation for Drell-Yan process

In the previous section we have discussed cross sections evaluated at fixed perturbative order in terms of the strong coupling α_s. We have seen that QCD offers a rich phenomenology when we take higher orders into account. In this section we will discuss

kinematical regions where such fixed order calculation gives a rather distorted image of the actual physics. To illustrate that, we exploit the Drell-Yan process, which we already discussed in the previous section. In this section we calculate the slightly simpler case where the cross section does not depend on the lepton pair rapidity. The cross section is given by

$$\frac{\mathrm{d}\sigma}{\mathrm{d}Q^2} = \sum_{a,b} \int_{Q^2/S}^{1} \mathrm{d}\xi_A \int_{Q^2/(S\xi_A)}^{1} \mathrm{d}\xi_B \; f_{a/A}(\xi_A,\mu)\; H_{ab}\left(z,\alpha_s,Q^2/\mu^2\right)\; f_{b/B}(\xi_B,\mu)\;. \quad (1.72)$$

The hard scattering function H_{ab} is dependent on the invariant pair mass of the observed final state Q^2, an arbitrary scale μ^2, the strong coupling α_s and a variable $z = Q^2/\hat{s}$ where $\hat{s}$ is the partonic center of mass energy $\hat{s} = \xi_A \xi_B S$. As we discussed the hard scattering function is a perturbative function an can be expanded as

$$H_{ab} = \sigma_0 \omega_{ab}\left(z, Q^2/\mu^2, \alpha_s\right) = \sigma_0 \left(\omega^{\mathrm{LO}}(z)\delta_{ab} + \frac{\alpha_s}{\pi}\omega_{ab}^{\mathrm{NLO}}(z, Q^2/\mu^2) + \mathcal{O}\left(\alpha_s^2\right)\right) \quad (1.73)$$

where we can use the methods discussed in the previous paragraphs to explicitly calculate the α_s-correction. In equation (1.73) we define the dimensionless hard scattering coefficients ω^{LO} and ω^{NLO} and $\sigma_0 = \frac{4\pi\alpha^2}{9\hat{s}Q^2}$. In the subsequent discussion, we neglect contributions arising at α_s-level, which are not given by a $q\bar{q}$ initial state. Fortunately, they play a subleading role in our kinematical region of interest. With the factor σ_0 the leading order is given by

$$\omega^{\mathrm{LO}} = \delta(1-z), \quad (1.74)$$

thus the NLO correction in the $q\bar{q}$ channel is given by [38]

$$\omega_{q\bar{q}}^{\mathrm{NLO}} = C_F \Bigg[2(1+z^2)\left(\frac{\ln(1-z)}{1-z}\right)_+ - \frac{1+z^2}{1-z}\ln z + \frac{1}{2}\left(\frac{2}{3}\pi^2 - 8\right)\delta(1-z) + P_{qq}(z)\ln\frac{Q^2}{\mu^2}\Bigg],$$

where the subscript + indicates the "plus"-distribution defined by

$$\int_0^1 \mathrm{d}z\; h(z)\,(g(z))_+ = \int_0^1 (h(z) - h(1))\, g(z)\;. \quad (1.75)$$

On closer examination of the α_s correction, we found terms that might be very important in the $z \to 1$ regime. We call the $z \to 1$ limit the "partonic threshold", since it defines a threshold where all the energy from the incoming $q\bar{q}$-pair is used to produce the two lepton final state. Therefore, the phase space for hard gluon emission into the

Table 1.1.: Threshold logarithms grouped into fixed order rows and resummation towers.

	Fixed Order $\Longrightarrow$			
$\Downarrow$Resummation	LO	1		
	NLO	$\alpha_s L^2$	$\alpha_s L$ α_s	
	NNLO	$\alpha_s^2 L^4$	$\alpha_s^2 L^3$ $\alpha_s^2 L^2$	$\alpha_s^2 L$ α_s^2
	...	...	...	...
	$\mathrm{N^kLO}$	$\underbrace{\alpha_s^k L^{2k}}_{\mathrm{LL}}$	$\underbrace{\alpha_s^k L^{2k-1}\ \alpha_s^k L^{2k-2}}_{\mathrm{NLL}}$	$\underbrace{\alpha_s^k L^{2k-3}\ \alpha_s^k L^{2k-4}}_{\mathrm{NNLL}}$

final state vanishes and only soft gluons are radiated at the partonic threshold. The logarithmic plus distributions

$$\left(\frac{\ln(1-z)}{1-z}\right)_+ \tag{1.76}$$

are a remainder from the IR-divergencies from such soft gluon diagrams. The ε-pole itself cancels among the virtual correction, whereas the distribution is still present in the cross section and gives a very large contribution in the threshold regime. It can be shown that these logarithms do appear at all orders of QCD perturbation theory. Thus, at perturbative order k we have terms of the form

$$\alpha_s^k \left(\frac{\ln^m(1-z)}{1-z}\right)_+, \quad \text{with } m \leq 2k\,. \tag{1.77}$$

Therefore, in order to obtain a meaningful result in the threshold regime, the threshold logarithms should be taken into account to all orders. The technique which exactly performs this all order treatment is called "treshold-resummation". We mention, that the effects from the threshold logarithms are even more enhanced by the shape of the PDFs. Due to the fact that the PDF are becoming extremely small towards small momentum fractions, the large momentum fraction and thus large z contributions are enhanced by the parton distributions.

The resummation of threshold logarithms may be achieved in Mellin transform space. The N-th Mellin moment of a function f is defined as

$$f^N = \int_0^1 \mathrm{d}x\; x^{N-1} f(x)\,. \tag{1.78}$$

If we take the Mellin moments with respect to the variable $\tau = Q^2/S$ of the Drell-Yan cross section, the convolution structure factorizes into the moments of the parton distributions and the partonic cross section,

$$\int_0^1 \mathrm{d}\tau \tau^{N-1} \frac{1}{\sigma_0} \frac{\mathrm{d}\sigma}{\mathrm{d}Q^2} = \sum_{a,b} f_{a/A}^N(\mu)\, \omega_{ab}^N(Q^2/\mu^2, \alpha_s)\, f_{b/B}^N(\mu) \tag{1.79}$$

where the N-moments of the hard scattering function and the parton distributions are given by

$$f_{a/A}^N(\mu) = \int_0^1 \mathrm{d}\xi_A\, \xi_A^{N-1} f_{a/A}(\xi_A, \mu)\,, \tag{1.80a}$$

$$f_{b/B}^N(\mu) = \int_0^1 \mathrm{d}\xi_B\, \xi_B^{N-1} f_{b/B}(\xi_B, \mu)\,, \tag{1.80b}$$

$$\omega_{ab}^N(Q^2/\mu^2, \alpha_s) = \int_0^1 \mathrm{d}z z^{N-1} \omega_{ab}(z, Q^2/\mu^2, \alpha_s)\,. \tag{1.80c}$$

The threshold limit $z \to 1$ corresponds to $N \to \infty$ in Mellin space. All contributions to the cross section that are smooth at $z = 1$, contribute to the moments only by corrections that vanish as powers of N for $N \to \infty$. Therefore, they play a minor role in our discussion. On the other hand, singular distributions at the partonic threshold give rise to logarithmic N-dependence

$$\int_0^1 \mathrm{d}z\, z^{N-1} \left(\frac{\ln^m(1-z)}{1-z} \right)_+ = \frac{(-1)^{m+1}}{m+1} \ln^{m+1} N + \dots\,. \tag{1.81}$$

When the singular terms at threshold are transformed to Mellin space, we find a double logarithmic structure, i.e. each power in α_s is accompanied by two powers of $\ln N$ in Mellin space. In figure 1.1 the all-order structure of threshold logarithms in Mellin space is shown, where $L \equiv \ln N$. In a leading logarithmic approximation (LL) only the most dominant class of logarithms is taken into account. This corresponds to the sum over the first column in figure 1.1. At the level of next-to leading logarithmic (NLL) accuracy the first three classes and at the level of next-to-next-to leading logarithmic accuracy (NNLL) the first five classes of logarithmic contributions are taken into account.

The resummation formalism for this process has been shown in detail at LL and NLL level in [39, 40] whereas results at NNLL accuracy are given in [41]. In this thesis we will get back how these results can be derived. For the moment we just state the results, in order to explore the basic properties of the resummed cross section. The all order structure of threshold logarithms is organized by treating them as exponentials, schematically given by

$$\omega_{ab}^{\text{resum.}}(N, Q^2/\mu^2, \alpha_s) = \exp\Big\{ \ln N h^{(1)}(\alpha_s \ln N) + h^{(2)}(\alpha_s \ln N) + \alpha_s h^{(3)}(\alpha_s \ln L) \Big\} C(\alpha_s) \tag{1.82}$$

where C collects all the far off shell dynamics. It is perturbative in α_s and in the case of Drell-Yan where the LO process is a color singlet, it is a scalar function that can for example be analytically matched to the fixed order calculation. The LL double logarithmic structure $\sim \alpha_s^k \ln^{2k} N$ from the first tower in figure 1.1 arises solely from the exponent $\ln N h^{(1)}$. The NLL structure arises if we additionally include $h^{(2)}$ and hence we get the NNLL structure by including the exponent $\alpha_s h^{(3)}$.

In our case the resummed cross section can be written as [41]

$$\omega_{q\bar{q}}^{\text{resum.}}(N, Q^2, Q^2/\mu^2, \alpha_s) = C_{q\bar{q}}(\alpha_s, Q^2/\mu^2)\Delta_{q\bar{q}}^{\text{DY}}(\alpha_s, Q^2, Q^2/\mu^2) \tag{1.83}$$

where the function Δ_{DY} takes care of the soft gluon emission contributions. We have to distinguish between two types of soft gluon radiation, soft collinear gluons or soft gluons radiated in a wide angle to the initial state partons.

$$\Delta_{q\bar{q}}^{\text{DY}}(\alpha_s, Q^2, Q^2/\mu^2) = 2\ln\Delta_q^N(Q^2, \mu^2) + \ln\Delta_{\text{DY}}^{\text{int.}}(Q^2) \tag{1.84}$$

The soft gluons that are emitted collinear to an initial state parton can be factored from the far off-shell process and can be resummed into the universal exponent

$$\ln\Delta_q^N(Q^2, \mu^2) = \int_0^1 \mathrm{d}x\, \frac{x^{N-1}-1}{1-x} \int_{\mu^2}^{(1-x)^2Q^2} \frac{\mathrm{d}\mu'}{\mu'^2}\, A(\alpha_s(\mu'^2))\,. \tag{1.85}$$

The wide angle soft gluon emissions, are resummed in the a process dependent exponent given by

$$\ln\Delta_{\text{DY}}^{\text{int.}}(Q^2) = \int_0^1 \mathrm{d}x\, \frac{x^{N-1}-1}{1-x} D_{\text{DY}}(\alpha_s((1-x)^2Q^2))\,. \tag{1.86}$$

The integrands in equations (1.85) and (1.86) are perturbative and given by,

$$A_q(\alpha_s) = \frac{\alpha_s}{\pi}A_q^{(1)} + \left(\frac{\alpha_s}{\pi}\right)^2 A_q^{(2)} + \left(\frac{\alpha_s}{\pi}\right)^3 A_q^{(3)} + \mathcal{O}(\alpha_s^4)\,, \tag{1.87a}$$

$$D_{\text{DY}}(\alpha_s) = \left(\frac{\alpha_s}{\pi}\right)^2 D_{\text{DY}}^{(2)} + \mathcal{O}(\alpha_s^3)\,, \tag{1.87b}$$

where the constants $A^{(i)}$ are the coefficients of the $1/(1-z)_+$ terms of the i-loop splitting functions $P_{qq}^{i-1}(x)$. Thus we have

$$A_q^{(1)} = C_F\,, \qquad A_1^{(2)} = \frac{1}{2}\,C_F\left[C_A\left(\frac{67}{18} - \frac{\pi^2}{6}\right) - \frac{5}{9}N_f\right]\,, \tag{1.88}$$

$$\begin{aligned} A_q^{(3)} = \frac{1}{4}C_F\Bigg[&C_A^2\left(\frac{245}{24} - \frac{67}{9}\zeta(2) + \frac{11}{6}\zeta(3) + \frac{11}{5}\zeta(2)^2\right) \\ &-\frac{1}{27}N_f^2 + C_F N_f\left(-\frac{55}{24} + 2\zeta(3)\right) \\ &+C_A N_f\left(-\frac{209}{108} + \frac{10}{9}\zeta(2) - \frac{7}{3}\zeta(3)\right)\Bigg]\,, \end{aligned}$$

$$D_{\text{DY}}^{(2)} = C_F\left[C_A\left(-\frac{1616}{27} + 56\zeta(2) + \frac{176}{3}\zeta(3)\right) + N_f\left(\frac{224}{27} - \frac{32}{3}\zeta(2)\right)\right]\,,$$

The next step is to calculate the exponential function $\Delta_{q\bar{q}}^{\mathrm{DY}}$ to the desired logarithmic order. To do so we need the definition of the strong coupling given in equation (1.28). The mass scale that arises from the RGE for the strong coupling is not necessarily the same mass scale as we have in equation (1.85). Therefore, we distinguish between the two scales and call the renormalization mass scale in equation (1.28) μ_R. The exponent is pleasantly organized to NLL accuracy as

$$\ln \Delta_{q\bar{q}}^{\mathrm{DY}} = 2 \ln N h^{(1)}(\lambda) + 2h^{(2)}(\lambda) + \mathcal{O}(\mathrm{NNLL}) \,, \tag{1.89}$$

with the variable

$$\lambda = \alpha_s b_0 \ln N \,, \tag{1.90}$$

where b_0 is the first coefficient of the QCD beta-function given in equation (1.25a). Thus we have

$$h^{(1)}(\lambda) = \frac{A_q^{(1)}}{2\pi b_0 \lambda} \left(2\lambda + (1-2\lambda)\ln(1-2\lambda)\right) \,, \tag{1.91a}$$

$$\begin{aligned} h^{(2)}(\lambda) = &-\frac{A_q^{(2)}}{2\pi^2 b_0^2}\left[2\lambda + \ln(1-2\lambda)\right] \\ &+\frac{A_q^{(1)} b_1}{2\pi b_0^3}\left[2\lambda + \ln(1-2\lambda) + \frac{1}{2}\ln^2(1-2\lambda)\right] \\ &-\frac{A_q^{(1)}}{2\pi b_0}\left[2\lambda + \ln(1-2\lambda)\right]\ln\frac{\mu_R^2}{Q^2} + \frac{A_q^{(1)}}{\pi b_0}\lambda \ln\frac{\mu^2}{Q^2} \,, \end{aligned} \tag{1.91b}$$

where we can conclude that the process dependent piece at first arises at NNLL level. We will come back to this in chapter 5. We want to mention that the resummed cross section is divergent for $\lambda = \frac{1}{2}$ as one can see in equation (1.91). This is the so called Landau singularity at

$$N_L = \exp\left(\frac{1}{2\alpha_s b_0}\right) \,, \tag{1.92}$$

which is caused by the unbound rise of $\alpha_s(\mu_R^2)$ towards small evaluation scales μ_R. This Landau singularity needs special care when we perform the inverse Mellin transformations, to ensure numerical convergence. The resummed cross section in equation (1.83) is given in Mellin space and needs an appropriate transformation to the physical space. In threshold resummation related calculations, this is usually performed numerically since the PDFs are not analytically known functions. The inverse Mellin transformation of the resummed cross section is given by a contour integral in the complex N-plane

$$\frac{\mathrm{d}\sigma^{\mathrm{resum.}}}{\mathrm{d}Q^2} = \sigma_0 \int_{c_N} \frac{\mathrm{d}N}{2\pi \mathrm{i}} f_{a/A}^N(\mu)\, \omega_{ab}^N(Q^2/\mu^2, \alpha_s)\, f_{b/B}^N(\mu) \,, \tag{1.93}$$

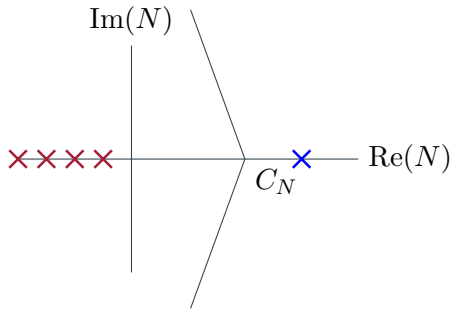

Figure 1.10.: Integration contour C_N in the complex N-plane. The crosses denote poles in the N-plane, where the rightmost blue cross is the Landau pole, whereas the red ones denote the poles emerging from the N-moments of the PDFs.

where c_N is an appropriate contour shown in figure 1.10. In this figure also the poles emerging from the moments of the PDFs (red crosses) and the Landau pole (blue cross) are shown. The contour is chosen following reference [42] to run between the rightmost pole from the moments of the PDFs and the Landau pole. This ensures numerical convergence, in a sense that one can show that a perturbative expansion of the resummed formula is free of factorially growing terms [42]. This special choice of the contour is called "Minimal-Prescription" and is used among all our threshold resummation studies.

Finally, we match the resummed result to a full fixed order calculation. Since, subleading terms at threshold, i.e. non singular terms for $z \to 1$ are not included in our resummed cross section so far. The most accurate results are expected by taking them both into account. This is done numerically by adding both the $\mathrm{N}^k\mathrm{LL}$ and the $\mathrm{N}^k\mathrm{LO}$, or the highest available fixed order result instead, i.e.

$$\mathrm{d}\sigma^{\mathrm{match}} = \left(\mathrm{d}\sigma^{\mathrm{resum.}}_{\mathrm{N}^k\mathrm{LL}} - \mathrm{d}\sigma^{\mathrm{resum.}}_{\mathrm{N}^k\mathrm{LL}}\Big|_{\mathcal{O}(\alpha_s^k)} \right) + \mathrm{d}\sigma^{\mathrm{full}}_{\mathrm{N}^k\mathrm{LO}} \,, \tag{1.94}$$

where the subtraction of the term $\mathrm{d}\sigma^{\mathrm{resum.}}_{\mathrm{N}^k\mathrm{LL}}\Big|_{\mathcal{O}(\alpha_s^k)}$ avoids double counting.

1.4.2. Resummation from factorization properties

A very sophisticated access to the all order structure of threshold logarithms is to exploit strong factorization properties of the cross section near the partonic threshold [39]. This is illustrated in figure 1.11 where the dominant momentum regions are shown. The far off-shell photon, is linked to the incoming partons through the hard-scattering amplitude $\mathcal{H}$ and the complex conjugate amplitude $\mathcal{H}^*$. The hard-scattering functions

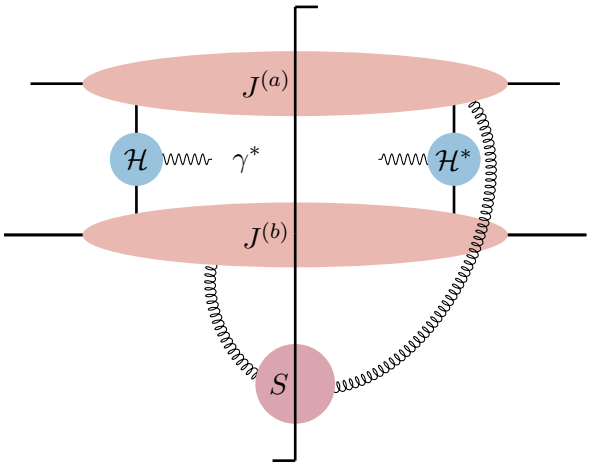

Figure 1.11.: Factorization for Drell-Yan cross section near partonic threshold.

contain the far off-shell, i.e. order Q^2 and higher, dynamics of the cross section. The hard functions are coupled to the incoming jets $J^{(a)}$ and $J^{(b)}$, which represent on-shell particles with momenta of the order Q. We assume that in the threshold-limit all on-shell partons with finite energy are included in these jet functions. In addition, the jet functions include all collinear radiation with respect to the incoming partons. The phase space which is left for on-shell radiation, is then limited to soft gluon emission. This is included in the function S which couples to the jet functions $J^{(a)}$ and $J^{(b)}$.

The dominant momentum regions in the threshold limit may be isolated quantitatively by introducing an appropriate weight. We assume the weight to be dimensionless and infrared safe. As was shown in [43], not every infrared safe weight leads to exponentiation of the cross section. In addition, the weight of particles within the jets and soft function must be independent and additive in the threshold limit. Thus we define the weights,

$$w = w_a + w_b + w_s = 1 - Q^2/S \tag{1.95}$$

with corrections that vanish as $\mathcal{O}(w^2)$ [44]. The general refactorized cross section is given by [44]

$$\begin{aligned}\sigma_0 \omega_{ab} = \mathcal{H}(p_i/\mu, \zeta_i) \int \frac{\mathrm{d}w_a}{w_a}\frac{\mathrm{d}w_b}{w_b}\frac{\mathrm{d}w_s}{w_s}\; J^{(a)}(p_a\cdot\zeta_a, w_a(Q/\mu))\; J^{(b)}(p_b\cdot\zeta_b, w_b(Q/\mu)) \\ \times S(w_s(Q/\mu), \zeta_i)\; \delta(w - w_a - w_b - w_s)\end{aligned} \tag{1.96}$$

where $i = a, b$. The vectors ζ_i are gauge fixing vectors using $\zeta_i \cdot A = 0$.

The convolution (1.96) factorizes into products by taking the moments

$$\sigma_0 \int_0^\infty \mathrm{d}w \mathrm{e}^{-Nw} \omega_{ab} = \mathcal{H}(p_i/\mu, \zeta_i)\ \tilde{S}(Q/\mu N, \zeta_i) \times \tilde{J}_a(p_a \cdot \zeta_a/\mu, Q/\mu N)\ \ \tilde{J}_b(p_b \cdot \zeta_a/\mu, Q/\mu N) \tag{1.97}$$

Each of the individual functions $\mathcal{H}$, $J^{(i)}$ and S require renormalization. Therefore, we introduce a set of anomalous dimensions, which determines the scale dependence of the quantities above, i.e.

$$\mu \frac{\mathrm{d}}{\mathrm{d}\mu} \ln \mathcal{H} = -\gamma_{\mathcal{H}}(\alpha_s)\ , \tag{1.98a}$$

$$\mu \frac{\mathrm{d}}{\mathrm{d}\mu} \ln J^{(i)} = -\gamma_{J^{(i)}}(\alpha_s)\ , \tag{1.98b}$$

$$\mu \frac{\mathrm{d}}{\mathrm{d}\mu} \ln S = -\gamma_S(\alpha_s)\ . \tag{1.98c}$$

The demand that the cross section is independent of the renormalization scale μ leads to

$$\gamma_{\mathcal{H}} + \gamma_S + \gamma_{J^{(a)}} + + \gamma_{J^{(b)}} = 0\ . \tag{1.99}$$

Therefore, the renormalization dependence of the individual functions must cancel in their product.

Solving equations (1.98) and imposing RGE invariance equation (1.99) we find an exponentiated structure for the jet functions $J^{(i)}$ [39, 44]. Furthermore, we recover the logarithmic all order structure given in equation (1.83). We mention, that the structure for QCD hard scattering, where all particles in the hard scattering are color charged, is highly more complex. In that case, soft gluon radiation non-collinear to the external partons is sensitive to their color state. Because of that, the factorization of the soft and hard functions is more complex and they will be linked by their color structure. Therefore, the functions $\mathcal{H}$ and S become matrices in space of color exchange operators. We will come back to this in chapter 5, where we use this method to resum threshold logarithms in the dihadron production process in pp scattering.

1.5. Conclusions and outlook

We showed in this chapter the problems and features that arise, if we try to face the theory of QCD with physical processes. We showed that QCD is a phenomenologically rich theory, starting from its Lagrangian. We outlined that QCD is an UV-divergent theory and needs consequently renormalization. This need for renormalization, brings in a key feature of the theory, which justifies most of our calculations: Asymptotic

Freedom. Therefore, if our physical process takes place at sufficiently high energies, the concept perturbation theory is legitimized.

We learned that most physical processes, involve parts where we can apply QCD perturbation theory and parts, which involve dynamics below an energy threshold where a perturbative expansion is useless. These non-perturbative parts of our calculation describe hadrons, that bound quarks and gluons into a confined colorless object. We introduced the concept of factorization that exactly decompose the cross section in the different regions, and allows us to obtain sensible answers from the theory. This is of course true as long as our physical observable fulfills the concept of infrared safety. The factorization formula, which itself is an approximation and which receives power suppressed corrections, decompose the cross section in the hard partonic part and the non-perturbative part described by parton distribution functions. These parton distribution functions are itself dependent on an energy scale where the process takes place. This scale dependence is described by the scale evolution, that gives QCD its great predictive power.

The subsequent chapters of this thesis, are all based on these fundamental concept of QCD perturbation theory and apply these concepts to nowadays research projects. So far, we discussed how we can handle hadronic initial states, such as present in the Drell-Yan cross section. But, also hadronic final states are interesting observables in nowadays high energy experiments. We introduce the concept of final state factorization in the next chapter, where we present a NLO calculation of single inclusive hadron production in lepton nucleon scattering. This study is motivated by the fact, that this process is indeed very interesting in the large field of spin physics. Since, in spin physics asymmetries are the physical quantity we want to look at, an accurate understanding of the unpolarized as well as the polarized cross sections is necessary. The polarized cross section is the topic of chapter 3 and 4 where we investigate the longitudinal double spin asymmetry respectively the single transverse spin asymmetry.

The chapters 5, 6 and 7 take a close look on threshold resummation effects in hadronic scattering. In these processes, all particles in the hard part of the cross section are color charged, which makes the determination of the all order structure of the threshold logarithms extremely challenging. In chapter 5 we present our beyond NLL calculation for dihadron production. And in chapters 6 and 7 we use the resummation formalism to determine approximate NNLO results for single jet production. We perform this calculation for unpolarized as well as longitudinally polarized initial states.

Chapter 2.

Single-Inclusive Production of Hadrons and Jets in Lepton-Nucleon Scattering at NLO

We present next-to-leading order (NLO) perturbative-QCD calculations of the cross sections for $\ell N \to hX$ and $\ell N \to \text{jet}\, X$. The main feature of these processes is that the scattered lepton is not observed, so that the hard scale that makes them perturbative is set by the transverse momentum of the hadron or jet. Kinematically, the two processes thus become direct analogs of single-inclusive production in hadronic collisions which, as has been pointed out in the literature, makes them promising tools for exploring transverse spin phenomena in QCD when the incident nucleon is transversely polarized. We find that the NLO corrections are sizable for the spin-averaged cross section. We also investigate in how far the scattering is dominated by the exchange of almost real (Weizsäcker-Williams) photons. We present numerical estimates of the cross sections for present-day fixed target experiments and for a possible future electron ion collider. This chapter is based on publications [3, 6].

2.1. Introduction

There has been growing interest recently, both experimentally [45–48] and theoretically [49–55], in the processes $\ell N \to hX$ and $\ell N \to \text{jet}\, X$, the single inclusive production of a hadron or jet at large transverse momentum in lepton-nucleon scattering. In contrast to the far more customary process $\ell N \to \ell' hX$ [56], for $\ell N \to hX$ the scattered lepton in the final state is not observed, so that the process is truly one-hadron

(or one-jet) inclusive. The reason for the interest in $\ell N \to hX$ comes from the study of single transverse-spin phenomena in hadronic scattering processes. It is well known that large single-spin asymmetries have been observed [57] for the process $pp^\uparrow \to hX$, where $p^\uparrow$ denotes a transversely polarized proton. To explain the large size of the asymmetries, and their persistence all the way from fixed-target to collider energies, has posed a major challenge to theory. Although a lot has been learned, it is fair to say that a fully satisfactory understanding has yet to be obtained. Measurements of corresponding asymmetries in the kinematically equivalent, but much simpler, processes $\ell N^\uparrow \to hX$, $\ell N^\uparrow \to \text{jet}\, X$ have the promise to shed new light on the mechanisms for single-spin asymmetries in QCD. First fairly precise experimental data for $\ell N^\uparrow \to hX$ have recently been released by the HERMES [46, 47] and Jefferson Lab Hall A [48] collaborations.

We note that at first sight one might consider the related process $\ell N^\uparrow \to \ell' X$ (which is just the standard inclusive deep-inelastic (DIS) process) to be equally suited for transverse-spin studies in lepton scattering. However, the analysis of the corresponding single-spin asymmetry is considerably more complex because higher order QED effects are required for the asymmetry to be non-vanishing [58–62]. In the same spirit as $\ell N^\uparrow \to hX$, also the processes $\vec{\ell} N^\uparrow \to hX$ [63] with longitudinal polarization of the lepton and $\ell N \to \Lambda^\uparrow X$ [64] with a transversely polarized Λ hyperon have been considered in the literature recently.

The proven method for analyzing single-inclusive processes such as $pp \to hX$ or $\ell N \to hX$ at large transverse momentum rests on QCD perturbation theory and collinear factorization. For single-transverse-spin observables, this involves a twist-3 formalism in terms of three-parton correlation functions of the nucleon or the fragmentation process [65–76]. Interestingly, the recent study [76] suggests that the twist-3 fragmentation effects could be the dominant source of the observed large transverse-spin asymmetries in $pp^\uparrow \to hX$. An alternative approach for describing the single-spin asymmetry in inclusive hadron production in $pp^\uparrow \to hX$ was devised in the context of a "generalized" parton model in which the dependence of parton distributions and fragmentation functions on transverse momentum is kept [77–80]. Although no such factorization in transverse momentum is known to be valid for a single-inclusive cross section, the approach has enjoyed considerable phenomenological success.

Both the collinear twist-3 approach and the generalized parton model have been used to obtain predictions for the spin asymmetry in $\ell N^\uparrow \to hX$. In Ref. [52] a leading order (LO) twist-3 analysis has been presented in terms of parton correlation functions that were previously extracted from data for $pp^\uparrow \to hX$. The results obtained in this way fail to describe the HERMES data [46, 47] for the spin asymmetries in $\ell N^\uparrow \to hX$. A comparison of perturbative calculations to the corresponding JLab data [48] is not possible as the data are for hadrons with transverse momenta below 1 GeV. The LO generalized parton model approach, on the other hand, appears to give results quite

consistent with the HERMES data [53–55].

In our view it is premature to draw any conclusions from these findings at LO. Given the kinematics (and the precision) of the present data, one may expect higher-order QCD corrections to the cross sections and the asymmetry to be important [52] for a meaningful comparison of data and theory. At least next-to-leading order (NLO) corrections should be included. We stress that the twist-3 formalism, although so far only developed to LO, offers a well-defined framework for a perturbative study of the transverse-spin asymmetry in $\ell N^\uparrow \to hX$. This is in contrast to the generalized parton model, for which there is likely no systematic way of going to higher orders in perturbation theory. That said, NLO calculations within the twist-3 formalism are technically very challenging, and only a few NLO calculations have been performed for the simpler Drell-Yan [81] and semi-inclusive deep-inelastic scattering (DIS) cases [82, 83].

In this chapter, we take a first step toward an NLO calculation of the transverse-spin asymmetry for $\ell N^\uparrow \to hX$ by computing the NLO corrections to the spin-averaged cross section for the process, which constitutes the denominator of the spin asymmetry. We present analytical results for the NLO partonic cross sections. To our knowledge, despite the vast amount of work performed for lepton proton scattering in the literature (see, for example [84–101]), this calculation has not been presented so far. We also present similar NLO calculations for the process $\ell N \to \text{jet}\, X$. We note that the process $\ell N \to \text{jet}\, X$ has also been extensively studied in terms of the concept of "1-jettiness" [102, 103]. Here one additionally writes the cross section differential in a variable τ_1 that characterizes the hadronic final state that is not associated with the produced jet or the nucleon beam remnant. In Ref. [103] the full NLO corrections for the 1-jettiness were computed, where a fully numerical approach was adopted. In principle, it should be possible to recover our NLO results by performing a (numerical) integration over τ_1 of the results of [103].

Because of the propagator of the exchanged photon, the cross section for $\ell N^\uparrow \to hX$ will contain contributions for which the photon is almost on-shell. This is not yet the case at LO where the high transverse momentum of the produced hadron requires the photon to be highly virtual. Starting from NLO, however, it may happen that the incoming lepton radiates the photon almost collinearly. This may then be followed by a $2 \to 2$ scattering process of the photon with a parton in the nucleon, which is perfectly capable of producing the hadron at high $P_{h\perp}$. In processes where the scattered lepton is observed, such as $\ell N \to \ell' hX$, one can in fact select such contributions by requiring the scattered lepton to have a low scattering angle. The incoming lepton then effectively acts merely as a source of quasi-real photons, and the process may be very accurately described in terms of a (perturbative) distribution function for photons in leptons known as the Weizsäcker-Williams (WW) distribution [56, 104–107]. This approach has been widely used with much success in the HERA physics program [56].

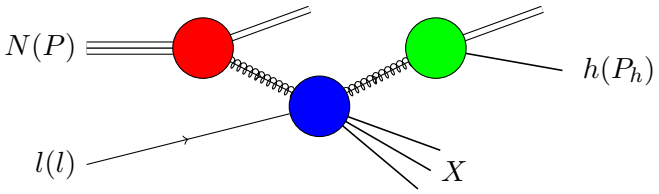

Figure 2.1.: Lepton nucleon scattering with an observed hadron $h(P_h)$ in the final state. The red and green blobs denote parton distribution and fragmentation functions. The blue blob stands for a hard process initiated by a lepton-quark or lepton-gluon initial state. Note: The unobserved final state X includes the final state lepton.

In the context of our NLO calculation for $\ell N \to hX$ it is therefore interesting to investigate whether also in this case the contributions by almost real photons dominate and the NLO corrections may be well approximated by a Weizsäcker-Williams type distribution. Since it is much easier to compute the latter contribution than the full NLO correction, this would mean that one could also obtain approximate NLO results for the transversely polarized cross section within the twist-3 framework by simply considering real photons. Given the complexity of a full NLO calculation for the twist-3 case, this would be a tremendous advantage. We note that the contributions to the spin-dependent cross sections for $\ell N \to \text{jet}\, X$ for real photons were discussed in [51], including the twist-3 contributions for the single-transverse spin case. Actual LO calculations for the twist-2 longitudinal spin-dependent cross section were presented in Ref. [108–110] for quasi-real photons. We will closely examine the contributions by quasi-real photons also in this chapter. Their relevance will of course also depend on the lepton species that is used, because the lepton mass leads to a lower limit on the virtuality of the photon.

This chapter is structured as follows. In Sec. 2.2 we present our NLO calculations for the partonic cross sections for $\ell N^\uparrow \to hX$ and $\ell N \to \text{jet}\, X$. We also discuss in some detail the Weizsäcker-Williams contribution and how the calculation can be done keeping a finite lepton mass. Section 2.3 presents numerical predictions for the NLO cross section to be expected at various fixed-target experiments and at a future Electron Ion Collider (EIC). Finally, we summarize our results in Sec. 2.4.

2.2. NLO calculation

2.2.1. General framework

In this section we present our derivation of the analytical NLO results for the processes $\ell N \to hX$ and $\ell N \to \text{jet}\, X$. The transverse momentum of the produced hadron or

jet sets a hard scale, so that perturbative methods may be used for treating the cross sections. We first consider $\ell(l) + N(P) \to h(P_h) + X$ (figure 2.1) cross sections and parton distribution/fragmentation functions. The momenta of the incoming parton, k^μ, and of the fragmenting parton, p^μ, which appear in the calculation of the partonic cross sections, are approximated as $k^\mu \simeq xP^\mu$ and $p^\mu \simeq P_h^\mu/z$, respectively. It is then convenient to work with the partonic Mandelstam variables

$$s = (k+l)^2 = xS,\ \ t = (k-p)^2 = \frac{x}{z}T,\ \ u = (l-p)^2 = \frac{U}{z}\,. \tag{2.1}$$

The general form of the factorized cross section for the inclusive hadron production process then is

$$\begin{aligned} E_h \frac{\mathrm{d}^3\sigma^{\ell N\to hX}}{\mathrm{d}^3 P_h} = \frac{1}{S}\sum_{i,f}\int_0^1 \frac{\mathrm{d}x}{x}\int_0^1 \frac{\mathrm{d}z}{z^2}\, f^{i/N}(x,\mu_F) \\ \times D^{h/f}(z,\mu_F)\,\hat{\sigma}^{i\to f}(s,t,u,\mu_F,\mu_R)\,, \end{aligned} \tag{2.2}$$

where $f^{i/N}(x,\mu_F)$ is the parton distribution function (PDF) for the incoming parton i in the nucleon N and $D^{h/f}(z,\mu_F)$ the corresponding fragmentation function (FF) for parton f fragmenting into hadron h, both evaluated at a factorization scale μ_F. We choose the factorization scales to be the same for the initial and the final state, and also equal to the renormalization scale. In equation (2.2), $\hat{\sigma}^{i\to f}$ is the partonic cross section for the lepton-parton scattering process, $\ell + i \to f + x$, with x an unobserved partonic final state including the unobserved lepton. The sum in equation (2.2) runs over the different species of partons, quarks, gluons and antiquarks. We note that the expression in equation (2.2) holds up to corrections that are suppressed by inverse powers of the produced hadron's transverse momentum $P_{h\perp}$.

The partonic cross sections $\hat{\sigma}^{i\to f}$ in equation (2.2) can be calculated in QCD perturbation theory. One may write their expansion in the strong coupling as

$$\hat{\sigma}^{i\to f} \;=\; \hat{\sigma}^{i\to f}_{\mathrm{LO}} + \frac{\alpha_s}{\pi}\,\hat{\sigma}^{i\to f}_{\mathrm{NLO}} + \mathcal{O}(\alpha_s^2)\,. \tag{2.3}$$

At lowest order (LO) only the tree-level process $\ell q \to q\ell$ shown in Fig. 2.2 contributes. The calculation of its cross section is straightforward. One finds

$$\hat{\sigma}^{q\to q}_{\mathrm{LO}} = 2\alpha_{\mathrm{em}}^2 e_q^2\,\frac{s^2+u^2}{t^2}\,\delta(s+t+u)\,, \tag{2.4}$$

where α_{em} is the fine structure constant and e_q is the quark's fractional charge.

At NLO, $\mathcal{O}(\alpha_s\alpha_{\mathrm{em}}^2)$, both virtual (Fig. 2.3) and real-emission diagrams (Figs. 2.4 and 2.5) contribute. We will address these in turn in the following subsections. One can see from Figs. 2.4 and 2.5 that beyond LO there are also new contributions where a gluon fragments or where an initial gluon enters the hard scattering process.

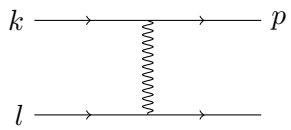

Figure 2.2.: LO diagram for lepton-quark scattering.

As is well known, all types of NLO contributions develop singularities at intermediate stages of the calculations, which we make manifest by using dimensional regularization with $D = 4-2\varepsilon$ space-time dimensions. The subsequent treatment of the singularities is standard in pQCD calculations. The only non-standard feature arises for the incoming lepton. If we assume for the moment that we have an incoming quark instead of a lepton in the diagrams in Figs. 2.4 and an exchanged gluon instead of a photon, then the diagram would make an NLO contribution to, say, $pp \to hX$. Being treated as massless, the initial quark would produce a singularity when it radiates the gluon collinearly. As is well understood, this singularity may be absorbed ("factorized") into the proton's quark PDF, exactly in the same way as for the incoming quark at the bottom of the diagram. In case of an incoming lepton, on the other hand, the lepton's mass ensures that no collinear singularity arises when the lepton radiates a collinear photon that subsequently participates in the hard scattering. In fact, keeping the lepton mass m_ℓ, the cross section will develop a logarithmic term of the form $\alpha_{\rm em} \log(\Lambda/m_\ell)$, where Λ represents a hard scale of the problem, and in the limit $m_\ell \to 0$ this logarithm precisely produces the required collinear singularity. In principle we should therefore perform the NLO calculation keeping the lepton mass finite. This is technically very cumbersome, and in fact not needed. We can adopt two different, and equivalent, approaches instead: In the first approach we neglect the lepton's mass and regularize the ensuing collinear pole in dimensional regularization. The pole is then subtracted (for example, in the $\overline{\rm MS}$ scheme) and absorbed into a "parton" distribution function for photons in a lepton. This distribution may be evaluated perturbatively in first-order QED, giving rise essentially to the well-known "Weizsäcker-Williams" distribution. This approach may in principle be extended to higher order in QED. In the second approach, we calculate the cross section for a massive lepton, keeping however only the leading

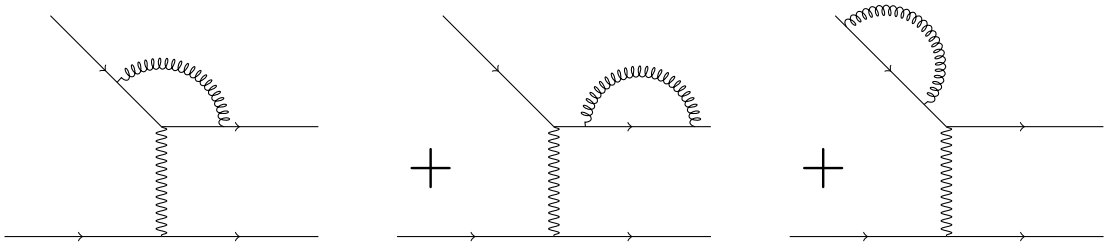

Figure 2.3.: Virtual diagrams at NLO. Self energy diagrams (right and middle graph) contribute in Feynman gauge.

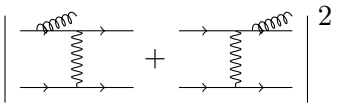

Figure 2.4.: NLO real-emission diagrams.$q \to q$ and $q \to g$ channels.

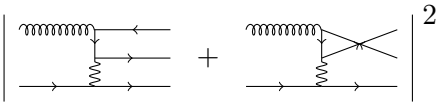

Figure 2.5.: NLO real-emission diagrams. $g \to q$ channel.

terms in m_ℓ which are of the form $\alpha_{\rm em}[\log(\Lambda/m_\ell) + \text{constant}]$. This is justified by the fact that all terms beyond this approximation are suppressed as powers of m_ℓ over the hard scale and hence numerically tiny. We note that although the logarithm can become large (as m_ℓ is small compared to typical QCD hard scales), the smallness of $\alpha_{\rm em}$ will usually make the term $\alpha \log(\Lambda/m_\ell)$ small enough to be regarded as a perturbative correction.

We will present our main calculation for the case of massless leptons and comment on the use of a finite lepton mass in the calculation later.

It is convenient to rewrite the x- and z-integrals in equation (2.2) in terms of new variables $v = 1 + t/s$ and $w = -u/(s+t)$. Using (3.1), we have

$$x = \frac{1-v}{vw}\frac{U}{T}\,, \quad z = \frac{-T}{(1-v)S}\,, \tag{2.5}$$

and equation (2.2) becomes

$$\begin{aligned} E_h \frac{\mathrm{d}^3\sigma^{\ell N\to hX}}{\mathrm{d}^3 P_h} = \left(\frac{-U}{S^2}\right) \sum_{i,f} \int_{\frac{U}{T+U}}^{1+\frac{T}{S}} \frac{\mathrm{d}v}{v(1-v)} \int_{\frac{1-v}{v}\frac{U}{T}}^{1} \frac{\mathrm{d}w}{w^2} \\ \times \frac{f^{i/N}(x,\mu_F)}{x} \frac{D^{h/f}(z,\mu_F)}{z^2} \hat{\sigma}^{i\to f}(v,w,\mu_F,\mu_R)\,. \end{aligned} \tag{2.6}$$

For ease of notation, we have kept the symbol $\hat{\sigma}^{i\to f}$ also for the cross section when expressed in terms of the new variables. We note that the invariant mass of the unobserved recoiling partonic final state is given by $s + t + u = sv(1-w)$. The function $\delta(s+t+u) \propto \delta(1-w)$ in the LO cross section (2.4) expresses the fact that at LO the recoil consists of a single parton.

2.2.2. Virtual contributions at NLO

At the NLO level, the virtual contributions shown in Fig. 2.3 contribute through their interference with the Born diagram. The virtual contributions thus have Born kinematics and are proportional to $\delta(1-w)$. Since we are only interested in QCD virtual corrections, only the quark line is affected, and we may adopt the result directly from the corresponding calculation in Ref. [38] for the basic photon-quark scattering diagrams in DIS. This gives

$$\hat{\sigma}^{q\to q}_{\mathrm{NLO,vir}} = \frac{C_F\alpha_s(\mu)}{2\pi}\frac{\Gamma(1-\varepsilon)^2\Gamma(1+\varepsilon)}{\Gamma(1-2\varepsilon)} \times\left(\frac{4\pi\mu^2}{-t}\right)^{\varepsilon}\left(-\frac{2}{\varepsilon^2}-\frac{3}{\varepsilon}-8\right)\hat{\sigma}^{q\to q}_{\mathrm{LO},\varepsilon}\,, \tag{2.7}$$

where

$$\hat{\sigma}^{q\to q}_{\mathrm{LO},\varepsilon} = 2\alpha_{\mathrm{em}}^2 e_q^2\frac{1}{sv}\left(\frac{1+v^2}{(1-v)^2}-\varepsilon\right)\delta(1-w)\,. \tag{2.8}$$

is the Born cross section computed in $4-2\varepsilon$ dimensions. Furthermore, $C_F = (N_c^2-1)/2N_c$, with N_c the number of colors.

2.2.3. Real-emission corrections at NLO

The real diagrams have $2\to 3$ topology. To obtain the desired contribution to an inclusive-parton cross section we need to integrate over the phase space of the lepton and the "unobserved" parton in the final state. This can be done in $4-2\varepsilon$ dimensions using the standard techniques available in the literature [111–113]. See Appendix C and D for further details.

After phase space integration, the result for the real-emission contribution for the $q\to q$ channel takes the form

$$\hat{\sigma}^{q\to q}_{\mathrm{NLO,real}} = \hat{\sigma}_A^{q\to q}(v,w,\varepsilon) + \frac{\hat{\sigma}_B^{q\to q}(v,w,\varepsilon)}{(1-w)^{1+2\varepsilon}}\,, \tag{2.9}$$

where both functions $\hat{\sigma}_A^{q\to q}$ and $\hat{\sigma}_B^{q\to q}$ carry a $1/\varepsilon$-pole, but are well-behaved in the limit $w\to 1$. Obviously, the second term in (2.9) requires special care in this limit since the denominator would lead to a non-integrable behavior for $\varepsilon = 0$. We deal with this limit by means of the expansion

$$(1-w)^{-1-2\varepsilon} = -\frac{1}{2\varepsilon}\delta(1-w) + \frac{1}{(1-w)_+} - 2\varepsilon\left(\frac{\ln(1-w)}{1-w}\right)_+ +\mathcal{O}(\varepsilon^2)\,, \tag{2.10}$$

where the plus distribution is defined in the usual way by

$$\int_0^1 dw\, f(w)\,[g(w)]_+ = \int_0^1 dw\, \left[f(w) - f(1)\right] g(w)\,. \tag{2.11}$$

This expansion makes the singularities in $1/\varepsilon$ explicit. When combined with the pole terms in $\hat{\sigma}_B^{q\to q}$, the term $\propto \delta(1-w)$ in (2.10) leads to a double pole term that cancels against the double pole in the virtual correction in equation (2.7). This well-known behavior reflects the cancelation of infrared singularities in partonic observables. The channels $q \to g$ and $g \to q$ are infrared finite at NLO.

2.2.4. Collinear subtraction for parton distribution functions and fragmentation functions

After the cancelation of infrared singularities between real and virtual contribution, the partonic cross sections still exhibit single poles that reflect collinear singularities arising when an "observed" parton (either the incoming one, or the one that fragments) becomes collinear with the unobserved parton. Figure 2.6 shows an initial state collinear singularity. The singularity has the form $\propto \frac{1}{\varepsilon} P_{qq} \hat{\sigma}_{ql\to ql}$ where P_{qq} is the first order Altarelli-Parisi splitting function (equation (2.13a)) and $\hat{\sigma}^{ql\to q}$ is the tree level cross section in d-dimensions which remains, if we remove the gluon and set the external momenta of the incoming quark to $y\,k$.

The factorization theorem states that these poles may be absorbed into the parton distribution functions or into the fragmentation functions. This procedure may be formulated in terms of renormalized parton densities and fragmentation functions (see, e.g., Ref. [114]). In fact, naive definitions of "bare" parton densities and fragmentation functions contain ultraviolet singularities that can be dealt with as well by using dimensional regularization. At NLO, the corresponding ultraviolet $1/\varepsilon$-poles that appear can be removed in the $\overline{\text{MS}}$ scheme by introducing "renormalized" functions in the form

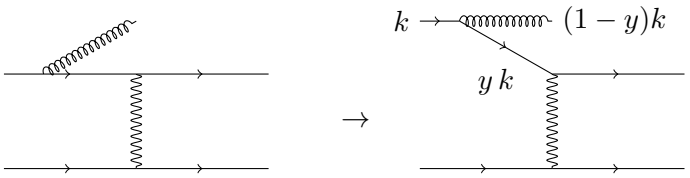

Figure 2.6.: Representative collinear singularity for an initial state quark in the $q \to q$ channel.

$$f^{q/N}_{\text{bare}}(x,\mu_F) = f^{q/N}_{\text{ren}}(x,\mu_F) + \frac{\alpha_s(\mu_F)}{2\pi}\frac{S_\varepsilon}{\varepsilon}\left(P_{qq}\otimes f^{q/N}_{\text{ren}}\right)(x,\mu_F) + \frac{\alpha_s(\mu_F)}{2\pi}\frac{S_\varepsilon}{\varepsilon}\left(P_{qg}\otimes f^{g/N}_{\text{ren}}\right)(x,\mu_F) + \mathcal{O}(\alpha_s^2)\,, \tag{2.12a}$$

$$D^{h/q}_{\text{bare}}(z,\mu_F) = D^{h/q}_{\text{ren}}(z,\mu_F) + \frac{\alpha_s(\mu_F)}{2\pi}\frac{S_\varepsilon}{\varepsilon}\left(P_{qq}\otimes D^{h/q}_{\text{ren}}\right)(z,\mu_F) + \frac{\alpha_s(\mu_F)}{2\pi}\frac{S_\varepsilon}{\varepsilon}\left(P_{gq}\otimes D^{g/N}_{\text{ren}}\right)(z,\mu_F) + \mathcal{O}(\alpha_s^2)\,, \tag{2.12b}$$

where we have the usual splitting functions

$$P_{qq}(y) = C_F\left[\frac{1+y^2}{(1-y)_+} + \frac{3}{2}\delta(1-y)\right]\,, \tag{2.13a}$$

$$P_{qg}(y) = T_R\left[y^2+(1-y)^2\right]\,, \tag{2.13b}$$

$$P_{gq}(y) = C_F\,\frac{1+(1-y)^2}{y}\,, \tag{2.13c}$$

(with $T_R = 1/2$), and where the "$\otimes$"-symbol indicates the convolution

$$(P\otimes f)(x) \equiv \int_x^1 \frac{dy}{y}\,P(y)\,f\left(\frac{x}{y}\right)\,. \tag{2.14}$$

The constant $S_\varepsilon \equiv (4\pi)^\varepsilon/\Gamma(1-\varepsilon)$ in (2.12a) and (2.12b) corresponds to the usual $\overline{\text{MS}}$ scheme. Inserting the bare distributions into the LO expression for the hadronic cross section, we obtain additional $\mathcal{O}(\alpha_s\alpha_{\text{em}}^2)$ contributions. These precisely cancel the collinear poles associated with the observed partons in the NLO partonic cross sections, for all three channels. We can express this contribution explicitly for the initial state collinear singularity in the $q\to q$ channel (figure (2.6)) as [113, 115]

$$\frac{\alpha_s}{\pi}\int_0^1 \mathrm{d}y\left(-\frac{1}{\varepsilon}+\gamma_E-\ln 4\pi\right)P_{qq}(y)\left(\frac{s}{\mu_F^2}\right)^\varepsilon \tilde{\sigma}^{ql\to q}(ys,yt,u,\varepsilon) \times\delta(y(s+t)+u)\,. \tag{2.15}$$

Note: The tilde on the σ denotes that the delta function, that fixes the invariant pair mass at zero in leading order is not part of $\tilde{\sigma}$.

Even after this procedure, one type of collinear singularity remains. It is generated by a momentum configuration where the exchanged photon is collinear to the incoming lepton. As discussed at the beginning of this section, the presence of this singularity is an artifact of neglecting the lepton's mass. In the following two subsections we discuss our treatment of this issue.

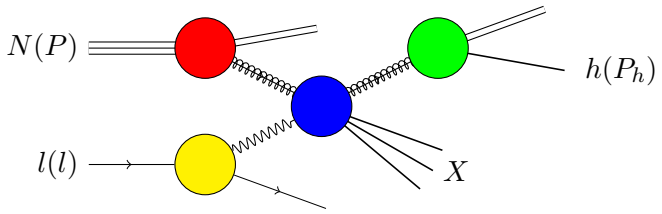

Figure 2.7.: General Weizsäcker-Williams contribution at NLO. The quasi-real photon entering the hard scattering part is treated as a parton in the lepton.

2.2.5. Weizsäcker-Williams contribution

One approach for dealing with the collinear lepton singularity is to introduce bare and renormalized QED parton distributions for the lepton, much in analogy with the procedure that we discussed in the previous section for the nucleon's parton distributions. The only differences are that for leptons the partons are the lepton itself and the photon, and that we can safely compute their distributions in QED perturbation theory. To lowest order in QED, we have just $f^{\ell/\ell}(y) = \delta(1-y)$, corresponding to the Born contribution in Fig. 2.2. The hard process involving an incoming lepton will always require two electromagnetic interactions and hence be of order α_{em}^2, as seen explicitly in equation (2.4). This is different for a hard process with an incoming photon such as $\gamma q \to qg$, which is of order $\alpha_{\text{em}}\alpha_s$. This implies that at NLO in QCD (at order $\alpha_{\text{em}}^2\alpha_s$) there will be contributions generated by the photon acting as a parton of the lepton and participating in the hard process. A generic picture for such types of contributions, known as Weizsäcker-Williams contributions, is shown in Fig. 2.7. In essence, the lepton merely serves as a source of real photons for the contributions shown in the figure. Like its nucleon counterpart, the corresponding photon-in-lepton distribution $f^{\gamma/\ell}(y)$ will require renormalization. Following (2.12a) we may write

$$f_{\text{bare}}^{\gamma/\ell}(y,\mu_0) = f_{\text{ren}}^{\gamma/\ell}(y,\mu_0) + \frac{\alpha_{\text{em}}}{2\pi}\frac{S_\varepsilon}{\varepsilon}\left(P_{\gamma\ell}\otimes f_{\text{ren}}^{\ell/\ell}\right)(y,\mu_0) + \dots \tag{2.16}$$

where $P_{\gamma\ell} = P_{gq}/C_F$ and the ellipses denote a term involving a photon-to-photon splitting that makes contributions beyond the order in α_{em} we consider here. Within the same reasoning, we can set $f_{\text{ren}}^{\ell/\ell}(y) = \delta(1-y)$ in (2.16).

The bare photon-in-lepton distribution $f_{\text{bare}}^{\gamma/\ell}$ in equation (2.16) can be defined analogously to the gluon distribution in a nucleon in terms of the matrix element (see also [51])

$$\begin{aligned}\Omega^{\mu\nu}(y) &\equiv n_\rho n_\sigma \int_{-\infty}^{\infty}\frac{d\lambda}{2\pi y}\,\mathrm{e}^{i\lambda y}\,\langle\ell|F_{\text{em}}^{\sigma\nu}(0)\,U[0;\lambda n]\,F_{\text{em}}^{\rho\mu}(\lambda n)|\ell\rangle,\\ &= \frac{-g_\perp^{\mu\nu}}{2(1-\varepsilon)}\,f_{\text{bare}}^{\gamma/\ell}(y,\mu_0)\,.\end{aligned} \tag{2.17}$$

In this definition n is a light-cone vector conjugate to the lepton momentum l, with $n^2 = 0$ and $l \cdot n = 1$. Furthermore, $F_{\rm em}^{\mu\nu} = \partial^\mu A^\nu - \partial^\nu A^\mu$ is the electromagnetic field-strength tensor, and we have inserted a (straight) Wilson line $U[0;\lambda n]$ that ensures the electromagnetic gauge invariance of the matrix element. The transverse projector in (2.17) is given as $g_\perp^{\mu\nu} = g^{\mu\nu} - l^\mu n^\nu - l^\nu n^\mu$.

Since the matrix element in (2.17) contains electromagnetic fields and elementary leptons in the in- and out-states we can compute it to LO in QED. In this calculation we keep a non-vanishing lepton mass m_ℓ in order to obtain an infrared-finite result. To order $\mathcal{O}(\alpha_{\rm em})$ we find,

$$f_{\rm bare}^{\gamma/\ell}(y,\mu_0) = \frac{\alpha_{\rm em}}{2\pi}\, P_{\gamma\ell}(y)\, S_\varepsilon \left[\frac{1}{\varepsilon} + \ln\left(\frac{\mu_0^2}{y^2 m_\ell^2}\right) - 1\right] + \mathcal{O}(\alpha_{\rm em}^2)\,, \tag{2.18}$$

where, as before, $S_\varepsilon \equiv (4\pi)^\varepsilon/\Gamma(1-\varepsilon)$. In close analogy to parton distributions of the nucleon we can perform an $\overline{\rm MS}$-renormalization of the distribution and obtain,

$$\begin{aligned} f_{\rm ren}^{\gamma/\ell}(y,\mu_0) &= f_{\rm bare}^{\gamma/\ell}(y,\mu_0) - \frac{\alpha_{\rm em}}{2\pi}\, P_{\gamma\ell}(y)\, \frac{S_\varepsilon}{\varepsilon} + \mathcal{O}(\alpha_{\rm em}^2) \\ &= \frac{\alpha_{\rm em}}{2\pi}\, P_{\gamma\ell}(y)\, \left[\ln\left(\frac{\mu_0^2}{y^2 m_\ell^2}\right) - 1\right] + \mathcal{O}(\alpha_{\rm em}^2)\,. \end{aligned} \tag{2.19}$$

This renormalized distribution is closely related to the 'classic' Weizsäcker-Williams distribution [104–107]. The logarithm in (2.19) may be derived from an integration over the photon's virtuality $-q^2$ (where q is the photon momentum). For the standard Weizsäcker-Williams distribution one performs this integration from the lower kinematic limit $m_\ell^2 y^2/(1-y)$ to an upper limit $Q_{\rm max}^2$ fixed by the experimental condition imposed on the scattered lepton. This gives rise to a term $\frac{\alpha_{\rm em}}{2\pi} P_{\gamma\ell}(y)\, \ln(Q_{\rm max}^2(1-y)/(y^2 m_\ell^2))$ in the photon spectrum, which can be recovered by an appropriate choice of the scale μ in (2.19).

For the contribution related to $f_{\rm ren}^{\gamma/\ell}$ the photon virtuality is then neglected everywhere else in the hard scattering. One thus considers scattering diagrams with a real incoming photon. We thus write the generic factorized cross section for the contribution as

$$\begin{aligned} E_h \frac{{\rm d}^3\sigma_{\rm WW}^{\ell N\to hX}}{{\rm d}^3 P_h} = \frac{1}{S}\sum_{i,f} \int_0^1 \frac{{\rm d}x}{x} \int_0^1 \frac{{\rm d}z}{z^2} \int_0^1 {\rm d}y\ \delta\left(y + \frac{t}{s+u}\right) \\ \times f^{i/N}(x,\mu_F)\, D^{h/f}(z,\mu_F)\, f_{\rm ren}^{\gamma/\ell}(y,\mu_0)\, \hat\sigma^{\gamma i\to f}, \end{aligned} \tag{2.20}$$

with the cross sections $\hat\sigma^{\gamma i\to f}$ describing the scattering $\gamma i \to f x$ of the photon off parton i in the nucleon (to be given below). At $\mathcal{O}(\alpha_s)$ we encounter three channels with an incoming photon: $\gamma q \to q(g)$, $\gamma q \to g(q)$, and $\gamma g \to q(\bar q)$ (the partons in parentheses are not observed). The relevant diagrams are as those shown in Figs. 2.4 and 2.5, but with the lepton lines removed and the virtual photon replaced by a real photon.

Being $2 \to 2$ diagrams, their calculation is straightforward. Inserting now the bare WW distribution we generate precisely the pole terms required to cancel the lepton collinear divergences discussed at the end of Sec. 2.2.4. This happens in the same way for all partonic channels. We note that the dependence on the scale μ associated with the lepton also disappears. This has to be the case, since for a finite lepton mass there would never be any lepton collinear divergences in the first place.

2.2.6. Calculation with $m_\ell \neq 0$

As we noted earlier, the presence of collinear singularities associated with lepton-photon splitting is really an artifact of neglecting the lepton's mass. In principle we should therefore perform a full calculation in which the lepton's mass is kept finite. This is trivial for the virtual diagrams, since the QCD corrections do not affect the lepton line. However, inclusion of a lepton mass considerably complicates the phase space integrations for the real diagram. Nevertheless, it is possible to compute the relevant integrals using the results given in Ref. [112]. One may then expand the result in powers of the lepton mass and neglect terms suppressed by powers of $\mathcal{O}(m_\ell)$. In this way, the "would-be" collinear singularity is regularized by the lepton mass and shows up as a term $\sim \ln(m_\ell^2)$. Terms independent of m_ℓ are also kept. All other parts of the calculation proceed as before, and the partonic cross section thus has the structure

$$\begin{aligned}\hat{\sigma}_{\mathrm{NLO}}^{i\to f}(v,w,m_\ell,\mu_F,\mu_0) = \hat{\sigma}_{\log}^{i\to f}(v,w,\mu_0)\ \ln(m_\ell^2/s) + \\ \hat{\sigma}_0^{i\to f}(v,w,\mu_F) + \mathcal{O}(m_\ell^2 \ln(m_\ell^2)).\end{aligned} \tag{2.21}$$

for each channel.

We have checked explicitly for all three channels that our two approaches for treating the initial lepton are equivalent: The full result obtained using the WW contribution in the previous subsection agrees with that for $m_\ell \neq 0$, as long as we only keep the leading terms as discussed in equation (2.21). The equivalence of the two approaches serves as an important check of our calculation and also explicitly demonstrates the universality of the WW-distribution.

2.2.7. Final results for single-inclusive hadron production

We now present our final results for the full partonic cross sections in analytic form. Combining the cross section (2.6) for massless leptons with the Weizsäcker-Williams

contribution (2.20), we may write the full NLO cross section as

$$E_h \frac{\mathrm{d}^3\sigma^{\ell N\to hX}}{\mathrm{d}^3P_h} = \left(\frac{-U}{S^2}\right)\sum_{i,f}\int_{\frac{U}{T+U}}^{1+\frac{T}{S}}\frac{\mathrm{d}v}{v(1-v)}\int_{\frac{1-v}{v}\frac{U}{T}}^{1}\frac{\mathrm{d}w}{w^2}\frac{f^{i/N}(x,\mu_F)}{x} \times\frac{D^{h/f}(z,\mu_F)}{z^2}\left[\hat{\sigma}^{i\to f}_{\mathrm{LO}}(v)+\frac{\alpha_s(\mu)}{\pi}\,\hat{\sigma}^{i\to f}_{\mathrm{NLO}}(v,w,\mu) +f^{\gamma/\ell}_{\mathrm{ren}}\left(\tfrac{1-v}{1-vw},\mu\right)\frac{\alpha_s(\mu)}{\pi}\,\hat{\sigma}^{\gamma i\to f}_{\mathrm{LO}}(v,w)\right]. \tag{2.22}$$

The LO contribution, present only for the channel $q\to q$ with an incoming quark that also fragments, was already given in (2.4). For the NLO term in this channel we find

$$\begin{aligned}\hat{\sigma}^{q\to q}_{\mathrm{NLO}}(v,w,\mu) = \frac{\alpha_{\mathrm{em}}^2 e_q^2 C_F}{svw}\Bigg[&A_0^{q\to q}\,\delta(1-w)+A_1^{q\to q}\left(\frac{\ln(1-w)}{1-w}\right)_+\\ &+\frac{1}{(1-w)_+}\Bigg\{B_1^{q\to q}\ln\left(\frac{1-v}{v(1-v(1-w))}\right)\\ &+B_2^{q\to q}\ln(1-v(1-w))+B_3^{q\to q}\ln\left(\frac{sv^2}{\mu^2}\right)\Bigg\}\\ &+C_1^{q\to q}\ln(v(1-w))+C_2^{q\to q}\ln\left(\frac{(1-v)w}{1-vw}\right)\\ &+C_3^{q\to q}\ln\left(\frac{1-v}{(1-vw)(1-v(1-w))}\right)\\ &+C_4^{q\to q}\ln\left(\frac{s}{\mu^2}\right)+C_5^{q\to q}\Bigg],\end{aligned} \tag{2.23}$$

where the coefficients $A_i^{q\to q}$, $B_i^{q\to q}$, $C_i^{q\to q}$ are functions of v and w and may be found in the Appendix A. The channels $q\to g$ and $g\to q$ have simpler expressions:

$$\begin{aligned}\hat{\sigma}^{q\to g}_{\mathrm{NLO}}(v,w,\mu) = \frac{\alpha_{\mathrm{em}}^2 e_q^2 C_F}{svw}\Bigg[&C_1^{q\to g}\ln(1-v(1-w))\\ &+C_2^{q\to g}\ln\left(\frac{1-v}{(1-vw)(1-v(1-w))}\right)\\ &+C_3^{q\to g}\ln\left(\frac{v(1-w)s}{\mu^2}\right)+C_4^{q\to g}\Bigg],\end{aligned} \tag{2.24}$$

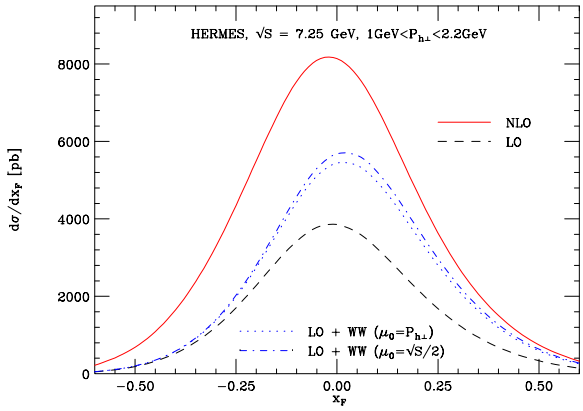

Figure 2.8.: Cross section for $\ell p \to \pi^+ X$ at HERMES, as function of x_F for 1 GeV $< P_{h\perp} <$ 2.2 GeV. The dashes line gives the LO prediction and the solid line the NLO one. The dotted and dot-dashed lines show the approximation (2.28) of the NLO cross section, using $\mu_0 = P_{h\perp}$ and $\mu_0 = \sqrt{S}/2$, respectively.

$$\hat{\sigma}^{g\to q}_{\rm NLO}(v,w,\mu) = \frac{\alpha_{\rm em}^2 e_q^2 T_R}{svw}\left[C_1^{g\to q}\ln\left(\frac{(1-v)w}{1-vw}\right)\right.$$
$$\left. + C_2^{g\to q}\ln\left(\frac{v(1-w)s}{\mu^2}\right) + C_3^{g\to q}\right]. \qquad (2.25)$$

The coefficients $C_i^{q\to g}$ and $C_i^{g\to q}$ are again given in the Appendix A.

We finally list the partonic cross sections for the Weizsäcker-Williams contributions:

$$\hat{\sigma}^{\gamma q\to q}_{\rm LO}(v,w) = \frac{C_F\alpha_{\rm em}e_q^2}{2s(1-v)}\frac{1+v^2w^2}{vw},$$
$$\hat{\sigma}^{\gamma q\to g}_{\rm LO}(v,w) = \frac{C_F\alpha_{\rm em}e_q^2}{2s(1-v)}\frac{1+(1-vw)^2}{1-vw},$$
$$\hat{\sigma}^{\gamma g\to q}_{\rm LO}(v,w) = \frac{T_R\alpha_{\rm em}e_q^2}{2s(1-v)}\frac{v^2w^2+(1-vw)^2}{vw(1-vw)}. \qquad (2.26)$$

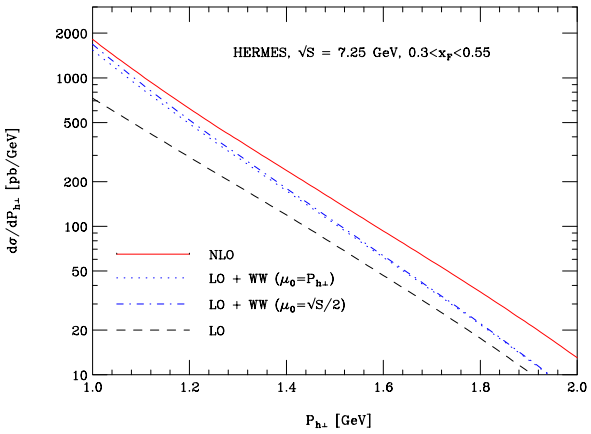

Figure 2.9.: Cross section for $\ell p \to \pi^+ X$ at HERMES as function of $P_{h\perp}$ for $0.3 < x_F < 0.55$. The dashes line gives the LO prediction and the solid line the NLO one. The dotted and dot-dashed lines show the approximation (2.28) of the NLO cross section, using $\mu_0 = P_{h\perp}$ and $\mu_0 = \sqrt{S}/2$, respectively.

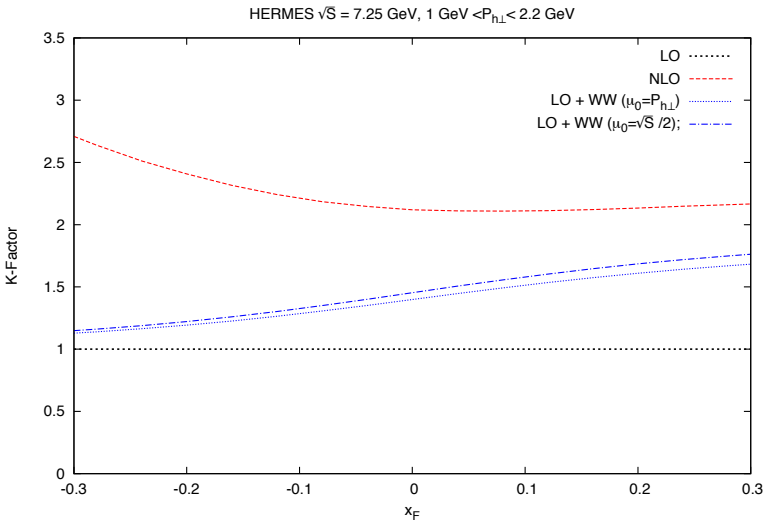

Figure 2.10.: K-factor (at a scale $\mu = P_{h\perp}$) for the HERMES experiment plotted vs. the Feynman variable x_F and a binned transverse momentum $P_{h\perp}$.

2.2.8. Single-inclusive jet production

Having computed the inclusive hadron production cross section at NLO the extension to single inclusive jet production is straightforward. The cross section for $\ell N \to \mathrm{jet}X$ may be written as

$$E_{\mathrm{J}}\frac{\mathrm{d}^3\sigma^{\ell N\to \mathrm{jet}X}}{\mathrm{d}^3P_{\mathrm{J}}} = \frac{1}{S}\sum_i \int_{\frac{-U}{S+T}}^1 \frac{\mathrm{d}w}{w}\, f^{i/N}\left(x=\tfrac{-U}{w(S+T)},\mu\right) \times\hat{\sigma}^{i\to\mathrm{jet}}\left(v=1+\frac{T}{S},w,\mu;R\right), \tag{2.27}$$

where E_{J} and $\vec{P}_{\mathrm{J}}$ are the energy and three-momentum of the jet and the hadronic Mandelstam variables are defined as before, now in terms of the jet momentum. The form of this expression follows from (2.6) by setting the fragmentation functions to $\delta(1-z)$. Of course, beyond LO, the partonic cross sections $\hat{\sigma}^{i\to\mathrm{jet}}$ for jet production differ from the ones for single-inclusive hadron production. This is evident from the fact that the latter are computed as "inclusive-parton" cross sections $\hat{\sigma}^{i\to f}$ which, as we saw in subsection 2.2.4, require collinear subtraction. This is in contrast to a jet cross section which is by itself infrared-safe, as far as the final state is concerned. Instead, it depends on the algorithm adopted to define the jet, as we have indicated by the dependence on a generic jet (size) parameter R in (3.16).

As was discussed in Refs. [116–118], even at NLO one may still go rather straightforwardly from the single-inclusive parton cross sections $\hat{\sigma}^{i\to f}$ to the $\hat{\sigma}^{i\to\mathrm{jet}}$, for any infrared-safe jet algorithm. The key is to properly account for the fact that at NLO two partons can fall into the same jet, so that the jet needs to be constructed from both. In fact, assuming the jet to be relatively narrow, one can determine the relation between $\hat{\sigma}^{i\to f}$ and $\hat{\sigma}^{i\to\mathrm{jet}}$ analytically [116]. This "Narrow Jet Approximation (NJA)" formally corresponds to the limit $R\to 0$ but turns out to be accurate even at values $R\sim 0.4-0.7$ relevant for experiment. We follow this approach in this work. In the NJA, the structure of the NLO jet cross section is of the form $\mathcal{A}\log(R)+\mathcal{B}$; corrections to this are of $\mathcal{O}(R^2)$ and are neglected. We note that to the order $\alpha_{\mathrm{em}}^2\alpha_s$ we consider in this chapter, the Weizsäcker-Williams terms only contribute to the R-independent piece $\mathcal{B}$. This is because for almost real exchanged photons it is at this order not possible to have two coalescing partons in the final state.

2.3. Numerical results

We now present phenomenological results for the NLO single-inclusive pion production cross section in lepton-proton scattering. As mentioned before, data on the transverse single-spin asymmetry for this reaction have been released by HERMES [46] and the Jefferson Lab Hall A Collaboration [48]. Unfortunately, corresponding cross sections

were not presented, and we will therefore provide predictions for these. Furthermore, we will also present predictions for COMPASS at CERN, for a future Electron-Ion-Collider (EIC), and for experiments at Jefferson Lab after the CEBAF upgrade to 12 GeV beam energy. Finally, at the end of this section we show some phenomenological results for the inclusive production of jets at the EIC.

As we saw in the previous subsections (see equation (2.22)), our NLO result can be formulated in such a way that it contains contributions involving the photon-in-lepton distribution $f_{\rm ren}^{\gamma/\ell}$ and LO photon-parton cross sections. These represent the contributions by quasi-real photons to the cross section. An interesting question is whether this part of the cross section dominates the NLO corrections, at least for a suitable choice of the scale μ in (2.19). We recall that the logarithm in (2.19) may be obtained by an integration over the photon's virtuality where only the $1/q^2$ propagator is kept for the photon, while q^2 is neglected everywhere else in the hard scattering. We now consider the cross section

$$\begin{aligned} E_h \frac{\mathrm{d}^3\sigma^{\ell N\to hX}}{\mathrm{d}^3P_h} = \left(\frac{-U}{S^2}\right) \sum_{i,f} \int_{\frac{U}{T+U}}^{1+\frac{T}{S}} \frac{\mathrm{d}v}{v(1-v)} \int_{\frac{1-v}{v}\frac{U}{T}}^{1} \frac{\mathrm{d}w}{w^2} \\ \times \frac{f^{i/N}(x,\mu_F)}{x} \frac{D^{h/f}(z,\mu_F)}{z^2} \\ \times \left[\hat{\sigma}_{\rm LO}^{i\to f}(v) + f_{\rm ren}^{\gamma/\ell}\left(\tfrac{1-v}{1-vw},\mu_0\right) \frac{\alpha_s(\mu)}{\pi}\, \hat{\sigma}_{\rm LO}^{\gamma i\to f}(v,w)\right] , \end{aligned} \tag{2.28}$$

which essentially corresponds to the full NLO one in (2.22), but with the terms $\hat{\sigma}_{\rm NLO}^{i\to f}$ dropped. In other words, we use the LO term and add the Weizsäcker-Williams contribution. For the latter, we choose the upper limit on $\sqrt{-q^2}$ in the photon spectrum as a large scale in the problem, $\mu_0 \sim P_{h\perp}$ or even $\mu_0 \sim \sqrt{S}/2$. This constitutes an attempt to obtain an approximation to the full NLO correction by assuming that the $1/q^2$-behavior of the hard cross sections is valid over most of the kinematical regime. In our studies we examine in this way the importance of the Weizsäcker-Williams contribution. As discussed in the Introduction, if the contribution plays a dominant role for the NLO corrections, this opens the door to approximate NLO calculations also for the spin-dependent case.

For all our calculations we use the CTEQ6.6M [31] set of parton distribution functions and the fragmentation functions of [119].

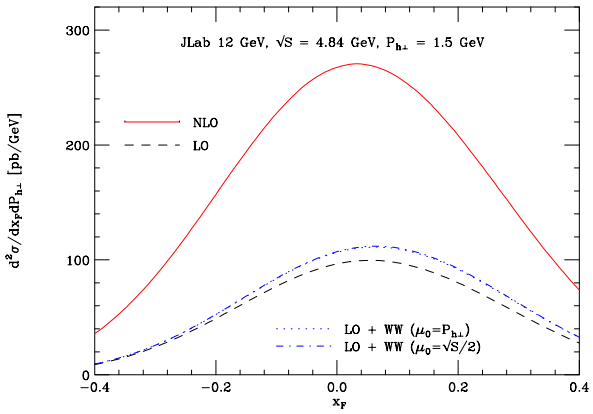

Figure 2.11.: Same as Figs. 2.8, but for $\ell\,^3$He scattering at beam energy 12 GeV after the CEBAF upgrade at Jefferson Lab. We have used a fixed $P_{h\perp} = 1.5$ GeV.

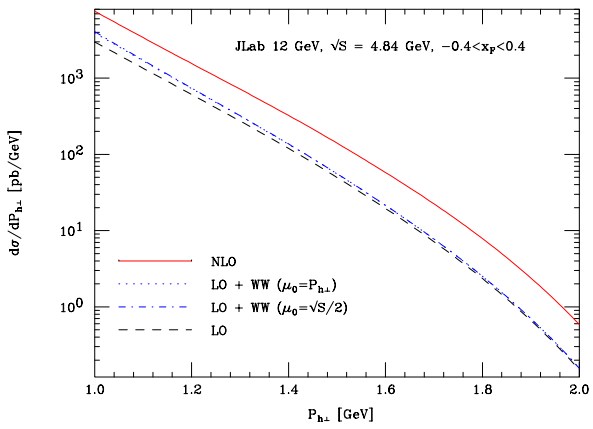

Figure 2.12.: Same as Fig 2.9, but for $\ell\,^3$He scattering at beam energy 12 GeV after the CEBAF upgrade at Jefferson Lab. We have integrated over $-0.4 \leq x_F \leq 0.4$.

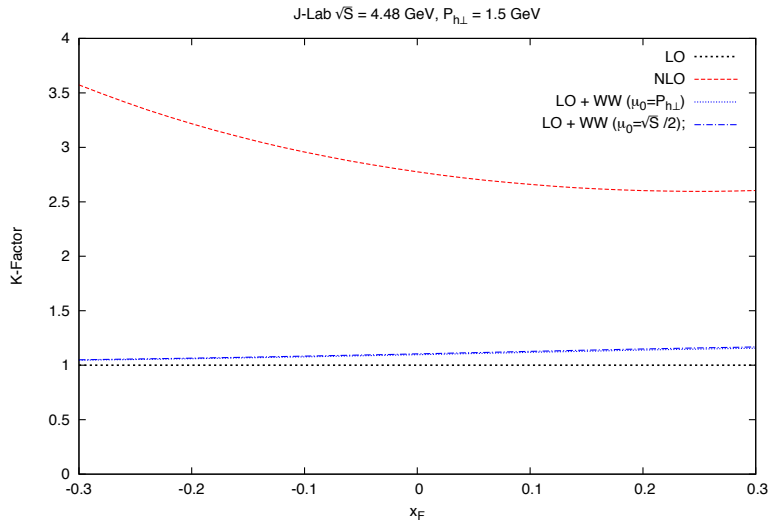

Figure 2.13.: K-factor (at a scale $\mu = P_{h\perp}$) for the 12 GeV upgrade at Jefferson Lab plotted vs. x_F and a fixed transverse momentum $P_{h\perp}$

HERMES

Figures 2.8, 2.9 and 2.10 present our results for π^+-production at HERMES at $\sqrt{S} = 7.25$ GeV. We fix the renormalization and factorization scales at $\mu = P_{h\perp}$. Fig In order to match the conventions used in $pp^\uparrow \to hX$, HERMES presents the spin asymmetry results in terms of the hadron's transverse momentum $P_{h\perp}$ and Feynman's $x_F = 2P_h^z/\sqrt{S}$, where P_h^z is the z-component of the hadron momentum in the center-of-mass frame of the collision, and where positive x_F is counted in the direction of the lepton beam. We have

$$\frac{d^2\sigma^{ep\to\pi X}}{dx_F\, dP_{h\perp}} = \frac{2\pi P_{h\perp}}{\sqrt{x_F^2 + x_T^2}}\, E_h \frac{d^3\sigma^{ep\to\pi X}}{d^3P_h}\,, \tag{2.29}$$

where $x_T = 2P_{h\perp}/\sqrt{S}$. The hadronic Mandelstam variables read

$$\begin{aligned} T &= -\frac{S}{2}\left(\sqrt{x_F^2 + x_T^2} + x_F\right)\,, \\ U &= -\frac{S}{2}\left(\sqrt{x_F^2 + x_T^2} - x_F\right)\,. \end{aligned} \tag{2.30}$$

Figure 2.8 shows the cross section as a function of x_F, integrated over 1 GeV $< P_{h\perp} <$ 2.2 GeV. This is the only $P_{h\perp}$ bin used in Ref. [46] with $P_{h\perp} > 1$ GeV. In Fig. 2.9 we examine the $P_{h\perp}$ dependence of the cross section for $0.3 < x_F < 0.55$. In both cases we find large NLO corrections; the NLO cross section is almost twice as large as

the LO one. As discussed above, we also examine in how far the Weizsäcker-Williams contribution drives the NLO corrections, using equation (2.28) with $\mu_0 = P_{h\perp}$ (dotted) and $\mu_0 = \sqrt{S}/2$ (dot-dashed). As one can see from the figures, the Weizsäcker-Williams contribution does lead to an increase over LO, but provides only about 50% to 70% of the NLO correction. This is likely to be attributed to the fact that the overall c.m.s. energy is rather low. The result with $\mu_0 = \sqrt{S}/2$ provides a slightly better description of the full NLO, although the differences are minor. We note that the WW approximation appears to work better for smaller transverse hadron momenta $P_{h\perp}$ and for larger x_F. The latter feature perhaps is at first sight surprising since positive x_F of the hadron imply on average backward scattering of the lepton, whereas the WW approximation should work better if the lepton is scattered in the forward direction. One can roughly understand this "shift" of the WW approximation towards positive x_F from the fact that $|T| \gg |U|$ for $x_F \to 1$ in equation (2.30). Since the dominant real-photon process $\gamma q \to q(g)$ in (2.26) has a $1/su$-behavior in contrast to the $1/t^2$-behaviour of the LO process, the WW approximation favors the region $x_F > 0$. The full NLO partonic cross section inherits the $1/t^2$-behaviour of the LO one, so that the Weizsäcker-Williams contribution can approximate it well only for $x_F > 0$. This behaviour is well confirmed by consulting figure 2.10, where the K-factors are shown. The K-factors are a measurement of the size of the higher order correction. They are defined by

$$K_i = \frac{\sigma_i}{\sigma_{\mathrm{LO}}} \,, \tag{2.31}$$

where the subscript i indicates the different higher order correction.

Scattering with the 12 GeV beam at the Jefferson Lab

Our NLO predictions for the cross section for $\ell\, {}^3\mathrm{He} \to \pi^+ X$ in 12 GeV scattering at the Jefferson Lab are shown in Figures 2.11, 2.12 and 2.13. For the x_F distribution on the left we have assumed a fixed transverse momentum $P_{h\perp} = 1.5$ GeV. On the right we show the $P_{h\perp}$ dependence of the cross section in the region $-0.4 < x_F < 0.4$. Again, the renormalization scale is fixed to the transverse hadron momentum, $\mu = P_{h\perp}$. Note that the rather modest c.m.s. energy available limits the possible size of $P_{h\perp}$ severely. For collisions using the present 6 GeV beam only transverse momenta outside the hard-scattering regime are possible, which is the reason why we cannot present any results for this case.

We again observe in Figures 2.11, 2.12 and 2.13 that the NLO corrections are very large with a NLO K-factor larger than 2.5. The Weizsäcker-Williams contribution is clearly insufficient to match the NLO result here.

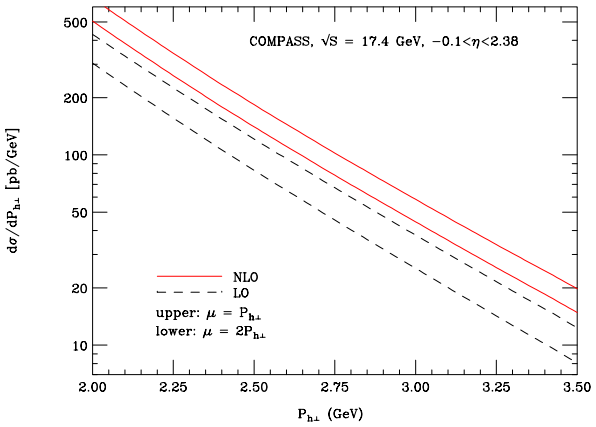

Figure 2.14.: Cross section for $\mu p \to \pi^0 X$ at COMPASS as function of $P_{h\perp}$ for $-0.1 \leq \eta \leq 2.38$. As before, the solid lines give the NLO results and the dashed lines the LO ones. We also present the LO and NLO results for the scale $\mu = 2P_{h\perp}$.

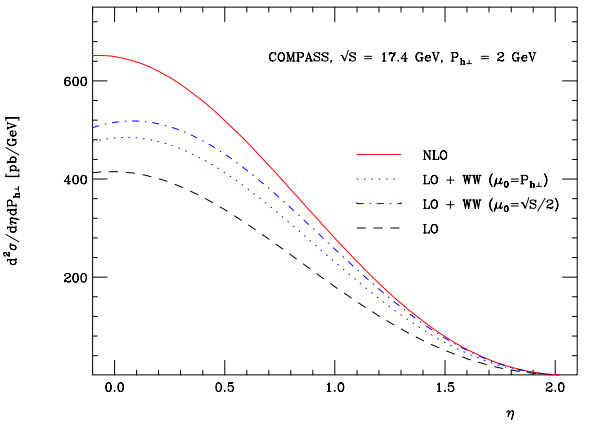

Figure 2.15.: Cross section for $\mu p \to \pi^0 X$ at COMPASS, as function of hadron pseudo-rapidity for fixed $P_{h\perp} = 2$ GeV. As before, the solid lines give the NLO results and the dashed lines the LO ones. The dotted and dot-dashed lines show the approximation (2.28) of the NLO cross section, using $\mu_0 = P_{h\perp}$ and $\mu_0 = \sqrt{S}/2$, respectively.

COMPASS

The results of our NLO analysis for COMPASS kinematics are shown in Figs. 2.15 and 2.14. COMPASS uses a muon beam with energy 160 GeV, resulting in $\sqrt{S} = 17.4$ GeV. Following the choice made by COMPASS, we use here the c.m.s. pseudorapidity η of the produced hadron rather than its Feynman-x_F. Pseudorapidity is counted as positive in the forward direction of the incident muon. We have

$$\frac{\mathrm{d}^2\sigma^{\mu p\to\pi^0 X}}{\mathrm{d}\eta\,\mathrm{d}P_{h\perp}} = 2\pi P_{h\perp} E_h \frac{\mathrm{d}^3\sigma^{\mu p\to\pi^0 X}}{\mathrm{d}^3 P_{h\perp}} \,, \tag{2.32}$$

where the hadronic Mandelstam variables read

$$\begin{aligned} T &= -P_{h\perp}\sqrt{S}\mathrm{e}^{+\eta} \,, \\ U &= -P_{h\perp}\sqrt{S}\mathrm{e}^{-\eta} \,. \end{aligned} \tag{2.33}$$

The COMPASS spectrometer roughly covers the region $-0.1 < \eta < 2.38$. From the η dependence shown in Fig. 2.15 for a fixed transverse momentum $P_{h\perp} = 2$ GeV we observe that the NLO corrections are significant but not as large as for HERMES and JLab. They amount to an increase over LO of roughly 30–40%. Strikingly, the Weizsäcker-Williams contribution is very small here, even for the choice $\mu_0 = \sqrt{S}/2$. This may be understood from the fact that the muon mass is about 200 times larger than the electron mass, resulting in a much smaller logarithm in the expression (2.19) for the photon spectrum, which then is largely cancelled by the non-logarithmic term.

For the $P_{h\perp}$ spectrum shown in Figure 2.14 we also show the results for a different choice of the factorization and renormalization scales, $\mu = 2P_{h\perp}$. As one can see, the scale dependence decreases somewhat when going from LO to NLO but remains fairly sizable.

Electron-Ion Collider

We finally also discuss the cross section for single-inclusive pion production in electron-proton collisions at a proposed future EIC [120] with $\sqrt{S} = 100$ GeV. Thanks to the higher energy of an EIC it will become possible to probe much larger transverse hadron momenta, where pQCD is expected to work better. Fig. 2.17 shows the η dependence of the cross section for a fixed transverse momentum $P_{h\perp} = 10$ GeV. Again we count positive η in the forward direction of the incoming lepton. The $P_{h\perp}$ dependence of the cross section is shown in Fig. 2.16, integrated over $|\eta| \leq 2$. The renormalization scale has again been fixed to the transverse hadron momentum, $\mu = P_{h\perp}$. As for COMPASS we found that the scale dependence slighty decreases for EIC kinematics when going from LO to NLO but remains relatively large.

We again find sizable NLO corrections. Overall, the Weizsäcker-Williams approximation works much better here than in the fixed-target regime. It describes the NLO cross

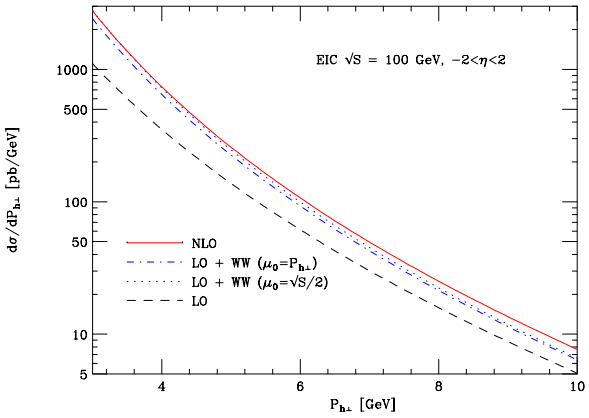

Figure 2.16.: Cross section for $ep \to \pi^+ X$ at an EIC with $\sqrt{S} = 100$ GeV as function of $P_{h\perp}$ integrated over $|\eta| \leq 2$. The lines are as in the previous figures.

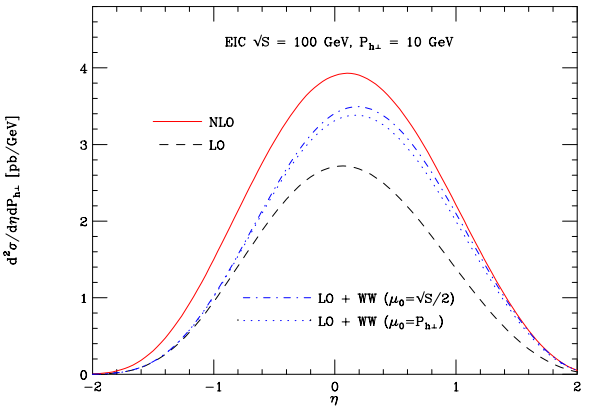

Figure 2.17.: Cross section for $ep \to \pi^+ X$ at an EIC with $\sqrt{S} = 100$ GeV as function of η at fixed $p_T = P_{h\perp} = 2$ GeV. The lines are as in the previous figures.

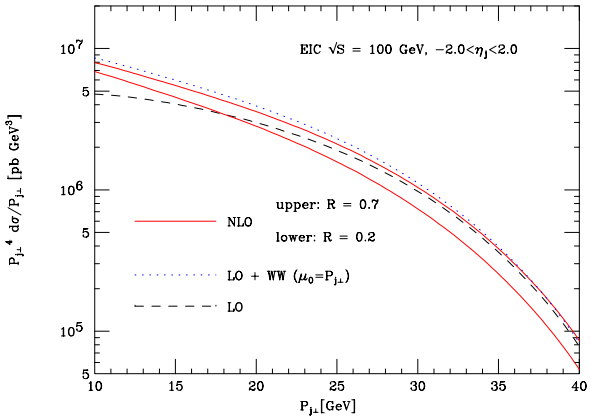

Figure 2.18.: Cross section for single-inclusive jet production at the EIC as function of $P_{\mathrm{J}\perp}$, integrated over $|\eta_{\mathrm{J}}| \leq 2$. We have used the NJA [116, 117] and the anti-k_t jet algorithm [121]. The solid lines show NLO prediction for two different values of the jet size parameter, $R = 0.7$ and $R = 0.2$, respectively. The dashed lines present the LO results, and the dotted ones the result for the approximation (2.28) of the NLO cross section, using $\mu_0 = P_{\mathrm{J}\perp}$.

section especially well when the hadron is produced in the electron forward direction. At mid-rapidity and negative rapidity the approximation tends to fall short of the full NLO result. From Fig. 2.16 we observe that that the Weizsäcker-Williams also works better for smaller $P_{h\perp}$.

Jet production at an EIC

Given the high energy of an EIC, also jet observables will be of much interest there [51]. For example, combined analysis of data for the transverse-spin asymmetries for $ep^{\uparrow} \to h\,X$ and $ep^{\uparrow} \to \mathrm{jet}\,X$ from a future EIC should allow for a clean separation of twist-3 parton correlations in the nucleon and in fragmentation. We therefore close this section by presenting predictions for the cross section for single-inclusive jet production, $ep \to \mathrm{jet}\,X$. Here we use the NJA formalism outlined in Sec. 2.2.8 to convert the single-hadron cross section into a jet one. We adopt the anti-k_t jet algorithm of [121]. In Fig. 2.19 we present the dependence of the cross section on the jet pseudo-rapidity η_{J} for a fixed transverse jet momentum of $P_{\mathrm{J}\perp} = 10$ GeV. We find once again that NLO contributions are large. We also observe that, compared to the case of hadron production considered in Fig. 2.17, the NLO cross section is much more peaked in the

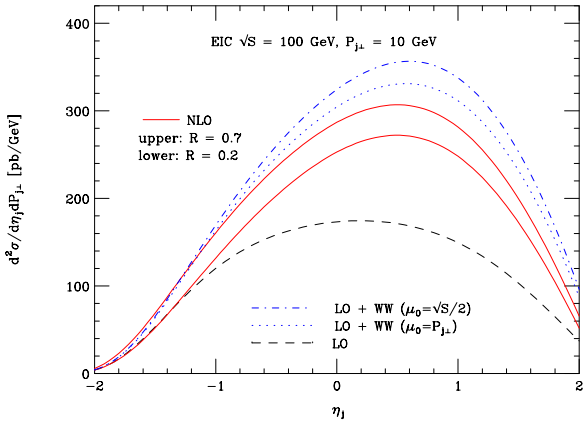

Figure 2.19.: Cross section for single-inclusive jet production at the EIC as a function of pseudorapidity η_{J} at a fixed transverse jet momentum $P_{\mathrm{J}\perp} = 10$ GeV. We have used the NJA [116, 117] and the anti-k_t jet algorithm [121]. The solid lines show NLO prediction for two different values of the jet size parameter, $R = 0.7$ and $R = 0.2$, respectively. The dashed lines present the LO results, and the dotted and dashed dotted the result for the approximation (2.28) of the NLO cross section, using $\mu_0 = P_{\mathrm{J}\perp}$ and also $\mu_0 = \sqrt{S}/2$.

forward electron region. The reason is that at large positive pseudo-rapidity $|T| \gg |U|$ in equation (2.33). Since the minimal value for the incoming parton's momentum fraction is $x_{\min} = -U/(S+T)$ in (3.16) rather small values of x are probed at large pseudo-rapidity where in turn the nucleon's parton distributions are large. On the other hand the fragmentation process suppresses the forward and backward regions in hadron production due to the large z-values probed, whereas in jet production the forward electron region is enhanced due to the absence of fragmentation.

In the figures 2.19 and 2.18, we show results for two different jet size parameters, $R = 0.7$ and $R = 0.2$. Dependence on R first occurs at NLO. As discussed at the end of Sec. 2.2.8, the first-order Weizsäcker-Williams contribution does not depend on R. It hence cannot give an accurate approximation of NLO in general. As the figure shows, the WW result happens to be rather close to the result for $R = 0.7$; this agreement, however, is essentially fortuitous.

2.4. Conclusions and outlook

We have performed next-to-leading order calculations of the partonic cross sections for the processes $\ell N \to hX$ and $\ell N \to \text{jet}\, X$, for which the scattered lepton in the final state is not detected. We have derived our results for a finite lepton mass, neglecting terms that are suppressed as powers of the mass over a hard scale. The results have been obtained in two ways. We have first set the mass to zero. We have regularized the ensuing collinear singularity in dimensional regularization and then subtracted it by introducing a Weizsäcker-Williams type photon distribution in the lepton. The latter can be computed in QED perturbation theory and effectively reinstates the leading lepton mass dependence, which is logarithmic plus constant. In the second approach, we have kept the lepton mass in the calculation directly, expanding all phase space integrals in such a way that the leading mass dependence is obtained. Both approaches give the same result.

We have presented phenomenological NLO predictions for various experimental setups, from fixed-target experiments (HERMES, JLab, COMPASS) to collider experiments at an EIC. We have found that the NLO corrections are large. We note that in the fixed target regime the bulk of the corrections comes from the plus distribution terms in equation (2.23), especially at negative x_F or rapidity. As is well known, the distributions are associated with the emission of soft gluons. Since they recur with increasing power at every higher order of perturbation theory, it may be worthwhile for future work to address their resummation to all orders, similarly to what was done for the photoproduction case $\ell N \to \ell' hX$ in [122].

The rather large size of the corrections that we find suggests that also the cross section

with transverse polarization of the initial nucleon may be subject to large NLO corrections. This would likely have ramifications for analyses of spin asymmetry data for $\ell N^\uparrow \to hX$ in terms of twist-3 parton correlation functions. As full NLO calculations for transverse single-spin observables are difficult, we have also investigated in how far it is possible to match our full NLO result for the spin-averaged cross section by adding just the Weizsäcker-Williams contribution to the LO one. We have found that this simplified approach does not appear to work well quantitatively. In other words, the NLO corrections do not appear to be dominated by quasi-real photons. Nonetheless, in order to obtain a first estimate of higher-order effects for the transverse-spin asymmetry, it may be worthwhile to use the Weizsäcker-Williams contribution for the case of transversely polarized nucleons, which is much simpler to do than the full NLO calculation and was already discussed in Ref. [51].

We again emphasize that our results suggest that contributions by quasi-real photons to the cross sections for the single-inclusive processes $\ell N \to hX$ and $\ell N \to \text{jet}\, X$ are not the dominant contributions, at least for large transverse hadron momenta $P_{h\perp} > 1\,\text{GeV}$. In other words, an experimental setup where the final state lepton is not observed in lepton-nucleon collisions does not automatically imply that one measures an (approximated) quasi-real photoproduction process. However, although quasi-real photons do not dominate, they typically do play a non-negligible role for the NLO corrections. As is well known, high-energy real photons may also exhibit their own partonic structure, in which case they are referred to as "resolved" photons (see Ref. [56]). The corresponding resolved-photon contributions are formally of the same order as the Weizsäcker-Williams contribution we have considered here. They are typically suppressed in the fixed-target regime. It may be interesting to address this contribution in future work, also in order to study its impact on the transverse single-spin asymmetries. The concept of "virtual photon structure" may also prove useful in this context (see, for example, Ref. [123]).

Chapter 3.

Double-Longitudinal Spin Asymmetry in Single-Inclusive Lepton Scattering at NLO

We calculate the double-spin asymmetries $A_{\rm LL}$ for the processes $\ell N \to hX$ and $\ell N \to$ jet X at next-to-leading order accuracy in perturbative QCD. We compare our theoretical results for $A_{\rm LL}$ to data from the SLAC E155 experiment, finding only partially satisfactory agreement. We conclude that measurements of $A_{\rm LL}$ and the relevant polarized and unpolarized cross sections should be performed at the present-day fixed-target lepton scattering experiments, as well as at a future electron ion collider, in order to verify our understanding of this process. We present predictions of the longitudinal double-spin asymmetry for these experiments. This chapter is based on publication [4].

3.1. Introduction

The single-inclusive production of hadrons (or jets) with large transverse momenta in lepton-nucleon collisions, $\ell N \to hX$, has attracted much interest in recent years from both the experimental [45–48, 124] and the theoretical sides [3, 6, 49, 51–55, 63, 64, 102, 103, 125, 126]. The main reason for this interest is that $\ell N \to hX$ may prove to be particularly useful for obtaining a better understanding of transverse (nucleon) spin effects. As is well known, measurements for the related purely hadronic process $pp \to hX$ have revealed large transverse single-spin asymmetries $A_{\rm N}$ [57], and the understanding of these large effects remains to pose a major challenge to theory. Since the process $\ell N \to hX$ is generally simpler to analyze theoretically, it is hoped that its transverse single-spin asymmetry will help us to identify the origins of the large effects observed in hadronic scattering.

The basis for the theoretical description of single-inclusive processes is collinear factorization in perturbative QCD (pQCD). In many instances, next-to-leading order (NLO) corrections, or even corrections beyond NLO, are found to be sizable for single-inclusive scattering [115, 127, 128]. Therefore, in order to be able to reliably confront data and theory for the single-transverse spin asymmetry for $\ell N \to hX$, it is crucial to have the NLO corrections for the cross sections entering the asymmetry. The recent study [52] of $A_{\rm N}$ in $\ell p \to hX$ at leading order (LO) suggests the presence of sizable NLO corrections: comparing to recent HERMES data [46] it was found that the LO theoretical prediction lies significantly higher than the data.

To compute the NLO corrections for the single-transverse spin asymmetry is a very complex task, however. The asymmetry is power-suppressed in QCD and involves twist-3 three-parton correlations. Higher-order calculations for higher-twist single-spin observables are notoriously difficult in pQCD and still relatively scarce [81]. As a first step towards an NLO calculation for the spin asymmetries in $\ell p \to hX$ (or $\ell p \to \mathrm{jet}\, X$), we have recently computed the NLO results for the respective spin-averaged cross sections [3, 6] that constitute the denominator of the asymmetries. Indeed, large NLO corrections were found for the various kinematic regimes of interest. We note that very recently even the next-to-next-to leading order calculation for the spin-averaged cross section for $\ell p \to \mathrm{jet}\, X$ was presented [126].

Unfortunately, so far no experimental data on the unpolarized cross sections exist that would allow for a comparison between theory and data. On the other hand, some data from SLAC [45] and HERMES [124] are available on the double-longitudinal spin asymmetry $A_{\rm LL}$, measured by scattering a longitudinally polarized lepton off a longitudinally polarized target. This asymmetry is of leading power in QCD and can hence be analyzed with standard techniques in pQCD. Therefore, prior to studying the more complex case of $A_{\rm N}$, we investigate $A_{\rm LL}$ at NLO in this chapter.

For the single-inclusive processes $\ell p \to hX$ and $\ell p \to \mathrm{jet}\, X$ the scattered lepton is not explicitly detected. As a result, there are contributions to the cross sections for which the incident lepton emits an almost real photon, followed by a hard photoproduction scattering process. Such contributions are formally NLO, but they are enhanced by the photon propagator. In Refs. [108] and [90] (at NLO, including resolved-photon contributions) the asymmetry $A_{\rm LL}$ for $\ell p \to hX$ was investigated under the approximation that the scattering is entirely dominated by the exchange of such quasi-real photons. However, as we found in [3], for the spin-averaged cross section this assumption is valid only in very limited kinematical regions. In general, a full NLO calculation is needed, for which the quasi-real photon contribution is just one among several. In this chapter we investigate in how far the assumption of dominant exchange of quasi-real photons is justified for the double-longitudinally polarized cross section and for $A_{\rm LL}$. In this context we also present new comparisons to the E155 data [45], on the basis of a full NLO calculation.

This chapter is structured as follows. In Sec. 3.2 we present our NLO calculations for the longitudinally polarized cross sections for $\ell N \to hX$ and $\ell N \to \text{jet}\, X$. Section 3.3 presents a comparison to the E155 data. Section 3.4 presents numerical predictions for the NLO double-spin asymmetry A_{LL} to be expected at various other fixed-target experiments and at a future Electron Ion Collider (EIC). Finally, we summarize our results in Sec. 3.5.

3.2. NLO calculation

3.2.1. Single-inclusive hadron production

In this section we briefly present our derivation of the analytical NLO results for the processes $\ell N \to hX$ and $\ell N \to \text{jet}\, X$ with longitudinally polarized initial particles. We will closely follow the previous chapter 2 in which we computed the corresponding unpolarized NLO cross sections. We will be brief and highlight only the differences arising for longitudinal polarization. We refer the reader to Ref. [3] for details concerning the calculation.

The transverse momentum of the produced hadron sets a hard scale, so that perturbative methods may be used for treating the cross sections. We first consider $\ell(l) + N(P) \to h(P_h) + X$, where we have introduced our notation for the four-momenta. We define the Mandelstam variables as $S = (P + l)^2$, $T = (P - P_h)^2$ and $U = (l - P_h)^2$. Furthermore, we denote the energy of the detected hadron by E_h and its three-momentum by $\vec{P}_h$. The momenta of the incoming parton, k^μ, and of the fragmenting parton, p^μ, which appear in the calculation of the partonic cross sections, are approximated as $k^\mu \simeq xP^\mu$ and $p^\mu \simeq P_h^\mu/z$, respectively. It is then convenient to work with the partonic Mandelstam variables

$$s = (k + l)^2 \approx xS,\;\; t = (k - p)^2 \approx \frac{x}{z}T,\;\; u = (l - p)^2 \approx \frac{U}{z}\,. \tag{3.1}$$

We will consider the following difference of cross sections:

$$\begin{aligned}\Delta\sigma \equiv \frac{1}{2}\Bigg[& E_h \frac{d^3\sigma^{\ell N \to hX}(S_L = +1, \lambda_e = +1)}{d^3P_h} \\ & - E_h \frac{d^3\sigma^{\ell N \to hX}(S_L = +1, \lambda_e = -1)}{d^3P_h}\Bigg]\,.\end{aligned} \tag{3.2}$$

In this expression S_L and λ_ℓ denote the helicities of the nucleon and the lepton, respectively. This choice of difference between polarized cross sections corresponds to the numerator of the longitudinal double-spin asymmetry $A_\parallel$ that was measured by the E155 experiment [45].

The general form of the factorized polarized cross section for inclusive hadron production process is then

$$\Delta\sigma = \frac{1}{S}\sum_{i,f}\int_0^1 \frac{dx}{x}\int_0^1 \frac{dz}{z^2}\,\Delta f^{i/N}(x,\mu)D^{h/f}(z,\mu)\,\Delta\hat{\sigma}^{i\to f}(s,t,u,\mu)\,, \tag{3.3}$$

where $\Delta f^{i/N}(x,\mu)$ is the helicity parton distribution function for the incoming parton i in the nucleon N and $D^{h/f}(z,\mu)$ the fragmentation function for parton f fragmenting into hadron h, both evaluated at a factorization scale μ. As in Ref. [3] we choose the factorization scales to be the same for the initial and the final state, and also equal to the renormalization scale. In equation (3.3), $\Delta\hat{\sigma}^{i\to f}$ is the longitudinally polarized cross section for the lepton-parton scattering process $\ell + i \to f + x$, with x an unobserved final state. The difference is defined in analogy with that in equation (3.2) The sum in equation (3.3) runs over the different species of partons, quarks, gluons and antiquarks. We note that the expression in equation (3.3) holds up to corrections that are suppressed by inverse powers of the produced hadron's transverse momentum $P_{h\perp}$.

It is convenient to rewrite the x- and z-integrals in equation (3.3) in terms of new variables $v \equiv 1 + t/s$ and $w \equiv -u/(s+t)$. Using (3.1), we have

$$x = \frac{1-v}{vw}\frac{U}{T}\,,\quad z = \frac{-T}{(1-v)S}\,, \tag{3.4}$$

and equation (3.3) becomes

$$\begin{aligned}\Delta\sigma = \left(\frac{-U}{S^2}\right)\sum_{i,f}\int_{\frac{U}{T+U}}^{1+\frac{T}{S}}\frac{dv}{v(1-v)}\int_{\frac{1-v}{v}\frac{U}{T}}^1\frac{dw}{w^2}\\ \times\frac{\Delta f^{i/N}(x,\mu)}{x}\frac{D^{h/f}(z,\mu)}{z^2}\,\Delta\hat{\sigma}^{i\to f}(v,w,\mu)\,,\end{aligned} \tag{3.5}$$

where $x = \frac{1-v}{vw}\frac{U}{T}$, $z = \frac{-T}{(1-v)S}$. For ease of notation, we have kept the symbol $\Delta\hat{\sigma}^{i\to f}$ also for the polarized cross section when expressed in terms of the new variables. We note that the invariant mass of the unobserved recoiling final state is given by $s + t + u = sv(1-w)$.

The partonic polarized cross sections $\Delta\hat{\sigma}^{i\to f}$ in equation (3.5) can be calculated in QCD perturbation theory. One may write their expansions in the strong coupling α_s as

$$\Delta\hat{\sigma}^{i\to f} \;=\; \Delta\hat{\sigma}^{i\to f}_{\rm LO} + \frac{\alpha_s}{\pi}\,\Delta\hat{\sigma}^{i\to f}_{\rm NLO} + \mathcal{O}(\alpha_s^2)\,. \tag{3.6}$$

As explained in detail in Ref. [3], there are contributions to the NLO cross section for which the photon exchanged between lepton and quark is almost real. These contributions are typically sizable. In fact they diverge when the mass of the lepton tends to

zero. Expanding the partonic cross section in the (small) lepton mass m_ℓ, one finds the structure

$$\Delta\hat{\sigma}^{i\to f}_{\rm NLO}(v,w,m_\ell,\mu) = \Delta\hat{\sigma}^{i\to f}_{\rm log}(v,w)\ \log(m_\ell/\mu) + \Delta\hat{\sigma}^{i\to f}_{0}(v,w,\mu/s) + \mathcal{O}(m_\ell^2\log(m_\ell)), \tag{3.7}$$

which exhibits the "mass singularity" as $m_\ell \to 0$. The scale μ is arbitrary and cancels between the first two pieces. The logarithmic part in (3.7) in a sense opens up new partonic channels at NLO, since it arises from configurations where the lepton radiates the photon collinearly, which subsequently participates as an initial particle in a photoproduction scattering process. Dropping all terms that vanish for $m_\ell = 0$ we arrive at the following form of the NLO cross section:

$$\begin{aligned}\Delta\sigma = \left(\frac{-U}{S^2}\right)\sum_{i,f}\int_{\frac{U}{T+U}}^{1+\frac{T}{S}}\frac{dv}{v(1-v)}\int_{\frac{1-v}{v}\frac{U}{T}}^{1}\frac{dw}{w^2} \\ \times\frac{\Delta f^{i/N}(x,\mu)}{x}\frac{D^{h/f}(z,\mu)}{z^2}\ \left[\Delta\hat{\sigma}^{i\to f}_{\rm LO}(v) + \frac{\alpha_s(\mu)}{\pi}\,\Delta\hat{\sigma}^{i\to f}_{\rm NLO}(v,w,\mu)\right. \\ \left. +\Delta f^{\gamma/\ell}\left(\tfrac{1-v}{1-vw},\mu\right)\ \frac{\alpha_s(\mu)}{\pi}\,\Delta\hat{\sigma}^{\gamma i\to f}_{\rm LO}(v,w)\right],\end{aligned} \tag{3.8}$$

where

$$\Delta f^{\gamma/\ell}(y,\mu) \equiv \frac{\alpha_{\rm em}}{2\pi}\ \Delta P_{\gamma\ell}(y)\ \log\left(\frac{\mu^2}{y^2 m_\ell^2}\right) + \mathcal{O}(\alpha_{\rm em}^2)\ , \tag{3.9}$$

is the polarized "photon-in-lepton" distribution, with $\alpha_{\rm em}$ the fine structure constant. It can be calculated perturbatively as discussed in Ref. [3] and involves the polarized lepton-photon splitting function $\Delta P_{\gamma/\ell}(y) = 2-y$. The $\Delta\hat{\sigma}^{\gamma i\to f}_{\rm LO}$ are the spin-dependent lowest-order scattering cross sections for $\gamma + i \to f + x$, computed with real incoming photons. They will be given below. We stress again that equation (3.8) is exact up to terms that vanish as $m_\ell \to 0$. The same result may be obtained in a calculation that treats the lepton as massless from the beginning. The ensuing collinear divergence may then be absorbed into a "bare" photon-in-lepton distribution and is canceled in this way [3].

For the LO partonic cross section in (3.8), present only for the channel $q \to q$ with an incoming quark that also fragments, one finds

$$\Delta\hat{\sigma}^{q\to q}_{\rm LO} = 2\alpha_{\rm em}^2 e_q^2\frac{1}{sv}\ \frac{1-v^2}{(1-v)^2}\ \delta(1-w)\ , \tag{3.10}$$

where e_q is the quark's fractional charge.

The NLO terms may be computed using the techniques discussed in [3]. The only new technical aspect concerns the use of the Dirac matrix γ_5 and the Levi-Civita tensor $\epsilon^{\mu\nu\rho\sigma}$ in dimensional regularization, which appear in the projections onto helicity states for the incoming particles. We use the 't Hooft-Veltman-Breitenlohner-Maison (HVBM) scheme [129, 130] throughout our calculation. For details of the application of these scheme in NLO calculations of single-inclusive cross sections we refer the reader to [131]. As is well-known, the HVBM scheme produces spurious terms that violate helicity conservation at the quark-gluon vertex [132]. This feature manifests itself in a spin-dependent splitting function $\Delta P_{qq}(y)$ in $d = 4 - 2\epsilon$ dimensions that differs from the spin-averaged one, $\Delta P_{qq}(y) = P_{qq}(y) + \varepsilon\, 4C_F(1-y)$. This may be corrected by a finite subtraction in the process of factorization of collinear singularities. This is the standard choice made in the literature and is also in accordance with all modern sets of NLO helicity parton distribution functions.

For the NLO term in thte $q \to q$ channel we find

$$\begin{aligned}
\Delta\hat{\sigma}^{q\to q}_{\rm NLO}(v,w,\mu) =& \frac{\alpha_{\rm em}^2 e_q^2 C_F}{svw}\Bigg[\Delta A_0^{q\to q}\,\delta(1-w) \\
&+ \Delta A_1^{q\to q}\left(\frac{\log(1-w)}{1-w}\right)_+ \\
&+ \frac{1}{(1-w)_+}\Bigg\{\Delta B_1^{q\to q}\log\left(\frac{1-v}{v(1-v(1-w))}\right) \\
&+ \Delta B_2^{q\to q}\log(1-v(1-w)) + \Delta B_3^{q\to q}\log\left(\frac{sv^2}{\mu^2}\right)\Bigg\} \\
&+ \Delta C_1^{q\to q}\log(v(1-w)) + \Delta C_2^{q\to q}\log\left(\frac{(1-v)w}{1-vw}\right) \\
&+ \Delta C_3^{q\to q}\log\left(\frac{1-v}{(1-vw)(1-v(1-w))}\right) \\
&+ \Delta C_4^{q\to q}\log\left(1-v(1-w)\right) \\
&+ \Delta C_5^{q\to q}\log\left(\frac{s}{\mu^2}\right) + \Delta C_6^{q\to q}\Bigg], \qquad (3.11)
\end{aligned}$$

where $C_F = 4/3$.The coefficients $\Delta A_i^{q\to q}$, $\Delta B_i^{q\to q}$, $\Delta C_i^{q\to q}$ are functions of v and w and may be found in the Appendix. Equation (3.11) contains the usual plus distributions defined as

$$\int_0^1 dw\, f(w)\,[g(w)]_+ = \int_0^1 dw\,\left[f(w) - f(1)\right] g(w)\,. \qquad (3.12)$$

For the channels $q \to g$ and $g \to q$ we find the simpler expressions

$$\begin{aligned}\Delta\hat{\sigma}^{q\to g}_{\rm NLO}(v,w,\mu) =& \frac{\alpha_{\rm em}^2 e_q^2 C_F}{svw}\Bigg[\Delta C_1^{q\to g}\log(1-v(1-w)) \\ &+ \Delta C_2^{q\to g}\log\left(\frac{1-v}{(1-vw)(1-v(1-w))}\right) \\ &+ \Delta C_3^{q\to g}\log\left(\frac{v(1-w)s}{\mu^2}\right) + \Delta C_4^{q\to g}\Bigg], \end{aligned} \tag{3.13}$$

and

$$\begin{aligned}\Delta\hat{\sigma}^{g\to q}_{\rm NLO}(v,w,\mu) =& \frac{\alpha_{\rm em}^2 e_q^2 T_R}{svw}\Bigg[\Delta C_1^{g\to q}\log\left(\frac{(1-v)w}{1-vw}\right) \\ &+ \Delta C_2^{g\to q}\log\left(\frac{v(1-w)s}{\mu^2}\right) + \Delta C_3^{g\to q}\Bigg], \end{aligned} \tag{3.14}$$

where $T_R = 1/2$. The coefficients $\Delta C_i^{q\to g}$ and $\Delta C_i^{g\to q}$ are again given in the Appendix. We finally list the spin-dependent partonic cross sections for the photon-initiated channels:

$$\begin{aligned}\Delta\hat{\sigma}^{\gamma q\to q}_{\rm LO}(v,w) &= \frac{2\pi\, C_F \alpha_{\rm em} e_q^2}{s(1-v)}\frac{1-v^2w^2}{vw}\,, \\ \Delta\hat{\sigma}^{\gamma q\to g}_{\rm LO}(v,w) &= \frac{2\pi\, C_F \alpha_{\rm em} e_q^2}{s(1-v)}\frac{vw(2-vw)}{1-vw}\,, \\ \Delta\hat{\sigma}^{\gamma g\to q}_{\rm LO}(v,w) &= -\frac{2\pi\, T_R \alpha_{\rm em} e_q^2}{s(1-v)}\frac{v^2w^2+(1-vw)^2}{vw(1-vw)}\,. \end{aligned} \tag{3.15}$$

3.2.2. Single-inclusive jet production

Having computed the NLO polarized cross section for inclusive hadron production the extension to single inclusive jet production is relatively straightforward, using the techniques of Refs. [116–118]. The spin-dependent cross section for $\ell N \to \text{jet}\, X$ may be written as

$$\begin{aligned}\Delta\sigma^{\ell N\to \text{jet}X} =& \frac{1}{S}\sum_i \int_{\frac{-U}{S+T}}^1 \frac{dw}{w}\,\Delta f^{i/N}\left(x=\tfrac{-U}{w(S+T)},\mu\right) \\ &\times\Bigg[\Delta\hat{\sigma}^{i\to\text{jet}}_{\text{incl. parton}}\left(v=1+\frac{T}{S},w,\mu\right) \\ &+ \Delta\hat{\sigma}^{i\to\text{jet}}_{R}\left(v=1+\frac{T}{S},w,\mu;R\right)\Bigg]\,. \end{aligned} \tag{3.16}$$

As indicated, the partonic cross section is the sum of two contributions. The first contains inclusive-parton cross sections $\Delta\hat{\sigma}^{i\to\text{jet}}_{\text{incl. parton}}$. This part of the cross section is obtained from (3.8) by setting the fragmentation functions to $\delta(1-z)$. Explicitly, we have

$$\Delta\hat{\sigma}^{i\to\text{jet}}_{\text{incl. parton}}(v,w,\mu) = \sum_f \Bigg[\Delta\hat{\sigma}^{i\to f}_{\text{LO}}(v) + \frac{\alpha_s(\mu)}{\pi}\,\Delta\hat{\sigma}^{i\to f}_{\text{NLO}}(v,w,\mu) + \Delta f^{\gamma/\ell}\left(\tfrac{1-v}{1-vw},\mu\right)\,\frac{\alpha_s(\mu)}{\pi}\,\Delta\hat{\sigma}^{\gamma i\to f}_{\text{LO}}(v,w)\Bigg], \tag{3.17}$$

where $v = 1 + T/S$. The inclusive-parton cross section has been integrated over the full phase space of the unobserved final-state particles, keeping the momentum of the observed particle fixed. This is not appropriate for an NLO jet cross section for which two final-state particles may jointly form the jet. As shown in Refs. [116–118], one can correct for this by introducing a subtraction piece. This piece is represented by the term involving $\Delta\hat{\sigma}_R^{i\to\text{jet}}$ in equation (3.16). As discussed further in [116–118] one may determine the $\Delta\hat{\sigma}_R^{i\to\text{jet}}$ analytically if one assumes that the jet size parameter R is relatively small. Without going into further detail we just quote the final results relevant for the spin-dependent cross section for $\ell N\to\text{jet}\,X$:

$$\begin{aligned}\Delta\hat{\sigma}_R^{q\to\text{jet}}(v,w,\mu;R) =& -\frac{\alpha_s(\mu)}{\pi}\frac{C_F\alpha_{\text{em}}^2 e_q^2}{svw}\,\Delta\mathcal{H}^{q\to q}(v,w)\\ &\times\Bigg[A_0^{\text{jet}}(v;R)\,\delta(1-w) + A_1^{\text{jet}}(v,w)\left(\frac{\log(1-w)}{1-w}\right)_+\\ &+ B_1^{\text{jet}}(v,w;R)\,\frac{1}{(1-w)_+} + C_1^{\text{jet}}(v,w;R)\Bigg] + \mathcal{O}(\alpha_s^2),\\ \Delta\hat{\sigma}_R^{g\to\text{jet}}(v,w,\mu;R) =& \mathcal{O}(\alpha_s^2).\end{aligned} \tag{3.18}$$

The coefficients A_0^{jet}, A_1^{jet}, B_1^{jet}, C_1^{jet} are given in the Appendix. They show that the NLO jet cross section has the form $\mathcal{A}\log(R)+\mathcal{B}+\mathcal{O}(R^2)$. The coefficient A_0^{jet} depends on the jet algorithm used to define the jet parameter R. The result given in the Appendix refers to the anti-k_T algorithm [121]. The hard-scattering function in (3.18) is related to the Born cross section in equation (3.10):

$$\Delta\mathcal{H}^{q\to q}(v,w) = \left.\frac{1-v'^2}{(1-v')^2}\right|_{v'=vw/(1-v(1-w))}. \tag{3.19}$$

We note that for the unpolarized cross section the same coefficients A_0^{jet}, A_1^{jet}, B_1^{jet}, C_1^{jet} appear, with however the hard part

$$\Delta\mathcal{H}^{q\to q}(v,w)\to\mathcal{H}^{q\to q} = \left.\frac{1+v'^2}{(1-v')^2}\right|_{v'=vw/(1-v(1-w))}. \tag{3.20}$$

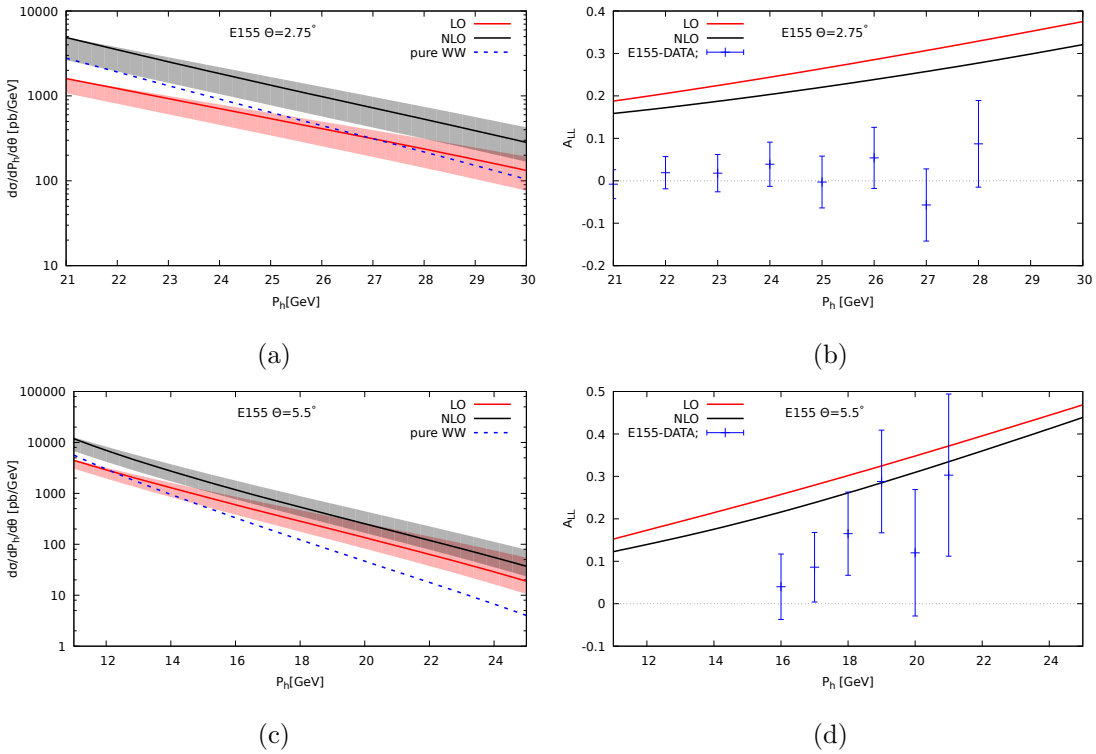

Figure 3.1.: Unpolarized cross sections ((a) and (c)) and longitudinal double-spin asymmetries A_{LL} for $ep \to \pi^+ X$, at scattering angle $\theta = 2.75°$ (upper panel) and $\theta = 5.5°$ (lower panel), respectively. We show LO and NLO results. The data are from E155 3.3. The blue line shows the pure Weizsäcker-Williams contributions by quasi-real photons. The bands in (a) and (c) represent the scale variation $1\,\mathrm{GeV} < \mu < 2P_{H\perp}$.

3.3. Phenomenological results

In this section we present numerical estimates for the longitudinal double-spin asymmetry A_{LL} for the kinematical setup of the SLAC E155 experiment [45]. Although HERMES also reports a measurement of A_{LL} [124] in $ep \to hX$, we cannot compare to their data. The reason is that the HERMES data are not fully single-inclusive but were taken with the requirement that the scattered electron not be seen within the detector acceptance. This is different from a fully single-inclusive measurement for which the electron may be in any region of phase space. Also, hadron transverse momenta are typically very low for the HERMES data.

E155 used an electron beam with energy $E = 48.35\,\mathrm{GeV}$ scattering off proton or

deuteron targets. The experiment measured the double-longitudinal spin asymmetry

$$A_{\mathrm{LL}}^{\ell N\to hX}(S,T,U) \equiv \frac{\Delta\sigma_{\mathrm{NLO}}^{\ell N\to hX}(S,T,U)}{\sigma_{\mathrm{NLO}}^{\ell N\to hX}(S,T,U)}. \tag{3.21}$$

at two scattering angles, $\theta = 2.75^\circ$ and $\theta = 5.5^\circ$, defined in the laboratory (target rest) frame, defined relative to the direction of the incident lepton beam. Hadrons with momenta $10\,\mathrm{GeV} \leq |\vec{P}_h| \leq 29\,\mathrm{GeV}$ were accepted, again defined in the laboratory frame. The asymmetry $A_{\mathrm{LL}}^{\ell N\to hX}$ was measured as a function of $|\vec{P}_h|$. Data were presented for identified pions and also for unidentified charged hadrons.

In order to compute $A_{\mathrm{LL}}^{\ell N\to hX}$ at NLO we use equation (3.8) for the spin-dependent cross section, accompanied by the results in equation (25) of Ref. [3] for the spin-averaged one. In the target rest frame, neglecting the mass of the produced hadron, we have

$$\begin{aligned} S &= (P+l)^2 \;=\; 2ME + M^2\,, \\ T &= (P-P_h)^2 \;=\; M^2 - 2M|\vec{P}_h|\,, \\ U &= (l-P_h)^2 \;=\; -2E|\vec{P}_h|(1-\cos\theta)\,, \end{aligned} \tag{3.22}$$

where M is the proton mass. We note that we find a rather strong decrease of our results (at the level of about 10%) if we drop the M^2 terms in (3.22). This is to be understood from the relatively modest beam energy and the forward kinematics. In principle we should include the full set of target mass corrections which, however, is beyond the scope of this article.

We note that the transverse hadron momentum is given in the rest-frame variables by $|\vec{P}_{h\perp}| = |\vec{P}_h|\sin(\theta)$. Since the transverse momentum sets the hard scale for the process we demand for our calculations that $|\vec{P}_{h\perp}| \geq 1$ GeV. For the scattering angle $\theta = 2.75^\circ$ this corresponds to a lower bound $|\vec{P}_h| \geq 20.9\,\mathrm{GeV}$ whereas for $\theta = 5.5^\circ$ we have $|\vec{P}_h| \geq 10.5\,\mathrm{GeV}$. Conversely, for $\theta = 2.75^\circ$ the data extend to $|\vec{P}_h| = 29\,\mathrm{GeV}$, corresponding to transverse momenta $|\vec{P}_{h\perp}| \leq 1.4\,\mathrm{GeV}$. For $\theta = 5.5^\circ$ the maximal hadron momentum in E155 is about $|\vec{P}_h| = 24\,\mathrm{GeV}$, yielding $|\vec{P}_{h\perp}| \leq 2.3\,\mathrm{GeV}$.

Throughout our calculations we use the NLO unpolarized parton distributions of [32], referred to as MSTW2008. For the helicity parton distributions we use the latest NLO set of [133] (DeFlorian2014). When dealing with deuteron targets we neglect nuclear binding effects and simply use $D = (p+n)/2$ along with the the isospin relations $f^{u/n} = f^{d/p}$ etc. for the up and down distributions in neutrons. Finally, for the pion fragmentation functions we choose the latest set of [119] (DSS14). This reference does not provide fragmentation functions for unidentified charged hadrons. For the latter we therefore use the earlier DSS sets [134].

The experiment E155 has released data for the channels $ep \to \pi^\pm X$, $ep \to h^\pm X$, $eD \to \pi^\pm X$ and $eD \to h^\pm X$. In the following we will briefly discuss each of these.

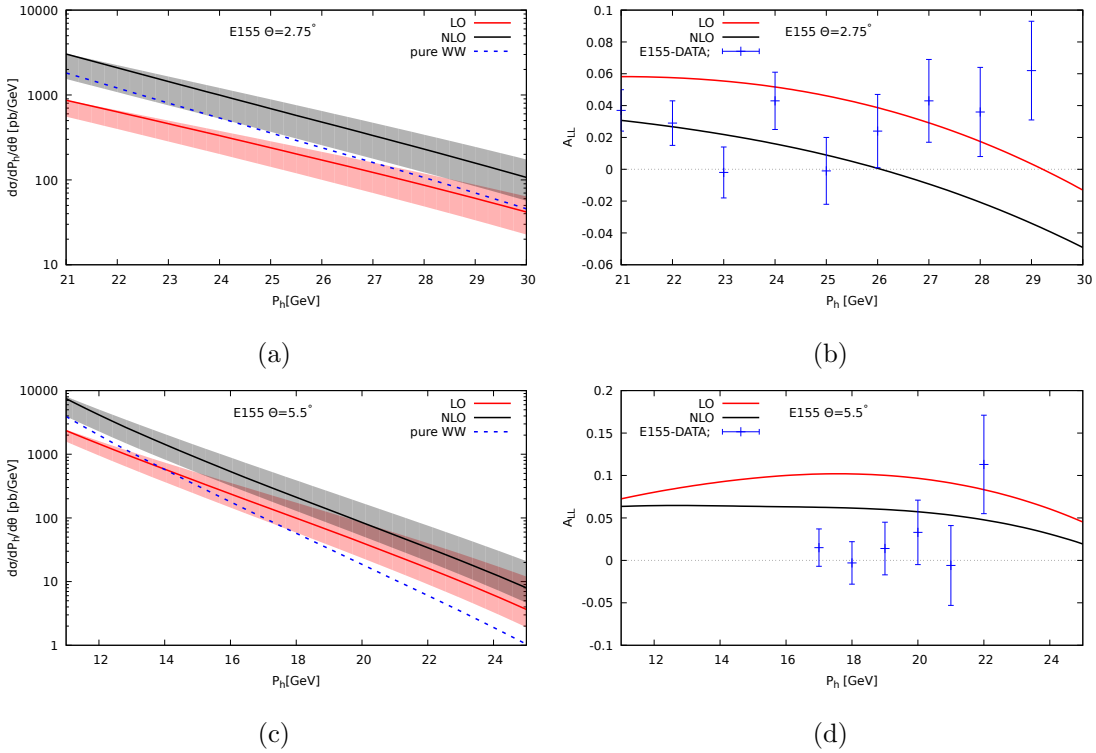

Figure 3.2.: Same as Figs. 3.1a - 3.1d, but for $ep \to \pi^- X$. Again, the upper panel corresponds to $\theta = 2.75°$ and the lower panel to $\theta = 5.5°$

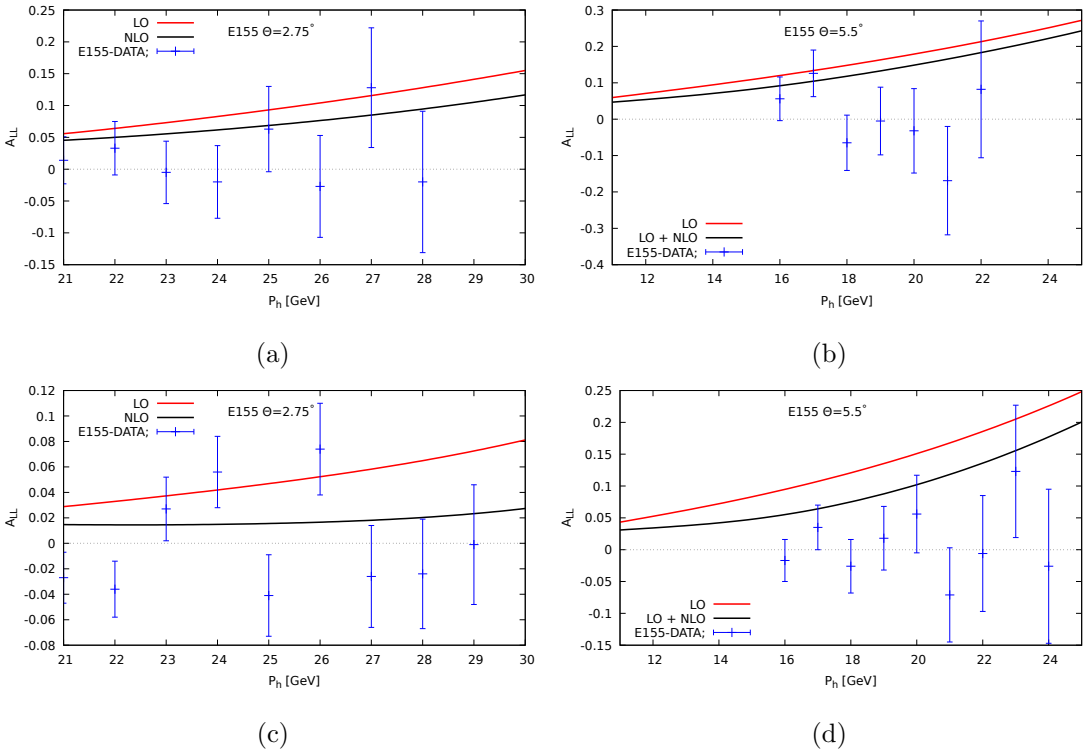

Figure 3.3.: Longitudinal double-spin asymmetries A_{LL} for $eD \to \pi^+ X$ (a),(b) and $eD \to \pi^- X$ (c),(d) for the scattering angles $\theta = 2.75°$ (a),(c) and $\theta = 5.5°$ (b),(d).

3.3.1. $ep \to \pi^+ X$

Figure 3.1a shows the unpolarized cross section for $ep \to \pi^+ X$ as a function of $|\vec{P}_{h\perp}|$ at a scattering angle of $\theta = 2.75°$. We plot

$$\frac{d\sigma^{\ell N \to hX}}{d|\vec{P}_h|\, d\theta} = 2\pi |\vec{P}_h| \sin(\theta) \left(E_h \frac{d\sigma^{\ell N \to hX}}{d^3 \vec{P}_h} \right), \tag{3.23}$$

at LO (lower solid line and band) and NLO (upper). The solid lines represent the cross sections computed at scale $\mu = |\vec{P}_{h\perp}| = |\vec{P}_h| \sin\theta$, while the bands are generated from the scale variation $1\,\mathrm{GeV} < \mu < 2P_{h\perp}$. The upper end of the band corresponds to the lowest scale. We find that the NLO corrections are large, with $K \equiv \sigma_{\mathrm{NLO}}/\sigma_{\mathrm{LO}}$-factors of about 2-3 at E155 for this scattering angle. The blue line in Fig. 3.1a represents the contribution to the cross section by quasi-real photons, obtained in the unpolarized case as (cf. equation (3.8) and see also equation (25) of Ref. [3]):

$$\begin{aligned} \sigma = \left(\frac{-U}{S^2} \right) \sum_{i,f} \int_{\frac{U}{T+U}}^{1+\frac{T}{S}} \frac{dv}{v(1-v)} \int_{\frac{1-v}{v}\frac{U}{T}}^{1} \frac{dw}{w^2} \frac{f^{i/N}(x,\mu)}{x} \\ \times \frac{D^{h/f}(z,\mu)}{z^2} f^{\gamma/\ell}\left(\tfrac{1-v}{1-vw}, \mu \right) \frac{\alpha_s(\mu)}{\pi} \hat{\sigma}_{\mathrm{LO}}^{\gamma i \to f}(v,w)\,. \end{aligned} \tag{3.24}$$

We refer to this contribution in the plots as "pure WW" contribution. We again adopt the scale $\mu = |\vec{P}_{h\perp}|$. As one can see, the real-photon contribution dominates the cross section only at the lower values of $|\vec{P}_h|$. Beyond $|\vec{P}_h| \approx 30$ GeV. This finding is at variance with the general assumption made in [45, 90, 108] that the bulk of inclusive-hadron events is produced by real photons. We note that for scattering angle $\theta = 2.75°$ real photons do dominate in the region where most of the data were taken.

This becomes different for scattering angle $\theta = 5.5°$; see Fig. 3.2c. Here the contribution by quasi-real photons does not really dominate anywhere in the regime of interest. We conclude that our full NLO calculation is required here for a meaningful comparison to the data. We note that the K-factors are slightly smaller at this scattering angle.

Turning to the corresponding spin asymmetries shown in Figs. 3.1b, 3.1d we find that the NLO corrections do not influence the asymmetries as much as the cross sections. Instead, a significant part of NLO corrections seems to cancel in the asymmetry. On the other hand, there is a clear trend for the asymmetry to decrease when going from LO to NLO. This helps to bring the theoretical results closer to the data. Still, even at NLO our results for the spin asymmetry are much higher than the data for $\theta = 2.75°$. For the angle $\theta = 5.5°$ we find a slightly better agreement, mostly because the data have larger error bars here. We note that for the kinematics that are relevant here the involved parton distributions and fragmentation functions are rather well constrained. It is conceivable that the disagreement we observe for the spin asymmetries indicates

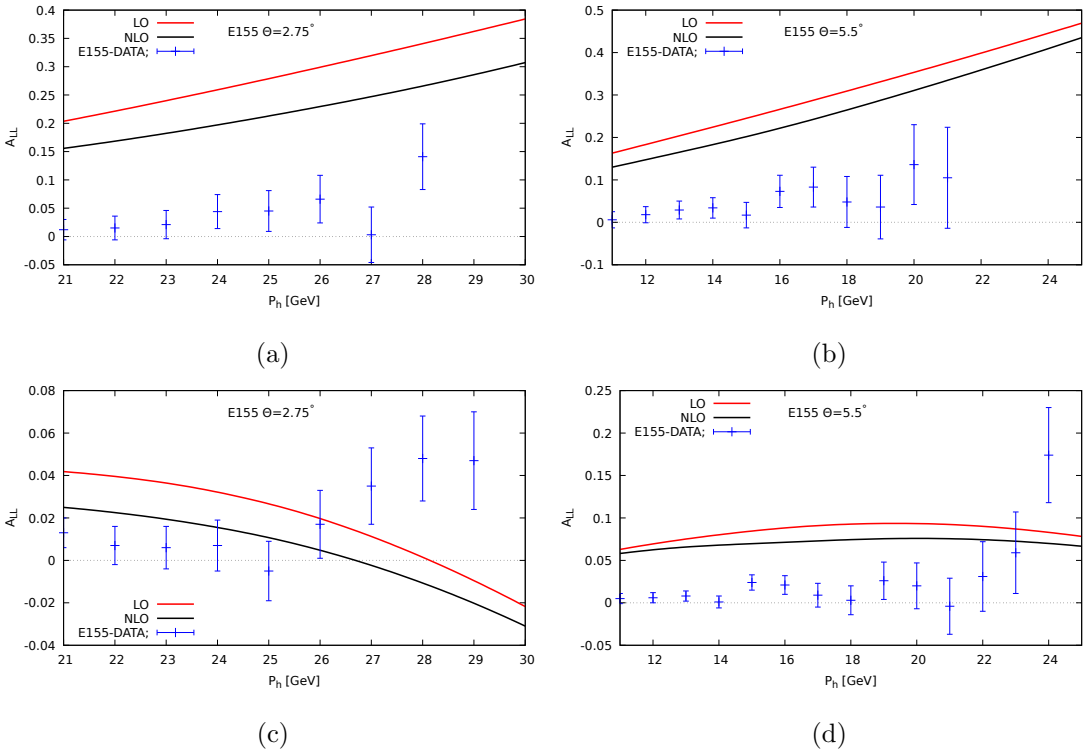

Figure 3.4.: Same as Figs. 3.3a - 3.3d, but for production of unidentified positive (a),(b) and negative (c),(d) hadrons off a proton target.

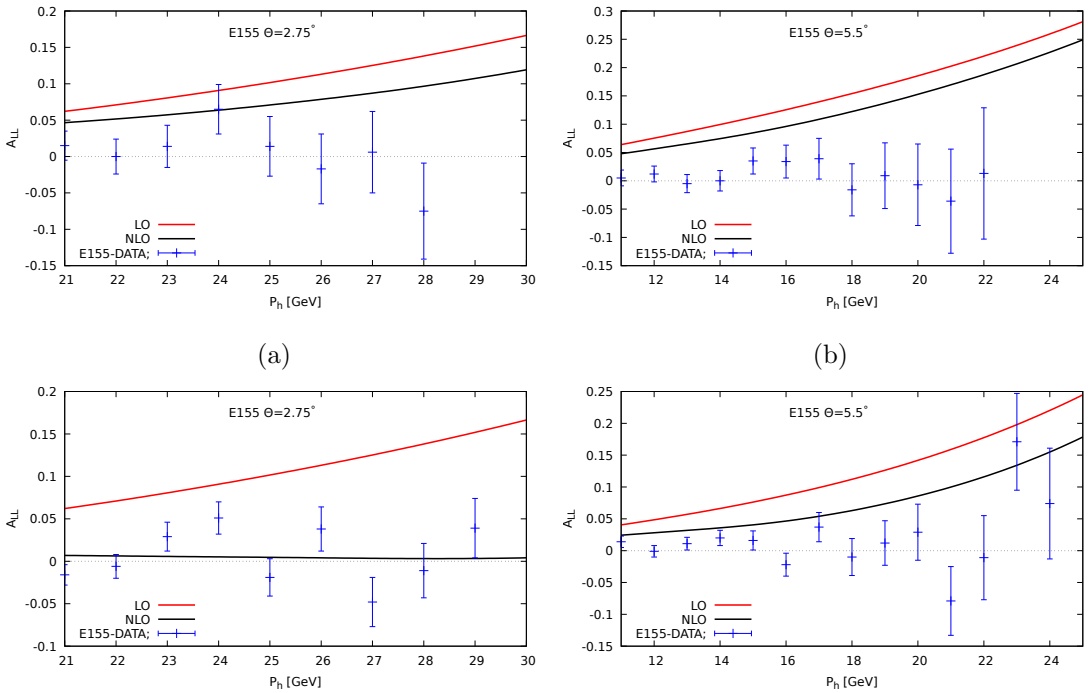

(a) (b)

(c) (d)

Figure 3.5.: Same as Figs. 3.3a - 3.3d, but for unidentified positive (a), (b) and negative (c), (d) hadrons produced off a deuteron target.

that perturbative-QCD methods are not yet applicable at such relatively low $|\vec{P}_{h\perp}|$. Higher-twist corrections might account for the difference, in particular for the data at $\theta = 2.75°$.

3.3.2. $ep \to \pi^- X$

In Figs. 3.2a – 3.2d we present our results for π^- production off a proton target. The plots of the unpolarized cross sections in Figs. 3.2a, 3.2c qualitatively resemble those for π^+-production, that is, we observe large K-factors and dominance of the real-photon contribution at the smaller π^- momenta for $\theta = 2.75°$. Also, as for π^+-production the contributions by real photons do not dominate for $\theta = 5.5°$. Since we find the same qualitative features of the cross section also for all other channels, $eD \to \pi^\pm X$, $ep \to h^\pm X$ and $eD \to h^\pm X$, we refrain from showing plots for their unpolarized cross sections.

In Figs. 3.2b, 3.2d we compare our results for the asymmetries to the E155 data and find a better agreement with the data than for π^+-production. Again we observe that the

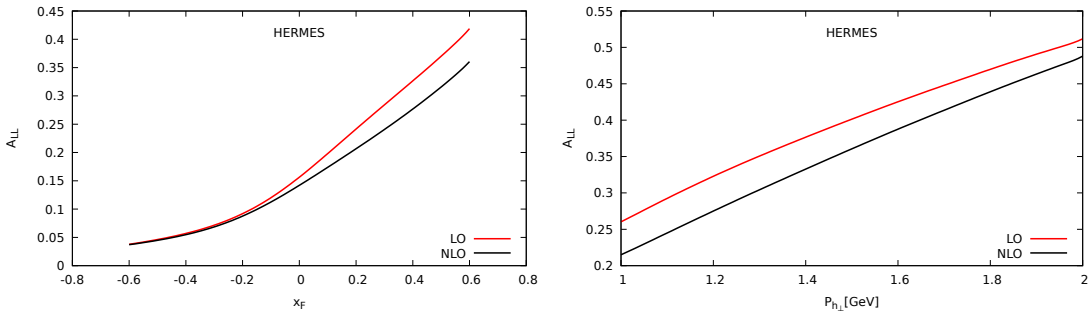

(a) (b)

Figure 3.6.: Longitudinal double-spin asymmetries A_{LL} for $ep \to \pi^+ X$ at HERMES, (a) as function of x_F for 1 GeV $< P_{h\perp} <$ 2.2 GeV, and (b) as function of $P_{h\perp}$ for $0.3 < x_F < 0.55$. The red line gives the LO prediction and the black line the NLO one.

NLO corrections are not as large for the asymmetries as they are for the cross sections. As before they tend to push the theory curves closer to the data. The spin asymmetries computed for the "pure WW" contributions by real photons agree with the data even better, in particular for $\theta = 5.5°$. It was already observed in Refs. [90, 108] that the asymmetry data are well described by the real-photon contributions. However, in the light of the fact that real photons do not produce the bulk of the cross section at this angle, we have to consider this agreement as coincidental.

3.3.3. $eD \to \pi^- X$

Figures 3.3a – 3.3d present numerical results for the asymmetries A_{LL} for pion production off a deuteron target. We observe an overall better agreement with the E155 data than for scattering off protons, especially for π^+-production. Again, the NLO corrections tend to improve the agreement, although by and large, the NLO results are somewhat higher than the data.

3.3.4. $ep \to h^{\pm} X$

We finally discuss the spin asymmetries for unidentified charged hadrons. Our results for production off a proton target are shown in Figs. 3.4a – 3.4d. We find that the NLO results are much higher than the E155 data for both scattering angles $\theta = 2.75°$ and $\theta = 5.5°$, irrespective of the charge of the produced hadrons.

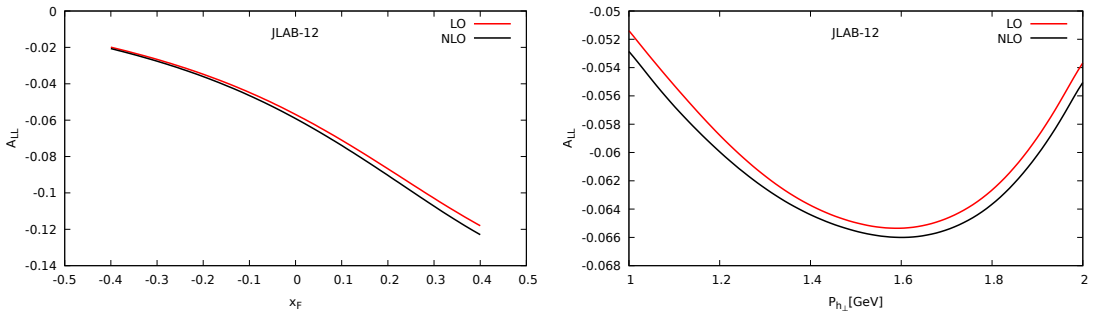

(a) (b)

Figure 3.7.: Same as Figs. 3.6a, 3.6b, but for $\ell\,^3$He scattering at beam energy 12 GeV after the CEBAF upgrade at Jefferson Lab. On the left we have chosen a fixed $P_{h\perp} = 1.5$ GeV, while for the $P_{h\perp}$ dependence on the right we have integrated over $-0.4 \leq x_F \leq 0.4$.

3.3.5. $eD \to h^{\pm}X$

The corresponding results for unidentified hadrons produced off a deuteron target are shown in Figs. 3.5a – 3.5d. Compared to the case of a proton target the theoretical curves are now overall much closer to the E155 data. This finding is in line with what we observed for pion production above.

3.4. Predictions

In view of the unclear situation concerning the comparison of NLO theory and E155 data we argue that it would be important to have independent data on the unpolarized cross section and the longitudinal double-spin asymmetry. We now present some phenomenological predictions for $A_{\rm LL}$ at NLO in single-inclusive pion production for HERMES, JLab12, COMPASS and the future EIC. For the latter, we also investigate the spin asymmetry in jet production. In the previous chapter 2 we have already presented results for the corresponding spin-averaged cross sections, and we compute the spin asymmetry for the same kinematics considered there. We always show LO and full NLO results, using the scale $\mu = |\vec{P}_{h\perp}|$. One of the findings of [3] (and of the comparison to the E155 data above) is that the real-photon contribution typically does not provide a faithful description of the full NLO corrections. In the following we hence refrain from showing results for the "pure WW" contribution.

In Figs. 3.6a, 3.6b we show the asymmetries in $ep \to \pi^+ X$ at $\sqrt{S} = 7.25$ GeV, as relevant for HERMES. The left figure shows the dependence of $A_{\rm LL}$ on the Feynman variable x_F, averaging the cross sections over $1\,\text{GeV} < P_{h\perp} < 2.2\,\text{GeV}$. Similar to

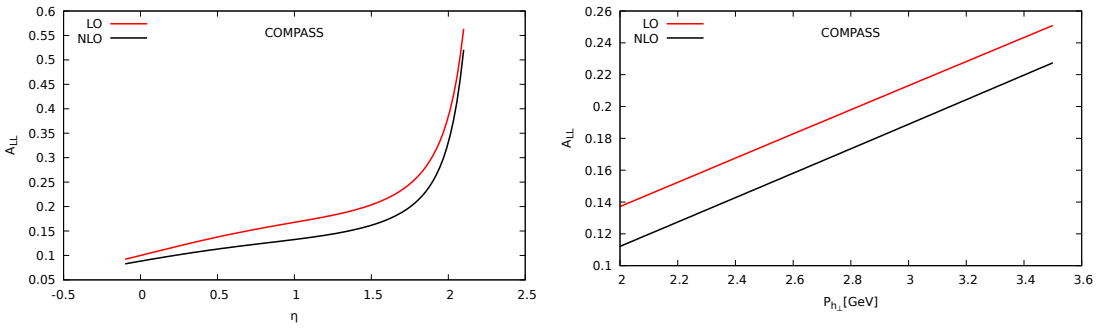

(a) (b)

Figure 3.8.: Longitudinal double-spin asymmetry $A_{\rm LL}$ for $\mu p \to \pi^0 X$ at COMPASS, (a) as function of pion pseudorapidity for fixed $P_{h\perp} = 2$ GeV, and (b) as function of $P_{h\perp}$ for $-0.1 \leq \eta \leq 2.38$. As before, the black line give the NLO result and the red line the LO one.

what we found for E155 the NLO corrections to the asymmetry are not large, despite large K-factors for the spin-averaged cross section (cf. Ref. [3]). We observe that the asymmetries grow toward larger Feynman-x_F where the NLO corrections become larger. Figure 3.6b shows the $P_{h\perp}$-dependence of $A_{\rm LL}$, with x_F averaged over $0.3 < x_F < 0.55$. Clearly, a very large spin asymmetry is expected for these kinematics.

Figures 3.7a, 3.7b show results for the spin asymmetry in $\ell\,^3$He scattering at beam energy of 12 GeV, corresponding to measurements possible with the CEBAF upgrade at Jefferson Lab. For the calculations of the unpolarized cross section we neglect nuclear effects for Helium and just set ^{3}He$= (2p + n)/3$ along with the usual isospin relations for the parton distributions. The situation is different for the helicity distributions. To a good approximation the two spins of the protons in a polarized ^{3}He nucleus are antiparallel. Effectively, the nucleus can be considered a polarized neutron target, with $\Delta f^{q/^3\mathrm{He}} = \Delta f^{q/n}$. Again, we then use isospin symmetry to obtain the neutron's helicity distributions. As seen from Figs. 3.7a, 3.7b, the resulting asymmetry is negative and much smaller in size than the one for a proton target found for HERMES kinematics. The NLO corrections affect the asymmetry only little. We stress that for the very modest beam energy at JLab12 the use of perturbative methods for analyzing the process $\ell N \to hX$ is questionable.

The COMPASS experiment employs a 160 GeV muon beam on a fixed target, resulting in a much larger center-of-mass energy of $\sqrt{S} = 17.4$ GeV. As a result, a wider $P_{h\perp}$-range can be probed. As we found in Ref. [3], this yields a more controlled perturbative framework, with the NLO corrections to the spin-averaged cross section amounting to only about $30 - 40\%$. Predictions for $A_{\rm LL}$ in $\mu p \to \pi^0 X$ at COMPASS are shown in Figs. 3.8a, 3.8b. On the left we plot the asymmetry as a function of pion's c.m.s.

pseudorapidity η, at a fixed transverse momentum $P_{h\perp} = 2\,\text{GeV}$. On the right, we show the $P_{h\perp}$-dependence of A_{LL}, averaging over $-0.1 \leq \eta \leq 2.38$. We find that the asymmetry is again reduced by the NLO corrections. Despite the relatively large energy A_{LL} is expected to be sizable.

Excellent opportunities for studies of single-inclusive hadron production would be provided by a future EIC [120]. Thanks to the high ep c.m.s. energy of an EIC, $\sqrt{S} =$ 100 GeV, it will become possible to probe much larger transverse hadron momenta where pQCD is expected to work better. We have presented numerical results in Ref. [3] (see Fig. 8a of this reference) for the η-dependence of the unpolarized cross section for $ep \to \pi^+ X$ at the EIC, at a relatively large fixed transverse hadron momentum $P_{h\perp} = 10\,\text{GeV}$. Our results indicated a milder modification of the LO result by NLO corrections for such a large transverse hadron momentum, with a K-factor of about 1.5. In particular, the NLO corrections are dominated by real photon contributions for positive pseudorapidities $\eta > 1$. We find for the η-dependence of the asymmetry A_{LL} at $P_{h\perp} = 10\,\text{GeV}$ that the effect of the NLO corrections is rather small.

Interestingly, NLO corrections to the asymmetry A_{LL} become quite important for a smaller fixed transverse hadron momentum $P_{h\perp} = 3$ GeV. In this case the event rate is about 200 times larger compared to the one at a large transverse momentum $P_{h\perp} =$ 10 GeV. In Fig. 2.17 we plot the asymmetry A_{LL} for $ep \to \pi^+ X$ at the EIC as a function of the pion's c.m.s. pseudorapidity η, at a fixed pion transverse momentum $P_{h\perp} = 3$ GeV. At midrapidity (where the event rate is largest) the asymmetry is about 2%. The asymmetry is considerably affected by NLO-corrections for pseudorapidities $\eta > 0.5$. In this region we observe a 60% reduction of the asymmetry when going from LO to NLO. This effect is generated by large K-factors of the unpolarized NLO cross section, caused by dominant real photon contributions. The unpolarized cross section receives positive enhancements from all partonic channels. On the other hand, the spin-dependent cross section obtains a relatively large negative contribution from the gluon-induced subprocess which partly compensates the large positive enhancements from the quark induced channels. Overall, this leads to an NLO correction that is smaller for the spin-dependent cross section than for the spin-averaged one, and consequently to a large NLO effect on the asymmetry. This sensitivity to gluon-induced processes at NLO indicates an opportunity to constrain the gluon's helicity distribution Δg at the EIC.

The $P_{h\perp}$-dependence of the spin asymmetry at the EIC is shown in Fig. 3.9b. As expected, the asymmetry becomes smaller at lower pion transverse momenta and the NLO correction lowers the asymmetry somewhat.

Given the high energy of an EIC, also jet observables will become available. Therefore, we also present predictions for the double-longitudinal spin asymmetry A_{LL} in $ep \to \text{jet}\, X$, using the NLO calculations described in Sec. 3.2.2. We adopt the anti-k_t jet

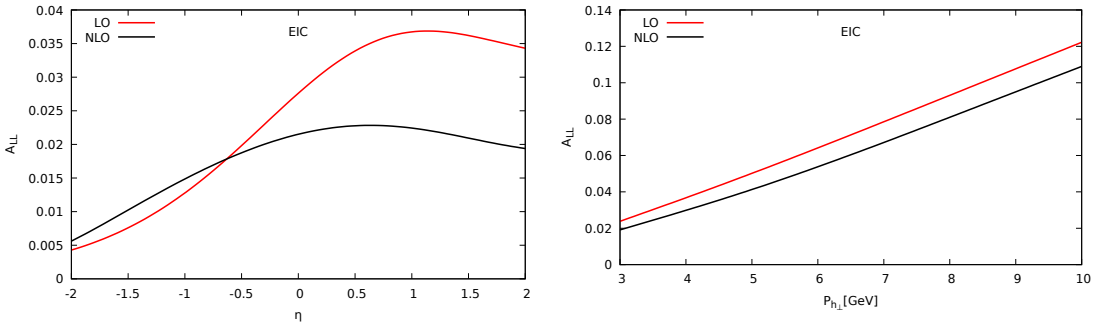

(a) (b)

Figure 3.9.: Longitudinal double-spin asymmetry A_{LL} for $ep \to \pi^+ X$ at an EIC with $\sqrt{S} = 100$ GeV, (a) as function of c.m.s. pseudorapidity η at fixed $P_{h\perp} = 3$ GeV, (b) as function of $P_{h\perp}$, integrated over $|\eta| \leq 2$. The lines are as in the previous figures.

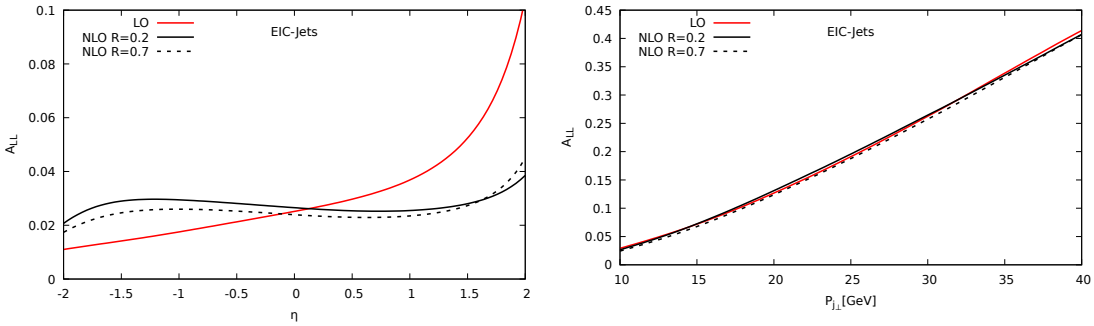

(a) (b)

Figure 3.10.: Longitudinal double-spin asymmetry for single-inclusive jet production at the EIC, (a) ass function of jet pseudorapidity η at a fixed transverse jet momentum $P_{\mathrm{J}\perp} = 10$ GeV, and (b) as function of $P_{\mathrm{J}\perp}$, integrated over $|\eta| \leq 2$. We have used the anti-k_t jet algorithm [121]. The dashed and dotted lines show NLO prediction for two different values of the jet size parameter, $R = 0.7$ and $R = 0.2$, respectively.

algorithm of [121]. Figure 3.10a shows the dependence of A_{LL} on the jet's pseudorapidity η at fixed jet transverse momentum $P_{j\perp} = 10\,\mathrm{GeV}$. We plot the NLO asymmetry for two jet sizes, $R = 0.2$ and $R = 0.7$. For negative jet-pseudorapidities the NLO corrections seem to increase the asymmetry with respect to the LO result, while they decrease for positive pseudorapidities. The $P_{\mathrm{J}\perp}$-dependence of the asymmetry is shown in Fig. 3.10b. It turns out to remain largely unaffected by the NLO corrections.

3.5. Conclusions

We have performed next-to-leading order calculations of the spin-dependent partonic cross sections for the processes $\ell N \to hX$ and $\ell N \to \mathrm{jet}\, X$ for longitudinal polarization of the initial particles. Based on these results we have computed the double-longitudinal spin asymmetry A_{LL} to NLO accuracy. We have found that the NLO corrections tend to reduce the size of the spin asymmetry.

We have presented detailed comparisons of our A_{LL} to the data by the SLAC E155 experiment which has measured the asymmetry for ep and eD scattering, in each case both for charged pions and for unidentified charged hadrons $h^{\pm}$. Data were recorded separately for two scattering angles, $\theta = 2.75^{\circ}$ and $\theta = 5.5^{\circ}$. No consistent picture emerges from the comparisons. By and large, the theoretical asymmetry lies higher than the data. For scattering off a deuteron target there is typically at least a qualitative agreement between the NLO calculation and the data. A notable exception is the asymmetry for $eD \to h^{+}X$. For scattering off a proton target, some of the asymmetries are very badly described, with the theoretical results being much higher than the data. This is the case especially for the asymmetries for $ep \to \pi^{+}X$ at the lower scattering angle and for $ep \to h^{+}X$ for both angles. Here

It is difficult to draw clear-cut conclusions from these findings. It is possible that non-perturbative power-suppressed contributions are still relevant in kinematic regimes relevant for E155, which would invalidate the use of QCD perturbation theory. Assuming that this is not the case, one question concerns the role of QCD corrections beyond NLO. As we have seen, the asymmetries decrease when going from LO to NLO so that it is conceivable that this trend will continue when even higher orders are taken into account. While a NNLO calculation of the spin-averaged cross section has now been carried out for $\ell N \to \mathrm{jet}\, X$ [126], no such calculation exists presently for $\ell N \to hX$ or for the double-spin asymmetry. On the other hand, it may well be that the bulk of the beyond-NLO corrections can be estimated using QCD threshold resummation techniques. A related study has recently been performed for the process $\ell N \to \ell' hX$ in photoproduction (that is, with an observed final-state lepton) [128], and it was indeed found that the higher-order corrections further suppress the asymmetry. However, this suppression will likely not be significant enough to bridge the partly large differences

between data and theory we find.

Arguably the physically most interesting explanation for the observed discrepancies would resort to changes in the helicity parton distributions. In this context it is interesting to note that recent data for the spin asymmetry $A_{\rm LL}$ in photoproduction via $\mu N \to \mu' h X$ published by COMPASS [135] also show a trend that the deuteron asymmetry is better described by theory than the proton one. On the other hand, given that the up and down helicity distributions which are mostly relevant here are rather well constrained, and that the NLO proton asymmetries for E155 kinematics would need to decrease very strongly (see for example Figs. 3.4a and 3.4b), it appears unlikely that the discrepancies are due to the helicity parton distributions alone. Clearly, further studies are needed here.

We hope that other experiments can obtain new data for $A_{\rm LL}$ in single-inclusive lepton scattering. We thus have presented predictions for the spin asymmetry for HERMES, JLab12, COMPASS and the electron ion collider. We expect that latter to provide particularly valuable information. Data, if available with sufficient precision and large lever arm in kinematics, might help to clarify whether the process can be reliably described by perturbative QCD. As discussed in the Introduction, this would in turn have important ramifications also for our understanding of single-transverse spin asymmetries, since a proper understanding of the simpler leading-twist observables in these single-inclusive processes is required before one can reliably address the more complicated transverse spin effects.

Chapter 4.

Single Hadron Production in Transversely Polarized Nucleon Lepton Scattering

4.1. Introduction

Single transverse spin asymmetries (SSA) in high energy reactions have attracted much theoretical and experimental interest over the last 3 decades. Large asymmetries have been observed in hadron-hadron and hadron-lepton interactions when one hadron is transversely polarized [46, 47, 124, 136–144].

The present calculation establishes a theoretical framework to calculate the single spin asymmetry for the process $lh^{\uparrow} \to hX$ beyond leading order. The process is schematically shown in figure 4.1. The asymmetry is given by the numbers of final state hadrons with large transverse momentum $P_{h\perp}$ produced either on left or the right side of the blue plane in figure 4.1, spanned by the momentum and spin direction of the initial state polarized hadron. The resulting "left-right" asymmetry can also be achieved by flipping the spin of the initial state polarized hadron. This leads to the definition

$$A_N(p_h) \equiv \frac{\sigma(p_h, \vec{s}_T) - \sigma(p_h, -\vec{s}_T)}{\sigma(p_h, \vec{s}_T) + \sigma(p_h, -\vec{s}_T)} = \frac{\Delta\sigma(p_h, \vec{s}_T)}{\sigma(p_h)} \,, \tag{4.1}$$

where $\vec{s}_T$ is the transverse spin vector and p_h the four momentum of the final state hadron.

The theoretical description of these asymmetries is challenging, since the leading collinear contribution vanishes. Therefore, the dependence on a single transverse spin is power-suppressed. Over the last years, a lot of theoretical progress has been achieved to understand the underlying mechanism leading to large asymmetries. These developments

follow two different approaches. The first one is the transverse momentum dependent (TMD) approach, where the parton distribution or fragmentation functions depend on an intrinsic partonic transverse momentum. The second approach is the so called twist-3 quark-gluon correlation function approach established in the early 90's [65, 66], which is suited if the observed final state has a large transverse momentum. We have focused on the latter, for the process $lh^{\uparrow} \to hX$, where the transverse momentum and rapidity of the final state hadron is observed.

In the history of particle physics, QCD has been successful in predicting spin-averaged cross sections at large momentum transfers. Therefore, scattering experiments with high-$P_{h\perp}$ final states can be interpreted very well by utilizing the pQCD ansatz, as described copiously in this thesis. However, extension of the pQCD formalism to polarized scattering, has not been completely straightforward. In the late 70's, significant single transverse-spin asymmetries have been observed in Λ and pion production processes [145, 146]. Unfortunately, at that time it was shown that pQCD predicts a vanishing single transverse-spin asymmetry towards high $P_{h\perp}$ [147]. This puzzle could be solved by Efremov and Teryaev in the mid 80's. They pointed out that in pQCD a non vanishing single transverse-spin asymmetry can be obtained, if one goes beyond the leading power [148–150]. Finally, in the early 90's Qiu and Sterman could consistently evaluate single transverse-spin asymmetries in terms generalized factorization theorems in pQCD [65, 66, 151]. The asymmetries are presented as a convolution using a twist-3 quark-gluon correlation function for the polarized hadron, and a short-distance partonic function calculable in perturbative QCD. The twist-3 quark-gluon correlation function reflects further interactions of quarks with the color field of the hadron. In [152] an important subtle has been pointed out, which finally justifies the assumptions for the hadronic twist-3 matrix element made in [65].

Single transverse-spin asymmetries described as a twist-3 effect, are remarkably complex and due to the large number of contributions very costly to calculate. It comes out, that the relevant twist-3 matrix elements are pure imaginary. Therefore, we need imaginary phase arising from the hard scattering process to obtain a real contribution. As was shown in [149], imaginary contributions in the hard scattering part arise whenever an internal line of the hard scattering functions goes on-shell. Such contributions are called pole contributions and we may use the distribution identity

$$\frac{1}{x \pm \mathrm{i}\varepsilon} = \mathrm{PV}\frac{1}{x} \mp \mathrm{i}\pi\delta(x) \; . \tag{4.2}$$

The delta distribution usually makes the the external partons, coming from the polarized hadron kinematically dependent. It was shown in [65, 66] that these contributions, grow near the edge of phase space, i.e. the gluon wich couples to the polarized hadron becomes soft. This observation was the breakthrough for the twist-3 approach to explain single transverse-spin asymmetries, since it shows that the theoretical predicted asymmetry is of comparable size with the experimental data.

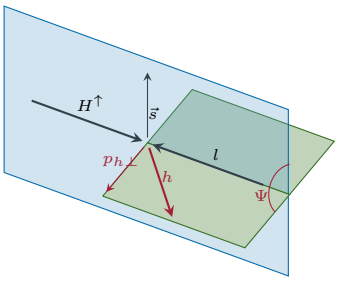

Figure 4.1.: Schematic SSA interaction. The blue plane is spanned by the beam direction and the hadron spin direction. The green one is given by the beam direction and the final state hadron direction.

Since that time, a lot of improvement for theoretical calculations using the twist-3 approach has been achieved. More pole contributions have been discovered, where other kinematical limits of the external particles are reached and of course the framework has been applied to various processes.

So far, however, phenomenological applications for the process $lh^\uparrow \to hX$ have been limited to zeroth order of QCD perturbation theory [52]. In general, for single spin asymmetries, QCD corrections to leading order are only available for more inclusive processes, like the transverse momentum weighted Drell-Yan cross Section [81] or semi-inclusive deep inelastic scattering [153, 154].

In the present chapter we investigate the NLO correction for the process $lh^\uparrow \to hX$. At NLO level various pole contributions arise from internal propagators in the hard scattering function. We focus on a contribution where the additional gluon from the polarized hadron becomes soft, which is the only pole contribution appearing already at LO.

Our aim for this project was to derive the leading-logarithmic contributions at NLO level, i.e. the prefactor of the logarithmic plus distribution. Utilizing some well established concepts of LO twist-3 calculations and prove their validity at NLO level, we were able to achieve our initial aspiration. Furthermore, we could calculate most of the real correction completely and we derived the complete ε-pole structure. This is a huge achievement for twist-3 calculations. In further work, we will derive the virtual NLO contribution, to complete our calculation. In this thesis we present our real correction result.

This chapter is organized as follows. In section 4.2 we introduce our notation and reformulate the unpolarized LO cross section, using a different notation as we used in chapter 2. In section 4.3, we perform the necessary collinear expansion of the hard scattering part and express the relevant twist-3 cross section in terms of gauge in-

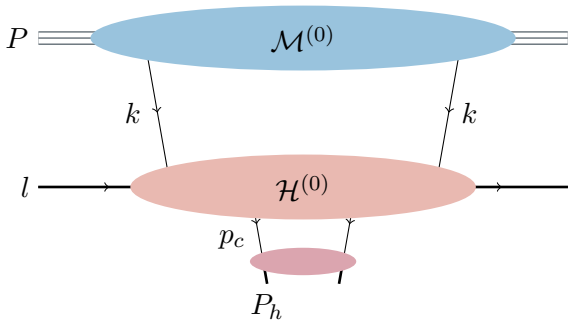

Figure 4.2.: Generic contribution to the single inclusive production of a hadron in lepton nucleon scattering. The upper blob represents the initial state nucleon and the middle blob the hard scattering process. The lower blob shows the fragmentation of a final state parton into a hadron.

variant quark-gluon correlation functions. In section 4.4, we recall the transverse spin dependent LO cross section, which was already discussed in [52]. The real correction at the soft gluon point is presented in section 4.5. In section 4.6 we present the twist 3 collinear subtraction terms and analyze the pole structure of the cross section. Finally, we present some of our analytical results in section 4.7.

4.2. Unpolarized leading order cross section

We consider the cross section $h(p) + l(l) \to \pi(P_h = z_c p_c) + X$ where the transverse momentum of the final state hadron $P_{h\perp}$ sets a hard scale, so that perturbative methods may be used to treat the cross section. X is the unobserved final state including the final state lepton. The Lorentz invariant cross section for this process can be written as

$$E_h \frac{d^3\sigma^{tw2}}{d^3P_h} = \frac{1}{S}\sum_{ac}\int \frac{\mathrm{d}z}{z^2}\frac{\mathrm{d}x}{x} f_a(x) D_c(z) H^{(0)}_{a,c} \tag{4.3}$$

where $H^{(0)}_{a,c}$ is the partonic hard scattering function. In equation (4.3) $f_a(x)$ is the parton distribution function (PDF) for the incoming parton a in the initial state nucleon and $D_c(z)$ the corresponding fragmentation function for parton c fragmenting into the observed hadron. We found it useful for reasons that will become clear in the next section, that we seperate the projectors onto the non-perturbative hadronic initial state matrix element from the hard scattering function

$$H^{(0)}_{a,c} = \frac{1}{2}\frac{1}{N_c}\mathrm{Tr}\left[\mathcal{H}^{(0)}_{a,c}(xp, l, p_c)\frac{1}{2}x\not{p}\right] \tag{4.4}$$

where the trace is in Dirac and color space for the quark line. The trace over the lepton part is included in $\mathcal{H}$.

The function $\mathcal{H}^{(0)}$ is perturbative and can be expanded in terms of α_s

$$\mathcal{H}^{(0)}_{a,c} = \mathcal{H}^{(0)}_{\mathrm{LO}}\delta_{ac} + \frac{\alpha_s}{\pi}\mathcal{H}^{(0)}_{\mathrm{NLO},a,c} + \mathcal{O}(\alpha_s^2) \ . \tag{4.5}$$

The leading order expression is given by

$$H^{(0)}_{\mathrm{LO},a,c} = \frac{1}{2N_c}\mathrm{Tr}\left[\mathcal{H}^{(0)}_{\mathrm{LO}}\frac{1}{2}x\not{p}\right]\delta_{ac} = 2\alpha_{em}e_a^2\frac{s^2+t^2}{u^2}\delta(s+t+u)\delta_{ac} \ , \tag{4.6}$$

where α_{em} is the fine structure constant and e_a is the quark's fractional charge. In equation (4.6) we used the partonic Mandelstam variables defined by

$$s = (xp + l)^2 \ , \tag{4.7a}$$
$$t = (xp - p_c)^2 \ , \tag{4.7b}$$
$$u = (l - p_c)^2 \ . \tag{4.7c}$$

We want to mention that the notation in this chapter differs from chapter 2 in this thesis. But, if we compare (4.6) with equation (2.4) we conclude, that the results remain the same.

4.3. Collinear expansion and parton correlations

In this section, we present the framework of the twist-3 calculation to calculate the SSA in the process $lh^{\uparrow} \to hX$. To extract the relevant twist-3 contribution to the cross section, we have to analyze the two contributions shown in figures 4.2 and 4.3. In these diagrams the partons from the polarized nucleon represented by the upper blob $\mathcal{M}^{(i)}$ are emitted into the hard scattering part $\mathcal{H}^{(i)}$. The superscripts on $\mathcal{H}$ and $\mathcal{M}$ denote the number of coherent gluons emitted from the polarized nucleon. The hard scattering process, that involves the partons coming from $\mathcal{M}$ and the incoming lepton, produce a hard final state parton with momentum p_c, which finally fragments into the observed hadron with momentum P_h. This fragmentation is denoted by the lowest blob. Therefore, the contribution to the twist-3 cross section can be written as

$$\sigma \sim \sum_{c=q,g}\int\frac{\mathrm{d}z}{z^2}D_c(z)\ w_c(xp, l, p_c = P_h/z) \ , \tag{4.8}$$

where we have factored the twist-2 fragmentation function away from the polarized hadronic- and the hard part, which is included in the function w_c. For simplicity, we do

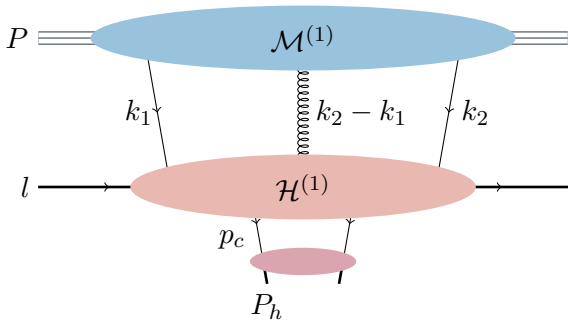

Figure 4.3.: Generic twist-3 contribution to the single inclusive production of a hadron in lepton nucleon scattering. The upper blob represents the initial state transversely polarized nucleon and the middle blob the hard scattering process. The additional gluon connecting the middle and lower blob, is responsible for the twist-3 effect induced by the polarized hadron. The lower blob shows the unpolarized fragmentation of a final state parton.

not explicitly write down the dependence on the parton type in the further discussion. In addition, we omit the dependence from D and w on factorization and renormalization scales, which are present in a NLO calculation. We will keep that in mind, when we get back to the NLO cross section in the next paragraph. Then w is given by

$$w(xp, l, p_c) = \int \frac{\mathrm{d}^4 k}{(2\pi)^4} \mathrm{Tr}\left[\mathcal{M}^{(0)}(k)\mathcal{H}^{(0)}(k, l, p_c)\right] + \int \frac{\mathrm{d}^4 k_1}{(2\pi)^4} \frac{\mathrm{d}^4 k_2}{(2\pi)^4} \mathrm{Tr}\left[\mathcal{M}^{(1),\sigma}(k)\mathcal{H}^{(1)}_{\sigma}(k_1, k_2, l, p_c)\right] , \tag{4.9}$$

where the trace is taken in Dirac and color space for the partonic part of $\mathcal{H}$ and the appropriate projectors coming from $\mathcal{M}$. Note, there is a second trace completely contained in $\mathcal{H}$ coming from the leptonic part of the scattering diagrams. The appropriate spin dependent nucleon matrix elements are given by [152]

$$\mathcal{M}^{(0)}_{ij}(k) = \int \mathrm{d}^4\xi \mathrm{e}^{\mathrm{i}k\xi} \langle pS_\perp | \overline{\Psi}_i(0)\Psi_j(\xi) | pS_\perp \rangle \tag{4.10a}$$

$$\mathcal{M}^{(1),\sigma}_{ij}(k_1, k_2) = \int \mathrm{d}^4\xi \int \mathrm{d}^4\eta \, \mathrm{e}^{\mathrm{i}k_1\xi}\mathrm{e}^{\mathrm{i}(k_2-k_1)\eta} \langle pS_\perp | \overline{\Psi}_i(0) g A^\sigma(\eta)\Psi_j(\xi) | pS_\perp \rangle \tag{4.10b}$$

where Ψ represents quark fields, p the momentum of the incoming nucleon and the vector n^μ can be regarded as light like with $n \cdot p = 1$. The ϵ-tensor has the convention $\epsilon^{0123} = 1$, the spin vector satisfies $S_\perp^2 = -1, S_\perp \cdot p = S_\perp \cdot n = 0$ and A^σ represents the additional coherent gluon field connecting the hard and soft part in figure 4.3. In order to extract the twist-3 contribution from equation (4.9) we expand the hard parts $\mathcal{H}^{(0)}$ and $\mathcal{H}^{(1)}$ with respect to the incoming parton momenta k, respectively k_1 and k_2, in the limit that they are collinear to the polarized hadron. This is the collinear expansion

[65–67, 155], which is always applied in the collinear factorization ansatz. Therefore, we have for the first term in equation (4.9)

$$\mathcal{H}^{(0)}(k,l,p_c) = \mathcal{H}^{(0)}(xp,l,p_c) + \left.\frac{\partial \mathcal{H}^{(0)}(k,l,p_c)}{\partial k^\alpha}\right|_{k=xp} \omega^\alpha{}_\beta\, k^\beta + \mathcal{O}((k_\perp)^2)\,, \tag{4.11}$$

with $n\cdot k = x$ and $\omega^{\alpha\beta} = g^{\alpha\beta} - p^\alpha n^\beta$. The terms $\mathcal{O}((k_\perp)^2)$ are twist-4 or higher and therefore irrelevant for our analysis. Using this expansion and performing the integration over k^- and $k_\perp$ component, we can rewrite the first part of equation (4.9) as

$$\begin{aligned}&\int \frac{\mathrm{d}^4k}{(2\pi)^4}\mathrm{Tr}\left[\mathcal{M}^{(0)}(k)\mathcal{H}^{(0)}(k,l,p_c)\right]\\ &\quad= \int \mathrm{d}x \mathrm{Tr}\left[M^{(0)}(x)\mathcal{H}^{(0)}(xp,l,pc) + \mathrm{i}\omega^\alpha{}_\sigma M^{(0),\sigma}_\partial(x)\left.\frac{\partial\mathcal{H}^{(0)}(k,l,p_c)}{\partial k_\alpha}\right|_{k=xp}\right]\end{aligned} \tag{4.12}$$

where we used $\omega^\alpha{}_\sigma\, k^\sigma \to \omega^\alpha{}_\sigma\, \partial^\sigma$. The remaining derivative in the second term has been shifted on the quark field by partial integration denoted by the subscript ∂ on M. Then the light cone parton correlators read

$$M^{(0)}_{ij}(x) = \int \frac{\mathrm{d}\kappa}{2\pi}\mathrm{e}^{\mathrm{i}\kappa x}\,\langle pS_\perp|\,\overline{\Psi}_i(0)\Psi_j(\kappa n)\,|pS_\perp\rangle \tag{4.13a}$$

$$M^{(0),\sigma}_{\partial,ij}(x) = \int \frac{\mathrm{d}\kappa}{2\pi}\mathrm{e}^{\mathrm{i}\kappa x}\,\langle pS_\perp|\,\overline{\Psi}_i(0)\partial^\sigma\Psi_j(\kappa n)\,|pS_\perp\rangle\ . \tag{4.13b}$$

The light cone matrix elements representing the transversely polarized hadron can be decomposed into its Dirac matrix structures. Obviously, only chiral even contributions will survive in the Dirac trace structure. Therefore, up to twist-4 or higher and chiral-odd contributions the matrix element is given by

$$M^{(0)}_{ij}(x) = (\gamma_5 \not{S}_\perp)_{ij} g_T(x)\,, \tag{4.14}$$

with $g_T(x)$ the chiral-even twist-3 quark distribution defined in [156]. Considering these matrix elements, we see immediately that the first term in equation (4.9) will not contribute in a leading order analysis for $\mathcal{H}^{(0)}$ [155]. This is due to the fact that $\mathcal{H}^{(0)}$ is manifestly real in the born approximation. Considering equations (4.12) and (4.13) we conclude that $M^{(0)}(x)$ and $\mathrm{i}\omega^\alpha{}_\beta M^{(0),\beta}_\partial(x)$ produce an overall i in the cross section formula. Therefore, equation (4.12) will not contribute to the cross section unless $\mathcal{H}^{(0)}$ provides an imaginary phase. As was shown in [155] this is not the case for the LO approximation. We want to stress, that in a NLO analysis the function $\mathcal{H}^{(0)}$ may obtain imaginary parts. This is evoked by internal propagators that reach their on-shell limit

in the edges of phase space in the real correction or by loop integration in case of virtual corrections. Consequently, we expect a contribution from $g_T(x)$ at this order. We will leave that for future research.

To investigate the second term in equation (4.9) we start with the collinear expansion of the hard scattering part $\mathcal{H}^{(1)}$, similarly to the first term in (4.9). We are considering now the middle blob of figure 4.3, where the momentum flow is clearly more complex compared to diagram 4.2. This is due to the additional coherent gluon carrying momentum $k_2 - k_1$ which is an additional degree of freedom. We define

$$\mathcal{H}^{(1)}(k_1, k_2, l, pc) \equiv \mathcal{H}^{(1)}_\beta(k_1, k_2, l, pc)p^\beta \ , \tag{4.15}$$

where its collinear expansion is given by

$$\mathcal{H}^{(1)}(k_1, k_2, l, pc) \ = \mathcal{H}^{(1)}(x_1 p, x_2 p, l, pc) + \sum_{i=1,2} \left.\frac{\partial \mathcal{H}^{(1)}(k_1, k_2, l, pc)}{\partial k_i^\alpha}\right|_{k_i = x_i p} \omega^\alpha{}_\sigma k_i^\sigma \ . \tag{4.16}$$

In the following discussion, we refer to the replacement $k_1 \to x_i p$ always as the collinear limit. We can insert the collinear expansion equation (4.16) into the second part of equation (4.9). We obtain

$$\begin{aligned}
&\int \frac{\mathrm{d}^4 k_1}{(2\pi)^4} \frac{\mathrm{d}^4 k_2}{(2\pi)^4} \ \mathrm{Tr}\left[\mathcal{M}^{(1),\sigma}(k)\mathcal{H}^{(1)}_\sigma(k_1, k_2, l, p_c)\right] \qquad (4.17)\\
&= \int \mathrm{d}x_1 \int \mathrm{d}x_2 \ \mathrm{Tr}\left[M^{(1)}_\sigma(x_1, x_2) n^\sigma \mathcal{H}^{(1)}(x_1 p, x_2 p, l, pc)\right] \\
&\quad + \int \mathrm{d}x_1 \int \mathrm{d}x_2 \ \mathrm{Tr}\left[\omega^\alpha{}_\sigma M^{(1),\sigma}(x_1, x_2)\mathcal{H}^{(1)}_\alpha(x_1 p, x_2 p, l, pc)\right] \\
&\quad + \int \mathrm{d}x_1 \int \mathrm{d}x_2 \sum_{j=1,2} \mathrm{Tr}\left[\mathrm{i}\omega^\alpha{}_\sigma M^{(1),\sigma}_{\partial_j}(x_1, x_2) \left.\frac{\partial \mathcal{H}^{(1)}(k_1, k_2, l, pc)}{\partial k_j^\alpha}\right|_{k_i = x_i p}\right] \ .
\end{aligned}$$

We shift the derivative on the light cone correlation functions by partial integration with respect to x_1 and x_2, where $x_i = n \cdot k_i$. Then the correlation functions are given by,

$$M^{(1),\sigma}(x_1, x_2) = \int \frac{\mathrm{d}\kappa}{2\pi} \int \frac{\mathrm{d}\lambda}{2\pi} \mathrm{e}^{\mathrm{i}\kappa x_1} \mathrm{e}^{\mathrm{i}\lambda(x_2 - x_1)} \left\langle pS_\perp \right| \overline{\Psi}(0) g A^\sigma(\lambda n) \Psi(\kappa n) \left| pS_\perp \right\rangle \tag{4.18a}$$

$$\begin{aligned}
M^{(1),\sigma}_{\partial 1}(x_1, x_2) = &\int \frac{\mathrm{d}\kappa}{2\pi} \int \frac{\mathrm{d}\lambda}{2\pi} \mathrm{e}^{\mathrm{i}\kappa x_1} \mathrm{e}^{\mathrm{i}\lambda(x_2 - x_1)} \qquad (4.18b)\\
&\times \left\langle pS_\perp \right| \overline{\Psi}(0) g A^\beta(\lambda n) n_\beta \partial^\sigma(\lambda n) \Psi(\kappa n) \left| pS_\perp \right\rangle
\end{aligned}$$

$$\begin{aligned}
M^{(1),\sigma}_{\partial 2}(x_1, x_2) = &\int \frac{\mathrm{d}\kappa}{2\pi} \int \frac{\mathrm{d}\lambda}{2\pi} \mathrm{e}^{\mathrm{i}\kappa x_1} \mathrm{e}^{\mathrm{i}\lambda(x_2 - x_1)} \qquad (4.18c)\\
&\times \left\langle pS_\perp \right| \overline{\Psi}(0) g \left[\partial^\sigma A^\beta(\lambda n) n_\beta + A^\beta(\lambda n) n_\beta \partial^\sigma\right] \Psi(\kappa n) \left| pS_\perp \right\rangle \ .
\end{aligned}$$

where it is important to note that $M^{(1),\perp}$ is power suppressed by a factor $1/p^+$ compared to $M^{(1),+}$ and gives therefore negligible subleading contributions to the twist-3 cross section. For the following discussion it is useful to further rewrite the correlators $M^{(1),\sigma}_{\partial 1}$ and $M^{(1),\sigma}_{\partial 2}$ as

$$M^{(1),\sigma}_{\partial 1}(x_1,x_2) - M^{(1),\sigma}_{\partial 2}(x_1,x_2) = -M^{(1),\sigma}_{F}(x_1,x_2) - \tilde{M}^{(1),\sigma}(x_1,x_2)\,, \tag{4.19}$$

We introduced two new matrix elements $M^{(1),\sigma}_{F}(x_1,x_2)$ and $\tilde{M}^{(1),\sigma}(x_1,x_2)$, where we can use equations (4.19) and (4.18) to arrange them as

$$\begin{aligned} M^{(1),\sigma}_{F}(x_1,x_2) &= \int\frac{\mathrm{d}\kappa}{2\pi}\int\frac{\mathrm{d}\lambda}{2\pi}\mathrm{e}^{\mathrm{i}\kappa x_1}\mathrm{e}^{\mathrm{i}\lambda(x_2-x_1)} \\ &\quad\times\langle pS_\perp|\,\overline{\Psi}(0)g\left[\partial^\sigma A^\beta(\lambda n)-\partial^\beta A^\sigma(\lambda n)\right]n_\beta\Psi(\kappa n)\,|pS_\perp\rangle\ , \end{aligned} \tag{4.20a}$$

$$\begin{aligned} \tilde{M}^{(1),\sigma}(x_1,x_2) &= \int\frac{\mathrm{d}\kappa}{2\pi}\int\frac{\mathrm{d}\lambda}{2\pi}\mathrm{e}^{\mathrm{i}\kappa x_1}\mathrm{e}^{\mathrm{i}\lambda(x_2-x_1)} \\ &\quad\times\langle pS_\perp|\,\overline{\Psi}(0)g\partial^\sigma A^\beta(\lambda n)n_\beta\Psi(\kappa n)\,|pS_\perp\rangle \\ &= \mathrm{i}(x_1-x_2)M^{(1),\sigma}(x_1,x_2)\,, \end{aligned} \tag{4.20b}$$

where the quantity in the first line can be identified as the F-type correlation function given in equation (4.26a) and [65, 155, 157]. It was discussed in [155] that the two terms in (4.20a) contribute at the same order with respect to the power of the large scale p^+.

If we insert these correlation functions into equation (4.17), we see immediately that the first term vanishes for the same reason as the first term in (4.9). The remaining terms can be rearranged as

$$\begin{aligned} &w(xp,l,p_c) \\ &=\int\mathrm{d}x_1\int\mathrm{d}x_2\ \mathrm{Tr}\left[\mathrm{i}\omega^\alpha{}_\beta M^{(1),\beta}_F(x_1,x_2)\,\frac{\partial\mathcal{H}^{(1)}(k_1,k_2,l,pc)}{\partial k_2^\alpha}\bigg|_{k_i=x_ip}\right] \\ &\quad+\int\mathrm{d}x_1\int\mathrm{d}x_2\ \mathrm{Tr}\Bigg[\omega^\alpha{}_\beta M^{(1),\beta}(x_1,x_2) \\ &\qquad\times\left\{(x_2-x_1)\,\frac{\partial\mathcal{H}^{(1)}(k_1,k_2,l,pc)}{\partial k_2^\alpha}\bigg|_{k_i=x_ip}+\mathcal{H}^{(1)}_\alpha(x_1p,x_2p,l,p_c)\right\}\Bigg] \\ &\quad+\int\mathrm{d}x_1\int\mathrm{d}x_2\ \mathrm{Tr}\Bigg[\omega^\alpha{}_\beta M^{(1),\beta}_{\partial 1}(x_1,x_2) \\ &\qquad\times\left\{\frac{\partial\mathcal{H}^{(1)}(k_1,k_2,l,pc)}{\partial k_1^\alpha}+\frac{\partial\mathcal{H}^{(1)}(k_1,k_2,l,pc)}{\partial k_2^\alpha}\right\}\bigg|_{k_i=x_ip}\Bigg]\,. \end{aligned} \tag{4.21}$$

As discussed in [155] the hard function $\mathcal{H}^{(1)}_{\alpha}(k_1, k_2, l, pc)$ fulfills the Ward identity for the coherent gluon

$$(k_2 - k_1)^{\alpha}\mathcal{H}^{(1)}_{\alpha}(k_1, k_2, l, pc) = 0 \tag{4.22}$$

This is indeed a most useful equality and is used copiously along our calculation. By using the identity above and equation (4.15) we conclude that

$$\left\{ \frac{\partial\mathcal{H}^{(1)}(k_1, k_2, l, pc)}{\partial k_1^{\alpha}} + \frac{\partial\mathcal{H}^{(1)}(k_1, k_2, l, pc)}{\partial k_2^{\alpha}} \right\}\Bigg|_{k_i = x_i p} = 0 \tag{4.23}$$

and

$$(x_2 - x_1)\, \frac{\partial\mathcal{H}^{(1)}(k_1, k_2, l, pc)}{\partial k_2^{\alpha}}\Bigg|_{k_i = x_i p} + \mathcal{H}^{(1)}_{\alpha}(x_1 p, x_2 p, l, p_c) = 0\ . \tag{4.24}$$

Therefore, the contribution to the twist-3 cross section arises solely from the first term in equation (4.21). Finally, we have

$$w(xp, l, p_c) = \int \mathrm{d}x_1 \int \mathrm{d}x_2\ \mathrm{Tr}\left[\mathrm{i}\omega^{\alpha}{}_{\beta} M_F^{(1),\beta}(x_1, x_2)\, \frac{\partial\mathcal{H}^{(1)}(k_1, k_2, l, pc)}{\partial k_2^{\alpha}}\Bigg|_{k_i = x_i p} \right]\ . \tag{4.25}$$

The name F-type correlation function, which we have defined in equations (4.20a) and (4.19), originates from the fact that in this definition the field strength tensor $F^{\mu\nu}n_{\nu}$ is inserted in the hadronic matrix element to generate the coherent gluon. The non-Abelian part of the field strength, will not contribute to our order. In the literature, two choices have been made to achieve gauge invariant twist-3 quark-gluon matrix elements. The matrix elements are eventually expressed in terms of either the the gluon field strength tensor $F^{\mu\nu}n_{\nu}$, or the transverse components of the covariant derivative, $D^{\mu} = \partial^{\mu} - \mathrm{i}gA^{\mu}$, with $\mu = \perp$. We refer to them as F-type correlation function or D-type correlation function respectively.

We can expand the F-type and D-type correlation functions as [155, 157]

$$M^{(1),\sigma}_{F,ij}(x_1, x_2) = \frac{M_N}{4}(\not{p})_{ij}\epsilon^{\sigma pnS_{\perp}} G_F(x_1, x_2) + \mathrm{i}\frac{M_N}{4}(\gamma_5\not{p})_{ij} S^{\sigma}_{\perp}\tilde{G}_F(x_1, x_2) \tag{4.26a}$$

$$M^{(1),\sigma}_{D,ij}(x_1, x_2) = \frac{M_N}{4}(\not{p})_{ij}\epsilon^{\sigma pnS_{\perp}} G_D(x_1, x_2) + \mathrm{i}\frac{M_N}{4}(\gamma_5\not{p})_{ij} S^{\sigma}_{\perp}\tilde{G}_D(x_1, x_2) \tag{4.26b}$$

up to twist-4 corrections. We introduce here the nucleon mass M_N to keep the non-perturbative Qiu-Sterman function [65–67] $G_F(x_1, x_2)$ dimensionless. The nucleon mass

seems appropriate here, since it represents a natural scale for chiral-symmetry breaking [155, 157]. The non perturbative functions satisfy the properties

$$G_F(x_1, x_2) = G_F(x_2, x_1) \,, \tag{4.27a}$$
$$\tilde{G}_F(x_1, x_2) = -\tilde{G}_F(x_2, x_1) \,, \tag{4.27b}$$
$$G_D(x_1, x_2) = -G_D(x_2, x_1) \,, \tag{4.27c}$$
$$\tilde{G}_D(x_1, x_2) = \tilde{G}_D(x_2, x_1) \,. \tag{4.27d}$$

The set of four functions, to define the non perturbative input in the twist-3 matrix elements is overcomplete. It is possible to use the QCD equations of motion to relate the functions

$$G_D(x_1, x_2) = \mathrm{PV}\frac{1}{x_1 - x_2} G_F(x_1, x_2) \,, \tag{4.27ea}$$
$$\tilde{G}_D(x_1, x_2) = \delta(x_1 - x_2)\tilde{g}(x_1) + \mathrm{PV}\frac{1}{x_1 - x_2}\tilde{G}_F(x_1, x_2) \,, \tag{4.27eb}$$

where PV denotes the principle value. The function $\tilde{g}(x_1)$ can be expressed in terms of the quark helicity distribution and the F-type functions [157]. In the following discussion we use the F-type functions $\left\{G_F(x_1, x_2),\ \tilde{G}_F(x_1, x_2)\right\}$ as a complete set of twist-3 correlation functions. The choice seems convenient, since the F-type functions are less singular then the D-type ones.

In equation (4.21) the first term contributes to the cross section only. In completion with equation (4.26a) we conclude, that in order to give a real contribution to the cross section the quantity $\partial\mathcal{H}^{(1)}/\partial k_2^\alpha|_{c.l.}$ must provide an imaginary part. In our calculation we focus on the so called pole contribution, where the imaginary part is provided from an internal propagator of $\mathcal{H}^{(1)}$ which is on its mass shell. In the subsequent sections, we will elaborate that $\mathcal{H}^{(1)}$ contains several propagators that can reach their on shell limit. We arrange them into four classes that belong to the following reduced propagators

$$\frac{1}{x_1 - x_2 + \mathrm{i}\epsilon} = \mathrm{PV}\frac{1}{x_1 - x_2} - \mathrm{i}\pi\delta(x_1 - x_2) \,, \tag{4.6a}$$
$$\frac{1}{x_i + \mathrm{i}\epsilon} = \mathrm{PV}\frac{1}{x_i} - \mathrm{i}\pi\delta(x_i) \,, \tag{4.6b}$$
$$\frac{1}{x_i - a + \mathrm{i}\epsilon} = \mathrm{PV}\frac{1}{x_i - a} - \mathrm{i}\pi\delta(x_i - a) \,, \tag{4.6c}$$
$$\frac{1}{f(q) + \mathrm{i}\epsilon} = \mathrm{PV}\frac{1}{f(q)} - \mathrm{i}\pi\delta(f(q)) \,, \tag{4.6d}$$

where PV denotes the "principle value". Equation (4.6a) produces a pole called soft-gluon pole (SGP), equation (4.6b) produces a soft-fermion pole (SFP) and equation (4.6c) a hard pole (HP). The pole in equation (4.6d) is a different pole, since it provides no restrictions on the collinear momentum fractions x_1 and x_2. The origin relies

in certain NLO corrections, coming from configurations where one of the unobserved particles is collinear to another external particle. Therefore, internal propagators of $\mathcal{H}^{(1)}$ can reach their on shell limit, coming from these collinear configurations. We call them collinear poles (CP).

4.4. Leading order pole contribution

The pole contribution for the process $h^{\uparrow}l \to hX$ at LO arises solely from the soft-gluon pole. The contributing diagrams are shown in figure 4.4, where the red bar denotes the internal propagator that is responsible for the imaginary part. This propagator is is the only propagator in the leading order approximation that can reach its on shell limit. The requirement for a large $p_{h\perp}$ for the final state hadron keeps the photon propagator off-shell at leading order. The quark propagator in the left diagram in figure 4.4 is given by

$$\frac{1}{\not{p}_c - (\not{k}_2 - \not{k}_1) + \mathrm{i}\varepsilon} \to \frac{(-\mathrm{i}\pi)}{2p \cdot p_c}\delta(x_1 - x_2) \tag{4.7}$$

where we take take the on-shell and collinear limit and use (4.2) to extract the imaginary phase from the propagator.

So far, we omitted the color index from the coherent gluon on $M^{(1)}$ and $\mathcal{H}^{(1)}$. Including that, the F-type correlation function at the soft gluon point, i.e. neglecting the second term of equation (4.26a), reads

$$M_{F,ij}^{\sigma,g}(x_1, x_2) = \frac{M_N}{4}\frac{2}{N_c^2 - 1}(\not{p}T^g)_{ij}\epsilon^{\sigma pnS_\perp}G_F(x_1, x_2) + \dots \ . \tag{4.8}$$

where ij are now associated with both color and Dirac indices. We regard p and n as light like vectors with $p^- = p_\perp = 0$, $n^+ = n_\perp = 0$ and $p \cdot n = 1$.

The hard part for LO SSA is derived by performing the collinear expansion of the diagrams in figure 4.4. We call the sum of these diagrams $\mathcal{H}^{(1)\sigma,g}(k_1, k_2, l, p_c)$, where σ and g are Lorentz and color indices of the additional twist-3 gluon. In the expressions for the leading order twist-2 cross section we explicitly write down the dependence on the parton species. In leading order the initial and the final state quark must be the same, even at twist-3 level. Therefore, we omit them in the following discussion. We can express the spin dependent cross section by using equations (4.8),(4.9),(4.22) and

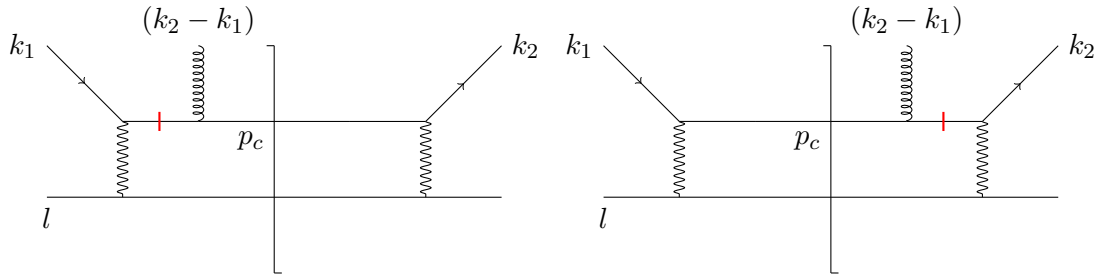

Figure 4.4.: LO contributions to SSA in the $ql \to ql$ channel, where the final state lepton is unobserved. The red lines denote the quark propagators causing the SGP by reaching their on shell limits.

(4.21) as

$$E_h \frac{d^3\sigma^{tw3}}{\mathrm{d}^3 P_h} = \frac{1}{S} \sum_{ac} \int \frac{\mathrm{d}z\, \mathrm{d}x_1\, \mathrm{d}x_2}{z^2} D_c(z) \times \mathrm{Tr}\left[\mathrm{i}\omega^{\alpha}{}_{\sigma} \left. \frac{\partial \mathcal{H}^{(1),g}_{\mathrm{LO}}(k_1, k_2, l, p_c) p_\beta}{\partial k^{\alpha}_{2\perp}} \right|_{\mathrm{c.l.}} M_F^{\sigma,g}(x_1, x_2) \right] , \tag{4.9}$$

where c.l. denotes the collinear limit given by $k_{1,2} \to x_{1,2} p$. The coherent soft gluon leaves the inner Dirac structure of the far off shell interaction unspoiled. Therefore, it is not necessary to carry out the derivative with respect to $k_{2\perp}$ on the twist-3 function. It has been shown [158, 159] that it turns into a derivative on the twist-2 function with respect to the momentum of the final state quark, which is plainly less exhausting to carry out. Then we have,

$$\left. \frac{\partial \mathcal{H}^{(1),g}_{\mathrm{LO}}(k_1, k_2, l, p_c) p_\sigma}{\partial k^{\alpha}_{2\perp}} \right|_{\mathrm{c.l.}} = \frac{1}{x_1 - x_2 + i\varepsilon} \frac{\mathrm{d}}{\mathrm{d}p_c^{\alpha}} \left(\mathcal{H}^{(0)}_{\mathrm{LO}}(x_1 p, l, p_c) \Big|_{\not{p}_c \to T^g \not{p}_c} \right) \tag{4.10}$$

where we can chose $\alpha = \perp$ because of the presence of the ϵ-tensor $\epsilon^{\alpha pns_\perp}$ in the cross section. The equation above has been named in the literature as the "Master Formula" [158, 159] and considerably simplifies the calculation. The replacement $\not{p}_c \to T^g \not{p}_c$ is necessary due to the color structure of the coherent gluon. Equation (4.10) includes the remnant of the internal propagator of $\mathcal{H}^{(1)}$ that produces the pole and the imaginary phase see equation (4.6a).

When we carry out the derivative in equation (4.10) we have to bear in mind that p_c is an on shell momentum that forces p_c to fulfill $p_c^2 = 0$. Therefore, we choose the plus component to be the dependent variable, i.e.

$$p_c^2 = 0 \quad \leftrightarrow \quad p_c = \left(p_c^+ = \frac{\vec{p}_\perp^{\,2}}{2p_c^-}, p^-, \vec{p}_\perp \right) . \tag{4.11}$$

The differential operator with respect to p_c is then given by,

$$\frac{d}{dp_c^\alpha} = \frac{\partial}{\partial p_c^\alpha} - \frac{p_{c\alpha} p^\lambda}{p \cdot p_c} \frac{\partial}{\partial p_c^\lambda} \,. \tag{4.12}$$

We rewrite the partonic part of the cross section in terms of the variables $w = \frac{-u}{s+t}$ and $v = 1 + \frac{t}{s}$ in analogy to the unpolarized process see chapter 2. The differentiation on p_c can then be rewritten as

$$\frac{d}{dp_c^\alpha} = \frac{2}{sv} \left(\frac{1}{v-1} p_{c\alpha} + l_\alpha \right) \frac{\partial}{\partial w} \,. \tag{4.13}$$

By using equations (4.8, 4.9, 4.10, 4.13) we obtain the twist-3 cross section,

$$\begin{aligned} E_h \frac{\mathrm{d}^3\sigma^{\mathrm{tw3}}}{\mathrm{d}^3 P_h} = \frac{\pi M_N}{S} \epsilon^{\alpha p n S_\perp} \sum_{ac} \int \frac{\mathrm{d}z}{z^2} D_c(z) \int \frac{\mathrm{d}x}{x} G_F(x,x) \\ \times \frac{2}{sv} \left(\frac{1}{v-1} p_{c\alpha} + l_\alpha \right) \frac{\partial H_{\mathrm{LO}}^{\prime(0)}(s,v,w)}{\partial w} \end{aligned} \tag{4.14}$$

where $H_{\mathrm{LO}}^{\prime(0)}$ can be calculated using the same methods as in the unpolarized case in equation (4.4). The prime on the function $H_{\mathrm{LO}}^{\prime(0)}$ indicates that the result must be modified by the color structure arising from the coherent gluon. The hard function is given by

$$H_{\mathrm{LO}}^{\prime(0)}(s,v,w) = \mathrm{Tr} \left[\frac{x \not{p} T^g}{(N_c^2 - 1)} \, \mathcal{H}_{\mathrm{LO}}^{(0)}(xp, l, p_c) \Big|_{\not{p}_c \to T^g \not{p}_c} \right] \tag{4.15}$$

where the function $\mathcal{H}_{\mathrm{LO}}^{(0)}$ is the same as defined in equation (4.5) for the twist-2 case. Therefore, we can rewrite

$$H_{\mathrm{LO}}^{\prime(0)} = C_{\mathrm{LO}} \tilde{\sigma}_{\mathrm{LO}}^{\mathrm{tw2}}(s,v) \delta(1-w) \,, \tag{4.16}$$

where $\tilde{\sigma}_{\mathrm{LO}}(s,v)$ is obtained by calculating the twist-2 2→2 Feynman diagrams for the process $ql \to ql$ and absorb the color algebra into the twist-3 leading order color factor $C_{\mathrm{LO}} = 1$.

$$\tilde{\sigma}_{\mathrm{LO}}^{\mathrm{tw2}}(s,v) = 2\alpha_{em}^2 e_a^2 \frac{1}{sv} \frac{1+v^2}{(1-v)^2} \tag{4.17}$$

We can further simplify equation (4.14) by using partial integration and the scale-invariance property $\tilde{\sigma}_{\mathrm{LO}}^{\mathrm{tw2}}$ [1], and rewrite the integrals in terms of v and w using

$$x = \frac{1-v}{vw} \frac{U}{T} \quad \text{and} \quad z = \frac{-T}{(1-v)S} \,. \tag{4.18}$$

[1] The scale invariance property from σ_{LO} in terms of the standard partonic Mandelstam variables is given by $\tilde{\sigma}_{\mathrm{LO}}^{\mathrm{tw2}}(s,t,u) = \tilde{\sigma}_{\mathrm{LO}}^{\mathrm{tw2}}(\lambda s, \lambda t, \lambda u)$.

Thus, we have

$$E_h \frac{\mathrm{d}^3\sigma^{tw3}}{\mathrm{d}^3 P_h} = C_{\mathrm{LO}} \frac{-\pi M_N}{T} \epsilon^{\alpha pnS_\perp} \sum_c \int_{v_{min}}^{v_{max}} \mathrm{d}v \int_{w_{min}}^{1} \frac{\mathrm{d}w}{w} D_c(z) \frac{2}{sv} \left(\frac{1}{v-1} p_{c\alpha} + l_\alpha \right) \tag{4.19}$$
$$\times \left\{ G_F(x,x) - x \frac{\mathrm{d}G_F(x,x)}{\mathrm{d}x} \right\} \tilde{\sigma}_{\mathrm{LO}}(s,v) \delta(1-w) \ ,$$

where the boundaries of integration are given by $v_{min} = U/(T+U)$, $v_{max} = 1 + \frac{T}{S}$ and $w_{min} = \frac{(1-v)U}{vT}$. Therefore, the twist-3 leading order partonic cross section is given by

$$\tilde{\sigma}_{\mathrm{LO}}^{\mathrm{tw3}}(s,v) = 2\alpha_{em}^2 e_a^2 \frac{-1}{s^2 v^2} \frac{1+v^2}{(1-v)^2} \tag{4.20}$$

Finally we make the observation, that the interplay of the master formula (4.10) and the scale invariance property of the partonic twist-2 cross section, considerably simplifies the twist-3 cross section. This is a very helpful tool and we use exactly the same mechanisms for parts of the NLO calculation. The presented LO calculation in this chapter is in accordance with the LO calculation in [52] for this process. We mention that the results in [52] are in a frame where l and p are collinear. In our calculation we keep it more general, where l and p are not necessarily collinear to each other. Therefore, we have the term proportional l^α present in the cross section formula. Due to the antisymmetry property of the ϵ-tensor, the term would cancel if we choose $l^\alpha = xp^\alpha$.

4.5. Real contribution at next-to leading order

The next-to leading order correction in α_s at twist-3 level is similar to twist-2 calculations, in a sense that the correction includes virtual and real contributions. In this section we calculate the real correction cross section, i.e. the $2 \to 3$ processes. We focus on contributions, where the Qiu-Sterman function is evaluated at equal arguments. Therefore, we have to evaluate $\mathcal{H}^{(1)}$ at the soft gluon point, where we identify two pole contributions that provide an imaginary phase fixing $x_1 = x_2$. On the one hand we have the obvious proper SGP contributions coming from propagators given in equation (4.6a), we refer to them as "pure"-SGP. On the other hand we have further contributions coming from hard poles, where the parameter a defined in equation (4.6c) is a function of the additional unobserved particle at NLO. Integrating over the phase space of the unobserved final state, we reach kinematical regions where these hard poles turn into soft poles.

To illustrate the two pole contributions, we show one of the twist-3 NLO diagrams in figure 4.5, where both contributions are present. The two propagators which may reach

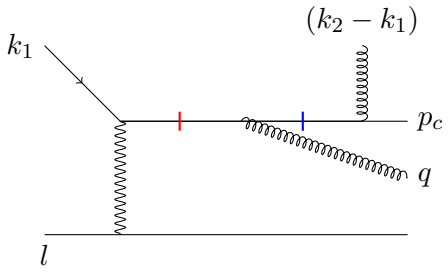

Figure 4.5.: Exemplary diagram for a $2 \to 3$ NLO twist-3 contribution. The red and the blue bars on the quark line indicate the the propagators, that may reach their on-shell limit. The blue bar marks the quark line carrying momentum $p_c - (k_2 - k_1)$, which is responsible for the pure SGP. The red bar denotes the quark line with momentum $p_c - (k_2 - k_1) + q$, which may reach the on-shell limit at the soft gluon point in certain edges of phase space.

their on-shell limit are marked by a red and a blue bar. The red bar is the origin of the pure SGP contribution, where we can use equation (4.7) to extract the imaginary phase. The blue bar in figure 4.5 denotes the propagator of the form

$$\frac{1}{\not k_1 - \not k_2 + \not p_c + \not q + \mathrm{i}\epsilon} \to \frac{(-\mathrm{i}\pi)}{2p \cdot (p_c + q)} \delta\left(x_1 - x_2 + \frac{p_c \cdot q}{p \cdot (p_c + q)}\right) (\not k_1 - \not k_2 + \not p_c + \not q) \,, \tag{4.21}$$

where we can expect contributions at the soft gluon point, for final state parton configurations where $p_c \cdot q = 0$.

In the subsequent sections we work out the cross section for the two pole contribution at the soft gluon point. As a forerunner we start to evaluate the $2 \to 3$ twist-2 function. Because similar to the LO case, we can use the twist-2 cross section to simplify the twist-3 result.

4.5.1. Unpolarized real NLO correction

We start with the unpolarized $2 \to 3$ cross section since we reduce parts of the twist-3 cross section to the twist-2 part, similar to LO. Despite the fact that this cross section has already discussed at NLO level in chapter 2, we rewrite the cross section in a slightly different notation since this is useful for our twist-3 calculation. For the real NLO twist-2 part we have to consider diagrams given on the left side of Fig. 4.6. The "blob" denotes the vertex function F that includes all the far of shell dynamics of the scattering amplitude. It is given by the two tree level five point amplitudes on the right side of Fig. 4.6. The bars on the end of the quark and gluon legs denote amputated parton lines, in a sense that the vertex function F not includes external factors like the

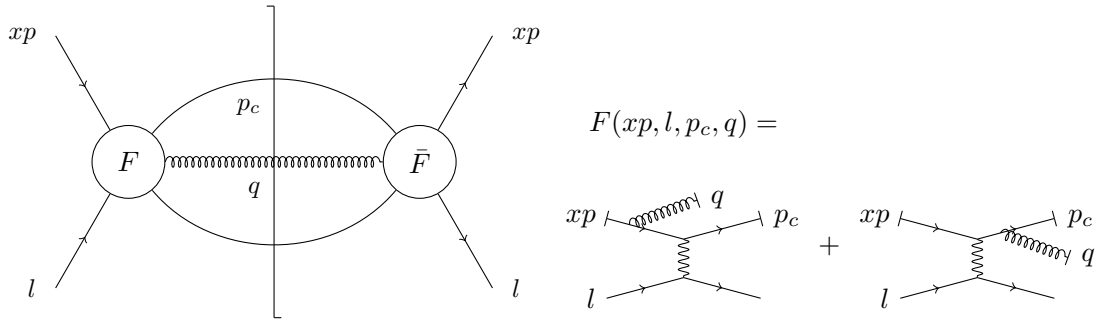

Figure 4.6.: Left: NLO Twist-2 2→3 scattering process.
Right: Definition of the quark-lepton-gluon vertex function. The bars at the end identify amputated lines.

projection on the hadronic functions or the gluon polarization tensor, whereas for the lepton line the on-shell spinors are included. To clarify our notation it is important to know that we have two Dirac traces in the hard part of our calculation, coming from the lepton and quark lines in figure 4.6. Whenever an expression contains $...\bar{F}....F....$ we assume the lepton trace to be implicit in this combination, whereas the quark trace is not contained. Therefore we can write the cross section as

$$E_h \frac{\mathrm{d}^2\sigma^{\mathrm{tw2}}}{d^3p_h} = \frac{1}{S}\sum_{ac}\int \frac{\mathrm{d}z}{z^2} D_c(z,\mu) \int \frac{\mathrm{d}x}{x} f_a(x,\mu) \frac{1}{2N_c} \mathrm{Tr}\left[\frac{1}{2} x\not{p}\tilde{\mathcal{H}}^{(0)}_{\mathrm{NLO},ac}(xp, l, p_c, \mu)\right] \tag{4.22}$$

where the trace indicates Dirac trace for the quark line as well as the color trace. According to that, the Dirac objects inside the trace belong always to the quark line. The sum runs over all parton flavors, we suppress these two indices in parts of the following discussion. At NLO level the parton distribution and the fragmentation function are dependent on an artificial mass scale μ, representing the factorization scale. The tilde on the hard function indicates the phase space integration for the additional unobserved gluon with momentum q. At NLO level, several divergencies will appear when we integrate the partonic function over phase space. To regulate them, we work in $n = 4 - 2\varepsilon$ dimensions. Thus we have,

$$\begin{aligned}\tilde{\mathcal{H}}^{(0)}_{\mathrm{NLO}}(xp, l, p_c, \mu) &= \mu^{2\varepsilon} \int \frac{\mathrm{d}^{(n-1)}q}{(2\pi)^{n-1} 2q^0} \bar{F}^{\mu}(xp, l, p_c, q) \not{p}_c d^{\mu\nu}(q, r) F^{\nu}(xp, l, p_c, q) \\ &\qquad \times \delta((xp + l - p_c - q)^2) \\ &= \mu^{2\varepsilon} \int \frac{\mathrm{d}^{(n-1)}q}{(2\pi)^{n-1} 2q^0} \mathcal{H}^{(0)}_{\mathrm{NLO}}(xp, l, p_c, q)\end{aligned} \tag{4.23}$$

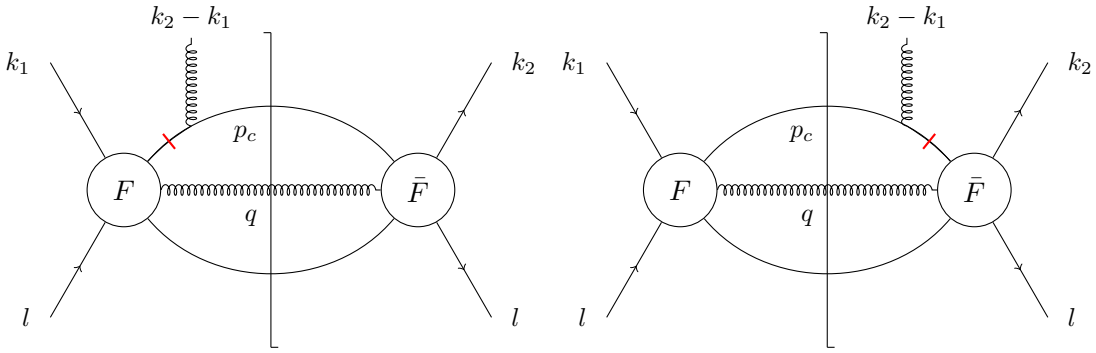

Figure 4.7.: Real emission diagrams for coherent gluon attaches the observed final state quark. The red bars denote the propagators that cause the SGP.

where $d^{\mu\nu}(q,r)$ denotes the polarization sum for the cut gluon line with momentum q and gauge vector r,

$$d^{\mu\nu}(q,r) = -g^{\mu\nu} + \frac{q^\mu r^\nu + q^\nu r^\mu}{q.r} \,. \tag{4.24}$$

We can indeed conclude that inserting equation (4.23) into equation (4.22) reproduces the real NLO contribution of chapter 2. Therefore, equation (4.22) is just a different notation that is useful by reformulating the twist-3 cross section in the next section.

4.5.2. Pure soft gluon pole contribution

The pure SGP contribution arise from on-shell propagators, that fix $x_1 = x_2$ independently from the phase space integration. It comes out, that the pure SGP contribution has two sub categories of diagrams. On the one hand diagrams where the coherent gluon is attached to the observed final state, and on the other hand where it is attached to the unobserved final state. We want to mention that the argument given in [67], that diagrams where the coherent gluon attaches an unobserved final state vanish among mirror diagrams, does not apply at NLO level. The reason for this cancellation is that the structure of the propagator that provides the imaginary phase is the same as the "on-shell" condition for the unobserved final state in the mirror-diagram and vice versa. After summing over the two mirror-diagrams they cancel among each other. Since this structure is violated at NLO, these diagrams give contributions to the cross section.

The twist-3 cross section for a generic initial state pole contribution at NLO can be

written as [159, 160]

$$E_h \frac{d^3\sigma^{tw3}_{\rm NLO}}{{\rm d}^3 P_h} = \frac{1}{S}\sum_{ac}\int \frac{{\rm d}z\,{\rm d}x_1\,{\rm d}x_2}{z^2} D_c(z,\mu) \times {\rm Tr}\left[i\omega^\alpha_\beta \left.\frac{\partial \tilde{\mathcal{H}}^{(1)g}_{\rm NLO}(k_1,k_2,l,p_c,\mu)}{\partial k^\alpha_{2\perp}}\right|_{\rm c.l.} M_F^{\beta,g}(x_1,x_2,\mu)\right] . \tag{4.25}$$

where it is important to mention, that the trace will produce ε dependent terms. The tilde on the hard function denotes the phase space integration for the additional final state particle coming from the α_s correction. Thus, we have

$$\tilde{\mathcal{H}}^{(1)g}_{\rm NLO}(k_1,k_2,l,p_c,\mu) = \mu^{2\varepsilon}\int \frac{{\rm d}^{(n-1)}q}{(2\pi)^{n-1}2q^0}\mathcal{H}^{(1)g}_{\rm NLO}(k_1,k_2,l,p_c,q) . \tag{4.26}$$

The function $\mathcal{H}^{(1)}_{\rm NLO}$ has two contributions

$$\mathcal{H}^{(1)}_{\rm NLO} = \mathcal{H}^{(1,{\rm U})}_{\rm NLO} + \mathcal{H}^{(1,{\rm O})}_{\rm NLO} , \tag{4.27}$$

where the U labels contributions where the coherent gluon attaches the unobserved final state and O for the observed final state. We neglect here the color index since the next step in the following section is essentially remodeling of the Dirac structure. For the LO contribution we exploit the master formula to calculate the cross section in an efficient way. For the pure SGP part of the NLO calculation we use the same strategy. Of course, before we can use the master formula, we have to prove its validity in a $2 \to 3$ process.

Coherent gluon on observed quark

In the following discussion we suppres spinor and color indices. The function $\mathcal{H}^{(1,{\rm O})}_{\rm NLO}$ receives contributions from diagrams where the twist-3 gluon attaches on the right and on the left side of the cut, see Fig. (4.7). We have to sum over both contributions

$$\mathcal{H}^{(1,{\rm O})}_{\rm NLO}(k_1,k_2,l,p_c,q) = \mathcal{H}^{(1,{\rm O})}_{\rm L}(k_1,k_2,l,p_c,q) + \mathcal{H}^{(1,{\rm O})}_{\rm R}(k_1,k_2,l,p_c,q) . \tag{4.28}$$

They are given by

$$\mathcal{H}^{(1,{\rm O})}_{\rm L}(k_1,k_2,l,p_c,q) = \big[\bar{F}_\mu(k_2,l,p_c,q)\, d^{\mu\nu}(q,r)\, L(k_1,k_2) \times F_\nu(k_1,l,k_1-k_2+p_c,q)\big]\,\delta((k_2+l-p_c-q)^2) \tag{4.29a}$$

$$\mathcal{H}^{(1,{\rm O})}_{\rm R}(k_1,k_2,l,p_c,q) = \big[\bar{F}_\mu(k_2,l,k_2-k_1+p_c,q)\, R(k_1,k_2)\, d^{\mu\nu}(q,r) \times F_\nu(k_1,l,p_c,q)\big]\,\delta((k_1+l-p_c-q)^2) \tag{4.29b}$$

The functions F are the same as defined in figure (4.6) with different arguments, and $d^{\mu\nu}(q,r)$ is the polarization sum for the cut gluon line defined in equation (4.24). The functions R and L represent factors associated with the attached twist-3 gluon. They include the propagator which produces the SGP, the projector onto the fragmentation function and the vertex of the gluon attachment contracted with p^σ.

$$L(k_1,k_2) = \not{p}_c \not{p} \frac{-1}{\not{k}_1 - \not{k}_2 + \not{p}_c + i\varepsilon} \tag{4.30a}$$

$$R(k_1,k_2) = \frac{-1}{\not{k}_2 - \not{k}_1 + \not{p}_c - i\varepsilon} \not{p} \not{p}_c \tag{4.30b}$$

We now perform the differentiation on equations (4.29a) and (4.29b) with respect to k_2, which is crucial to observe the twist-3 contribution. By doing that, $\partial/\partial k_2^\alpha$ hits either L or R, or other factors in $\mathcal{H}^{(1)g}_{\mathrm{R,L}}$. We thus needs

$$L(k_1,k_2)|_{\mathrm{c.l.}} = L(x_1 p, x_2 p) = \not{p}_c \frac{-1}{x_1 - x_2 + i\varepsilon} \tag{4.31a}$$

$$R(k_1,k_2)|_{\mathrm{c.l.}} = R(x_1 p, x_2 p) = \not{p}_c \frac{1}{x_1 - x_2 + i\varepsilon} \tag{4.31b}$$

$$\left.\frac{\partial L}{\partial k_2^\alpha}\right|_{\mathrm{c.l.}} = \frac{1}{2p\cdot p_c} \not{p}_c \not{p} \gamma_\alpha \frac{1}{x_1 - x_2 + i\varepsilon} - \frac{p_{c\alpha}}{p\cdot p_c} \not{p}_c \left(\frac{1}{x_1 - x_2 + i\varepsilon}\right)^2 \tag{4.32a}$$

$$\left.\frac{\partial R}{\partial k_2^\alpha}\right|_{\mathrm{c.l.}} = \frac{1}{2p\cdot p_c} \frac{1}{x_1 - x_2 + i\varepsilon} \gamma_\alpha \not{p} \not{p}_c + \frac{p_{c\alpha}}{p\cdot p_c} \left(\frac{1}{x_1 - x_2 + i\varepsilon}\right)^2 \not{p}_c \tag{4.32b}$$

By carrying out the derivative $\left.\frac{\partial \mathcal{H}^{(1)g}_{\mathrm{NLO}}}{\partial k_2^\alpha}\right|_{\mathrm{c.l.}}$ we obtain three different types of pole terms. (I) double pole terms coming from equations (4.32a) and (4.32b), (II) single pole terms coming from equations (4.32a) and (4.32b) or (III) single pole terms appearing when the derivative hits other terms in $\mathcal{H}^{(1)g}_{\mathrm{NLO}}$. The double pole term (I) reads:

$$\begin{aligned}
&\left.\frac{\partial \mathcal{H}^{(1,\mathrm{O})}_{\mathrm{NLO}}}{\partial k_2^\alpha}\right|^{(\mathrm{I})}_{\mathrm{c.l.}} \\
&= \left(\frac{p_{c\alpha}}{p\cdot p_c}\right)\left(\frac{1}{x_1 - x_2 + i\varepsilon}\right)^2 \Bigg[- \Big[\bar{F}_\mu(x_2 p, l, p_c, q)\, d^{\mu\nu}(q,r)\, \not{p}_c \\
&\quad \times F_\nu(x_1 p, l, (x_1 - x_2)p + p_c, q)\Big] \delta((x_2 p + l - p_c - q)^2) \\
&\quad + \Big[\bar{F}_\mu(x_2 p, l, (x_2 - x_1)p + p_c, q)\ \not{p}_c\, d^{\mu\nu}(q,r)\, F_\nu(x_1 p, l, p_c, q)\Big] \\
&\quad \times \delta((x_1 p + l - p_c - q)^2)\Bigg]
\end{aligned} \tag{4.33}$$

The function which multiplies the pole in equation (4.33) can be expanded with respect to x_2 around x_1 up to $\mathcal{O}(x_2 - x_1)$. Afterwards, we multiply the $\mathcal{O}(x_2 - x_1)$ expansion to the double pole term, then we are left with a double and a single pole term. The double pole terms cancel among mirror diagrams. After the double poles are canceled, we can transform the derivative with respect to x_2 from the taylor-expansion into a derivative with respect to p_c. We end up with,

$$\frac{\partial \mathcal{H}^{(1,\mathrm{O})}_{\mathrm{NLO}}}{\partial k_2^\alpha}\bigg|^{(\mathrm{I})}_{\mathrm{c.l.}} = \left(\frac{p_{c\alpha}}{p\cdot p_c}\right)\left(\frac{1}{x_1 - x_2 + i\varepsilon}\right)\Bigg[p^\mu \frac{\partial}{\partial p_c^\mu}\Bigg\{\Big[\bar{F}_\mu(x_1 p, l, p_c, q) \times d^{\mu\nu}(q,r)\, \not{p}_c\, F_\nu(x_1 p, l, p_c, q)\Big]\delta((x_1 p + l - p_c - q)^2)\Bigg\}\Bigg]\,. \tag{4.34}$$

We must choose the gauge vector r independent of p_c. This is important, otherwise we would get further contributions when the derivative hits the polarization sum. The single pole terms for $\frac{\partial L}{\partial k_2^\alpha}$ and $\frac{\partial R}{\partial k_2^\alpha}$ are

$$\begin{aligned}&\frac{\partial \mathcal{H}^{(1,\mathrm{O})}_{\mathrm{NLO}}}{\partial k_2^\alpha}\bigg|^{(\mathrm{II})}_{\mathrm{c.l.}} \\ &= \left(\frac{1}{2p\cdot p_c}\right)\left(\frac{1}{x_1 - x_2 + i\varepsilon}\right)\delta((x_1 p + l - p_c - q)^2) \\ &\quad\times\Big[\bar{F}_\mu(x_1 p, l, p_c, q)\, d^{\mu\nu}(q,r)\,(2p\cdot p_c \gamma_\alpha - 2p_{c,\alpha}\not{p}) F_\nu(x_1 p, l, p_c, q)\Big]\,.\end{aligned} \tag{4.35}$$

We collect the single pole terms of type (III) and get

$$\begin{aligned}\frac{\partial \mathcal{H}^{(1,\mathrm{O})}_{\mathrm{NLO}}}{\partial k_2^\alpha}\bigg|^{(\mathrm{III})}_{\mathrm{c.l.}} &= \left(\frac{1}{x_1 - x_2 + i\varepsilon}\right)\delta((x_1 p + l - p_c - q)^2) \\ &\quad\Bigg\{\frac{\partial}{\partial p_c^\alpha}\Big[\bar{F}_\mu(x_1 p, l, p_c, q)\, d^{\mu\nu}(q,r)\, \not{p}_c\, F_\nu(x_1 p, l, p_c, q)\Big] \\ &\quad - \Big[\bar{F}_\mu(x_1 p, l, p_c, q)\, d^{\mu\nu}(q,r)\, \gamma_\alpha\, F_\nu(x_1 p, l, p_c, q)\Big]\Bigg\}\,.\end{aligned} \tag{4.36}$$

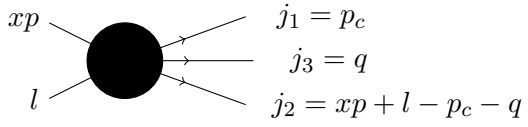

Figure 4.8.: Momentum labeling for a generic $2 \to 3$ process.

Finally, after we calculate all necessary derivative terms and take the collinear limit we can add terms of types (I) + (II) + (III) and get

$$\begin{aligned}
&\frac{\partial \mathcal{H}^{(1,\mathrm{O})}_{\mathrm{NLO}}(k_1,k_2,l,p_c,q)}{\partial k_2^\alpha}\bigg|^{(\mathrm{I})+(\mathrm{II})+(\mathrm{III})}_{\mathrm{c.l.}} \\
&= \left(\frac{1}{x_1 - x_2 + i\varepsilon}\right)\left(\frac{\partial}{\partial p_c^\alpha} - \frac{p_{c\alpha}p^\lambda}{p\cdot p_c}\frac{\partial}{\partial p_c^\lambda}\right) \\
&\quad \times\Big[\bar{F}(x_1 p, l, p_c, q) d(q,r)\, \not{p}_c\, F(x_1 p, l, p_c, q)(x_1 \not{p} + \not{l} - \not{p}_c - \not{q})\Big] \\
&\quad \times\delta((x_1 p + l - p_c - q)^2)\,. \qquad (4.37)
\end{aligned}$$

Comparing this result with equation (4.23) leads immediately to

$$\begin{aligned}
&\frac{\partial \mathcal{H}^{(1,\mathrm{O})}_{\mathrm{NLO}}(k_1,k_2,l,p_c,q)}{\partial k_2^\alpha}\bigg|^{(\mathrm{I})+(\mathrm{II})+(\mathrm{III})}_{\mathrm{c.l.}} \\
&= \frac{1}{x_1 - x_2 + i\varepsilon}\left(\frac{\partial}{\partial p_c^\alpha} - \frac{p_{c\alpha}p^\lambda}{p\cdot p_c}\frac{\partial}{\partial p_c^\lambda}\right)\mathcal{H}^{(0)}_{\mathrm{NLO}}(x_1 p, l, p_c, q)\Big|_{\not{p}_c \to T^g \not{p}_c} \qquad (4.38)
\end{aligned}$$

where the replacement $\not{p}_c \to T^g \not{p}_c$ includes the color structure of the coherent gluon. With the help of equation (4.38) we can relate the SGP twist-3 real emission contributions to the corresponding twist-2 partonic function. Therefore, equation (4.38) is the "master formula" for $2 \to 3$ processes, where the coherent gluon is attached to the observed final state. We can use this formula to rewrite equation (4.25) as

$$\begin{aligned}
E_h \frac{\mathrm{d}^3\sigma^{\mathrm{tw3}}}{\mathrm{d}^3 P_h} = \frac{\pi M_N}{S}\epsilon^{\alpha pnS_\perp}\sum_{ac}\int\frac{\mathrm{d}z}{z^2}D_c(z,\mu)\int\frac{\mathrm{d}x}{x}G_F(x,x,\mu) \\
\times\mu^{2\varepsilon}\int\frac{\mathrm{d}^{(n-1)}q}{(2\pi)^{n-1}2q^0}\left(\frac{\partial}{\partial p_c^\alpha} - \frac{p_{c\alpha}p^\lambda}{p\cdot p_c}\frac{\partial}{\partial p_c^\lambda}\right)H'^{(0)}_{\mathrm{NLO}}(x_1 p, l, p_c, q) \qquad (4.39)
\end{aligned}$$

with

$$H'^{(0)}_{\mathrm{NLO}}(x_1 p, l, p_c, q, \varepsilon) = \mathrm{Tr}\left[\frac{x\not{p}T^g}{(N_c^2-1)}\,\mathcal{H}^{(0)}_{\mathrm{NLO}}(xp, l, p_c)\Big|_{\not{p}_c \to T^g \not{p}_c}\right]\,. \qquad (4.40)$$

We can further rewrite the partonic function by introducing a set of Mandelstam variables $s = (xp + l)^2$, $s_{ik} = (j_i + j_k)^2$, $t_i = (xp - j_i)^2$ and $u_i = (l - j_i)^2$, where the

momentum labeling is shown in figure 4.8. The function $\mathcal{H}^{(0)}_{\rm NLO}$ can be expressed in terms of these kinematical quantities. Obviously, the set of 10 Mandelstam variables is over-determined. Therefore, we can use momentum conservation to eliminate the momentum j_2, i.e. s_{12}, t_2, u_2 and s_{23}. Then the partonic function reads

$$H'^{(0)}_{\rm NLO} = C_O\ \hat{\sigma}^{\rm tw-2}_{2\to3}(s, s_{13}, t_1, t_3, u_1, u_3, \varepsilon)\delta(s + s_{13} + t_1 + t_3 + u_1 + u_3)\ , \tag{4.41}$$

where $\hat{\sigma}^{\rm tw-2}_{2\to3}$ is the twist-2 partonic $2 \to 3$ cross section without colour factors that are included in C_O. For this process $C_O = -1/(2N_c)$. When we use the master formula which we have proven to be valid at NLO level, we have to carry out the differentiation on the twist-2 partonic function $\mathcal{H}^{(0)}_{\rm NLO}$ with respect to p_c. For our subsequent analysis it is important that p has only plus component, i.e. $p = (p^+, 0, \vec{0})$. Therefore, we can rewrite the differential operator as

$$\begin{aligned}\frac{\mathrm{d}}{\mathrm{d}p_c^\alpha} H'^{(0)}_{\rm NLO} &= \left(\frac{\mathrm{d}s_{13}}{\mathrm{d}p_c^\alpha}\frac{\partial}{\partial s_{13}} + \frac{\mathrm{d}u_1}{\mathrm{d}p_c^\alpha}\frac{\partial}{\partial u_1}\right) H'^{(0)}_{\rm NLO} \\ &= \left(2\left[-\frac{t_3}{t_1}p_{c\alpha} + q_\alpha\right]\frac{\partial}{\partial s_{13}} - 2\left[\frac{s}{t_1}p_{c\alpha} + l_\alpha\right]\frac{\partial}{\partial u_1}\right) H'^{(0)}_{\rm NLO}\ ,\end{aligned} \tag{4.42}$$

where $\alpha = \perp$. The derivative in equation (4.42) hits either $\hat{\sigma}_{2\to3}$ or the delta function of equation (4.41). When the derivatives hits the delta function we convert them by partial integration with respect to x to a derivative term on the Qiu-Sterman function. Inserting equation (4.42) into equation (4.39) and performing partial integration we obtain the following result

$$\begin{aligned}E_h\frac{\mathrm{d}^3\sigma_O^{tw3}}{\mathrm{d}^3P_h} = C_O\frac{\pi M_N}{S}\sum_{ac}\int\frac{\mathrm{d}z}{z^2}D_c(z,\mu)\int\frac{\mathrm{d}x}{x}\mu^{2\varepsilon}\int\frac{\mathrm{d}^{(n-1)}q}{(2\pi)^{n-1}2q^0}\frac{1}{t_2} \\ \times\Bigg[\left(-2\frac{t_3}{t_1}\epsilon^{p_cpnS_\perp} + 2\epsilon^{qpnS_\perp}\right)\left\{\hat{\sigma}\left(G_F(x,x,\mu) - x\frac{dG_F(x,x,\mu)}{dx}\right)\right. \\ \left. + \left(\hat{\sigma} + u_1\frac{\partial\hat{\sigma}}{\partial u_1} + u_3\frac{\partial\hat{\sigma}}{\partial u_3} - (u_3+u_1)\frac{\partial\hat{\sigma}}{\partial s_{13}}\right)G_F(x,x,\mu)\right\} \\ + \left(-2\frac{s}{t_1}\epsilon^{p_cpnS_\perp} - 2\epsilon^{lpnS_\perp}\right)\left\{\hat{\sigma}\left(G_F(x,x,\mu) - x\frac{\mathrm{d}G_F(x,x,\mu)}{dx}\right)\right. \\ \left.\left. + \left(\hat{\sigma} + s_{13}\frac{\partial\hat{\sigma}}{\partial s_{13}} + u_3\frac{\partial\hat{\sigma}}{\partial u_3} - (u_3+s_{13})\frac{\partial\hat{\sigma}}{\partial u_1}\right)G_F(x,x,\mu)\right\}\right] \\ \times\delta(s + s_{13} + t_1 + t_3 + u_1 + u_3)\end{aligned} \tag{4.43}$$

where $\hat{\sigma} \equiv \hat{\sigma}^{\rm tw2}_{2\to3}(s, s_{13}, t_1, t_3, u_1, u_3, \varepsilon)$. To obtain formula (4.43) we use the fact that the mass dimension of $\hat{\sigma}_{2\to3}$ is -2. Therefore, we have the relation

$$\hat{\sigma}^{\rm tw2}_{2\to3}(\lambda s, \lambda s_{13}, \lambda t_1, \lambda t_3, \lambda u_1, \lambda u_3) = \frac{\hat{\sigma}^{\rm tw2}_{2\to3}(s, s_{13}, t_1, t_3, u_1, u_3)}{\lambda}\ , \tag{4.44}$$

from this follows

$$-\hat{\sigma}^{\mathrm{tw2}}_{2\to3} = s\frac{\partial\hat{\sigma}^{\mathrm{tw2}}_{2\to3}}{\partial s} + t_1\frac{\partial\hat{\sigma}^{\mathrm{tw2}}_{2\to3}}{\partial t_1} + t_3\frac{\partial\hat{\sigma}^{\mathrm{tw2}}_{2\to3}}{\partial t_3} + u_1\frac{\partial\hat{\sigma}^{\mathrm{tw2}}_{2\to3}}{\partial u_1} + u_3\frac{\partial\hat{\sigma}^{\mathrm{tw2}}_{2\to3}}{\partial u_3} + s_{13}\frac{\partial\hat{\sigma}^{\mathrm{tw2}}_{2\to3}}{\partial s_{13}} \ . \quad (4.45)$$

For the actual calculation, q integration for terms that multiply the tensor structure $\epsilon^{qpnS_\perp}$ is very inconvenient. Therefore, we decompose this part of the integral as

$$\epsilon^{\alpha pnS_\perp}\int\frac{\mathrm{d}^3q}{(2\pi)^3 2q^0}q^\alpha\ldots = \epsilon^{\alpha pnS_\perp}\left(Ap_c^\alpha + Bl^\alpha + Cxp^\alpha\right) \ . \quad (4.46)$$

The justification of this ansatz relies in the fact that the final result should only depend on the external momenta of our physical process. Since the C term vanishes in conjunction with the ϵ-tensor, we can project on the A and B terms in our expansion and conclude that $\epsilon^{qpnS_\perp}$ can be replaced by

$$\epsilon^{qpnS_\perp} \to \frac{-1}{2t_1u_1}(-u_1t_3 + ss_{13} - t_1u_3)\epsilon^{p_cpnS_\perp} + \frac{-1}{2su_1}(-u_1t_3 - ss_{13} + t_1u_3)\epsilon^{lpnS_\perp} \ . \quad (4.47)$$

Then the cross section formula (4.43) is given by

$$\begin{aligned}
E_h\frac{\mathrm{d}^3\sigma_O^{tw3}}{\mathrm{d}^3P_h} = C_O\frac{\pi M_N}{S}\sum_{ac}\int\frac{\mathrm{d}z}{z^2}D_c(z,\mu)\int\frac{\mathrm{d}x}{x}\left(2\frac{s}{t_1}\epsilon^{p_cpnS_\perp} + 2\epsilon^{lpnS_\perp}\right)\\
\mu^{2\varepsilon}\int\frac{\mathrm{d}^{(n-1)}q}{(2\pi)^{n-1}2q^0}\frac{-1}{t_2}\Bigg[\frac{1}{su_1}\left(-u_1t_3 - ss_{13} + t1u_3\right)\\
\times\Bigg\{\hat{\sigma}\left(G_F(x,x,\mu) - x\frac{dG_F(x,x,\mu)}{dx}\right)\\
+\left(\hat{\sigma} + u_1\frac{\partial\hat{\sigma}}{\partial u_1} + u_3\frac{\partial\hat{\sigma}}{\partial u_3} - (u_3+u_1)\frac{\partial\hat{\sigma}}{\partial s_{13}}\right)G_F(x,x,\mu)\Bigg\}\\
-2\Bigg\{\hat{\sigma}\left(G_F(x,x,\mu) - x\frac{\mathrm{d}G_F(x,x,\mu)}{dx}\right)\\
+\left(\hat{\sigma} + s_{13}\frac{\partial\hat{\sigma}}{\partial s_{13}} + u_3\frac{\partial\hat{\sigma}}{\partial u_3} - (u_3+s_{13})\frac{\partial\hat{\sigma}}{\partial u_1}\right)G_F(x,x,\mu)\Bigg\}\Bigg]\\
\times\delta(s + s_{13} + t_1 + t_3 + u_1 + u_3) \ . \quad (4.48)
\end{aligned}$$

For the phase space integration over q we use the results given in Appendix C and D applying the same methods we already used in chapter (2).

Coherent gluon on unobserved final state gluon

As we mentioned before, non-vanishing contributions from coherent gluon attachments on unobserved final state are present at NLO. Those contributions are shown in figure

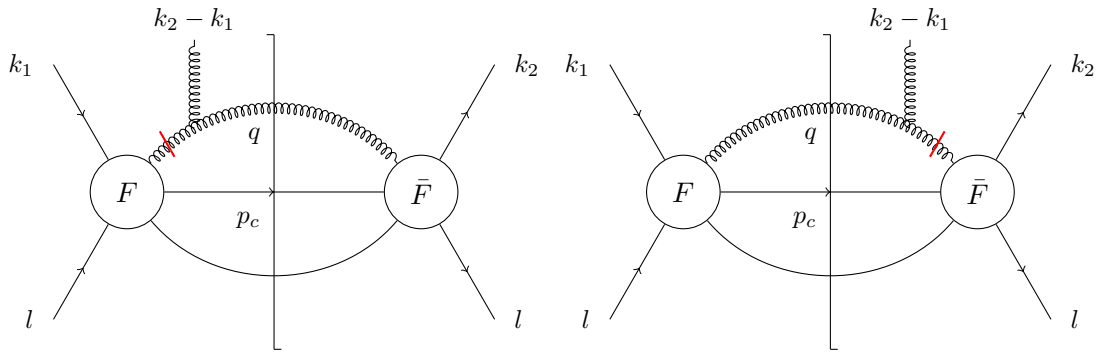

Figure 4.9.: Real emission diagrams for a coherent gluon attaching the unobserved final state gluon. The red bars denote the propagators which cause the SGP.

(4.9). Using the same methods as for the configuration where the coherent gluon attaches the observed final state, we can prove the master formula ansatz to be correct and obtain

$$\left.\frac{\partial \mathcal{H}^{(1,\mathrm{U})}_{\mathrm{NLO}}(k_1,k_2,l,p_c,q)}{\partial k_2^\alpha}\right|_{\mathrm{c.l.}} = \frac{1}{x_1 - x_2 + i\varepsilon}\left(\frac{\partial}{\partial q^\alpha} - \frac{p_{c\alpha}p^\lambda}{p\cdot q}\frac{\partial}{\partial q^\lambda}\right) \times \mathcal{H}^{(0)}_{\mathrm{NLO}}(x_1 p, l, p_c, q)\Big|_{\delta_{dd'}\to \mathrm{i}f_{dgd'}} , \tag{4.49}$$

as the master formula for adding a coherent gluon to the final state unobserved gluon. The replacement $\delta_{dd'} \to \mathrm{i}f_{dgd'}$ is necessary due to the color structure of the coherent gluon in our cross section. We like to emphasize that the replacement differs compared to equation (4.38), since the coherent gluon is attached to a final state gluon. Therefore, we could give a more general definition of the master formula which is valid also for different partonic channels

$$\left.\frac{\partial \mathcal{H}^{(1,\mathrm{O,U})}_{\mathrm{NLO}}(k_1,k_2,l,p_c,q)}{\partial k_2^\alpha}\right|_{\mathrm{c.l.}} = \frac{1}{x_1 - x_2 + i\varepsilon}\left(\frac{\partial}{\partial j_i^\alpha} - \frac{p_{c\alpha}p^\lambda}{p\cdot j_i}\frac{\partial}{\partial j_i^\lambda}\right) \times \mathcal{H}^{(0)}_{\mathrm{NLO}}(x_1 p, l, j_1, j_2)\Big|_{\mathrm{c.r.}} , \tag{4.50}$$

where c.r. is the color replacement dependent on whether the coherent gluon is attached to a quark or a gluon. We have $\delta_{dd'} \to \mathrm{i}f_{dgd'}$ when the twist-3 gluon is attached to a final state gluon and $\not{j}_i \to T^g \not{j}_i$ for a final state quark.

From equation (4.49) we can proceed with the same methods as in the previous section

and obtain the cross section formula

$$
\begin{aligned}
E_h\frac{\mathrm{d}^3\sigma_U^{tw3}}{\mathrm{d}^3P_h} = C_U\frac{\pi M_N}{S}\sum_{ac}\int\frac{\mathrm{d}z}{z^2}D_c(z,\mu)\int\frac{\mathrm{d}x}{x}\left(2\frac{s}{t_1}\epsilon^{p_cpnS_\perp}+2\epsilon^{lpnS_\perp}\right)\\
\times\mu^{2\varepsilon}\int\frac{\mathrm{d}^{(n-1)}q}{(2\pi)^{n-1}2q^0}\frac{-1}{u_1t_2t_3}\Bigg[\\
(u_1t_3+ss_{13}-t_1u_3)\times\Bigg\{\frac{t_1}{s}\hat{\sigma}\left(G_F(x,x,\mu)-x\frac{dG_F(x,x,\mu)}{dx}\right)\\
+\left(\hat{\sigma}+u_1\frac{\partial\hat{\sigma}}{\partial u_1}+u_3\frac{\partial\hat{\sigma}}{\partial u_3}-(u_3+u_1)\frac{\partial\hat{\sigma}}{\partial s_{13}}\right)G_F(x,x,\mu)\Bigg\}\\
+(-u_1t_3+ss_{13}-t_1u_3)\times\Bigg\{\hat{\sigma}\left(G_F(x,x,\mu)-x\frac{dG_F(x,x,\mu)}{dx}\right)\\
+\left(\hat{\sigma}+s_{13}\frac{\partial\hat{\sigma}}{\partial s_{13}}+u_1\frac{\partial\hat{\sigma}}{\partial u_1}-(u_1+s_{13})\frac{\partial\hat{\sigma}}{\partial u_3}\right)G_F(x,x,\mu)\Bigg\}\Bigg]\\
\times\delta(s+s_{13}+t_1+t_3+u_1+u_3)\,,
\end{aligned}
\tag{4.51}
$$

where the color factor is given by $C_U = N_C/2$.

Pure soft gluon pole results

We can evaluate the cross section formulas (4.48) and (4.51) by using standard methods for phase space integration given in Appendix C and D. We discuss in this section the results in the quark fragmentation channel. The final result for the pure SGP contribution is given by

$$
E_h\frac{\mathrm{d}^3\sigma_{SGP}^{tw3}}{\mathrm{d}^3P_h} = E_h\frac{\mathrm{d}^3\sigma_U^{tw3}}{\mathrm{d}^3P_h}+E_h\frac{\mathrm{d}^3\sigma_O^{tw3}}{\mathrm{d}^3P_h}\,. \tag{4.52}
$$

The pure SGP part is the only part in the real correction, where contributions $\propto \left(G_F(x,x,\mu)-x\frac{dG_F(x,x,\mu)}{dx}\right)$ appear. Beneath this combination of derivative and non-derivative Qiu-Sterman functions, we have pure non derivative terms in equations (4.48) and (4.51). Therefore, we can cast the pure SGP contribution into the form

$$
\begin{aligned}
E_h\frac{\mathrm{d}^3\sigma_{SGP}^{tw3}}{\mathrm{d}^3P_h} = \frac{-\pi M_N}{T}\epsilon^{\alpha pnS_\perp}\sum_c\int_{v_{min}}^{v_{max}}\mathrm{d}v\int_{w_{min}}^{1}\frac{\mathrm{d}w}{w}D_c(z,\mu)\left(\frac{2}{v-1}p_{c\alpha}+2l_\alpha\right)\\
\times\left\{\left(G_F(x,x,\mu)-x\frac{\mathrm{d}G_F(x,x,\mu)}{\mathrm{d}x}\right)A(s,v,w,\mu,\epsilon)+G_F(x,x,\mu)B(s,v,w,\mu,\epsilon)\right\}\,.
\end{aligned}
\tag{4.53}
$$

The function $B(s,v,w,\mu,\epsilon)$ has divergent terms of the form

$$B(s,v,w,\mu,\epsilon) \propto \frac{h(s,v,w)}{(1-w)^{(2+\varepsilon)}} \tag{4.54}$$

with $h(s,v,1) \neq 0$. Since these badly divergent terms do not vanish among pure SGP contributions, this is a clear indicator that there are additional parts in our cross section we have not included so far. Fortunately, the HP diagrams that we discuss in the next section, provide exactly the same singularities that cancel among those found in the pure SGP part. Therefore, we postpone the discussion of the pure SGP non-derivative part and hark back to them when we calculate the HP contribution.

The A term in equation (4.53) can be cast into the form

$$\begin{aligned} &A(s,v,w,\mu,\epsilon) \\ =&\alpha_{em}^2 e_a^2 \frac{\alpha_s}{\pi}\left(\frac{4\pi\mu}{s}\right)^{2\varepsilon}\left[A_1\left\{\frac{\delta(1-w)}{\varepsilon^2}+4\left(\frac{\ln(1-w)}{1-w}\right)_+\right\}+A_3\delta(1-w)+A_4\left(\frac{1}{1-w}\right)_+\right. \\ &\left.+\frac{1}{\varepsilon}\left\{A_{21}\delta(1-w)-2A_1\left(\frac{1}{1-w}\right)_+ + A_{22}\right\}+A_6\right] \end{aligned} \tag{4.55}$$

where the coefficient functions A_i depend on the variables w, v and s. The function A_6 contains all the regular parts that are non singular at the upper boundary of the w integral.

The derivative part of the pure SGP contribution has singularities from collinear and soft configurations in the hard scattering function. Due to the fact that we use dimensional regularization, this is reflected in contributions $\propto \frac{1}{\varepsilon^2}$ and $\propto \frac{1}{\varepsilon}$. We mention that our calculation assumes a massless lepton, and we regulate the singularity from collinear lepton-photon contributions in dimensional regularization as well.

The double pole $\propto \frac{1}{\varepsilon^2}$ appears in the observed and the unobserved part coming from soft final state gluon configurations. It is given by,

$$A_1 = (C_O + C_U)\frac{-2}{s^2 v^2}\frac{v^2+1}{(1-v)^2} \tag{4.56}$$

where we obtain that similar to twist-2 NLO the prefactor of $\frac{1}{\varepsilon^2}$ and $\left(\frac{\ln(1-w)}{1-w}\right)_+$ is Born like. It is important to mention that the $\frac{1}{\varepsilon^2}$ must cancel against virtual corrections, which must have the same color factor as the real part $C_O + C_U = C_F$.

4.5.3. Hard pole contribution

As discussed in the literature [155] hard-pole contributions are pole contributions arising from internal propagators of $\mathcal{H}^{(1)}$ that makes x_1 and x_2 kinematics dependent. In our

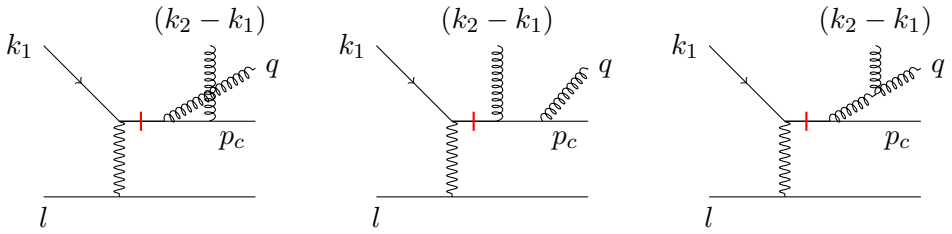

Figure 4.10.: Hard Pole diagrams that lead to a vanishing coherent gluon momentum in kinematical edges of the phase space. The red bar indicates the propagators that produces the necessary imaginary part by reaching their on-shell limit.

calculation, a spectrum of such hard poles are present. If we look at the possible "on-shell" propagators in $\mathcal{H}^{(1)}$, we find among other hard poles propagators

$$\frac{1}{\not{k}_1 - \not{k}_2 + \not{p}_c + \not{q} + \mathrm{i}\epsilon} \tag{4.57}$$

which give rise to the delta function $(-\mathrm{i}\pi)\delta\left((x_2 - x_1) + \frac{p_c \cdot q}{p \cdot (p_c + q)}\right)$ in the collinear limit. Therefore, we get a contribution from hard poles at NLO with equal arguments in the Qiu-Sterman function from phase space configurations where $p_c \cdot q \to 0$. Since this is a hard pole contribution, we can not proceed by using the master formula equation (4.50) as in the previous section. We exploit here a more formal argument to carry out the k_2 derivative in a novel way, i.e. by using the Ward identity. This method has been already used in LO processes, where HP configuration are present [155]. After we work through all HP contributions, we identify 12 diagrams which involve poles of the form mentioned above. We show them basically in figure 4.10. Those diagrams interfere with the quark-lepton-gluon vertex function $\bar{F}(k_1, l, p_c, q)$ shown in figure 4.6, which give six different contribution. Including their mirror diagrams, we end up with 12 HP diagrams that contribute at the soft gluon point. We call the sum of the three types of diagrams shown in figure 4.10, $D^{\mathrm{HP},g,h}_{\mu,\beta}(k_1, k_2, l, p_c, q)$ where μ indicates the Lorentz index for the final state gluon and β for the coherent gluon and g and h denote their color index. We suppress open Dirac indices here. It was shown in [155] that the sum of the diagrams of figure 4.10 fulfills the Ward identity, i.e.

$$(k_1 - k_2)^\beta D^{\mathrm{HP},g}_{\mu,\beta}(k_1, k_2, l, p_c, q) = 0\,. \tag{4.58}$$

We call the sum of the 12 twist-3 HP diagrams before phase space integration $\mathcal{H}^{(1),\mathrm{HP}}_{\beta}$. To obtain the physical cross section we have to do the same expansion as we perform in the SGP case in equation (4.16). Again the zeroth order cancels out, and we are left with the first term in equation (4.21). Therefore, we have to calculate the derivative

term $\left.\frac{\partial \mathcal{H}^{(1),\mathrm{HP}}(k_1,k_2,l,pc)}{\partial k_2^\alpha}\right|_{k_i=x_i p}$. We can express

$$\mathcal{H}^{(1),\mathrm{HP}}_{\beta,g}(k_1,k_2,l,p_c,q) = \bar{F}^h_\nu(k_1,l,p_c,q)\not{p}_c d^{\mu\nu}(q,r) D^{\mathrm{HP},g,h}_{\mu,\beta}(k_1,k_2,l,p_c,q) \times\delta((k_2+l-p_c-q)^2) + \text{mirr.} \tag{4.59}$$

where +mirr. indicates that we need to include not only the contributions in figure 4.10 but also their mirror diagrams. In this framework, $\mathcal{H}^{(1),\mathrm{HP}}_{\beta,g}$ also satisfies

$$(k_1-k_2)^\beta \mathcal{H}^{(1),\mathrm{HP}}_{\beta,g}(k_1,k_2,l,p_c,q) = 0\,, \tag{4.60}$$

which is a very important feature that simplifies the ∂k_2^α derivative enormously. If we carry out the derivative with respect to k_2 on equation (4.60), we see immediately

$$(x_2-x_1)\left.\frac{\partial \mathcal{H}^{(1),\mathrm{HP}}_{\alpha,g}(k_1,k_2,l,pc)p^\alpha}{\partial k_2^\beta}\right|_{k_i=x_i p} - \mathcal{H}^{(1),\mathrm{HP}}_{\beta,g}(x_1 p, x_2 p, l, p_c, q) = 0\,. \tag{4.61}$$

Thus we have,

$$\left.\frac{\partial \mathcal{H}^{(1),\mathrm{HP}}_{\alpha}(k_1,k_2,l,pc)p^\alpha}{\partial k_2^\beta}\right|_{k_i=x_i p} = \frac{1}{x_2-x_1}\mathcal{H}^{(1),\mathrm{HP}}_{\beta}(x_1 p, x_2 p, l, p_c, q)\,. \tag{4.62}$$

The identity above simplifies our calculation of the hard pole diagrams considerably. To carry out the derivative on $\mathcal{H}^{(1),\mathrm{HP}}$ with respect to k_2 we just leave the Lorentz index present from the coherent gluon uncontracted and divide the result by (x_2-x_1). Due to the constraints from the pole condition the quantity (x_2-x_1) is just a combination of kinematical variables. To calculate $\mathcal{H}^{(1),\mathrm{HP}}$ explicitly we use standard Feynman rules and replace the on-shell propagator in figure 4.10 by

$$\frac{1}{\not{k}_1-\not{k}_2+\not{p}_c+\not{q}+\mathrm{i}\epsilon} \to (-\mathrm{i}\pi)\frac{(\not{k}_1-\not{k}_2+\not{p}_c+\not{q})}{2p\cdot(p_c+q)}\delta\left((x_2-x_1)+\frac{p_c\cdot q}{p\cdot(p_c+q)}\right)\,. \tag{4.63}$$

The delta distribution eliminates one of the x_1 or x_2 integration in equation (4.21). Therefore, we can rewrite the first and solely remaining term in (4.21) as

$$\begin{aligned} &E_h\frac{\mathrm{d}^3\sigma^{tw3}_{HP}}{\mathrm{d}^3P_h} \\ &= \frac{\pi M_N}{S}\sum_{ac}\int\frac{\mathrm{d}z}{z^2}\int\frac{\mathrm{d}x}{x}D_c(z,\mu)\left(2\frac{s}{t_1}\epsilon^{p_c p n S_\perp}+2\epsilon^{lpnS_\perp}\right) \\ &\quad\times\mu^{2\varepsilon}\int\frac{\mathrm{d}^{(n-1)}q}{(2\pi)^{n-1}2q^0}G_F(x,x(1-\tilde{x}),\mu)\mathcal{M}_{HP}(t_3,s_{13},u_2)\,\delta((k_2+l-p_c-q)^2)\,, \end{aligned} \tag{4.64}$$

where $\tilde{x} = -\frac{s_{13}}{t_1+t_3}$ and we use that $G_F(x_1, x_2) = G_F(x_2, x_1)$. $\mathcal{M}_{HP}(t_3, s_{13}, u_2)$ is the partonic hard pole function and is defined by

$$\mathcal{M}_{HP}(t_3, s_{13}, u_2) \left(2\frac{s}{t_1}p^\alpha + 2l^\alpha\right) \delta((k_2 + l - p_c - q)^2) \\ = \frac{p \cdot (p_c + q)}{p_c \cdot q} \mathrm{Tr}\left[\mathrm{i}\omega^{\alpha\beta} \frac{x\not{p} T^g}{(N_c^2 - 1)} \mathcal{H}^{(1),\mathrm{HP}}_{\beta,g}(x_1 p, x_2 p, l, p_c, q)\right] . \quad (4.65)$$

For simplicity, we denote only t_3, s_{13}, u_2 as the arguments of the partonic function. Surely, there are other Mandelstam variables present in $\mathcal{M}_{HP}$, but after extensive partional fractioning, the angular dependent variables in the denominator reduce to these three. Therefore, the function $\mathcal{M}_{HP}$ has singularities if one of the variables $t_3, s_{13}, u_2 \to 0$. The structure of the last line in equation (4.64) is the matter of interest for our following discussion and we rename it as HP. Despite the fact, the arguments of the Qiu-Sterman function are non diagonal, we could reach kinematical points in the phase space integration, i.e. $s_{13} \to 0$, where we evaluate G_F at equal arguments. This is of course highly non trivial since $\mathcal{M}_{HP}$ is soft and collinear divergent in this point. This is due to the fact, that the HP cross section in equation (4.62) has the extra factor $1/(x_2 - x_1)$ which gives an additional singularity at the soft gluon point, on top of which is present in $\mathcal{H}^{(1),\mathrm{HP}}_\beta$ anyway. Parts of this extra divergence cancels the unpleasant singularities in the SGP contribution equation (4.54). For simplicity we absorb the delta distribution in the last line of equation (4.64) which leads to the standard three particle phase space and we can rewrite the HP contribution as

$$HP = \int \mathrm{d}PS_3 \; G_F(x, x(1-\tilde{x}), \mu) \mathcal{M}_{HP}(t_3, s_{13}, u_2) . \quad (4.66)$$

To extract the soft-gluon point contribution from this expression we start with the Taylor-expansion for the Qiu-Sterman function $G_F(x, x(1-\tilde{x}))$ with respect to $\tilde{x}$ around $\tilde{x} = 0$, i.ie

$$G_F(x, x(1-\tilde{x}), \mu) \\ = G_F(x, x, \mu) - \tilde{x}\frac{x}{2}\frac{\mathrm{d}}{\mathrm{d}x} G_F(x, x, \mu) + \sum_{k=2}^{\infty} \frac{(-\tilde{x})^k}{k!} \left(x^k \frac{\mathrm{d}^k G_F(x, y, \mu)}{\mathrm{d}y^k}\right)\Big|_{y=x} \quad (4.67)$$

We label the terms

$$HP_1 = \int \mathrm{d}PS_3 \; G_F(x, x, \mu) \mathcal{M}_{HP}(t_3, s_{13}, u_2) \quad (4.68a)$$

$$HP_2 = \int \mathrm{d}PS_3 \left(-\tilde{x}\frac{x}{2}\frac{\mathrm{d}}{\mathrm{d}x} G_F(x, x, \mu)\right) \mathcal{M}_{HP}(t_3, s_{13}, u_2) \quad (4.68b)$$

$$HP_3 = \int \mathrm{d}PS_3 \left(\sum_{k=2}^{\infty} \frac{(-\tilde{x})^k}{k!} \left(x^k \frac{\mathrm{d}^k G_F(x, y, \mu)}{\mathrm{d}y^k}\right)\Big|_{y=x}\right) \mathcal{M}_{HP}(t_3, s_{13}, u_2) , \quad (4.68c)$$

so that

$$HP = HP_1 + HP_2 + HP_3 \; . \tag{4.69}$$

HP_1 is highly soft and collinear divergent. To obtain the contribution to the cross section, we reinsert HP1 in equation (4.64),

$$\begin{aligned} E_h \frac{\mathrm{d}^3\sigma^{tw3}_{HP1}}{\mathrm{d}^3 P_h} = & \frac{\pi M_N}{S} \sum_{ac} \int \frac{\mathrm{d}z}{z^2} \int \frac{\mathrm{d}x}{x} D_c(z,\mu) \left(2\frac{s}{t_1} \epsilon^{p_c pnS_\perp} + 2\epsilon^{lpnS_\perp} \right) \\ & \times \mu^{2\varepsilon} \int \frac{\mathrm{d}^{(n-1)}q}{(2\pi)^{n-1} 2q^0} G_F(x,x,\mu) \mathcal{M}_{HP}(t_3, s_{13}, u_2) \; \delta((k_2 + l - p_c - q)^2) \\ = & \frac{-\pi M_N}{T} \epsilon^{\alpha pnS_\perp} \sum_c \int_{v_{min}}^{v_{max}} \mathrm{d}v \int_{w_{min}}^{1} \frac{\mathrm{d}w}{w} D_c(z,\mu) \left(\frac{2}{v-1} p_{c\alpha} + 2l_\alpha \right) \\ & \times G_F(x,x,\mu) C(s,v,w,\mu,\epsilon) \; . \end{aligned} \tag{4.70}$$

$\mathcal{M}_{HP}(t_3, s_{13}, u_2)$ has terms $\sim 1/(t_3^2 s_{13})$, $1/(t_3 s_{13}^2)$, $s_{23}/(t_3^2 s_{13}^2)$, that lead to manifest divergent terms

$$C(s,v,w,\mu,\epsilon) \sim \frac{h(s,v,w)}{(1-w)^{(2+\varepsilon)}} \; . \tag{4.71}$$

But fortunately, these divergent terms are exactly the same as we found in the pure SGP contribution and cancel in the sum with the B term defined in equation (4.53). Thus the combination

$$\int_{w_{min}}^{1} \mathrm{d}w \; \left(B(s,v,w,\mu,\epsilon) + C(s,v,w,\mu,\epsilon) \right) \; , \tag{4.72}$$

is well behaved at the upper boundary of the w integration. This is indeed a clear sign that the NLO result at the soft-gluon point is not given solely by the pure SGP part. At NLO we have soft collinear pole contributions that cancel among the two pole contributions at the soft gluon point.

HP_2 is a derivative term on the Qiu-Sterman function. In contrast to HP_1, the extra factor $\tilde{x}$ makes all the problematic terms in $\mathcal{M}_{HP}(t_3, s_{13}, u_2)$ well behaved, in a sense that they can be integrated using standard methods, described in appendix C and D.

There is one exception concerning the phase space integration for HP_1 and HP_2. In the inner Dirac structure of $\mathcal{H}^{(1),\mathrm{HP}}$ terms proportional to $\sim (x_2 - x_1)\not{p}$ are present which produce an extra factor $1/(t_1 + t_3)$, which is new compared to standard twist-2 single inclusive calculations. We can calculate those integrals by using the methods of

appendix C in [112], the integrals are given in group 2 and 3. We need one new integral, which is given in appendix E in this thesis.

Now, we come to the third contribution of the Taylor-expansion in equation (4.67). The extraction of the $G_F(x,x)$ part of HP_3 is quite more challenging than for the other two contributions of HP. We start with the observation that the only term from the Taylor-expansion that is affected by the phase space integral is $\tilde{x}$. Thus we can write

$$\begin{aligned} HP_3 &= \sum_{k=2}^{\infty} \frac{(-1)^k}{k!} \left(x^k \frac{\mathrm{d}^k G_F(x,y)}{\mathrm{d}y^k} \right) \Big|_{y=x} \int \mathrm{d}PS_3 \; \tilde{x}^k \mathcal{M}_{HP}(t_3, s_{13}, u_2) \\ &= \sum_{k=0}^{\infty} \frac{(-1)^k}{(k+2)!} \left(x^{k+2} \frac{\mathrm{d}^{k+2} G_F(x,y)}{\mathrm{d}y^{k+2}} \right) \Big|_{y=x} \int \mathrm{d}PS_3 \; \tilde{x}^{k+2} \mathcal{M}_{HP}(t_3, s_{13}, u_2) \; . \end{aligned} \tag{4.73}$$

Unfortunately, the term $\tilde{x}^{k+2}\mathcal{M}$ is not integrable by using the standard methods for single inclusive phase space integration. Therefore, we are not able to obtain the finite part from HP_3 so far and we leave that for future research. On the other hand, we developed a framework, where we can obtain the collinear $1/\varepsilon$ pole structure from HP_3. This is very important, since the knowledge of the pole structure is the first step towards a deep insight how the interplay of the different NLO contributions work. To do so, we have to identify the collinear regions of $\tilde{x}^{k+2}\mathcal{M}$. We want to remind the reader that $\mathcal{M}_{HP}(t_3, s_{13}, u_2)$ has the following denominator structure

$$\mathcal{M}_{HP}(t_3, s_{13}, u_2)|_{\text{poles}} = \left\{ \frac{1}{s_{13}}; \; \frac{1}{s_{13}^2}; \; \frac{1}{t_3}; \frac{1}{t_3^2}; \; \frac{1}{u_2}; \; \frac{1}{u_2^2} \right\} \; , \tag{4.74}$$

where only denominators are listed that eventually produce a collinear pole. We see immediately, that the factor $\tilde{x}^{k+2}$ makes the $\tilde{x}^{k+2}\mathcal{M}$ finite for $s_{13} \to 0$. This is due to the fact that $\tilde{x}^{k+2} \sim s_{13}^{k+2}$ and $k \geq 0$. Concerning that we identify two collinear regions in HP_3, these are $u_2 \to 0$ and $t_3 \to 0$. Therefore, we can decompose

$$\tilde{x}^2 \mathcal{M} = \mathcal{M}_1 + \mathcal{M}_2 + \mathcal{M}_3 \; , \tag{4.75}$$

where $\mathcal{M}_1$ is singular as $u_2 \to 0$, $\mathcal{M}_2$ is singular as $t_2 \to 0$, and $\mathcal{M}_3$ is completely finite.

We first consider the phase space integration for $\tilde{x}^k \mathcal{M}_1$ or more precisely the extraction of its $1/\varepsilon$ pole part. We arranged the terms in a way that $\tilde{x}^k \mathcal{M}_1$ is divergent for $u_2 \to 0$. For the angular integration we work in the rest frame of the two unobserved final states, but we are free to choose which of the three observed momenta defines the direction of the z-axis (see appendix D). Here we choose that the initial state lepton defines the z-axis, i.e. we use "set 1". In that frame, u_2 has its simplest structure

$$u_2 = u_2^0 (1 - \cos\theta_1) \; , \tag{4.76}$$

where we conclude that the collinear limit is defined by $\theta_1 \to 0$. In this frame, our integrand has terms $\sim 1/u_2$ and $\sim 1/u_2^2$. Therefore, we can further decompose $\tilde{x}^k \mathcal{M}_1$ in these two contributions,

$$\tilde{x}^k \mathcal{M}_1 = \frac{\mathcal{N}_1^1(v, w, \theta_1, \theta_2)}{s u_2^0 (1 - \cos\theta_1)} + \frac{\mathcal{N}_1^2(v, w, \theta_1, \theta_2)}{(u_2^0 (1 - \cos\theta_1))^2} \tag{4.77}$$

where the functions $\mathcal{N}_1^i(s, v, w, \theta_1, \theta_2)$ are dependent on the kinematical variables s, v, w and the two spherical angles between the two unobserved final states θ_1 and θ_2. It turned out, that if we Taylor expand N_2^1 around $\cos\theta_1 = 1$ that the zeroth order cancels, i.e.

$$\mathcal{N}_1^2(v, w, \theta_1, \theta_2) = (1 - \cos\theta_1)\tilde{\mathcal{N}}_1^2(v, w, \cos\theta_2) + \mathcal{O}((1 - \cos\theta_1)^2) \,, \tag{4.78}$$

whereas the expansion for N_1^1 starts at zeroth order

$$\mathcal{N}_1^1(s, v, w, \theta_1, \theta_2) = \tilde{\mathcal{N}}_1^1(v, w, \cos\theta_2) + \mathcal{O}((1 - \cos\theta_1)) \,. \tag{4.79}$$

We can combine these terms and end up with

$$\begin{aligned} \tilde{x}^k \mathcal{M}_1 = \frac{1}{1 - \cos\theta_1} \left(\frac{\tilde{\mathcal{N}}_1^2(v, w, \cos\theta_2)}{(u_2^0)^2} + \frac{\tilde{\mathcal{N}}_1^1(v, w, \cos\theta_2)}{s u_2^0} \right) \\ + \mathcal{O}((1 - \cos\theta_1)^0) \end{aligned} \tag{4.80}$$

where $\mathcal{O}((1 - \cos\theta_1)^0)$ indicates that there are finite terms we have not included so far. It is important to mention that equation (4.80) is independent of k since $\tilde{x} \to 1$ for $\cos\theta_1 \to 1$. Since, the expansion for N_2^1 starts with a term $\sim (1 - \cos\theta_1)$ there is no term $1/(1 - \cos\theta_1)^2$ left. In other words, in our leading collinear term we have θ_1-dependence only through $1/(1 - \cos\theta_1)$ as an overall factor. For the θ_2 dependence we obtain two different terms in our leading collinear expansion. We have on the one hand terms that are independent of θ_2 on the other hand terms that are proportional $\cos^2\theta_2$. Therefore, we need two angular integrals here

$$\begin{aligned} I^1_{\text{col.}} &= \int_0^\pi \mathrm{d}\theta_1 \int_0^\pi \mathrm{d}\theta_2 \; \sin^{1-2\varepsilon}\theta_1 \sin^{-2\varepsilon}\theta_2 \; \frac{1}{(1 - \cos\theta_1)} = \frac{-\pi}{\varepsilon} + \mathcal{O}(\varepsilon^0) \,, \\ I^2_{\text{col.}} &= \int_0^\pi \mathrm{d}\theta_1 \int_0^\pi \mathrm{d}\theta_2 \; \sin^{1-2\varepsilon}\theta_1 \sin^{-2\varepsilon}\theta_2 \; \frac{\cos^2\theta_2}{(1 - \cos\theta_1)} = \frac{-\pi}{2\varepsilon} + \mathcal{O}(\varepsilon^0) \,. \end{aligned} \tag{4.81}$$

By using the two integrals we find:

$$\int \mathrm{d}PS_3 \; \tilde{x}^k \mathcal{M}_1 = \frac{1}{\varepsilon} f(s, v, w) + \mathcal{O}(\varepsilon^0) \tag{4.82}$$

where $f(s,v,w)$ is a simple rational function. The finite terms, that are $\mathcal{O}(\varepsilon^0)$ are again not included in our calculation. To complete the calculation for $\mathcal{M}_1$ we must insert $f(s,v,w)$ into equation (4.73) and convert the infinite series back into normal expression in terms of G_F. Inserting equation (4.82) into (4.73) we get

$$\begin{aligned}
&\sum_{k=0}^{\infty} \frac{(-1)^k}{(k+2)!} \left(x^{k+2} \frac{\mathrm{d}^{k+2} G_F(x,y)}{\mathrm{d}y^{k+2}} \right)\Big|_{y=x} \frac{f(s,v,w)}{\varepsilon} \\
&\quad = \sum_{k=2}^{\infty} \frac{(-1)^k}{k!} \left(x^{k} \frac{\mathrm{d}^{k} G_F(x,y)}{\mathrm{d}y^{k}} \right)\Big|_{y=x} \frac{f(s,v,w)}{\varepsilon} \\
&\quad = \left(G_F(x,0) + \frac{x}{2} \frac{\mathrm{d}}{\mathrm{d}x} G_F(x,x) - G_F(x,x) \right) \frac{f(s,v,w)}{\varepsilon} \,, \qquad (4.83)
\end{aligned}$$

with

$$f(s,v,w) = \alpha_{em}^2 e_a^2 \frac{\alpha_s}{\pi} \left(vwC_F - \frac{N_C}{2} \right) \frac{(v^2(2w^2-2w+1) - 2vw + 1)}{s^2(v-1)^2 v^2 w^2 (vw-1)} \,. \qquad (4.84)$$

in the q-fragmentation channel. Equation (4.83) shows that a soft-fermion-pole arises, which is a very interesting result from our calculation. These poles should cancel among SFP contribution where the pole is manifest in the whole NLO phase space.

Next, we consider $\tilde{x}^k \mathcal{M}_2$ and extract its pole part. In that case, the divergence appear if $t_3 \to 0$. We choose here the parton momentum coming from the polarized hadron to define the z-direction, i.e. "set 1". In that frame with $t_3 = t_3^0(1+\cos\theta_1)$, the collinear limit is defined by $\theta_1 \to \pi$. We can perform the same expansion as in the $u_2 \to 0$ case. We find that the leading collinear term is again proportional to $\sim 1/(1+\cos\theta_1)$ and also has no soft piece. But, in contrast to the $u_2 \to 0$ case, the result is k dependent. The reason for this behavior is that from the collinear limit $t_3 \to 0$ follows that $\tilde{x} \to 1-w$. We find for the pole part

$$\begin{aligned}
\int \mathrm{d}PS_3 \, \tilde{x}^k \mathcal{M}_2 = \frac{1}{\varepsilon} \Big(&(1-w)^{k+1} g_1(v,w) + (k+1)(1-w)^k g_2(v,w) \Big) \\
&+ \mathcal{O}(\varepsilon^0) \qquad (4.85)
\end{aligned}$$

where g_1 and g_2 are simple rational functions given in the q fragmentation channel as

$$g_1(v,w,s) = \alpha_{em}^2 e_a^2 \frac{\alpha_s}{\pi} N_C \frac{v^2+1}{2s^2(v-1)^2 v^3 w^2} \,, \qquad (4.86a)$$

$$g_2(v,w,s) = \alpha_{em}^2 e_a^2 \frac{\alpha_s}{\pi} N_C \frac{\left(v^2+1\right)(w+1)}{2s^2(v-1)^2 v^3 w} \,. \qquad (4.86b)$$

The next step is to insert this result into equation (4.73) and rewrite the sum into combinations of Qiu-Sterman functions. This is surely more challenging as in the $u_2 \to 0$

case, since our result is k dependent. We start with the g_1 part

$$\begin{aligned}
&\sum_{k=0}^{\infty}\frac{(-1)^k}{(k+2)!}\left(x^{k+2}\frac{\mathrm{d}^{k+2}G_F(x,y)}{\mathrm{d}y^{k+2}}\right)\Big|_{y=x}(1-w)^{k+1}\frac{g_1(v,w,s)}{\varepsilon}\\
&\quad=\frac{1}{\varepsilon}\frac{g_1(v,w,s)}{1-w}\sum_{k=2}^{\infty}\frac{(-1)^k}{k!}\left(x^{k}\frac{\mathrm{d}^{k}G_F(x,y)}{\mathrm{d}y^{k}}\right)\Big|_{y=x}(1-w)^{k}\\
&\quad=\frac{1}{\varepsilon}\frac{g_1(v,w,s)}{1-w}\left[\frac{G_F(x,xw)-G_F(x,x)}{1-w}+\frac{x}{2}\frac{\mathrm{d}}{\mathrm{d}x}G_F(x,x)\right]
\end{aligned}\tag{4.87}$$

Likewise we can rewrite the g_2 part,

$$\begin{aligned}
&\sum_{k=0}^{\infty}\frac{(-1)^k}{(k+2)!}\left(x^{k+2}\frac{\mathrm{d}^{k+2}G_F(x,y)}{\mathrm{d}y^{k+2}}\right)\Big|_{y=x}(k+1)(1-w)^{k}\frac{g_2(v,w,s)}{\varepsilon}\\
&\quad=-\frac{1}{\varepsilon}g_2(v,w,s)\frac{\partial}{\partial w}\left[\sum_{k=0}^{\infty}\frac{(-1)^k}{(k+2)!}\left(x^{k+2}\frac{\mathrm{d}^{k+2}G_F(x,y)}{\mathrm{d}y^{k+2}}\right)\Big|_{y=x}(1-w)^{k+1}\right]\\
&\quad=-\frac{1}{\varepsilon}g_2(v,w,s)\frac{\partial}{\partial w}\left[\frac{G_F(x,xw)-G_F(x,x)}{1-w}+\frac{x}{2}\frac{\mathrm{d}}{\mathrm{d}x}G_F(x,x)\right]\\
&\quad=-\frac{1}{\varepsilon}g_2(v,w,s)\frac{\partial}{\partial w}\left[\frac{G_F(x,xw)-G_F(x,x)}{1-w}\right]
\end{aligned}\tag{4.88}$$

where it is important that $\partial/\partial w$ is a partial derivative. Therefore, it acts only on the explicit dependence on w and because of this, the derivative term in the third line cancels out. We can merge our results in equations (4.83),(4.87) and (4.88) in equation (4.68c) and we end up with

$$\begin{aligned}
HP_3 = \quad&\frac{1}{\varepsilon}f(s,v,w)\left[G_F(x,0)+\frac{x}{2}\frac{\mathrm{d}}{\mathrm{d}x}G_F(x,x)-G_F(x,x)\right]\\
&+\frac{1}{\varepsilon}\frac{g_1(v,w,s)}{1-w}\left[\frac{G_F(x,xw)-G_F(x,x)}{1-w}+\frac{x}{2}\frac{\mathrm{d}}{\mathrm{d}x}G_F(x,x)\right]\\
&-\frac{1}{\varepsilon}g_2(v,w,s)\frac{\partial}{\partial w}\left[\frac{G_F(x,xw)-G_F(x,x)}{1-w}\right]\,.
\end{aligned}\tag{4.89}$$

Now, we are able to extract the whole ε-pole structure from the HP contribution and even a new pole structure arises, which we identify as a SFP. This is indeed very interesting since it demonstrates that one should also include SFP contributions because they are connected by their pole structure.

We want to mention, that the partonic functions for the $2 \to 3$ process, HP and SGP contributions, are cross checked by a calculation using a different ansatz as we showed above. We used for the cross check formula (20) in [161], which is also called "master formula", but it should not be mixed up with our equation (4.50). The two calculations lead to the exact same result.

4.6. Evolution equation and collinear subtraction

4.6.1. Evolution equation for the Qiu-Sterman function

To obtain the factorization contribution we have to include beneath the twist-2 evolution of the fragmentation function, the twist-3 evolution of the Qiu-Sterman function. The evolution kernel for the quark-gluon-quark correlator is highly non trivial. Over the last decade a lot of progress has been made to determine this function using different formulations [83, 162–164]. A complete picture is given in [165–167]. The result presented in [167] includes a "new"-HP contribution, coming from gluon-quark-quark or quark-quark-gluon correlations. So far, we have not included them into our $2 \to 3$ calculation and therefore we neglect them. For the non-derivative part of the Qiu-Sterman function the evolution kernel is given by

$$\begin{aligned}\frac{\partial}{\partial \ln \mu^2} G_F(x,x,\mu^2) =& \frac{\alpha_s}{2\pi} \int_x^1 \frac{\mathrm{d}z}{z} \Bigg\{ \left[P_{qq}\left(\frac{x}{z}\right) - C_A \delta\left(1-\frac{x}{z}\right) \right] G_F(z,z,\mu^2) \\ &+ \frac{C_A}{2} \left[\frac{1+\frac{x}{z}}{1-\frac{x}{z}} \left(G_F(z,x,\mu^2) - G_F(z,z,\mu^2) \right) + \frac{x}{z} G_F(z,z,\mu^2) \right] \Bigg\}\end{aligned} \tag{4.90}$$

where P_{qq} is the usual quark to quark splitting function given in equation (1.70). In the literature, evolution kernels have been discussed for non-derivative Qiu-Sterman contributions [83, 162–167]. However, we need the evolution equation for the LO combination $G_F(x,x) - x\,\mathrm{d}/\mathrm{d}x\, G_F(x,x)$. To obtain the derivative part of the evolution equation we take the derivative with respect to x of equation (4.90). We find,

$$\begin{aligned}&\frac{\partial}{\partial \ln \mu^2} \left(G_F(x,x,\mu^2) - x \frac{\mathrm{d}}{\mathrm{d}x} G_F(x,x,\mu^2) \right) = \\ &\frac{\alpha_s}{2\pi} \Bigg\{ \int_x^1 \frac{\mathrm{d}z}{z} \Bigg[\left[P_{qq}\left(\frac{x}{z}\right) - \frac{C_A}{2} \delta\left(1-\frac{x}{z}\right) \right] \left(G_F(z,z,\mu^2) - x \frac{\mathrm{d}}{\mathrm{d}x} G_F(z,z,\mu^2) \right) \\ &\quad + \frac{C_A}{2} \left(1 - \left(1+\frac{x}{z}\right) x \frac{\mathrm{d}}{\mathrm{d}x} \right) \left(\frac{\left(G_F(z,x,\mu^2) - G_F(z,z,\mu^2) \right)}{1-\frac{x}{z}} \right) \Bigg] \Bigg\} .\end{aligned} \tag{4.91}$$

Finally, by including the twist-2 kernels given in chapter 2 all evolution kernels are available to obtain the correct collinear subtraction term.

4.6.2. Collinear subtraction

In the the $2 \to 3$ process, we have certain collinear contributions that produce $\frac{1}{\varepsilon}$-poles, which must be subtracted into the bare distributions $G_F^{(0)}$, $D^{(0)}$ and the bare photon in

lepton distribution $f^{(0)}_{\gamma\ell}$. We refer to chapter 2 where this subtraction method, and the photon in lepton distribution is explained in detail. The subtraction terms defined in equation 2.12b and 2.16 has the same structure in the twist-3 case. We mention that the splitting kernels are convoluted with the leading order partonic functions $q\ell \to q\ell$ and $\gamma q \to \gamma q$, which have to be replaced by the twist-3 ones.

To subtract the initial state photon-lepton collinear singularity, we use the Weizsäcker-Williams contribution defined in equations 2.18 and 2.19. The singularity appears in our cross section, because we assume the lepton to be massless. Therefore, as discussed in in chapter 2 and [3], we could either assume a massive lepton throughout the whole calculation, or we assume a massles lepton and absorb the appearing pole it into the bare Weizsäcker-Williams distribution given in equation (2.18). Both strategies, lead to the same result. Therefore, we perform a massless calculation, since this is convenient for phase space integration. However, the factorization contribution is then depended on the lepton mass. We found that the ε-pole from the photon-lepton singularity turns into

$$\frac{1}{\varepsilon} \to -\ln\left(\frac{\mu^2}{m_\ell^2}\right) , \tag{4.92}$$

with m_ℓ the lepton mass.

Pole contributions where the initial state quark radiates a collinear final state gluon are absorbed into the combination $G_F^{(0)}(x,x,\mu) - \frac{\mathrm{d}}{\mathrm{d}x} G_F^{(0)}(x,x,\mu)$ of bare Qiu-Sterman functions as follows

$$\begin{aligned} G_F(x,x,\mu) - \frac{\mathrm{d}}{\mathrm{d}x} G_F(x,x,\mu) = G_F^{(0)}(x,x,\mu) - \frac{\mathrm{d}}{\mathrm{d}x} G_F^{(0)}(x,x,\mu) \qquad (4.93) \\ + \frac{1}{\varepsilon}\frac{\alpha_s}{2\pi}\left\{ \int_x^1 \frac{\mathrm{d}z}{z}\left[\left[P_{qq}\left(\frac{x}{z}\right) - \frac{C_A}{2}\delta\left(1-\frac{x}{z}\right)\right]\left(G_F(z,z,\mu^2) - x\frac{\mathrm{d}}{\mathrm{d}x} G_F(z,z,\mu^2)\right)\right.\right. \\ \left.\left. + \frac{C_A}{2}\left(1 - \left(1+\frac{x}{z}\right)x\frac{\mathrm{d}}{\mathrm{d}x}\right)\left(\frac{\left(G_F(z,x,\mu^2) - G_F(z,z,\mu^2)\right)}{1-\frac{x}{z}}\right)\right]\right\} . \end{aligned}$$

The Qiu-Sterman function in the last line has the explicit dependence on x in its argument, which is different to twist-2 factorization terms. In initial state factorization the term x/z becomes w. The differential in the last term in equation (4.93) reproduces exactly the pole-term coming from the g_2 contribution in equation (4.88).

Finally, we have determined the complete ε-pole structure in the $2 \to 3$ process at the soft twist-3 gluon point and the appropriate collinear subtraction term. We can add all

ε-poles from equations (4.53) and (4.64) and find the remaining poles

$$E_h \frac{\mathrm{d}^3\sigma^{tw3}_{\mathrm{pole}}}{\mathrm{d}^3 P_h} = \frac{-\pi M_N}{T}\epsilon^{\alpha pnS_\perp}\sum_c \int_{v_{min}}^{v_{max}} \mathrm{d}v \int_{w_{min}}^{1} \frac{\mathrm{d}w}{w} D_c(z,\mu)\left(\frac{2}{v-1}p_{c\alpha} + 2l_\alpha\right) \tag{4.94}$$
$$\times\left\{\left(G_F(x,x,\mu) - x\frac{\mathrm{d}G_F(x,x,\mu)}{\mathrm{d}x}\right)P_1(s,v,w,\mu,\epsilon) + G_F(x,x,\mu)P_2(s,v,w,\mu,\epsilon)\right\}.$$

with

$$P_1(s,v,w,\mu,\epsilon) \tag{4.95a}$$
$$= \alpha_{em}^2 e_a^2 \frac{\alpha_s}{\pi}\left(\frac{4\pi\mu}{s}\right)^{2\varepsilon}\left[C_F\left\{\frac{1}{\varepsilon^2}\frac{-2}{s^2v^2}\frac{v^2+1}{(1-v)^2} + \frac{1}{\varepsilon}\frac{(2\ln(1-v)-3)\left(v^2+1\right)}{s^2(v-1)^2v^2}\right\}\right.$$
$$\left.\times\,\delta(1-w)\right],$$

$$P_1(s,v,w,\mu,\epsilon) \tag{4.95b}$$
$$= \alpha_{em}^2 e_a^2 \frac{\alpha_s}{\pi}\left(\frac{4\pi\mu}{s}\right)^{2\varepsilon}\left[C_F\frac{1}{\varepsilon}\frac{-2}{s^2v^2}\frac{\left(v^2+1\right)}{(v-1)^2} - N_C\frac{1}{\varepsilon}\frac{(v+1)}{s^2v(v-1)^2}\right]\delta(1-w).$$

The ε-poles which are present in (4.94) must cancel among the poles in the virtual correction to secure factorization.

4.7. Real correction results

So far, we derived the complete pure SGP correction and parts of the HP contribution, as well as the complete ε-pole structure from these contributions. Therefore, we could achieve several important results for the real part of the NLO calculation:

- The complete real correction to the derivative part on the Qiu-Sterman function.
- The complete ε-pole structure at the soft gluon point
- The complete distribution part from the HP contribution at the soft gluon point.
- Most of the non-singular parts of the HP contribution.

The regular part in the HP contribution which we did not obtained so far, arises solely in the HP3 contribution. The HP1 and HP2 contributions are derived completely.

However, the results are lengthy and therefore we can not show them completely. In the subsequent section, we highlight some results from our calculation. A very interesting observation can be made concerning the logarithmic plus distributions. They have the structure

$$E_h \frac{\mathrm{d}^3\sigma^{tw3}_{\log}}{\mathrm{d}^3 P_h} = \frac{-\pi M_N}{T}\epsilon^{\alpha pnS_\perp}\sum_c \int_{v_{min}}^{v_{max}} \mathrm{d}v \int_{w_{min}}^{1} \frac{\mathrm{d}w}{w} D_c(z,\mu)\left(\frac{2}{v-1}p_{c\alpha}+2l_\alpha\right) \times\left(G_F(x,x,\mu)-x\frac{\mathrm{d}G_F(x,x,\mu)}{\mathrm{d}x}\right)\sigma^{tw3}_{\mathrm{LO}}\frac{\alpha_s}{\pi}4C_F\left(\frac{\ln(1-w)}{1-w}\right)_+ \tag{4.96}$$

where $\sigma^{tw3}_{\mathrm{LO}}$ is the twist 3 leading order partonic cross section defined in equation (4.20). The Leading logarithmic threshold correction, is evoked by soft collinear gluon radiation to the initial and final state quark. Since soft gluon emission is spin-independent, the relative correction remains the same.

In our calculation we obtain also full control over $\frac{1}{(1-w)_+}$-terms. They are given by

$$E_h \frac{\mathrm{d}^3\sigma^{tw3}_{\mathrm{plus}}}{\mathrm{d}^3 P_h} = \frac{-\pi M_N}{T}\epsilon^{\alpha pnS_\perp}\sum_c \int_{v_{min}}^{v_{max}} \mathrm{d}v \int_{w_{min}}^{1} \frac{\mathrm{d}w}{w} D_c(z,\mu)\left(\frac{2}{v-1}p_{c\alpha}+2l_\alpha\right) \times\left\{\left(G_F(x,x,\mu)-x\frac{\mathrm{d}G_F(x,x,\mu)}{\mathrm{d}x}\right)E_1(s,v,w,\mu)+G_F(x,x,\mu)E_2(s,v,w,\mu)\right\} \tag{4.97}$$

with

$$E_1(s,v,w,\mu) = \alpha^2_{em}e_a^2\frac{\alpha_s}{\pi}\left\{C_F\left(\frac{-4\left(1+v^2\right)}{s^2(1-v)^2v^2}\ln\left(\frac{sv(1-v)}{\mu^2}\right)-\frac{4}{s^2v^2}\right) -N_C\frac{\left(1+v^2\right)}{s^2(1-v)^2v^2}\right\}\left(\frac{1}{1-w}\right)_+ . \tag{4.98a}$$

$$E_1(s,v,w,\mu) = \alpha^2_{em}e_a^2\frac{\alpha_s}{\pi}\left\{C_F\frac{-2\left(1+v^2\right)}{s^2v^2}-N_C\frac{1+v^2}{2s^2(1-v)^2v^2}\right\}\left(\frac{1}{1-w}\right)_+ . \tag{4.98b}$$

where the relative prefactor compared to LO for the term $\sim \ln\left(\frac{sv(1-v)}{\mu^2}\right)$ in E_1 is again the same as in the unpolarized case. This is due to the fact, that these contributions are a remnant of collinear quark gluon configurations of the external particles. Due to the Dirac structure of the cross section, such contributions may factored away from the inner born structure of the partonic scattering.

4.8. Conclusions

In this chapter we derived the real NLO correction for the process $h^{\uparrow} l \to \pi X$. Within the twist-3 collinear factorization formalism we first studied the pole contribution which arises when the coherent gluon becomes soft. We found a remarkably complex structure of the NLO contributions. We found on the one hand real corrections, that produce a pure SGP and on the other hand we found real corrections that produce SGP contributions in certain regions of phase space of the unobserved final state particles.

In our calculation we have obtained full control over terms $\sim \left(\frac{\ln(1-w)}{1-w}\right)_+$ and $\sim \left(\frac{1}{1-w}\right)_+$. We could show, that the relative prefactor compared to LO for the logarithmic plus distribution is the same as in the unpolarized case. This is indeed a very interesting result and supports the fact that soft gluon emission is spin independent.

We could derive the complete collinear pole structure from the two real SGP contributions and we showed that the pole structure we found in the evolution kernel cancels most of them. The remaining poles are accompanied by the delta distribution $\delta(1-w)$ which may cancel among the virtual NLO correction. So far, we have not included the virtual contribution and we leave that for future research. We could show that the highly non-trivial ε-pole structure can not be isolated concerning the poles that fix the arguments of the Qiu-Sterman function. Therefore, we will derive beneath the SGP all HP and SFP contributions in future work. This is crucial for a deep understanding of the twist-3 cross section at NLO.

Chapter 5.

Toward NNLL Threshold Resummation for Hadron Pair Production in Hadronic Collisions

We investigate QCD threshold resummation effects beyond the next-to-leading logarithmic (NLL) order for the process $H_1H_2 \to h_1h_2X$ at high invariant mass of the produced hadron pair. We take into account the color structure of the underlying partonic hard-scattering cross sections and determine the relevant hard and soft matrices in color space that contribute to the resummed cross section at next-to-next-to-leading logarithmic (NNLL) accuracy. We present numerical results for fixed-target and collider regimes. We find a significant improvement compared to previous results at NLL accuracy. In particular, the scale dependence of the resummed cross section is greatly reduced. Use of the most recent set of fragmentation functions also helps in improving the comparison with the experimental data. Our calculation provides a step towards a systematic NNLL extension of threshold resummation also for other hadronic processes, in particular for jet production. This chapter is based on publications [2, 7]

5.1. Introduction

The resummation of threshold logarithms in partonic hard-scattering cross sections contributing to hadronic scattering has received an ever-growing attention in recent years. On the one hand, resummation is phenomenologically relevant in many kinematical situations, ranging from fixed-target energies all the way to the LHC. At the same time, it offers insights into the structure of perturbative corrections at higher orders, which

among other things may provide benchmarks for explicit full fixed-order calculations in QCD.

Threshold logarithms typically arise when the initial partons have just enough energy to produce the observed final state. In this case, the phase space available for gluon bremsstrahlung vanishes, resulting in large logarithmic corrections. Taking the hadron-pair production cross section to be discussed in this chapter as an example, the partonic threshold is reached when $\hat{s} = \hat{m}^2$, that is, $\hat{\tau} \equiv \hat{m}^2/\hat{s} = 1$, where $\sqrt{\hat{s}}$ is the partonic center-of-mass system (c.m.s.) energy and $\hat{m}$ the pair mass of two outgoing produced partons that eventually fragment into the observed hadron pair. The leading large contributions near threshold arise as $\alpha_s^k \left[\ln^{2k-1}(1-\hat{\tau})/(1-\hat{\tau})\right]_+$ at the kth order in perturbation theory, where α_s is the strong coupling and the "plus" distribution will be defined below. There is a double-logarithmic structure, with two powers of the logarithm arising for every new order in the coupling. Subleading terms have fewer logarithms, so that the threshold logarithms in the perturbative series take the general form

$$\sum_{k=0}^{\infty} \sum_{\ell=1}^{2k} \alpha_s^k \, \mathcal{A}_{k,\ell} \left(\frac{\ln^{2k-\ell}(1-\hat{\tau})}{1-\hat{\tau}} \right)_+ , \tag{5.1}$$

with perturbative coefficients $\mathcal{A}_{k,\ell}$. One often refers to the all-order set of logarithms with a fixed ℓ as the ℓth tower of logarithms. As has been established in the literature [39, 40, 168–170], threshold logarithms exponentiate after taking an integral transform conjugate to the relevant kinematical variable ($\hat{\tau}$ in the above example). Under this transform the threshold logarithms translate into logarithms of the transform variable N. The exponent may itself be written as a perturbative series and is only *s*ingle-logarithmic in the transform variable. Ignoring for the moment the color structure of the underlying partonic cross section, the structure of the resummed cross section becomes in transform space

$$\left(1 + \alpha_s C^{(1)} + \alpha_s^2 C^{(2)} + \ldots\right) \exp\left[\sum_{k=1}^{\infty} \sum_{\ell=1}^{k+1} \mathcal{B}_{k,\ell} \alpha_s^k \, \ln^{\ell}(N) \right] , \tag{5.2}$$

again with coefficients $\mathcal{B}_{k,\ell}$ and with "matching coefficients" $C^{(k)}$ that ensure that at every fixed order the resummed cross section agrees with the exact fixed-order one, up to corrections suppressed at threshold. They contain the full virtual corrections at order α_s^k, corresponding to contributions $\propto \delta(1-\hat{\tau})$ in the partonic cross section, and may be compared by comparison to a full fixed-order calculation performed near threshold. Thanks to the exponentiated single-logarithmic structure of the exponent, knowledge of the two leading towers $\alpha_s^k \ln^{k+1}(N)$ and $\alpha_s^k \ln^k(N)$, along with the coefficient $C^{(1)}$, is sufficient to predict the *t*hree leading towers in the perturbative series (5.1) for the cross section in $\hat{\tau}$-space. This is termed "next-to-leading logarithmic" (NLL) resummation. At full next-to-next-to-leading logarithmic (NNLL) accuracy, one needs three towers in

the exponent and the two-loop coefficient $C^{(2)}$, already providing control of five towers in the partonic cross section.

While NLL resummation was the state of the art for many years, much progress has been made recently on extending the framework to NNLL accuracy, or even beyond. The most advanced results have been obtained for color-singlet processes such as Higgs production, where NNLL [171–173] and, most recently, even studies up to the N^{3}LL level [174, 175] have been obtained, in which seven towers of logarithms are fully taken into account to all orders. This became possible when all threshold distributions at three-loop order were computed [176]. For processes that are not characterized by a color-singlet lowest-order (LO) hard scattering reaction, progress beyond NLL has also been made. For such processes, the resummation framework becomes more complex because the interference between soft emissions by the various external partons in the hard scattering process becomes sensitive to the color structure of the hard scattering itself. This requires a color basis for the partonic scattering process which, as will be reviewed below, leads to a matrix structure of the soft emission [40, 170, 177–179]. This ultimately turns the exponential in (5.2) into a sum of exponentials, each with its own set of matching coefficients $C^{(k)}$. An extensive list of color-non-singlet reactions of this type along with corresponding references to NLL studies may be found in [180]. Resummation studies beyond NLL have been presented in the context of top quark (pair) production [181–195], for single-inclusive hadron production [180], and for squark and gluino production [196–198]. At present, full NNLL resummation in the sense described above is not yet possible for most processes, since the required two-loop matching coefficients are usually not yet available (see, however, the recent calculation [199] for massless scattering). Nonetheless, with knowledge of the one-loop matching coefficients an improvement of the resummation framework becomes possible already, providing control of four (instead of five at full NNLL) towers in the partonic cross sections. A prerequisite for this is that the appropriate color structure be taken into account for all ingredients in the resummed expression.

In this chapter, we will develop such a partial NNLL resummation for the process of di-hadron production in hadronic collisions, collecting all necessary ingredients. Previously, Ref. [200] presented a NLL study for this process which forms the basis for this chapter. Kinematically, hadron pair production shares many features with the much simpler color-singlet Drell-Yan process, if one confronts the produced partonic pair mass $\hat{m}$ with the invariant mass of the lepton pair. The interesting aspect of di-hadron production is that it possesses all the color complexity of the underlying $2 \to 2$ QCD hard scattering. As such, the process becomes an ideal test for the study of QCD resummation beyond NLL and can serve as a template for reactions of more significant phenomenological interest, especially single or two-jet production in hadronic collisions. That said, di-hadron production is phenomenologically relevant in its own right as experimental data as a function of the pair's mass are available from various fixed-target experiments [201–204], as well as from the ISR [205]. In addition, di-hadron

cross sections are also accessible at the Relativistic Heavy Ion Collider (RHIC).

This chapter is structured as follows. In Sec. 5.2 we recall the basic formulas for the di-hadron cross section as a function of pair mass at fixed order in perturbation theory, and display the role of the threshold region. In order for this thesis to be self-contained, we recall a number of results from [200]. Section 5.3 presents details of the NNLL threshold resummation for the cross section. In particular, we derive the various hard and soft matrices in color space that are needed for the analysis. Here, we make use of one-loop results available in the literature [206–208] and compare to related work [209]. In Sec. 5.4 we give phenomenological results, comparing the threshold resummed calculations at NLL and NNLL to some of the available experimental data. Finally, we summarize our results in Sec. 5.5.

5.2. Hadron pair production near partonic threshold

5.2.1. Perturbative cross section

As in [200], we consider the process $H_1(P_a)+H_2(P_b) \to h_1(P_c)+h_2(P_d)+X$ at measured pair invariant mass squared,

$$M^2 \equiv (P_c + P_d)^2 \,, \tag{5.3}$$

and at c.m.s. rapidities η_1, η_2 of the two produced hadrons. It is convenient to introduce

$$\begin{aligned} \Delta\eta &= \frac{1}{2}(\eta_1 - \eta_2) \,, \\ \bar{\eta} &= \frac{1}{2}(\eta_1 + \eta_2) \,. \end{aligned} \tag{5.4}$$

For sufficiently large M^2, the cross section for the process can be written in the factorized form

$$\begin{aligned} M^4 \frac{\mathrm{d}\sigma^{H_1H_2\to h_1h_2X}}{\mathrm{d}M^2\mathrm{d}\Delta\eta\mathrm{d}\bar{\eta}} &= \sum_{abcd} \int_0^1 \mathrm{d}x_a \mathrm{d}x_b \mathrm{d}z_c \mathrm{d}z_d \, f_a^{H_1}(x_a,\mu_F) f_b^{H_2}(x_b,\mu_F) \\ &\quad \times z_c D_c^{h_1}(z_c,\mu_F) z_d D_d^{h_2}(z_d,\mu_F) \, \omega_{ab\to cd}\left(\hat{\tau}, \Delta\eta, \hat{\eta}, \alpha_s(\mu_R), \frac{\mu_R}{\hat{m}}, \frac{\mu_F}{\hat{m}}\right) \,, \end{aligned} \tag{5.5}$$

where $\hat{\eta}$ is the average rapidity in the partonic c.m.s., which is related to $\bar{\eta}$ by

$$\hat{\eta} = \bar{\eta} - \frac{1}{2}\ln\left(\frac{x_a}{x_b}\right) \,. \tag{5.6}$$

The quantity $\Delta\eta$ is a difference of rapidities and hence boost invariant. The average and relative rapidities for the hadrons and their parent partons are the same, since all particles are taken to be massless. The functions $f_{a,b}^{H_{1,2}}$ in equation (5.5) are the parton

distribution functions for partons a, b in hadrons $H_{1,2}$ and $D_{c,d}^{h_{1,2}}$ the fragmentation functions for partons c, d fragmenting into the observed hadrons $h_{1,2}$. The distribution functions are evaluated at a factorization scale μ_F that we choose to be the same for the initial and the final state. μ_R denotes the renormalization scale, which may differ from μ_F. The partonic momenta are given in terms of the hadronic ones by $p_a = x_a P_a$, $p_b = x_b P_b$, $p_c = P_c/z_c$, $p_d = P_d/z_d$. We introduce

$$\begin{aligned} S &= (P_a + P_b)^2 \,, \\ \tau &\equiv \frac{M^2}{S} \,, \\ \hat{s} &\equiv (x_a P_a + x_b P_a)^2 = x_a x_b S \,, \\ \hat{m}^2 &\equiv \left(\frac{P_c}{z_c} + \frac{P_d}{z_d}\right)^2 = \frac{M^2}{z_c z_d} \,, \\ \hat{\tau} &\equiv \frac{\hat{m}^2}{\hat{s}} = \frac{M^2}{x_a x_b z_c z_d S} = \frac{\tau}{x_a x_b z_c z_d} \,. \end{aligned} \tag{5.7}$$

The $\omega_{ab\to cd}$ in equation (5.5) are the hard-scattering functions for the contributing partonic processes $ab \to cdX'$, where X' denotes some additional unobserved partonic final state. Since the cross section in equation (5.5) has been written in a dimensionless form, the $\omega_{ab\to cd}$ can be chosen to be functions of $\hat{m}^2/\hat{s} = \hat{\tau}$ and the ratios of $\hat{m}$ to the factorization and renormalization scales, as well as the rapidities and the strong coupling. They may be computed in QCD perturbation

$$\omega_{ab\to cd} = \left(\frac{\alpha_s}{\pi}\right)^2 \left[\omega_{ab\to cd}^{\mathrm{LO}} + \frac{\alpha_s}{\pi}\,\omega_{ab\to cd}^{\mathrm{NLO}} + \left(\frac{\alpha_s}{\pi}\right)^2 \omega_{ab\to cd}^{\mathrm{NNLO}} + \ldots\right] . \tag{5.8}$$

Here we have separated the overall power of $\mathcal{O}(\alpha_s^2)$, which arises because the leading order partonic hard-scattering processes are the ordinary $2 \to 2$ QCD scatterings.

5.2.2. Threshold limit

The limit $\hat{\tau} \to 1$ corresponds to the partonic threshold, where the hard-scattering uses all available energy to produce the pair. This is kinematically similar to the Drell-Yan process, if one thinks of the hadron pair replaced by a lepton pair. The presence of fragmentation of course complicates the analysis somewhat, because only a fraction $z_c z_d$ of $\hat{m}^2$ is used for the invariant mass of the observed hadron pair. As shown in [200], it is useful to introduce the variable

$$\tau' \equiv \frac{\hat{m}^2}{S} = \frac{M^2}{z_c z_d S} \,, \tag{5.9}$$

which may be viewed as the "τ-variable" at the level of produced partons when fragmentation has not yet been taken into account, akin to the variable $\tau = Q^2/S$ in Drell-Yan.

At LO, one has $\hat{\tau} = 1$ and also $\hat{\eta} = 0$. One can therefore write the LO term as

$$\omega^{\rm LO}_{ab\to cd}\left(\hat{\tau}, \Delta\eta, \hat{\eta}\right) = \delta\left(1-\hat{\tau}\right)\,\delta\left(\hat{\eta}\right)\,\omega^{(0)}_{ab\to cd}(\Delta\eta)\;, \tag{5.10}$$

where $\omega^{(0)}_{ab\to cd}$ is a function of $\Delta\eta$ only. According to (5.6), the second delta-function implies that $\bar{\eta} = \frac{1}{2}\ln(x_a/x_b)$. At next-to-leading order (NLO), or overall $\mathcal{O}(\alpha_s^3)$, one can have $\hat{\tau} \neq 1$ and $\hat{\eta} \neq 0$. In general, as discussed in [200], near partonic threshold the kinematics becomes "LO like". One has:

$$\begin{aligned}\omega_{ab\to cd}\left(\hat{\tau}, \Delta\eta, \hat{\eta}, \alpha_s(\mu_R), \frac{\mu_R}{\hat{m}}, \frac{\mu_F}{\hat{m}}\right) &= \delta\left(\hat{\eta}\right)\,\omega^{\rm sing}_{ab\to cd}\left(\hat{\tau}, \Delta\eta, \alpha_s(\mu_R), \frac{\mu_R}{\hat{m}}, \frac{\mu_F}{\hat{m}}\right)\\ &+ \omega^{\rm reg}_{ab\to cd}\left(\hat{\tau}, \Delta\eta, \hat{\eta}, \alpha_s(\mu_R), \frac{\mu_R}{\hat{m}}, \frac{\mu_F}{\hat{m}}\right)\;,\end{aligned} \tag{5.11}$$

where all singular behavior near threshold is contained in the functions $\omega^{\rm sing}_{ab\to cd}$. Threshold resummation addresses this singular part to all orders in the strong coupling. All remaining contributions, which are subleading near threshold, are collected in the "regular" functions $\omega^{\rm reg}_{ab\to cd}$. Specifically, for the NLO corrections, one finds the following structure:

$$\begin{aligned}\omega^{\rm NLO}_{ab\to cd}\left(\hat{\tau}, \Delta\eta, \hat{\eta}, \frac{\mu_R}{\hat{m}}, \frac{\mu_F}{\hat{m}}\right) &= \delta\left(\hat{\eta}\right)\,\left[\omega^{(1,0)}_{ab\to cd}\left(\Delta\eta, \frac{\mu_R}{\hat{m}}, \frac{\mu_F}{\hat{m}}\right)\,\delta(1-\hat{\tau})\right.\\ &\left.+\,\omega^{(1,1)}_{ab\to cd}\left(\Delta\eta, \frac{\mu_F}{\hat{m}}\right)\,\left(\frac{1}{1-\hat{\tau}}\right)_+ + \omega^{(1,2)}_{ab\to cd}(\Delta\eta)\left(\frac{\log(1-\hat{\tau})}{1-\hat{\tau}}\right)_+\right]\\ &+\,\omega^{\rm reg,NLO}_{ab\to cd}\left(\hat{\tau}, \Delta\eta, \hat{\eta}, \frac{\mu_R}{\hat{m}}, \frac{\mu_F}{\hat{m}}\right)\;,\end{aligned} \tag{5.12}$$

where the singular part near threshold is represented by the functions $\omega^{(1,0)}_{ab\to cd}, \omega^{(1,1)}_{ab\to cd}, \omega^{(1,2)}_{ab\to cd}$, which are again functions of only $\Delta\eta$, up to scale dependence. The "plus"-distributions are defined by

$$\int_{x_0}^1 f(x)\left(g(x)\right)_+ {\rm d}x \equiv \int_{x_0}^1 \left(f(x)-f(1)\right)\,g(x){\rm d}x - f(1)\int_0^{x_0} g(x){\rm d}x\;. \tag{5.13}$$

The functions $\omega^{(1,0)}_{ab\to cd}, \omega^{(1,1)}_{ab\to cd}, \omega^{(1,2)}_{ab\to cd}$ were derived in [200] from an explicit NLO calculation near threshold. We will use these results below as an useful check on the resummed formula and on the matching coefficients.

5.2.3. Mellin and Fourier transforms

In order to prepare the resummation of threshold logarithms, we take integral transforms of the cross section. Following [200], we first write the hadronic cross section in

equation (5.5) as

$$M^4 \frac{\mathrm{d}\sigma^{H_1H_2\to h_1h_2X}}{\mathrm{d}M^2\mathrm{d}\Delta\eta\mathrm{d}\bar{\eta}} = \sum_{cd}\int_0^1 \mathrm{d}z_c\,\mathrm{d}z_\mathrm{d}\,z_c\,D_c^{h_1}(z_c,\mu_F)\,z_d\,D_d^{h_2}(z_d,\mu_F) \times\Omega_{H_1H_2\to cd}\left(\tau',\Delta\eta,\bar{\eta},\alpha_s(\mu_R),\frac{\mu_R}{\hat{m}},\frac{\mu_F}{\hat{m}}\right), \tag{5.14}$$

where $\tau' = \hat{m}^2/S = \hat{\tau}x_a x_b$ and

$$\Omega_{H_1H_2\to cd}\left(\tau',\Delta\eta,\bar{\eta},\alpha_s(\mu_R),\frac{\mu_R}{\hat{m}},\frac{\mu_F}{\hat{m}}\right) \equiv \sum_{ab}\int_0^1 \mathrm{d}x_a\,\mathrm{d}x_b \times f_a^{H_1}(x_a,\mu_F)\,f_b^{H_2}(x_b,\mu_F)\,\omega_{ab\to cd}\left(\hat{\tau},\Delta\eta,\hat{\eta},\alpha_s(\mu_R),\frac{\mu_R}{\hat{m}},\frac{\mu_F}{\hat{m}}\right). \tag{5.15}$$

Taking Mellin moments of this function with respect to τ' and a Fourier transform in $\bar{\eta}$, we obtain

$$\begin{aligned}&\int_{-\infty}^{\infty}\mathrm{d}\bar{\eta}\,\mathrm{e}^{i\nu\bar{\eta}}\int_0^1\mathrm{d}\tau'\,\left(\tau'\right)^{N-1}\Omega_{H_1H_2\to cd}\left(\tau',\Delta\eta,\bar{\eta},\alpha_s(\mu_R),\frac{\mu_R}{\hat{m}},\frac{\mu_F}{\hat{m}}\right)\\ &=\sum_{ab}\tilde{f}_a^{H_1}(N+1+i\nu/2,\mu_F)\tilde{f}_b^{H_2}(N+1-i\nu/2,\mu_F)\\ &\quad\tilde{\omega}_{ab\to cd}\left(N,\nu,\Delta\eta,\alpha_s(\mu_R),\frac{\mu_R}{\hat{m}},\frac{\mu_F}{\hat{m}}\right),\end{aligned} \tag{5.16}$$

where $\tilde{f}_a^H(N,\mu_F) \equiv \int_0^1 x^{N-1}f_a^H(x,\mu_F)dx$, and

$$\begin{aligned}&\tilde{\omega}_{ab\to cd}\left(N,\nu,\Delta\eta,\alpha_s(\mu_R),\frac{\mu_R}{\hat{m}},\frac{\mu_F}{\hat{m}}\right)\\ &\equiv\int_{-\infty}^{\infty}d\hat{\eta}\,\mathrm{e}^{i\nu\hat{\eta}}\int_0^1 d\hat{\tau}\,\hat{\tau}^{N-1}\,\omega_{ab\to cd}\left(\hat{\tau},\Delta\eta,\hat{\eta},\alpha_s(\mu_R),\frac{\mu_R}{\hat{m}},\frac{\mu_F}{\hat{m}}\right).\end{aligned} \tag{5.17}$$

Near threshold, keeping only the singular terms in (5.11), the right-hand-side of this reduces to

$$\begin{aligned}&\int_0^1 d\hat{\tau}\,\hat{\tau}^{N-1}\,\omega_{ab\to cd}^{\mathrm{sing}}\left(\hat{\tau},\Delta\eta,\alpha_s(\mu_R),\frac{\mu_R}{\hat{m}},\frac{\mu_F}{\hat{m}}\right)\\ &\equiv\tilde{\omega}_{ab\to cd}^{\mathrm{resum}}\left(N,\Delta\eta,\alpha_s(\mu_R),\frac{\mu_R}{\hat{m}},\frac{\mu_F}{\hat{m}}\right).\end{aligned} \tag{5.18}$$

We have labeled the new function on the right by the superscript "resum" as it is this quantity that contains all threshold logarithms and that threshold resummation addresses. As discussed in [200], it is important here that we consider fixed $\hat{m}$ and fixed renormalization/factorization scales, which is achieved by isolating the fragmentation functions as in equation (5.14). Note that $\tilde{\omega}_{ab\to cd}^{\mathrm{resum}}$ depends on the Mellin variable N only. All dependence on the Fourier variable ν resides in the moments of the parton distribution functions.

5.3. Threshold resummation for hadron-pair production

In this section we present the framework for threshold resummation for di-hadron production at NNLL. We start by giving the main result and discussing its structure. Subsequently, we will describe the various new ingredients in more detail.

5.3.1. Resummation formula at next-to-next-to-leading logarithm

For di-hadron production near threshold, all gluon radiation is soft. Since all four external partons in the hard scattering are "observed" in the sense that they are either incoming or fragmenting partons, each of them makes the same type of (double-logarithmic) contribution to the resummed cross section in moment space, given by a "jet" function Δ_i^N $(i = a, b, c, d)$ that takes into account soft and collinear gluon radiation off an external parton [200, 210, 211]. In addition, large-angle soft emission is sensitive to the color state of the hard scattering, giving rise to a trace structure in color space [40, 177, 178]. The resummed partonic cross section in moment space then takes the following form [40, 170, 177–179, 200]:

$$\begin{aligned}
&\tilde{\omega}_{ab\to cd}^{\text{resum}}\left(N, \Delta\eta, \alpha_s(\mu_R), \frac{\mu_R}{\hat{m}}, \frac{\mu_F}{\hat{m}}\right) \\
&= \Delta_a^{N+1}\left(\alpha_s(\mu_R), \frac{\mu_R}{\hat{m}}, \frac{\mu_F}{\hat{m}}\right) \Delta_b^{N+1}\left(\alpha_s(\mu_R), \frac{\mu_R}{\hat{m}}, \frac{\mu_F}{\hat{m}}\right) \\
&\quad \times \Delta_c^{N+2}\left(\alpha_s(\mu_R), \frac{\mu_R}{\hat{m}}, \frac{\mu_F}{\hat{m}}\right) \Delta_d^{N+2}\left(\alpha_s(\mu_R), \frac{\mu_R}{\hat{m}}, \frac{\mu_F}{\hat{m}}\right) \\
&\quad \times \mathrm{Tr}\left\{ H\left(\Delta\eta, \alpha_s(\mu_R)\right) \mathcal{S}_N^\dagger\left(\Delta\eta, \alpha_s(\mu_R), \frac{\mu_R}{\hat{m}}\right) \right. \\
&\quad \left. S\left(\alpha_s(\hat{m}/\bar{N}), \Delta\eta\right) \mathcal{S}_N\left(\Delta\eta, \alpha_s(\mu_R), \frac{\mu_R}{\hat{m}}\right) \right\}_{ab\to cd} \\
&\quad \times \xi_R\left(\alpha_s(\mu_R), \frac{\mu_R}{\hat{m}}\right) \xi_F^{abcd}\left(\alpha_s(\mu_R), \frac{\mu_F}{\hat{m}}\right) \ . \qquad (5.19)
\end{aligned}$$

This form is valid to all logarithmic order, up to corrections that are suppressed by powers of $1/N$, or $1 - \hat{\tau}$. The additional functions $\xi_{R,F}$ do not contain threshold logarithms but are N-independent. They serve to improve the dependence of the resummed cross section on the scales μ_R and μ_F. We will now discuss the various functions in equation (7.10) and their NNLL expansions.

Jet functions

The radiative functions Δ_i^N are familiar from threshold resummation for the Drell-Yan process. They exponentiate logarithms that arise due to soft-collinear gluon emission by the initial and final-state partons. In the $\overline{\text{MS}}$ scheme, they are given by [39, 41, 171,

212]

$$\Delta_i^N\left(\alpha_s(\mu_R),\frac{\mu_R}{\hat{m}},\frac{\mu_F}{\hat{m}}\right)=R_i(\alpha_s(\mu_R))\,\exp\left\{\right. \tag{5.20}$$
$$\left.\int_0^1 \mathrm{d}z\,\frac{z^{N-1}-1}{1-z}\left[\int_{\mu_F^2}^{(1-z)^2\hat{m}^2}\frac{\mathrm{d}\mu^2}{\mu^2}A_i(\alpha_s(\mu))+D_i(\alpha_s((1-z)\hat{m}))\right]\right\}.$$

The functions A_i and D_i may be calculated perturbatively as series in α_s,

$$\begin{aligned}A_i(\alpha_s)&=\frac{\alpha_s}{\pi}A_i^{(1)}+\left(\frac{\alpha_s}{\pi}\right)^2A_i^{(2)}+\left(\frac{\alpha_s}{\pi}\right)^3A_i^{(3)}+\mathcal{O}(\alpha_s^4)\\ D_i(\alpha_s)&=\left(\frac{\alpha_s}{\pi}\right)^2D_i^{(2)}+\mathcal{O}(\alpha_s^3)\,,\end{aligned} \tag{5.21}$$

where, up to NNLL, one needs the coefficients [213–220]

$$\begin{aligned}A_i^{(1)}&=C_i\,,\qquad A_i^{(2)}=\frac{1}{2}\,C_i\left[C_A\left(\frac{67}{18}-\frac{\pi^2}{6}\right)-\frac{5}{9}N_f\right]\,,\\ A_i^{(3)}&=\frac{1}{4}C_i\left[C_A^2\left(\frac{245}{24}-\frac{67}{9}\zeta(2)+\frac{11}{6}\zeta(3)+\frac{11}{5}\zeta(2)^2\right)\right.\\ &\qquad-\frac{1}{27}N_f^2+C_FN_f\left(-\frac{55}{24}+2\zeta(3)\right)\\ &\qquad\left.+C_AN_f\left(-\frac{209}{108}+\frac{10}{9}\zeta(2)-\frac{7}{3}\zeta(3)\right)\right]\,,\\ D_i^{(2)}&=C_i\left[C_A\left(-\frac{101}{27}+\frac{11}{3}\zeta(2)+\frac{7}{2}\zeta(3)\right)+N_f\left(\frac{14}{27}-\frac{2}{3}\zeta(2)\right)\right]\,,\end{aligned} \tag{5.22}$$

with N_f the number of flavors and

$$C_q=C_F=\frac{N_c^2-1}{2N_c}=\frac{4}{3}\,,\quad C_g=C_A=N_c=3\,. \tag{5.23}$$

The D_i term in the radiative factor Δ_i^N first appears at NNLL accuracy [39, 41, 171, 212]. It takes into account logarithms that arise from soft gluons that are emitted at large angles. Incoming and outgoing external lines of a given parton type carry the same D_i term, as discussed in the Appendix.

Finally, the coefficient R_i in equation (5.20) ensures that our soft functions for this process are defined relative to that for the Drell-Yan process; again see the Appendix for details. To the order we consider, we have

$$R_i(\alpha_s)\;=\;1-\frac{3\alpha_s}{4\pi}\,A_i^{(1)}\,\zeta(2)+\mathcal{O}(\alpha_s^2)\,. \tag{5.24}$$

Evaluating the integrals in equation (5.20), one obtains an explicit expression for the NNLL expansion of the function Δ_i^N:

$$\Delta_i^N\left(\alpha_s(\mu_R), \frac{\mu_R}{\hat{m}}, \frac{\mu_F}{\hat{m}}\right) = \tilde{R}_i(\alpha_s(\mu_R)) \exp\left\{h_i^{(1)}(\lambda)\, \ln \bar{N} + h_i^{(2)}\left(\lambda, \frac{\mu_R}{\hat{m}}, \frac{\mu_F}{\hat{m}}\right) + \alpha_s(\mu_R)\, h_i^{(3)}\left(\lambda, \frac{\mu_R}{\hat{m}}, \frac{\mu_F}{\hat{m}}\right)\right\} . \tag{5.25}$$

Here $\tilde{R}_i$ is a combination of R_i in equation (5.24) and a π^2-term arising in the NNLL expansion [171]:

$$\tilde{R}_i(\alpha_s) \;=\; 1 + \frac{\alpha_s}{4\pi}\, A_i^{(1)}\, \zeta(2) + \mathcal{O}(\alpha_s^2) . \tag{5.26}$$

In (5.25) we have furthermore defined $\lambda = b_0 \alpha_s(\mu_R) \ln(N \mathrm{e}^{\gamma_E})$ with γ_E the Euler constant. In the following we denote $N\mathrm{e}^{\gamma_E} \equiv \bar{N}$. The functions $h_i^{(1)}, h_i^{(2)}, h_i^{(3)}$ read

$$h_i^{(1)}(\lambda) = \frac{A_i^{(1)}}{2\pi b_0 \lambda}\left(2\lambda + (1-2\lambda)\ln(1-2\lambda)\right) , \tag{5.27a}$$

$$\begin{aligned} h_i^{(2)}\left(\lambda, \frac{\mu_R}{\hat{m}}, \frac{\mu_F}{\hat{m}}\right) = &-\frac{A_i^{(2)}}{2\pi^2 b_0^2}\left[2\lambda + \ln(1-2\lambda)\right] \\ &+\frac{A_q^{(1)} b_1}{2\pi b_0^3}\left[2\lambda + \ln(1-2\lambda) + \frac{1}{2}\ln^2(1-2\lambda)\right] \\ &-\frac{A_i^{(1)}}{2\pi b_0}\left[2\lambda + \ln(1-2\lambda)\right]\ln\frac{\mu_R^2}{\hat{m}^2} + \frac{A_i^{(1)}}{\pi b_0}\lambda \ln\frac{\mu_F^2}{\hat{m}^2} , \end{aligned} \tag{5.27b}$$

and [41, 212]

$$\begin{aligned} &h_i^{(3)}\left(\lambda, \frac{\mu_R}{\hat{m}}, \frac{\mu_F}{\hat{m}}\right) \\ &= \frac{2A_i^{(1)}}{\pi}\zeta(2)\frac{\lambda}{1-2\lambda} - \frac{A_i^{(2)} b_1}{2\pi^2 b_0^3}\frac{1}{1-2\lambda}\left[2\lambda + \ln(1-2\lambda) + 2\lambda^2\right] \\ &\quad + \frac{A_i^{(1)} b_1^2}{2\pi b_0^4 (1-2\lambda)}\left[2\lambda^2 + 2\lambda\ln(1-2\lambda) + \frac{1}{2}\ln^2(1-2\lambda)\right] \\ &\quad + \frac{A_i^{(1)} b_2}{2\pi b_0^3}\left[2\lambda + \ln(1-2\lambda) + \frac{2\lambda^2}{1-2\lambda}\right] + \frac{A_i^{(3)}}{\pi^3 b_0^2}\frac{\lambda^2}{1-2\lambda} \\ &\quad + \frac{A_i^{(2)}}{\pi^2 b_0}\lambda \ln\frac{\mu_F^2}{\hat{m}^2} - \frac{A_i^{(1)}}{2\pi}\lambda\ln^2\frac{\mu_F^2}{\hat{m}^2} + \frac{A_i^{(1)}}{\pi}\lambda\ln\frac{\mu_R^2}{\hat{m}^2}\ln\frac{\mu_F^2}{\hat{m}^2} \\ &\quad - \frac{1}{1-2\lambda}\left(\frac{A_i^{(1)} b_1}{2\pi b_0^2}\left[2\lambda + \ln(1-2\lambda)\right] - \frac{2A_i^{(2)}}{\pi^2 b_0}\lambda^2\right)\ln\frac{\mu_R^2}{\hat{m}^2} \\ &\quad + \frac{A_i^{(1)}}{\pi}\frac{\lambda^2}{1-2\lambda}\ln^2\frac{\mu_R^2}{\hat{m}^2} - \frac{D_i^{(2)}}{2\pi^2 b_0}\frac{\lambda}{1-2\lambda} . \end{aligned} \tag{5.28}$$

Here b_0, b_1, b_2 are the first three coefficients of the QCD beta function which are given by equation (1.25) and [16, 17].

Color trace contribution

Next we discuss the trace $\mathrm{Tr}\{H\mathcal{S}_N^\dagger S\mathcal{S}_N\}$ in color space in equation (7.10). We note that this is the only contribution to the resummed cross section that depends on the difference of the rapidities $\Delta\eta$. Each of the factors $H_{ab\to cd}$, $\mathcal{S}_{N,ab\to cd}$, $S_{ab\to cd}$ is a matrix in the space of color exchange operators [40, 177, 178]. The $H_{ab\to cd}$ are the hard-scattering functions. They are perturbative and have the expansions

$$H_{ab\to cd}\left(\Delta\eta,\alpha_s\right)=\left(\frac{\alpha_s}{\pi}\right)^2\left[H^{(0)}_{ab\to cd}\left(\Delta\eta\right)+\frac{\alpha_s}{\pi}H^{(1)}_{ab\to cd}\left(\Delta\eta\right)+\mathcal{O}(\alpha_s^2)\right]\,. \tag{5.29}$$

The LO (i.e. $\mathcal{O}(\alpha_s^2)$) contributions $H^{(0)}_{ab\to cd}$ may be found in [40, 177–179]. For resummation beyond NLL accuracy, one needs all entries of the NLO hard-scattering matrices $H^{(1)}_{ab\to cd}$. These matrices may be extracted from a color decomposed one-loop calculation [200, 209]. We will outline the derivation of the first-order corrections $H^{(1)}_{ab\to cd}$ in Section 5.3.2. We note that they depend in principle also on the renormalization scale μ_R, in the form of a term $\propto \ln(\mu_R/\hat{m})H^{(0)}_{ab\to cd}$. This dependence, however, has been absorbed into the contribution involving the function ξ_R in (7.10); see below.

The $S_{ab\to cd}$ are known as soft functions. In general, they depend on the rapidity difference $\Delta\eta$ and on the strong coupling whose argument is to be set to $\hat{m}/\bar{N}$ [40, 177, 178, 188]. This dependence on $\hat{m}/\bar{N}$ and hence on N occurs first at NNLL. The soft functions have the expansion

$$S_{ab\to cd}\left(\alpha_s(\hat{m}/\bar{N}),\Delta\eta\right)=S^{(0)}_{ab\to cd}+\frac{\alpha_s(\hat{m}/\bar{N})}{\pi}S^{(1)}_{ab\to cd}\left(\Delta\eta\right)+\mathcal{O}(\alpha_s^2)\,. \tag{5.30}$$

Relating the coupling at scale $\hat{m}/\bar{N}$ to that at scale μ_R, one can construct the explicit N-dependence of the soft matrix at NLO. To the accuracy of resummation that we are considering in this work, it is sufficient to use

$$\alpha_s(\hat{m}/\bar{N})=\frac{\alpha_s(\mu_R)}{1-2\lambda}\,. \tag{5.31}$$

The LO expressions $S^{(0)}_{ab\to cd}$, which are independent of $\Delta\eta$, may also be found in [40, 177–179]. Like the hard-scattering matrices $H^{(1)}_{ab\to cd}$, at NNLL accuracy, we need the explicit expressions for the full NLO soft-matrices $S^{(1)}_{ab\to cd}$. These may be extracted by performing a color-decomposed calculation of the $2\to 3$ contributions to the partonic cross sections in the eikonal approximation, as will be described in Section 5.3.3.

The resummation of wide-angle soft gluons is contained in $\mathcal{S}_{ab\to cd}$. The two exponentials $\mathcal{S}_N^\dagger$ and $\mathcal{S}_N$ that enclose the soft function $S_{ab\to cd}$ within the trace structure appear when solving the renormalization group equation for the soft function [40, 177–179]. The exponentials are given in terms of soft anomalous dimensions $\Gamma_{ab\to cd}$:

$$\mathcal{S}_{N,ab\to cd}\left(\Delta\eta,\alpha_s(\mu_R),\frac{\mu_R}{\hat{m}}\right)=\mathcal{P}\exp\left[\frac{1}{2}\int_{\hat{m}^2}^{\hat{m}^2/\bar{N}^2}\frac{d\mu^2}{\mu^2}\Gamma_{ab\to cd}\left(\Delta\eta,\alpha_s(\mu)\right)\right]\,, \tag{5.32}$$

where $\mathcal{P}$ denotes path ordering. The soft anomalous dimension matrices start at $\mathcal{O}(\alpha_s)$,

$$\Gamma_{ab\to cd}\left(\alpha_s, \Delta\eta\right) = \frac{\alpha_s}{\pi}\,\Gamma^{(1)}_{ab\to cd}\left(\Delta\eta\right) + \left(\frac{\alpha_s}{\pi}\right)^2 \Gamma^{(2)}_{ab\to cd}(\Delta\eta) + \mathcal{O}(\alpha_s^3)\,. \tag{5.33}$$

Their first-order terms are presented in [40, 177–179, 221]. We will discuss the $\Gamma_{ab\to cd}$ matrices in more detail in Section 5.3.3. For NNLL resummation, we also need to take into account the second-order contributions $\Gamma^{(2)}_{ab\to cd}$ which were derived in [222–225] and are determined by the one-loop terms:

$$\Gamma^{(2)}_{ab\to cd}(\Delta\eta) = \frac{K}{2}\Gamma^{(1)}_{ab\to cd}(\Delta\eta)\,, \tag{5.34}$$

where $K = C_A(67/18 - \pi^2/6) - 5N_f/9$. We also give here our result for the NNLL expansion of the integral in equation (5.32):

$$\begin{aligned}
&\ln \mathcal{S}_{N,ab\to cd}\left(\Delta\eta, \alpha_s, \frac{\mu_R}{\hat{m}}\right) \\
&= \Gamma^{(1)}_{ab\to cd}\left(\Delta\eta\right)\left[\frac{\ln(1-2\lambda)}{2\pi b_0} + \frac{\alpha_s}{\pi}\frac{1}{2b_0^2\pi(1-2\lambda)}\right. \\
&\qquad\left.\times\left(b_1\pi(2\lambda + \ln(1-2\lambda)) - b_0\lambda\left(K + 2\pi b_0 \ln\frac{\mu_R^2}{\hat{m}^2}\right)\right)\right]\,.
\end{aligned} \tag{5.35}$$

We note that in our phenomenological applications we follow [200] and perform the exponentiation of the matrices numerically by iterating the exponential series to an adequately high order.

In order to clarify the roles of the various matrices appearing in the color trace, it is instructive to analyze the structure of the resummed cross section (7.10) in Mellin space after expansion to NLO:

$$\begin{aligned}
&\tilde{\omega}^{\text{resum}}_{ab\to cd}\left(N, \Delta\eta, \alpha_s(\mu_R), \frac{\mu_R}{\hat{m}}, \frac{\mu_F}{\hat{m}}\right) \\
&= \left(\frac{\alpha_s(\mu_R)}{\pi}\right)^2\left[\mathrm{Tr}\{H^{(0)}S^{(0)}\}_{ab\to cd}\left\{1 + 2b_0\alpha_s(\mu_R)\ln\frac{\mu_R^2}{\hat{m}^2}\right.\right. \\
&\quad + \frac{\alpha_s(\mu_R)}{\pi}\sum_{i=a,b,c,d}\left(A_i^{(1)}\ln^2\bar{N} + \frac{1}{4}A_i^{(1)}\zeta(2)\right. \\
&\quad \left.\left.+\left(A_i^{(1)}\ln\bar{N} + \frac{1}{2}B_i^{(1)}\right)\ln\frac{\mu_F^2}{\hat{m}^2}\right)\right\} \\
&\quad + \frac{\alpha_s(\mu_R)}{\pi}\,\mathrm{Tr}\Big\{ - \left[H^{(0)}(\Gamma^{(1)})^\dagger S^{(0)} + H^{(0)}S^{(0)}\Gamma^{(1)}\right]\ln\bar{N} \\
&\quad \left. + H^{(1)}S^{(0)} + H^{(0)}S^{(1)}\Big\}_{ab\to cd}\right] + \mathcal{O}(\alpha_s^4)
\end{aligned} \tag{5.36}$$

Here the term $\propto \zeta(2)$ arises from the coefficient $\tilde{R}_i$ in (5.26). We have anticipated the contributions by the functions ξ_R and ξ_F in (7.10) that will be specified in the next subsection. ξ_R yields the term involving the renormalization scale, and ξ_F contributes the ones $\propto B_i^{(1)}$, with

$$B_q^{(1)} = -\frac{3}{2} C_F \;, \qquad B_g^{(1)} = -2\pi b_0 \;. \tag{5.37}$$

The term $\mathrm{Tr}\{H^{(0)} S^{(0)}\}_{ab\to cd}$ in (5.36) is proportional to the LO function $\omega^{(0)}_{ab\to cd}(\Delta\eta)$ introduced in equation (5.10). In [200] (as in many previous studies of threshold resummation for hadronic hard-scattering), the combination $\mathrm{Tr}[H^{(1)} S^{(0)} + H^{(0)} S^{(1)}]$, which carries no dependence on N, was extracted as a whole by matching the expression in equation (5.36) to the NLO calculation at threshold. Of course, this is not sufficient for determining the full first-order matrices $H^{(1)}$ and $S^{(1)}$. However, it is a valid approach at NLL accuracy, where the three most dominant towers of logarithms are taken into account. For a given fixed-order expansion to $\mathcal{O}(\alpha_s^k)$, the following terms are under control:

$$\alpha_s^k \, \left\{ \ln^{2k} \bar{N}, \;\; \ln^{2k-1} \bar{N}, \;\; \ln^{2k-2} \bar{N} \right\} \;. \tag{5.38}$$

It is straightforward to see that the hard and soft matrices will contribute to the third tower of threshold logarithms always in the combination $\mathrm{Tr}\{H^{(1)} S^{(0)} + H^{(0)} S^{(1)}\}_{ab\to cd}$ in the following way:

$$\left(\frac{\alpha_s}{\pi}\right)^k \frac{\sum_i A_i^{(1)}}{(k-1)!} \, \mathrm{Tr}\left\{ H^{(1)} S^{(0)} + H^{(0)} S^{(1)} \right\}_{ab\to cd} \ln^{2k-2} \bar{N} \;. \tag{5.39}$$

Hence, to NLL, it is sufficient to know the combined expression of $H^{(1)}$ and $S^{(1)}$ instead of having to compute the full matrices separately. It is then legitimate to that order to approximate the trace term in the resummed formula by

$$\mathrm{Tr}\left\{ H \mathcal{S}_N^\dagger S \mathcal{S}_N \right\}_{ab\to cd,\mathrm{N}LL} = \left(1 + \frac{\alpha_s}{\pi} C^{(1),\mathrm{N}LL}_{ab\to cd}\right) \mathrm{Tr}\left\{ H^{(0)} \mathcal{S}_N^\dagger S^{(0)} \mathcal{S}_N \right\}_{ab\to cd} \;, \tag{5.40}$$

where

$$C^{(1),\,\mathrm{N}LL}_{ab\to cd}\,(\Delta\eta) \equiv \frac{\mathrm{Tr}\left\{ H^{(1)} S^{(0)} + H^{(0)} S^{(1)} \right\}_{ab\to cd}}{\mathrm{Tr}\left\{ H^{(0)} S^{(0)} \right\}_{ab\to cd}} \;. \tag{5.41}$$

This was the approach adopted in [200] and also, for example, in studies on single-inclusive hadron [226] or jet production [1, 227].

On the other hand, in order to control the fourth tower of logarithms, $\alpha_s^k \ln^{2k-3} \bar{N}$, one needs to know $H^{(1)}$ and $S^{(1)}$ explicitly as they also appear separately in various

combinations with the anomalous dimension matrices. Computation of the full matrices is therefore a necessary ingredient for NNLL resummation. Clearly, having the matrices at hand, one can compute also the known combination $\mathrm{Tr}\{H^{(1)}S^{(0)} + H^{(0)}S^{(1)}\}_{ab\to cd}$, which provides an important cross-check on them. We stress further that, in order to fully take into account also the fifth tower $\alpha_s^k \ln^{2k-4}\bar{N}$ at NNLL, one would need to know the full matrices $H^{(2)}$ and $S^{(2)}$ and perform a matching to NNLO. Although $H^{(2)}$ became available very recently [199], this is beyond the scope of the present work.

We finally note that a new feature which first appears at NNLL is that the hard-scattering matrix H obtains an imaginary part. This is because H is constructed from virtual corrections to partonic $2 \to 2$ scattering, which contain logarithms of ratios of space- and timelike invariants. We write

$$H = H_R + iH_I \tag{5.42}$$

with H_R and H_I real. It turns out that H_R is a symmetric matrix, whereas H_I is antisymmetric; see Section 5.3.2. Hence, the hard-scattering matrix H as a whole is hermitian, as it should be. The imaginary part H_I contributes to the resummed cross section due to the fact that the remaining terms inside the color trace in the resummed cross section (7.10), $M \equiv \mathrm{e}^{\Gamma^\dagger} S \mathrm{e}^{\Gamma}$, also develop an imaginary part since the anomalous dimension matrices are complex-valued [40, 177, 178]. M is also hermitian as the soft matrix S is symmetric, and therefore we may also decompose $M = M_R + iM_I$ with M_R symmetric and M_I antisymmetric. The trace $\mathrm{Tr}\{HM\}$ is then real, as it must be, but both the real and imaginary parts of H, M contribute:

$$\mathrm{Tr}\{HM\} = \mathrm{Tr}\{H_R M_R\} - \mathrm{Tr}\{H_I M_I\} \ . \tag{5.43}$$

Note that the contribution by the imaginary part of H drops out from $\mathrm{Tr}[H^{(1)}S^{(0)} + H^{(0)}S^{(1)}]$, so that it is not present at NLL. Performing an analytical fixed-order expansion of our NNLL resummed result, we find that the imaginary parts of H and M first start to play a role at $\mathrm{N^3LO}$, where they contribute to the fifth tower, $\alpha_s^3 \ln^2 \bar{N}$. We note, however, that the imaginary parts of $\Gamma_{ab\to cd}$ also contribute to the real part of M, since $M = \mathrm{e}^{\Gamma^\dagger} S \mathrm{e}^{\Gamma}$. It turns out that they already appear in the *fourth* tower of logarithms. In this way we see that the imaginary parts of the various contributions are important ingredients of the NNLL resummed cross section.

Functions ξ_R and ξ_F

The N-independent function ξ_F^{abcd} in equation (7.10) addresses the factorization scale dependence of the cross section [40, 177–179, 228]:

$$\ln \xi_F^{abcd}\left(\alpha_s(\mu_R), \frac{\mu_F}{\hat{m}}\right) = -\frac{1}{2}\sum_{i=a,b,c,d}\int_{\mu_F^2}^{\hat{m}^2}\frac{d\mu^2}{\mu^2}\frac{\alpha_s(\mu)}{\pi}B_i^{(1)} \ , \tag{5.44}$$

where we are summing over all four external partons. The coefficients $B_i^{(1)}$, which have been given in equation (5.37), correspond to the δ-function contributions to the corresponding LO diagonal parton-to-parton splitting functions and thus depend on whether the considered parton i is a quark or a gluon. As follows from [229], the function ξ_F^{abcd} takes into account all N-independent pieces corresponding to the evolution of parton distributions and fragmentation functions between scales μ_F and $\hat{m}$. Again its first-order contribution would explicitly appear in $H_{ab\to cd}^{(1)}$, from where it has been absorbed. It is straightforward to expand (5.44) to the desired NNLL accuracy.

ξ_R governs the renormalization scale dependence of the resummed cross section. This function was also introduced in [179]. ξ_R essentially serves to set the scale in the strong coupling constant in the overall factor α_s^2 (see equation (5.8)) of the cross section to $\hat{m}$:

$$\ln \xi_R \left(\alpha_s(\mu_R), \frac{\mu_R}{\hat{m}}\right) = 2 \int_{\mu_R^2}^{\hat{m}^2} \frac{d\mu^2}{\mu^2} \beta(\alpha_s(\mu)) \,. \tag{5.45}$$

Evaluating the integral while keeping only the first two terms in the QCD β-function,

$$\beta(\alpha_s) \equiv \frac{1}{\alpha_s} \frac{d\alpha_s}{d\log(\mu^2)} = -b_0 \alpha_s - b_1 \alpha_s^2 + \mathcal{O}(\alpha_s^3) \,, \tag{5.46}$$

and expanding the result up to second order in α_s, we find

$$\ln \xi_R \left(\alpha_s, \frac{\mu_R}{\hat{m}}\right) = 2b_0 \alpha_s \ln \frac{\mu_R^2}{\hat{m}^2} + \alpha_s^2 \left(2b_1 \ln \frac{\mu_R^2}{\hat{m}^2} + b_0^2 \ln^2 \frac{\mu_R^2}{\hat{m}^2}\right) \,. \tag{5.47}$$

Here b_0, b_1 are as given in (1.25). The first term on the right reproduces the explicit μ_R-dependence of the first-order hard-scattering function that we have chosen to pull out of $H_{ab\to cd}^{(1)}$. The additional terms generated by this expression produce higher-order scale-dependent contributions that will occur in the perturbative series. When combined with resummation at NNLL level, they necessarily help to stabilize the cross section with respect to changes in μ_R, as we shall discuss in more detail now.

Following [230] and suppressing all arguments except for the renormalization scale, we write the perturbative expansion of a generic partonic cross section ω as

$$\omega = \sum_{k=0}^{\infty} \alpha_s^{k+2}(\mu_R)\, \omega^{(k)}(\mu_R) \,. \tag{5.48}$$

The LO coefficient $\omega^{(0)}$ is independent of μ_R; all higher-order terms depend on μ_R through the logarithm $L \equiv \ln(\mu_R^2/\hat{m}^2)$. Truncating the series at some fixed $k = n$, the uncertainty introduced by the renormalization scale dependence is of the order of $\mathcal{O}(\alpha_s(\mu_R)^{n+3})$. In the following we consider as an example the renormalization scale

dependence after truncation to next-to-next-to-leading order (NNLO), which is given by

$$\begin{aligned}\omega|_{\text{NNLO}} &= \alpha_s^2(\mu_R)\,\omega^{(0)} + \alpha_s^3(\mu_R)\,\omega^{(1)}(\mu_R) + \alpha_s^4(\mu_R)\,\omega^{(2)}(\mu_R) \\ &= \alpha_s^2(\mu_R)\,\omega^{(0)} + \alpha_s^3(\mu_R)\,\left(\omega'^{(1)} + 2b_0\,L\,\omega^{(0)}\right) \\ &\quad + \alpha_s^4(\mu_R)\,\left(\omega'^{(2)} + 3b_0\,L\,\omega'^{(1)} + (3b_0^2\,L^2 + 2b_1\,L)\,\omega^{(0)}\right)\,, \end{aligned} \tag{5.49}$$

where the coefficients $\omega'^{(k)}$ denote the terms in $\omega^{(k)}$ that do not carry any dependence on μ_R. As is well-known, the μ_R-dependence of the NNLO cross section is entirely determined by the NLO terms in the perturbative expansion.

We may now compare the general expression in equation (5.49) to an NNLO expansion of the resummed cross section $\tilde{\omega}^{\text{resum}}$ at either NLL or NNLL. First of all, we find that the NLO scale dependence and the contribution $(3b_0^2\,L^2 + 2b_1\,L)\,\omega^{(0)}$ at NNLO are entirely reproduced by the exponential ξ_R in equations (5.45) and (5.47). The interesting term at NNLO is now the term $3b_0\,L\,\omega'^{(1)}$ in the last line. Out of the five towers of threshold logarithms that appear at NNLO, the renormalization scale dependence resides only in the lowest three. Indeed, as can be seen from the explicit NLO expansion given in equation (5.36), the coefficient $\omega'^{(1)}$ contains terms proportional to $\ln^2\bar{N}$, $\ln\bar{N}$, 1 which, at NNLO, correspond to the 3$^{\text{rd}}$, 4$^{\text{th}}$ and 5$^{\text{th}}$ towers. If we now compare to the NNLO expansion of the NLL-resummed cross section, we find that only the scale dependence of the 3$^{\text{rd}}$ tower is correctly reproduced. For the 4$^{\text{th}}$ and 5$^{\text{th}}$ tower, that are not fully taken into account at NLL, we find a factor of $2b_0\,L$ instead of $3b_0\,L$ multiplying the corresponding part of the coefficient $\omega'^{(1)}$. If instead resummation is performed at NNLL, the scale dependence in the 4$^{\text{th}}$ tower is correctly reproduced as well, whereas in the 5$^{\text{th}}$ tower the incorrect factor $2b_0\,L$ remains. (In addition, of course, the scale-independent coefficient $\omega'^{(2)}$ also changes). As it turns out, going from NLL to NNLL leads to a dramatic reduction of the renormalization scale uncertainty of the resummed cross section, as will be seen in our numerical studies in Sec. 5.4.

5.3.2. Hard-scattering function

In this Section we present our derivation of the matrices $H^{(1)}_{ab\to cd}$. We note that these were also determined in [209]; the results of our independent computation are in agreement with that reference. As the resulting expressions become rather lengthy in general, we present explicit results only for the simplest partonic channel, $qq' \to qq'$. For ease of notation, we will usually drop the ubiquitous subscript "$qq' \to qq'$" of the matrices. We also refer the reader to Ref. [179], where many details of the relevant color bases have been collected. In fact, for each partonic channel we adopt the corresponding color basis from that reference. We note that our choice differs from the one in [209], where an overcomplete basis was chosen for the $gg \to gg$ channel.

Color basis and lowest-order contribution

We consider the partonic process

$$q(p_1,a)q'(p_2,b) \to q(p_3,c)q'(p_4,d) \;, \tag{5.50}$$

where the p_i are the momenta of the incoming and outgoing quarks, and the indices a, b, c, d denote their color. Given the fact that the leading-order process has only a t-channel contribution, it is convenient to choose the t-channel octet-singlet color basis which leads to a simple form for the lowest-order hard-scattering matrix $H^{(0)}$. The contributing color tensors in this basis are given by (1=octet, 2=singlet)

$$\begin{aligned} \mathcal{C}_1 &\equiv T^g_{ca}T^g_{db} = \frac{1}{2}\left(\delta_{ad}\,\delta_{bc} - \frac{1}{N_c}\,\delta_{ac}\,\delta_{bd}\right) \;, \\ \mathcal{C}_2 &\equiv \delta_{ac}\delta_{bd} \;, \end{aligned} \tag{5.51}$$

where T^g is the generator in the fundamental representation and the indices a, b, c, d will be kept implicit throughout most of our discussion. The soft and hard functions become matrices in this basis, whose entries are determined as the coefficients multiplying the respective tensor structures. The elements of the leading-order contribution to the soft function $S^{(0)}$ in equation (5.30) are given by $(I, J = 1, 2)$

$$(S^{(0)})_{JI} \equiv \mathrm{Tr}[\mathcal{C}_J^\dagger \mathcal{C}_I] \equiv \sum_{a,b,c,d=1}^{N_c} \mathcal{C}_J^* \mathcal{C}_I \;. \tag{5.52}$$

In our basis one finds

$$S^{(0)} = \begin{pmatrix} \frac{N_c^2-1}{4} & 0 \\ 0 & N_c^2 \end{pmatrix} \;. \tag{5.53}$$

We next color-decompose the Born amplitude for the process as

$$M^{(0)} = \sum_I h_I^{(0)} \mathcal{C}_I \;. \tag{5.54}$$

Squaring the amplitude and summing (averaging) over external colors and helicities, we find

$$\begin{aligned} \frac{1}{4N_c^2} \sum_{a,b,c,d=1}^{N_c} |M^{(0)}|^2 &= \frac{1}{4N_c^2} \sum_{a,b,c,d=1}^{N_c} \sum_{IJ} h_I^{(0)} h_J^{(0)*} \mathcal{C}_J^* \mathcal{C}_I \\ &= \frac{1}{4N_c^2} \sum_{IJ} h_I^{(0)} h_J^{(0)*} S_{JI}^{(0)} \equiv \mathrm{Tr}[H^{(0)} S^{(0)}] \;, \end{aligned} \tag{5.55}$$

where

$$(H^{(0)})_{IJ} \equiv \frac{1}{4N_c^2}\, h_I^{(0)} h_J^{(0)*} \;. \tag{5.56}$$

While the matrix $H^{(0)}$ follows from a simple direct calculation, we extract it from the results of [206], since we can then follow the same strategy for the one-loop results given there. The color-decomposed tree-level four-point helicity amplitudes for $qq' \to qq'$ are given in [206] as

$$\begin{aligned}\mathcal{A}_{\text{tree}}^{\lambda\lambda'} &= \left(\delta_{ad}\,\delta_{bc} - \frac{1}{N_c}\,\delta_{ac}\,\delta_{bd}\right) a_{4;0}^{\lambda\lambda'} \\ &\equiv \mathcal{C}_1 \times \left(2a_{4;0}^{\lambda\lambda'}\right) + \mathcal{C}_2 \times 0\,, \end{aligned} \tag{5.57}$$

where $\lambda\lambda'$ denotes the helicity configuration of the initial partons. For a given pair of helicity settings we have $h_{I=1}^{(0)} = 2a_{4;0}$, $h_{I=2}^{(0)} = 0$. The squares of the two helicity amplitudes are

$$\begin{aligned}|a_{4;0}^{--}|^2 &= \frac{s^2}{t^2}\,, \\ |a_{4;0}^{-+}|^2 &= \frac{u^2}{t^2}\,, \end{aligned} \tag{5.58}$$

with the Mandelstam variables

$$\begin{aligned} s = (p_1+p_2)^2 &= \hat{m}^2\,, \\ t = (p_1-p_3)^2 &= -\hat{m}^2 \frac{e^{-\Delta\eta}}{e^{\Delta\eta}+e^{-\Delta\eta}}\,, \\ u = (p_1-p_4)^2 &= -\hat{m}^2 \frac{e^{\Delta\eta}}{e^{\Delta\eta}+e^{-\Delta\eta}}\,. \end{aligned} \tag{5.59}$$

Averaging over external colors and helicities appropriately, following equation (5.55), we obtain the lowest-order hard-scattering matrix as

$$H^{(0)} = \begin{pmatrix} \frac{2}{N_c^2}\frac{s^2+u^2}{t^2} & 0 \\ 0 & 0 \end{pmatrix} \equiv \begin{pmatrix} h_0 & 0 \\ 0 & 0 \end{pmatrix}\,, \tag{5.60}$$

in agreement with [179]. As expected, its only entry is in the "octet-octet" corner, thanks to our choice of color basis.

Hard part at one loop

The hard-scattering matrix $H_{ab\to cd}$ is a perturbative function that contains all contributions associated with momenta of the order of the hard scale $\hat{m}$. Since in the threshold regime there is no phase space for hard on-shell radiation, only purely virtual

contributions contribute to $H_{ab\to cd}$. Writing the virtual one-loop amplitude as (again we suppress the indices for the external particles)

$$M^{(1),\mathrm{virt}} = \sum_I \tilde{h}_I^{(1)} \mathcal{C}_I \,, \tag{5.61}$$

and considering the interference with the Born amplitude, the elements of the first-order contribution $H^{(1)}_{ab\to cd}$ are obtained from the finite part of

$$(\tilde{H}^{(1)})_{IJ} \equiv \frac{1}{4N_c^2} \left(\tilde{h}_I^{(1)} h_J^{(0)*} + h_I^{(0)} \tilde{h}_J^{(1)*} \right) \,. \tag{5.62}$$

Most of the one-loop amplitudes that we need are given in [206]. For the gluonic channel $gg \to gg$, we additionally use the results of [207, 208]. For the process $qq' \to qq'$, the one-loop four-point helicity amplitudes are given in [206] as

$$\begin{aligned} \mathcal{A}_{1\mathrm{loop}}^{\lambda\lambda'} = & \left(\delta_{ad}\,\delta_{bc} - \frac{1}{N_c}\,\delta_{ac}\,\delta_{bd} \right) a_{4;1}^{\lambda\lambda'} + \delta_{ad}\,\delta_{bc}\, a_{4;2}^{\lambda\lambda'} \\ = & \quad \mathcal{C}_1 \times 2 \left(a_{4;1}^{\lambda\lambda'} + a_{4;2}^{\lambda\lambda'} \right) + \mathcal{C}_2 \times \frac{1}{N_c} a_{4;2}^{\lambda\lambda'} \,. \end{aligned} \tag{5.63}$$

From this we can determine the $\tilde{h}_I^{(1)}$. Keeping in mind that we have pulled out an overall factor α_s/π in our definition of the hard-scattering matrix $H^{(1)}$, cf. equation (5.29), we have $\tilde{h}_{I=1}^{(1)} = 2(a_{4;1}^{\lambda\lambda'} + a_{4;2}^{\lambda\lambda'})$ and $\tilde{h}_{I=2}^{(1)} = a_{4;2}^{\lambda\lambda'}/N_c$. As shown in [206], the $a_{4;1}^{\lambda\lambda'}$, $a_{4;2}^{\lambda\lambda'}$ are proportional to the tree-level $a_{4;0}^{\lambda\lambda'}$ in (5.57) for each helicity configuration:

$$\begin{aligned} a_{4;1}^{\lambda\lambda'} = & \quad C_\Gamma\, F_{4;1}^{\lambda\lambda'} a_{4;0}^{\lambda\lambda'} \,, \\ a_{4;2}^{\lambda\lambda'} = & \quad C_\Gamma\, F_{4;2}^{\lambda\lambda'} a_{4;0}^{\lambda\lambda'} \,, \end{aligned} \tag{5.64}$$

where in our normalization

$$C_\Gamma \;=\; \frac{e^{\gamma_E \varepsilon}}{4}\, \frac{\Gamma^2(1-\varepsilon)\,\Gamma(1+\varepsilon)}{\Gamma(1-2\varepsilon)} \,. \tag{5.65}$$

Here dimensional regularization with $D = 4 - 2\varepsilon$ dimensions is used. The $F_{4;1}^{\lambda\lambda'}$, $F_{4;2}^{\lambda\lambda'}$ are functions of the Mandelstam variables. Using the shorthand notation

$$L(t) = \log\frac{-t}{s} \,, \quad L(u) = \log\frac{-u}{s} \,, \quad L(s) = -i\pi \,, \tag{5.66}$$

we have from [206]:

$$
\begin{aligned}
F_{4;1}^{--} &= N_c\left[-\frac{2}{\varepsilon^2}-\frac{3}{\varepsilon}+2\frac{L(s)}{\varepsilon}+L^2(t)-\frac{2}{3}L(t)\left(1+3L(s)\right)+\frac{13}{9}+\pi^2\right]\\
&\quad+N_f\left[\frac{2}{3}L(t)-\frac{10}{9}\right]-\frac{1}{N_c}\Bigg[-\frac{2}{\varepsilon^2}-\frac{3}{\varepsilon}-\frac{2}{\varepsilon}(L(s)-L(t)-L(u))\\
&\quad-8-L^2(t)+\frac{u^2-s^2}{2s^2}\left((L(t)-L(u))^2+\pi^2\right)\\
&\quad+2L(t)(1+L(s)-L(u))-\frac{1}{s}(uL(t)+tL(u))\Bigg]+4\pi b_0\log\left(\frac{\mu_R^2}{\hat{m}^2}\right),\\
F_{4;1}^{-+} &= N_c\left[-\frac{2}{\varepsilon^2}-\frac{3}{\varepsilon}+2\frac{L(s)}{\varepsilon}+L^2(t)-\frac{2}{3}L(t)\left(1+3L(s)\right)+\frac{13}{9}+\pi^2\right]\\
&\quad+N_f\left[\frac{2}{3}L(t)-\frac{10}{9}\right]-\frac{1}{N_c}\Bigg[-\frac{2}{\varepsilon}-\frac{3}{\varepsilon}-\frac{2}{\varepsilon}(L(s)-L(t)-L(u))\\
&\quad-8-L^2(t)+L(t)(3+2L(s)-2L(u))\Bigg]\\
&\quad+\left(N_c+\frac{1}{N_c}\right)\left[\frac{s^2-u^2}{2u^2}(L^2(t)-2L(s)L(t))+\frac{t}{u}(L(t)-L(s))\right]\\
&\quad+4\pi b_0\log\left(\frac{\mu_R^2}{\hat{m}^2}\right),\\
F_{4;2}^{--} &= 2C_F\Bigg[\frac{2}{\varepsilon}(L(u)-L(s))+\frac{u^2-s^2}{2s^2}\left(L^2(t)+L^2(u)+\pi^2\right)\\
&\qquad+\frac{t}{s}(L(t)-L(u))+2L(s)L(t)-\frac{u^2+s^2}{s^2}L(t)L(u)\Bigg],\\
F_{4;2}^{-+} &= 2C_F\Bigg[\frac{2}{\varepsilon}(L(u)-L(s))-\frac{s^2-u^2}{2u^2}L^2(t)-\frac{t}{u}(L(t)-L(s))\\
&\qquad-2L(t)L(u)+\frac{s^2+u^2}{u^2}L(t)L(s)\Bigg].
\end{aligned}
\tag{5.67}
$$

Note that the loop corrections have imaginary parts arising from the analytic continuation of Mandelstam variables into the physical region $s>0;\ t,u<0$. They appear in the finite part as well as in the pole contributions.

From this we can construct the matrix $\tilde{H}^{(1)}$ defined in equation (5.62) as

$$\tilde{H}^{(1)} = \frac{C_\Gamma}{4N_c^2} \begin{pmatrix} \tilde{H}_{11}^{(1)} & \tilde{H}_{12}^{(1)} \\ \tilde{H}_{21}^{(1)} & \tilde{H}_{22}^{(1)} \end{pmatrix} , \tag{5.68}$$

with

$$\tilde{H}_{11}^{(1)} = 16 \left(\mathcal{R}e \left(F_{4;2}^{--} + F_{4;1}^{--} \right) \frac{s^2}{t^2} + \mathcal{R}e \left(F_{4;2}^{-+} + F_{4;1}^{-+} \right) \frac{u^2}{t^2} \right) , \tag{5.69a}$$

$$\tilde{H}_{12}^{(1)} = \frac{4}{N_c} \left(F_{4;2}^{--*} \frac{s^2}{t^2} + F_{4;2}^{-+*} \frac{u^2}{t^2} \right) , \tag{5.69b}$$

$$\tilde{H}_{21}^{(1)} = \frac{4}{N_c} \left(F_{4;2}^{--} \frac{s^2}{t^2} + F_{4;2}^{-+} \frac{u^2}{t^2} \right) , \tag{5.69c}$$

$$\tilde{H}_{22}^{(1)} = 0 . \tag{5.69d}$$

The full expression for this matrix is rather lengthy. It has the following explicit structure:

$$\begin{aligned} \tilde{H}^{(1)} = \frac{1}{2} \Bigg[& \left(-\frac{4C_F}{\varepsilon^2} - \frac{6C_F}{\varepsilon} \right) H^{(0)} - \frac{L(s)}{\varepsilon} \frac{C_F}{N_c} \begin{pmatrix} 0 & -1 \\ 1 & 0 \end{pmatrix} \\ & - \frac{2}{\varepsilon} L(t) \frac{h_0}{N_c} \begin{pmatrix} 1 & 0 \\ 0 & 0 \end{pmatrix} + \frac{1}{\varepsilon} L(u) \frac{h_0}{N_c} \begin{pmatrix} 2(N_c^2 - 2) & C_F \\ C_F & 0 \end{pmatrix} \\ & + 4\pi b_0 \log \left(\frac{\mu_R^2}{\hat{m}^2} \right) H^{(0)} \Bigg] + H^{(1)} , \end{aligned} \tag{5.70}$$

where h_0 and $H^{(0)}$ have been given in (5.60). Following [231], we have identified the finite part in the last line with the first-order correction to the hard-scattering matrix. This finite part is a function of the Mandelstam variables only. As one can see, the explicit dependence on the renormalization scale μ_R has been separated from $H^{(1)}$. It is proportional to $H^{(0)}$ and therefore fully taken into account by the exponential ξ_R in equation (5.45), as discussed in Sec. 5.3.1.

To present our final results for $H^{(1)}$, we adopt the notation of Ref. [209], where the matrix was derived in the context of the soft-collinear effective theory. We find full

agreement with the result in their equation (39):

$$\begin{aligned}
\left(H^{(1)}\right)_{11} =& \ \mathcal{R}e\left\{\frac{1}{2N_c^2}\Big[\frac{s^2+u^2}{t^2}\left(-4C_F L(t)^2+2X_1(s,t,u)L(t)+2Y\right)\right.\\
&\left.+\frac{s^2}{t^2}(C_A-4C_F)Z(s,t,u)-\frac{u^2}{t^2}(2C_A-4C_F)Z(u,t,s)\Big]\right\},\\
\left(H^{(1)}\right)_{21} =& \frac{1}{2N_c^2}\Big[\frac{s^2+u^2}{t^2}X_2(s,t,u)L(t)-\frac{s^2}{t^2}\frac{C_F}{2C_A}Z(s,t,u)\\
&+\frac{u^2}{t^2}\frac{C_F}{2C_A}Z(u,t,s)\Big],\\
\left(H^{(1)}\right)_{12} =& \left(H^{(1)}\right)_{21}^{*},\\
\left(H^{(1)}\right)_{22} =& \,0\,,
\end{aligned} \tag{5.71}$$

with [209]

$$\begin{aligned}
X_1(s,t,u) =& \ 6C_F-4\pi b_0+8C_F[L(s)-L(u)]\\
&-2C_A[2L(s)-L(t)-L(u)]\,,\\
X_2(s,t,u) =& \frac{2C_F}{C_A}[L(s)-L(u)]\,,\\
Y =& \ C_A\left(\frac{10}{3}+\pi^2\right)+C_F\left(\frac{\pi^2}{3}-16\right)+\frac{5}{3}4\pi b_0\,,\\
Z(s,t,u) =& \frac{t}{s}\left(\frac{t+2u}{s}[L(u)-L(t)]^2+2[L(u)-L(t)]+\pi^2\frac{t+2u}{s}\right).
\end{aligned} \tag{5.72}$$

There are several ways of checking the validity of the results. The simplest one is to compute

$$\mathrm{Tr}\left[\tilde{H}^{(1)}\,S^{(0)}\right], \tag{5.73}$$

which should reproduce the known one-loop virtual correction to $qq' \to qq'$ scattering given in [206]. This indeed turns out to be the case. Since $S^{(0)}$ is diagonal in our basis, this provides a check on the diagonal elements of $H^{(1)}$.

We also note that the pole terms of the NLO virtual amplitudes $M^{(1),\mathrm{virt}}$ in (5.61), including their imaginary parts, have been predicted in [231, 232] to be given by

$$\tilde{h}_I^{(1)}|_{\substack{\mathrm{pole}\\ \mathrm{terms}}} = \frac{1}{2}\left[-C_F\left(\frac{2}{\varepsilon^2}+\frac{3}{\varepsilon}\right)\mathbb{1}+\frac{1}{\varepsilon}\Gamma^{(1)}_{qq'\to qq'}\right]_{IJ} h_J^{(0)}\,, \tag{5.74}$$

where $\mathbb{1}$ denotes the 2×2 unit matrix and $\Gamma^{(1)}_{qq'\to qq'}$ is the soft anomalous dimension matrix introduced in (5.32) which possesses imaginary parts (the explicit result for $\Gamma^{(1)}_{qq'\to qq'}$

is given in equation (5.85) below). We have verified that this correctly reproduces the pole terms in the $\tilde{h}_I^{(1)}$.

In the way described in this subsection we have determined the one-loop hard-scattering matrix for each partonic channel contributing to di-hadron production. As one can see in equations (5.70),(5.71), for $qq' \to qq'$ the final expression always contains the squares of the tree-level helicity amplitudes $a_{4;0}$. This becomes different for partonic channels involving both external quarks and gluons.

5.3.3. Soft function

We now turn to the computation of the first-order correction $S^{(1)}_{ab\to cd}$ to the soft function in equation (5.30). Again we present explicit results only for the qq' channel, although we have of course considered all partonic channels. In fact, in the course of the study of qq' scattering we find a general construction rule for the soft matrix $S^{(1)}_{ab\to cd}$ that turns out to be applicable to all partonic channels.

Color structure of diagrams in the eikonal approximation

In order to to compute the soft matrix at NLO for qq' scattering, we need to consider the process $q(p_1)+q'(p_2) \to q(p_3)+q'(p_4)+g(k)$, where g denotes a radiated gluon with soft momentum k. The diagrams are treated in the eikonal approximation, decomposed according to our color basis. They are shown in Fig. 5.1. The blobs on either side of the cut denote a Born hard part that can be a color-octet or a singlet. There are six diagrams labeled "34" or "12" for example, depending on the external legs between which the additional gluon is exchanged. Eventually, all contributions must be summed. Using the notation of the previous subsection, each of the diagrams in Fig. 5.1 has the structure

$$\sum_{IJ} h_I^{(0)} h_J^{(0)*} \, (\mathcal{R}_{ij})_{JI} \, I_{ij} \;, \tag{5.75}$$

where ij labels the diagram, I_{ij} is an integral over the eikonal factor corresponding to the diagram that we will specify below, and the $(\mathcal{R}_{ij})_{JI}$ form a 2×2 matrix with entries labeled by JI =octet-octet, singlet-octet, etc. For example, for the "octet-octet" entry

of $\mathcal{R}_{34}$ we have

$$\begin{aligned}(\mathcal{R}_{34})_{\substack{J=\text{octet}\\I=\text{octet}}} &= \sum_{\substack{a,b,c,d,c',d'\\g,g_1,g_2}} T^{g_2}_{bd'} T^{g_2}_{ac'}\, T^{g}_{d'd} T^{g}_{c'c}\, T^{g_1}_{db} T^{g_1}_{ca} \\ &= \sum_{g,g_1,g_2} \mathrm{Tr}[T^{g_2} T^{g} T^{g_1}]\,\mathrm{Tr}[T^{g_2} T^{g} T^{g_1}] \\ &= -\frac{N_c^2-1}{4N_c} = -\frac{C_F}{2}\,. \end{aligned} \tag{5.76}$$

Here g corresponds to the color of the gluon exchanged between the external legs, while g_1 and g_2 are those for the gluons in the amplitudes on the two sides of the cut. Computing in this way the matrices $\mathcal{R}_{ij}$ for all diagrams, we find:

$$\begin{aligned}\mathcal{R}_{12} = \mathcal{R}_{34} &= \frac{C_F}{2}\begin{pmatrix} -1 & N_c \\ N_c & 0 \end{pmatrix}, \\ \mathcal{R}_{13} = \mathcal{R}_{24} &= \frac{C_F}{2}\begin{pmatrix} -\frac{1}{2} & 0 \\ 0 & 2N_c^2 \end{pmatrix}, \\ \mathcal{R}_{14} = \mathcal{R}_{23} &= \frac{C_F}{2}\begin{pmatrix} \frac{1}{2}(N_c^2-2) & N_c \\ N_c & 0 \end{pmatrix}. \end{aligned} \tag{5.77}$$

For the sum of all diagrams we thus have

$$\sum_{ij} \mathcal{R}_{ij}\, I_{ij} = \frac{C_F}{2}\begin{pmatrix} (RJ)_{11} & (RJ)_{12} \\ (RJ)_{21} & (RJ)_{22} \end{pmatrix}, \tag{5.78}$$

with

$$(RJ)_{11} = \frac{1}{2}(I_{13}+I_{24}) - I_{12} - I_{34} - \frac{N_c^2-2}{2}(I_{14}+I_{23}) \tag{5.79a}$$

$$(RJ)_{12} = N_c(I_{12}+I_{34}-I_{14}-I_{23}) \tag{5.79b}$$

$$(RJ)_{21} = (RJ)_{12} \tag{5.79c}$$

$$(RJ)_{22} = -2N_c^2(I_{13}+I_{24}) \tag{5.79d}$$

We note that the eikonal factor for the interference between initial- and final-state emission has an extra minus sign which we included here.

Integrals I_{ij}

Next, we need to specify and compute the I_{ij}. They are essentially given by eikonal factors integrated over the gluon phase space. They are normalized relative to the

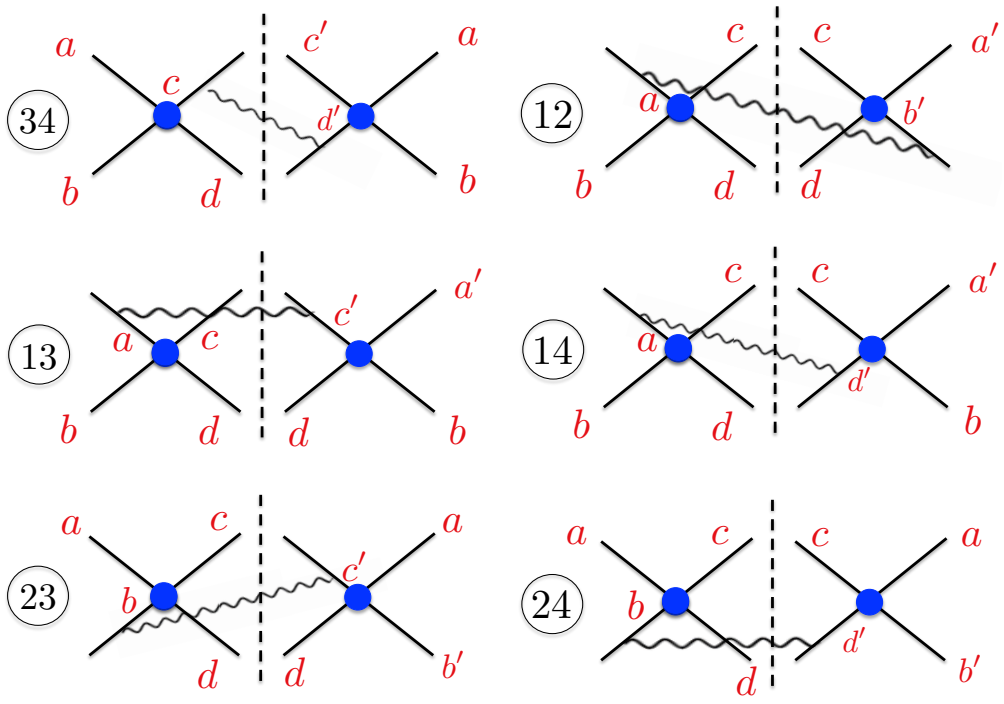

Figure 5.1.: Diagrams relevant for the calculation of the NLO soft matrix $S^{(1)}$. The blobs represent a Born amplitude and the letters are color indices.

Born cross section. Adopting the three-particle phase space in $D = 4 - 2\varepsilon$ dimensions from [200] (see also [188]), one has

$$I_{ij} = -\frac{\alpha_s}{\pi}\frac{s}{4\pi}e^{\varepsilon\gamma_E}\frac{\Gamma(1-\varepsilon)}{\Gamma(1-2\varepsilon)}\int_0^1 d\hat{\tau}\,\hat{\tau}^{-\varepsilon}(1-\hat{\tau})^{1-2\varepsilon}\int d\Omega\,\frac{p_i\cdot p_j}{(p_i\cdot k)(p_j\cdot k)}\,, \tag{5.80}$$

where

$$\int d\Omega = \int_0^\pi d\psi \sin^{1-2\varepsilon}\psi \int_0^\pi d\theta\, \sin^{-2\varepsilon}\theta\,. \tag{5.81}$$

We work in the c.m.s. of the incoming partons; ψ and θ are the gluon's polar and azimuthal angles relative to the plane defined by the directions of incoming and outgoing hard partons. The relevant angular integrals are well-known [111]:

$$\begin{aligned}&\int d\Omega\,\frac{1}{(1-\cos\psi)^j(1-\cos\psi\cos\chi-\sin\psi\cos\theta\sin\chi)^k}\\ &\quad= 2\pi\frac{\Gamma(1-2\varepsilon)}{\Gamma(1-\varepsilon)^2}\,2^{-j-k}\,B(1-\varepsilon-j,1-\varepsilon-k)\,{}_2F_1\left(j,k,1-\varepsilon,\cos^2\frac{\chi}{2}\right)\,,\end{aligned} \tag{5.82}$$

with the Hypergeometric function ${}_2F_1$. Performing the integrations over $d\Omega$, but leaving the integration over $\hat{\tau}$ (or, equivalently, gluon energy) aside for the moment, we find near threshold

$$\begin{aligned}\frac{dI_{12}}{d\hat{\tau}} &= \frac{dI_{34}}{d\hat{\tau}} = -\frac{\alpha_s}{\pi}\left[\left(\frac{1}{\varepsilon^2}-\frac{\pi^2}{4}\right)\delta(1-\hat{\tau}) - \frac{2}{\varepsilon}\,\frac{1}{(1-\hat{\tau})_+}\right.\\ &\qquad\left. +4\left(\frac{\ln(1-\hat{\tau})}{1-\hat{\tau}}\right)_+\right]\,,\\ \frac{dI_{13}}{d\hat{\tau}} &= \frac{dI_{24}}{d\hat{\tau}} = -\frac{\alpha_s}{\pi}\left[\left(\frac{1}{\varepsilon^2}-\frac{\pi^2}{4}-\frac{1}{\varepsilon}\ln\left(-\frac{t}{s}\right)-\mathrm{Li}_2\left(-\frac{u}{t}\right)\right)\delta(1-\hat{\tau})\right.\\ &\quad +2\left(-\frac{1}{\varepsilon}+\ln\left(-\frac{t}{s}\right)\right)\,\frac{1}{(1-\hat{\tau})_+} + 4\left(\frac{\ln(1-\hat{\tau})}{1-\hat{\tau}}\right)_+\Bigg]\,,\\ \frac{dI_{23}}{d\hat{\tau}} &= \frac{dI_{14}}{d\hat{\tau}} = \frac{dI_{13}}{d\hat{\tau}}\Big|_{t\leftrightarrow u},\end{aligned} \tag{5.83}$$

where Li_2 denotes the Dilogarithm function.

Extraction of $S^{(1)}$

Combining equations (5.78) and (5.83), we obtain

$$\begin{aligned}
&\sum_{ij} \mathcal{R}_{ij} \frac{dI_{ij}}{d\hat{\tau}} \\
&= C_F \frac{\alpha_s}{\pi} \Bigg[\left\{ \delta(1-\hat{\tau}) \left(\frac{1}{2\varepsilon^2} - \frac{\pi^2}{8} \right) - \frac{1}{\varepsilon} \frac{1}{(1-\hat{\tau})_+} + 2 \left(\frac{\ln(1-\hat{\tau})}{1-\hat{\tau}} \right)_+ \right\} \\
&\qquad \times \begin{pmatrix} N_c^2 - 1 & 0 \\ 0 & 4N_c^2 \end{pmatrix} + \left\{ \delta(1-\hat{\tau}) \frac{1}{2\varepsilon} - \frac{1}{(1-\hat{\tau})_+} \right\} \\
&\qquad \times \begin{pmatrix} \ln\left(-\frac{t}{s}\right) + (2-N_c^2) \ln\left(-\frac{u}{s}\right) & -2N_c \ln\left(-\frac{u}{s}\right) \\ -2N_c \ln\left(-\frac{u}{s}\right) & -4N_c^2 \ln\left(-\frac{t}{s}\right) \end{pmatrix} \\
&+ \delta(1-\hat{\tau}) \frac{1}{2} \begin{pmatrix} \mathrm{Li}_2\left(-\frac{u}{t}\right) + (2-N_c^2) \mathrm{Li}_2\left(-\frac{t}{u}\right) & -2N_c \mathrm{Li}_2\left(-\frac{t}{u}\right) \\ -2N_c \mathrm{Li}_2\left(-\frac{t}{u}\right) & -4N_c^2 \mathrm{Li}_2\left(-\frac{u}{t}\right) \end{pmatrix} \Bigg] . \qquad (5.84)
\end{aligned}$$

In the first term we recognize the lowest-order soft matrix of equation (5.53). The matrix in the second term has a direct relation to the one-loop soft anomalous dimension matrix $\Gamma^{(1)}_{qq'\to qq'}$ introduced in (5.32),(5.33), which in our color basis is given by [179]

$$\Gamma^{(1)}_{qq'\to qq'} = \begin{pmatrix} \frac{1}{N_c}(2S - T - U) + 2C_F U & 2(U-S) \\ \frac{C_F}{N_c}(U-S) & 2C_F T \end{pmatrix} , \qquad (5.85)$$

with

$$S = 0, \quad T = \ln\left(\frac{-t}{s}\right) + i\pi, \quad U = \ln\left(\frac{-u}{s}\right) + i\pi \, . \qquad (5.86)$$

An equally possible choice is $S = -i\pi, T = \ln\left(\frac{-t}{s}\right), U = \ln\left(\frac{-u}{s}\right)$, which matches the logarithms in equation (5.66). One easily checks that $\Gamma^{(1)}_{qq'\to qq'}$ differs for the two choices only by a term proportional to the unit matrix which commutes with all other matrices and hence cancels in the final result. This holds true for all partonic channels. Note that even for the resummed cross section only the combination $\mathrm{e}^{\Gamma^\dagger} S \mathrm{e}^{\Gamma}$ contributes. One easily checks that the matrix in the second line of the right-hand-side of (5.84) is given

by $-[(\Gamma^{(1)})^\dagger S^{(0)} + S^{(0)}\Gamma^{(1)}]/C_F$. Hence, we have after some reordering of terms:

$$\begin{aligned}
&\sum_{ij} \mathcal{R}_{ij}\, \frac{dI_{ij}}{d\hat{\tau}} \\
&\quad = \frac{\alpha_s}{\pi}\Bigg[\delta(1-\hat{\tau})\left\{\frac{2C_F}{\varepsilon^2}S^{(0)} - \frac{1}{2\varepsilon}\left[(\Gamma^{(1)})^\dagger S^{(0)} + S^{(0)}\Gamma^{(1)}\right]\right\} \\
&\qquad - \frac{4C_F}{\varepsilon}\frac{1}{(1-\hat{\tau})_+}S^{(0)} + 8C_F\left(\frac{\ln(1-\hat{\tau})}{1-\hat{\tau}}\right)_+ S^{(0)} \\
&\qquad + \frac{1}{(1-\hat{\tau})_+}\left[(\Gamma^{(1)})^\dagger S^{(0)} + S^{(0)}\Gamma^{(1)}\right] \\
&\qquad + \frac{C_F}{2}\delta(1-\hat{\tau})\Bigg\{\begin{pmatrix} \mathrm{Li}_2\left(-\frac{u}{t}\right) + (2-N_c^2)\,\mathrm{Li}_2\left(-\frac{t}{u}\right) & -2N_c\,\mathrm{Li}_2\left(-\frac{t}{u}\right) \\ -2N_c\,\mathrm{Li}_2\left(-\frac{t}{u}\right) & -4N_c^2\,\mathrm{Li}_2\left(-\frac{u}{t}\right)\end{pmatrix} \\
&\qquad - \pi^2 S^{(0)}\Bigg\}\Bigg]\,. \qquad (5.87)
\end{aligned}$$

Each of the terms in this equation has a transparent interpretation. The pole terms $\propto \delta(1-\hat{\tau})$ in the first line will be canceled by corresponding terms in the virtual correction; see equation (5.74). The single pole term $\propto 1/(1-\hat{\tau})_+$ will be canceled by collinear factorization in the eikonal approximation, as described in the Appendix. The next two terms precisely match the threshold logarithms at NLO, as becomes evident by going to Mellin-moment space and comparing to (5.36). The remaining term involves the one-loop soft matrix we are interested in. More precisely, since $S^{(1)}$ appears in the Mellin-space expression for the resummed cross section, and since the moments of $(\ln(1-\hat{\tau})/(1-\hat{\tau}))_+$ are given by $\frac{1}{2}(\ln^2\bar{N} + \pi^2/6)$ (up to corrections suppressed as $1/N$), all terms $\propto \pi^2$ match when comparing to (5.36), and we are just left with

$$S^{(1)} \;=\; \frac{C_F}{2}\begin{pmatrix} \mathrm{Li}_2\left(-\frac{u}{t}\right) + (2-N_c^2)\,\mathrm{Li}_2\left(-\frac{t}{u}\right) & -2N_c\,\mathrm{Li}_2\left(-\frac{t}{u}\right) \\ -2N_c\,\mathrm{Li}_2\left(-\frac{t}{u}\right) & -4N_c^2\,\mathrm{Li}_2\left(-\frac{u}{t}\right)\end{pmatrix}. \qquad (5.88)$$

This is our final result for the one-loop soft matrix for this process. A powerful check on the result comes from comparison with the full cross section at NLO: Inserting our $S^{(1)}$ along with $H^{(1)}$ from equation (5.71) into (5.36), we verify that the resulting expression correctly reproduces all threshold logarithms *a*nd all constant terms in the NLO partonic cross section.

As it turns out, we can give a very simple rule for obtaining $S^{(1)}$ directly from $S^{(0)}$ and the anomalous dimension matrix $\Gamma^{(1)}$. This becomes already evident from comparison of the two matrices in the second and third lines of (5.84): They have identical structure, except that each logarithm has to be replaced by a dilogarithm with suitably modified

argument,

$$\ln\left(-\frac{t}{s}\right) \to \mathrm{Li}_2\left(-\frac{u}{t}\right) ,$$
$$\ln\left(-\frac{u}{s}\right) \to \mathrm{Li}_2\left(-\frac{t}{u}\right) . \tag{5.89}$$

The deeper reason for this is of course that already in the integrals (5.83) the logarithm and the dilogarithm always appear in the same ratio in the term $\propto \delta(1-\hat{\tau})$. Since we know how the matrix in the second line of (5.84) is expressed in terms of $S^{(0)}$ and $\Gamma^{(1)}$, we also know how to construct $S^{(1)}$: Compute the combination $-1/2\left((\Gamma^{(1)})^\dagger S^{(0)} + S^{(0)}\Gamma^{(1)}\right)$ and substitute each logarithm according to (5.89). As the integrals I_{ij} are the same no matter which process we are considering, this simple construction rule works for all partonic channels. All necessary ingredients, the $\Gamma^{(1)}_{ab\to cd}$ and the $S^{(0)}_{ab\to cd}$, may be found in the Appendix of Ref. [179]; we therefore do not present the explicit expressions for the resulting $S^{(1)}_{ab\to cd}$ for all the other channels, which become rather lengthy. It is likely that the simple rule we find is a special property of the pair mass kinematics we are considering here.

5.3.4. Inverse Mellin and Fourier transforms and matching procedure

In order to produce phenomenological results for the resummed case, we need to perform inverse Mellin transform and Fourier transforms. The Mellin inverse requires a prescription for dealing with the singularity in the perturbative strong coupling constant in the NNLL expansions of the resummed exponents. As in [200] we will use the *Minimal Prescription* developed in [42], which relies on use of the NNLL expanded forms given in Sec. 5.3.1 and on choosing a Mellin contour in complex-N space that lies to the *l*eft of the poles at $\lambda = 1/2$ and $\lambda = 1$ in the Mellin integrand. The function $\Omega_{H_1H_2\to cd}$ in (5.15) is obtained as [200]

$$\begin{aligned}
&\Omega^{\mathrm{resum}}_{H_1H_2\to cd}\left(\tau', \Delta\eta, \bar{\eta}, \alpha_s(\mu_R), \frac{\mu_R}{\hat{m}}, \frac{\mu_F}{\hat{m}}\right) \\
&\quad = \frac{1}{2\pi}\int_{-\infty}^{\infty} d\nu\, \mathrm{e}^{-i\nu\bar{\eta}} \int_{C_{MP}-i\infty}^{C_{MP}+i\infty} \frac{dN}{2\pi i}\, \left(\tau'\right)^{-N} \\
&\qquad \times \sum_{ab} \tilde{f}_a^{H_1}(N+1+i\nu/2, \mu_F)\tilde{f}_b^{H_2}(N+1-i\nu/2, \mu_F) \\
&\qquad \times \tilde{\omega}^{\mathrm{resum}}_{ab\to cd}\left(N, \nu, \Delta\eta, \alpha_s(\mu_R), \frac{\mu_R}{\hat{m}}, \frac{\mu_F}{\hat{m}}\right),
\end{aligned} \tag{5.90}$$

a with a suitable Mellin contour consistent with the minmal prescription. As shown in [200], it is straightforward to perform the convolution of the inverted resummed $\Omega^{\mathrm{resum}}_{H_1H_2\to cd}$ with the fragmentation functions, as given by (5.14).

As in [200], we match the resummed cross section to the full NLO one, by expanding the resummed cross section to $\mathcal{O}(\alpha_s^3)$, subtracting the expanded result from the resummed one, and adding the full NLO cross section:

$$d\sigma^{\text{match}} = \left(d\sigma^{\text{resum}} - d\sigma^{\text{resum}}\Big|_{\mathcal{O}(\alpha_s^3)} \right) + d\sigma^{\text{NLO}} \,. \tag{5.91}$$

For the NLO cross section we use the results of [233]. In this way, NLO is taken into account in full, and the soft-gluon contributions beyond NLO are resummed in the way described above. Of course, for a full NNLL resummed cross section one would prefer to match to an NNLO calculation, which however is not available for this observable yet.

5.4. Phenomenological results

We now examine the numerical effects of our approximate NNLL resummation in comparison to the NLL and NLO results shown in [200]. Since the NNLL effects are generally rather similar for the experimental situations considered in [200], we show only two representative examples here. We will also make predictions for the di-hadron cross section at RHIC, where one would expect the effects of resummation to be smaller.

Our examples from [200] concern the NA24 [201] and the CCOR [205] $pp \to \pi^0\pi^0$ scattering experiments. The fixed-target experiment NA24 recorded data at a beam energy of $E_p = 300$ GeV, while CCOR operated at the ISR collider at $\sqrt{S} = 62.4$ GeV. Both experiments employed the cuts $p_T^{\text{pair}} < 1$ GeV, $|Y| < 0.35$, and $|\cos\theta^*| < 0.4$. Here, p_T^{pair} and Y are the transverse momentum and rapidity of the pion pair, respectively, which are given in terms of the individual pion transverse momenta $p_{T,i}$ and of $\Delta\eta, \bar{\eta}$ in (5.4) by

$$\begin{aligned} p_T^{\text{pair}} &= |p_{T,1} - p_{T,2}| \,, \\ Y &= \bar{\eta} - \frac{1}{2} \ln \left(\frac{p_{T,1}\, \mathrm{e}^{-\Delta\eta} + p_{T,2}\, \mathrm{e}^{\Delta\eta}}{p_{T,1}\, \mathrm{e}^{\Delta\eta} + p_{T,2}\, \mathrm{e}^{-\Delta\eta}} \right) \,, \end{aligned} \tag{5.92}$$

where LO kinematics have been assumed as appropriate in the threshold regime. Furthermore, $\cos\theta^*$ is the cosine of the scattering angle in the partonic c.m.s. and is for LO kinematics given by

$$\cos\theta^* = \frac{1}{2} \left(\frac{p_{T,1}}{p_{T,2} + p_{T,1}\cosh(2\Delta\eta)} + \frac{p_{T,2}}{p_{T,1} + p_{T,2}\cosh(2\Delta\eta)} \right) \sinh(2\Delta\eta) \,. \tag{5.93}$$

For details on the kinematical variables, see [200]. Thanks to our way of organizing the threshold resummed cross section, inclusion of cuts on any of these variables is straightforward.

In all our calculations, we use the CTEQ6M5 set of parton distribution functions [31], along with its associated value of the strong coupling constant. As compared to our results in [200], we update to the latest "de Florian-Sassot-Stratmann" (DSS) set of fragmentation functions [119]. We note that one might object that the use of NLO parton distribution functions and fragmentation functions is not completely justified for obtaining NNLL resummed predictions. However, since fragmentation functions evolved at NNLO are not yet available in any case, we have decided to stick to NLO functions throughout. As in [200], we choose the renormalization and factorization scales to be equal, $\mu_R = \mu_F \equiv \mu$, and we give them the values M and $2M$, in order to investigate the scale dependence of the results.

Figure 5.2 shows the comparison to the NA24 [201] data. As known from [200], the full NLO cross section and the first-order expansion of the resummed expression, that is, the last two terms in equation (5.91), agree to a remarkable degree. Their difference actually never exceeds 1% for the kinematics relevant for NA24. We recall these results by the dashed lines and the crosses in the figure. They provide confidence that the soft-gluon terms constitute the dominant part of the cross section, so that their resummation is sensible. The dot-dashed lines in the figure present the NLL results, computed by dropping all NNLL terms and matching to NLO via equations (5.40),(5.41), as in [200]. As found there, resummation leads to a significant enhancement of the theoretical prediction and provides a much better description of the NA24 data [201] than for the NLO calculation. Finally, the two solid lines show our NNLL resummed results. The key observations are that the two NNLL results for scales $2M$ and M are very close together and both roughly fall within the "band" spanned by the two NLL results for the two scales. One also notices that the NNLL curves have a slope somewhat less steep than the NLL ones. Given the relatively large uncertainties of the data, it is fair to say that the main effects are already taken into account at NLL. However, the precision of the NNLL calculation, in particular the strong reduction of the scale dependence, still provides a significant theoretical and phenomenological improvement.

In order to assess the improvement in scale dependence in a more detailed way, we show in Fig. 5.3 results for the predicted cross section as a function of μ/M (where again $\mu_R = \mu_F \equiv \mu$), using a fixed pair invariant mass $M = 5.125$ GeV, which corresponds to the left-most point in Fig. 5.2. The dot-dashed line corresponds to the variation of the NLL resummed cross section, where for ξ_R in equation (5.47) we include only the first term in the exponent, i.e. $2b_0\alpha_s \ln(\mu_R^2/\hat{m}^2)$. This is the only term justified for a cross section resummed to this accuracy. We note that keeping this term in the exponent or expanding the exponential to first order (as done in [200]) makes only a modest numerical difference. At NNLL, we include the full exponent ξ_R in equation (5.47), keeping in mind the discussion following equation (5.49). Our result for the scale variation of the NNLL resummed cross section is shown as a solid line in Fig. 5.3. One observes a very strong improvement when going from NLL to NNLL, with the NNLL resummed cross section rather flat even out to scales as large as $\mu = 10M$.

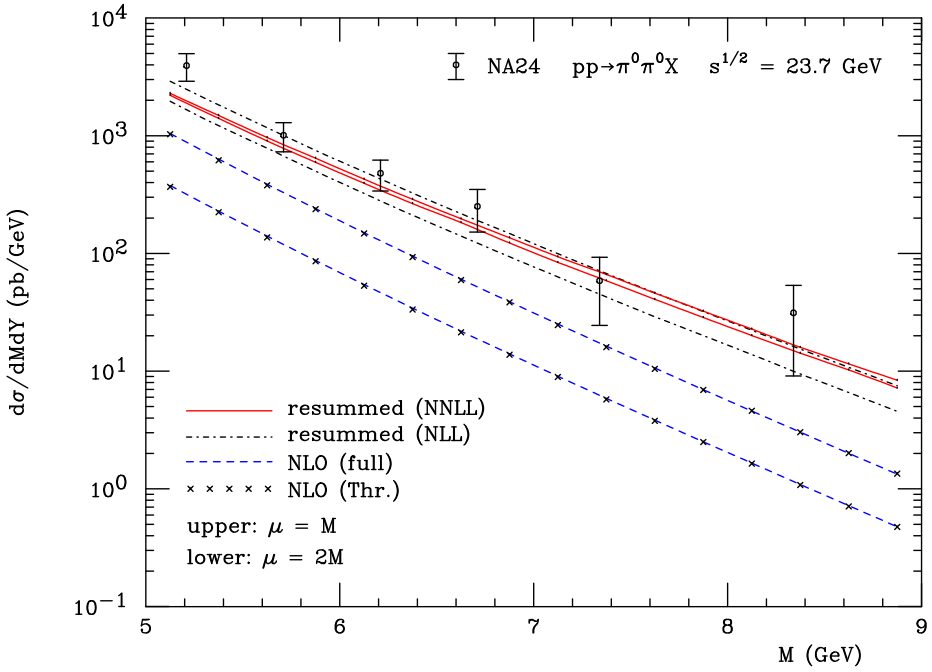

Figure 5.2.: Comparison of NLO (dashed), NLL resummed (dot-dashed) and NNLL resummed (solid) calculations of the cross section for $pp \to \pi^0\pi^0 X$ to the NA24 data [201], for two different choices of the renormalization and factorization scales, $\mu_R = \mu_F = M$ (upper lines) and $\mu_R = \mu_F = 2M$ (lower lines). The crosses display the NLO $\mathcal{O}(\alpha_s)$ expansion of the resummed cross section.

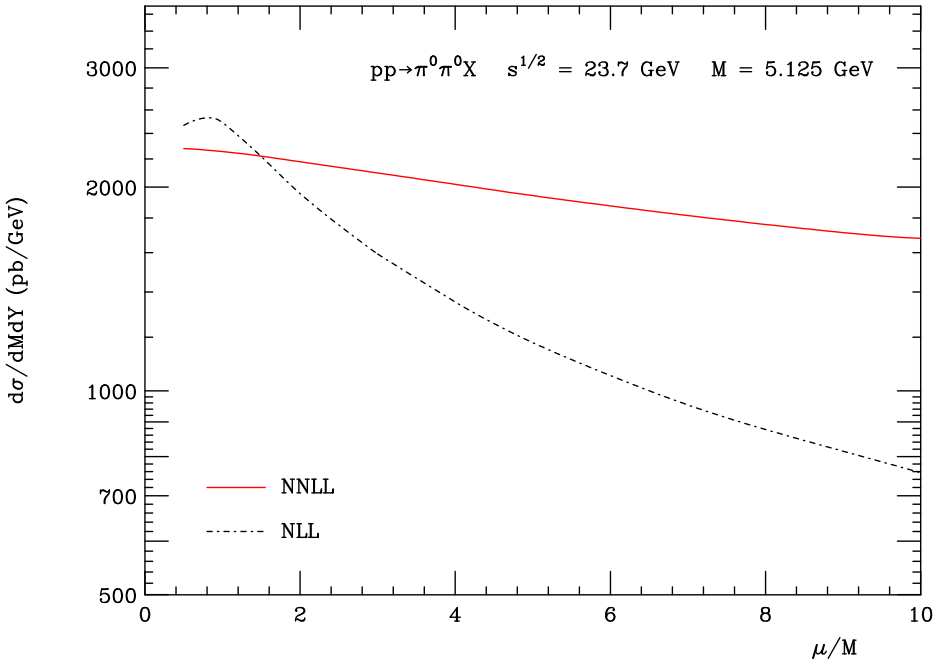

Figure 5.3.: Comparison of the scale dependence of the NLL resummed (dot-dashed) and the NNLL resummed (solid) cross sections for NA24 kinematics. We choose a pion pair invariant mass of $M = 5.125$ GeV and show the variation of the cross sections as a function of μ/M, where $\mu_R = \mu_F = \mu$.

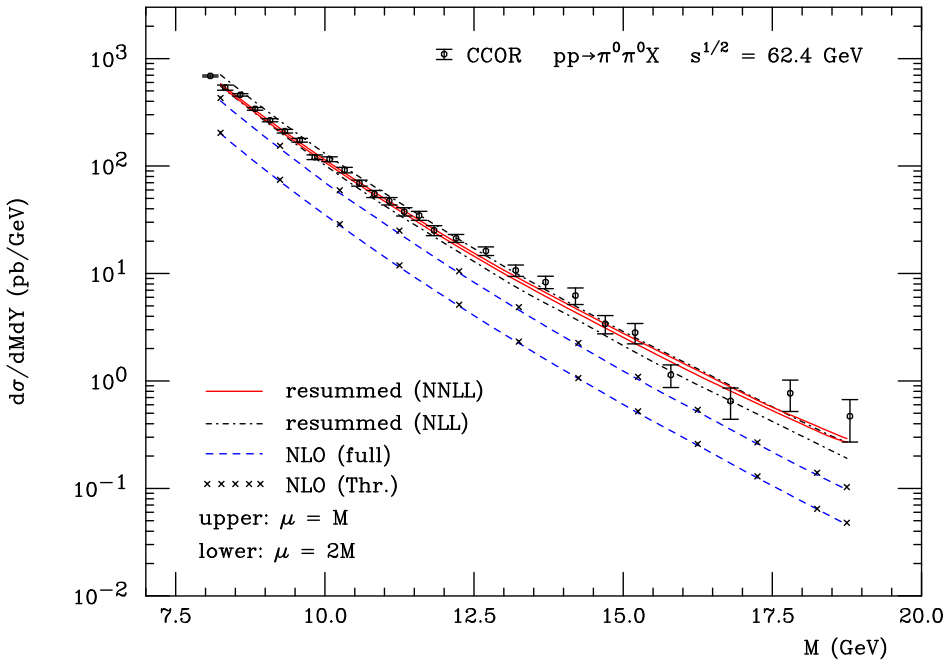

Figure 5.4.: Same as Fig. 5.2, but for pp collisions at $\sqrt{S} = 62.4$ GeV. The data are from CCOR [205].

Figure 5.4 shows the comparison of our results to the CCOR data [205]. The main features of the results are very similar to those in Fig. 5.2. Again the scale dependence is strongly reduced at NNLL. As a side remark we note that the new fragmentation functions of [119] also help to achieve a much better description of the data than we found in our previous study [200].

Finally, we consider di-hadron production in pp collisions at RHIC with a c.m.s. energy of $\sqrt{S} = 200$ GeV. For simplicity, we use the same cuts as for the NA24 experiment. In Fig. 5.5, we show our results for an invariant mass range of $M = 10 - 75$ GeV. We find that at this energy the full NLO (dashed) and the NLO expansion of the resummed result (crosses) do not match quite as well as observed for fixed target scattering in Fig. 5.2, although the agreement is usually at the 10% level or better. Threshold resummation again yields a sizable enhancement over NLO, but the effects are somewhat

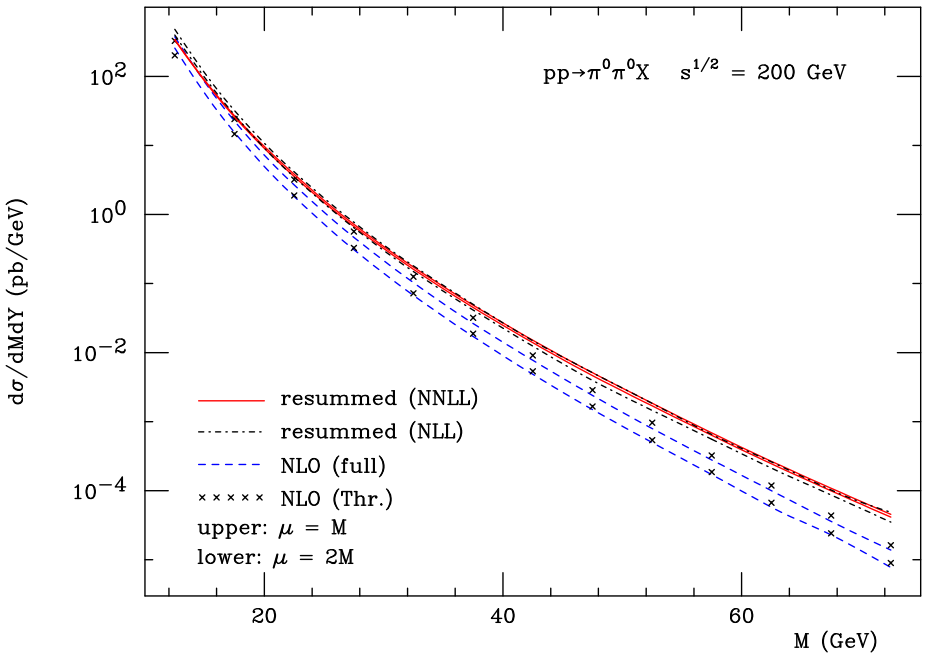

Figure 5.5.: Di-hadron production at RHIC at a center-of-mass energy of $\sqrt{S} = 200$ GeV. The full NLO result (dashed) is shown in comparison to the NLO expansion of the resummed result (crosses). The solid line shows the NNLL resummed cross section. As before, we use the scales $\mu_R = \mu_F = M$ and $\mu_R = \mu_F = 2M$.

smaller than in the fixed-target regime, since at RHIC's higher energy one is typically further away from threshold. Also here, the NNLL-resummed result is nearly within the NLL scale uncertainty band and shows a reduced scale dependence.

5.5. Conclusions

We have extended the threshold resummation framework for di-hadron production in hadronic collisions, $H_1H_2 \to h_1h_2X$, beyond the next-to-leading logarithmic level. To achieve this, we have determined the first-order corrections to the hard-scattering func-

tion H and the soft function S, which both are matrices in color space. With these, it becomes possible to resum four towers of threshold logarithms in the perturbative series. In our numerical studies, we have found that the NNLL resummed results fall within the scale uncertainty band of the NLL resummed calculation. They also show a much reduced scale dependence.

There are important further applications of our work. Of particular interest are di-jet, single-inclusive jet and single-inclusive hadron cross sections, all of which have much phenomenological relevance at present-day collider experiments. Given the promising results we have obtained for di-hadron production, we may expect that a similar resummation at NNLL for these reactions would also improve the theoretical QCD prediction.

Chapter 6.

Approximate NNLO Corrections to Hadronic Jet Production

We determine dominant next-to-next-to-leading order QCD corrections to single-inclusive jet production at the LHC and Tevatron, using the established threshold resummation framework. In contrast to previous literature on this topic, our study incorporates all of the following features: (1) It properly accounts for the way a jet is defined in experiment and treated in available full next-to-leading order calculations, (2) It includes the three leading classes of logarithmic terms in the perturbative expansion, and (3) It is adapted to the full kinematics in jet transverse momentum and rapidity relevant for experiments. A recent full next-to-next-to-leading order calculation in the purely gluonic channel allows us to assess the region where our approximate corrections provide an accurate description. We expect our results to be important on the way to precision jet phenomenology at the LHC and as benchmark for further full next-to-next-to-leading order calculations. This chapter is based on publication [1].

6.1. Introduction.

The production of high-transverse-momentum hadron jets plays a fundamental role at the LHC [234] and at Tevatron [235]. Jets are produced very copiously, making them precision probes of the physics of the Standard Model and beyond. Theoretical calculations whose precision matches that achievable in experiment are of critical importance. The efforts made in this context have spanned more than three decades now, culminating so far with the recent calculation of the next-to-next-to-leading order (NNLO) perturbative corrections to jet production in the "gluon-only" channel [236, 237].

As complete NNLO calculations of jet production are probably still a few years away, it is useful to determine approximate NNLO results, at least in certain kinematical

regimes. This is possible thanks to the fact that the perturbative series for the partonic cross sections contains classes of logarithmic terms that often dominate. Resummation techniques in QCD [238] allow to determine the all-order structure of these logarithmic terms, and one therefore also obtains the logarithms present at NNLO. Knowledge of approximate NNLO expressions is very useful, since it potentially offers an avenue toward more precise phenomenology than available on the basis of the presently known full next-to-leading order (NLO) corrections. It also serves as benchmark for future full NNLO calculations.

The logarithms just mentioned arise near a threshold from which the production of a jet becomes possible in a partonic collision. They are hence known as "threshold logarithms". The threshold is set by a vanishing invariant mass $\sqrt{s_4}$ of the partonic system that recoils against the observed jet. At the kth order of perturbation theory, one finds threshold corrections to the Born cross section of the form $\alpha_s^k[\log^m(z)/z]_+$, with $0 \leq m \leq 2k-1$, where $z = s_4/s$ with $\sqrt{s}$ the center-of-mass energy of the incoming partons. The systematic resummation of these logarithms to all orders in the strong coupling α_s was derived for the case of jet production in [238], where explicit next-to-leading logarithmic (NLL) results were given that in principle allow to resum the three "towers" of logarithms with $m = 2k-1, 2k-2, 2k-3$.

An important "subtlety" was pointed out in [238] concerning the threshold logarithms in jet production: the structure of the logarithmic corrections depends on whether or not the jet is assumed to be massless at partonic threshold, even at the leading-logarithmic (LL) level. If the jet is taken to be massless at threshold, an approach for which we will use the term "scheme (1)" in the following, leading-logarithmic corrections arise in the resummed perturbative function describing the jet. If, on the other hand, the jet is permitted to have a non-vanishing invariant mass at threshold ("scheme (2)"), the leading logarithms cancel, leaving behind a non-leading logarithm whose coefficient depends on jet "size" parameter R introduced by the jet algorithm. The difference between the two schemes may be understood from the fact that fewer final states contribute in scheme (1) than in scheme (2) [238].

Approximate NNLO corrections for jet production have been derived in [239–241], adopting scheme (1). As one can see in the very recent study [240], the NLO terms predicted for scheme (1) fail to match a full NLO calculation [242] even in a regime where threshold logs are known to dominate. This becomes particularly evident from the fact that the threshold terms for scheme (1) do not carry any dependence on the jet parameter R, whereas the full NLO results do. These features observed in [240] are in fact not surprising: explicit analytical NLO calculations [116, 117] have shown that jets produced close to partonic threshold do span a range of jet masses. Indeed, for any jet algorithm the jet produced in the perturbative calculation can evidently contain two or more partons and hence have a non-vanishing invariant mass. This is even the case at exact threshold $z = 0$, when for example only a single parton recoils against the entire

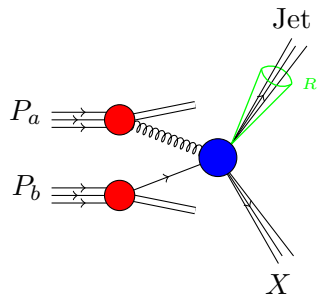

Figure 6.1.: Schematic visualization of the $hh \to \text{Jet}X$ cross section. The red blobs represents the PDFs of the incoming hadrons with momenta P_a and P_b. The blue blob represents the partonic hard scattering part.

jet. The maximally allowed jet mass at threshold will depend on the parameter R used in the jet algorithm.

Thus, the assumption of massless jets at threshold that was made in previous studies [239–241] does not appear to be appropriate. Instead, the resummation ought to be carried out within scheme (2). A resummed study in this scheme was in fact performed in [227], where however only the rapidity-integrated cross section was considered, for which the resummation simplifies considerably. Integration over all rapidity is not quite adequate for comparisons with experimental data. In this chapter we present new predictions for the NNLO threshold terms, using scheme (2) and keeping full dependence on rapidity in the calculation. We will also go beyond the previous studies [239, 240] by determining all three most leading logarithmic contributions $\propto (\log^3(z)/z)_+$, $(\log^2(z)/z)_+$, $(\log(z)/z)_+$ at NNLO. The last of these is new; it may be obtained by matching the resummation framework to a full NLO calculation. For the latter we choose that of [116, 117], which provides analytical results for the partonic cross sections. The calculation was performed assuming that the produced jet is rather narrow ("narrow-jet approximation" (NJA)). It has been shown that this approximation is extremely accurate even at relatively large jet sizes of $R \sim 0.7$.

6.2. Theoretical framework

The factorized cross section for the single-inclusive production of a jet with transverse momentum p_T and pseudorapidity η may be written as

$$\frac{p_T^2 \mathrm{d}^2\sigma}{\mathrm{d}p_T^2 \mathrm{d}\eta} = \sum_{ab} \int_0^{V(1-W)} \mathrm{d}z \int_{\frac{VW}{1-z}}^{1-\frac{1-V}{1-z}} \mathrm{d}v \, x_a f_a(x_a, \mu_f) \times x_b f_b(x_b, \mu_f) \frac{\mathrm{d}\hat{\sigma}_{ab}}{\mathrm{d}v \mathrm{d}z}(v, z, p_T, \mu_r, \mu_f, R), \tag{6.1}$$

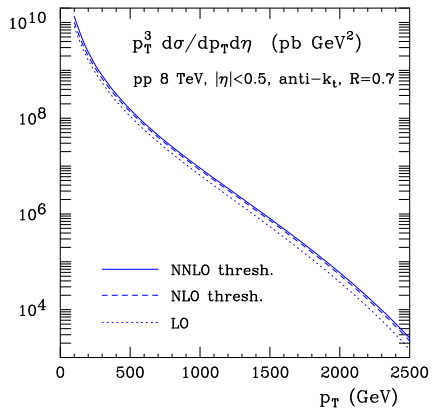

Figure 6.2.: Differential cross section for jet production in pp-collisions at the LHC at $\sqrt{S} = 8$ TeV, using the anti-k_t algorithm with $R = 0.7$.

where $V = 1 - x_T e^{-\eta}/2$, $VW = x_T e^{\eta}/2$, with $x_T = 2p_T/\sqrt{S}$ and the hadronic center-of-mass energy $\sqrt{S}$. The sum runs over all partonic collisions producing the jet; $d\hat{\sigma}_{ab}$ denote the corresponding partonic hard-scattering cross sections and f_a, f_b the parton distribution functions at momentum fractions $x_a = VW/v(1-z)$, $x_b = (1-V)/(1-v)(1-z)$. The partonic cross sections are computed in QCD perturbation theory. As indicated, besides depending on p_T and the usual renormalization and factorization scales μ_r, μ_f, they are functions of the partonic kinematic variables, which we have chosen as

$$v = \frac{u}{t+u}, \qquad z = \frac{s_4}{s}, \tag{6.2}$$

where $s = x_a x_b S$ is the partonic center-of-mass energy squared, $t = (p_a - p_J)^2$, $u = (p_b - p_J)^2$ (with $p_{a,b}$ and p_J the four-momenta of the initial partons and the jet, respectively), and s_4 is the invariant mass squared of the "unobserved" partonic system recoiling against the jet. We stress that the $d\hat{\sigma}_{ab}$ also depend on the algorithm adopted to define the jet, as indicated by the generic jet parameter R in equation (6.1). We always assume the jet to be defined by the anti-k_t algorithm [121].

The perturbative series for each of the partonic scattering cross sections may be cast

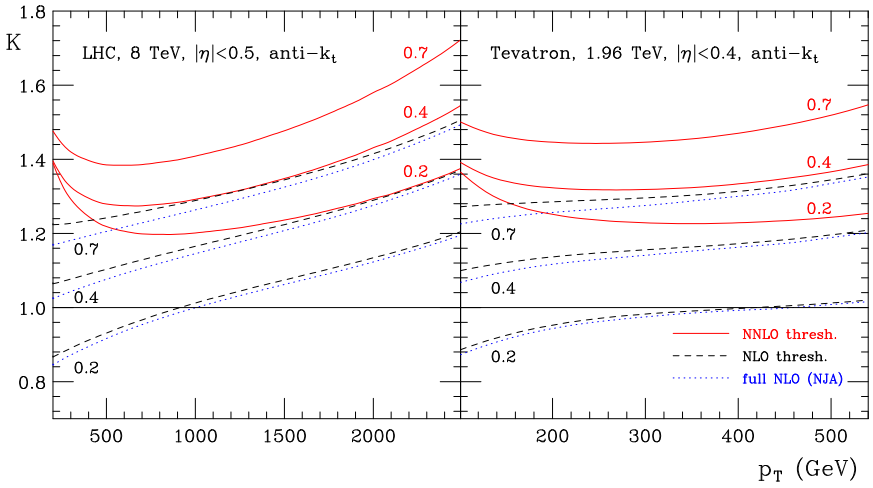

Figure 6.3.: Left: K-factors for jet production in pp-collisions at the LHC at $\sqrt{S}$ = 8 TeV for $R = 0.2, 0.4, 0.7$, using the anti-k_t algorithm. Right: Same for $p\bar{p}$ collisions at the Tevatron at $\sqrt{S} = 1.96$ TeV.

into the form

$$\frac{sd\hat{\sigma}_{ab}}{dvdz} = \left(\frac{\alpha_s}{\pi}\right)^2 \left[\omega_{ab}^{(0)} + \frac{\alpha_s}{\pi}\omega_{ab}^{(1)} + \left(\frac{\alpha_s}{\pi}\right)^2 \omega_{ab}^{(2)} + \mathcal{O}(\alpha_s^3)\right], \tag{6.3}$$

where $\alpha_s \equiv \alpha_s(\mu)$ is the strong coupling constant, and where each of the $\omega_{ab}^{(k)}$ is a function of v, z and, for $k > 0$, of R and p_T/μ (we choose from now on $\mu_r = \mu_f \equiv \mu$). At lowest order we have

$$\omega_{ab}^{(0)}(v, z) \equiv \tilde{\omega}_{ab}^{(0)}(v)\delta(z), \tag{6.4}$$

since the recoiling system is a single massless parton. Hence $z = 0$ sets a threshold for the process to take place, since the transverse momentum of the observed jet always needs to be balanced. At higher orders in perturbation theory, the hard scattering functions contain logarithmic distributions in z, with increasing powers of logarithms as the perturbative order increases. More precisely, one has near the threshold at $z = 0$:

$$\alpha_s^k \omega_{ab}^{(k)} \sim \alpha_s^k \left(\frac{\log^m(z)}{z}\right)_+, \quad \text{with } 0 \leq m \leq 2k-1. \tag{6.5}$$

Here $\int_0^1 dz g(z)[f(z)]_+ \equiv \int_0^1 dz(g(z) - g(0))f(z)$. As one can see, two additional powers of the logarithm arise for every order of perturbation theory. Due to the integration against the parton distribution functions, which are steeply falling functions of momentum fraction, the threshold region $z \to 0$ typically makes significant contributions to the hadronic cross section. This is particularly the case when the kinematic boundary of the hadronic reaction is approached, that is, when $x_T \cosh\eta \to 1$.

As is well known, the large logarithmic corrections arising in the threshold region are associated with the emission of soft or collinear gluons. It is therefore possible to systematically determine the structure of the corrections to all orders and to resum the "towers" of logarithms with $m = 2k-1, 2k-2, \ldots$. This may be used to derive approximate beyond-NLO corrections for hadronic jet production, by expanding the resummed result appropriately to the desired order [227, 239, 240]. To achieve the all-order resummation, one considers Mellin moments in $(1-z)$ of the partonic cross section:

$$\Omega_{ab}(v, N) \equiv \int_0^1 \mathrm{d}z(1-z)^{N-1} \frac{s\mathrm{d}\hat{\sigma}_{ab}}{\mathrm{d}v\mathrm{d}z}. \tag{6.6}$$

In moment space, the resummed hard-scattering function $\Omega_{ab}^{\mathrm{res}}$ can at large N be written as [180, 238]

$$\begin{aligned}\Omega_{ab}^{\mathrm{res}}(v, N) = &\sum_{c,d} \Delta_a(N_a)\, \Delta_b(N_b)\, J_c^{(\mathrm{jet})}(N, R)\, J_d^{(\mathrm{recoil})}(N) \\ &\times \Delta_{ab\to cd}^{(\mathrm{int})}(N, v)\, \Delta_c^{(\mathrm{ng})}(N),\end{aligned} \tag{6.7}$$

where $N_a = vN$, $N_b = (1-v)N$ and the sum runs over the two final-state partons c, d in an underlying $ab \to cd$ subprocess. Here it is assumed that parton c produces the jet (in a way that we shall clarify below), while the recoiling parton d remains unobserved. Each of the terms is also a function of $\alpha_s(\mu)$ and $\log(\mu^2/s)$, which we have not written explicitly. Each of the functions $\Delta_a, \Delta_b, J_c^{(\mathrm{jet})}, J_d^{(\mathrm{recoil})}$ is an exponential. Δ_a, Δ_b resum threshold logarithms arising from soft/collinear radiation off the incoming hard partons. Their expressions are very well known and may be found in the form we need them in, for example, [180]. Likewise, also the expression for gluon radiation off the "unobserved" recoiling parton d is standard and may be found there. Δ_a, Δ_b and $J_d^{(\mathrm{recoil})}$ contain all the leading logarithmic pieces $\propto (\log^3(z)/z)_+, (\log^2(z)/z)_+$ in $\omega_{ab}^{(2)}$.

A crucial point of our study concerns the function $J_c^{(\mathrm{jet})}$ used for the actual jet. As was shown in [238], this function takes different forms depending on whether one assumes the jet to become itself massless at threshold or not. These two forms differ even at leading logarithmic level. For scheme (2) introduced earlier, we have to next-to-leading logarithmic accuracy [238]:

$$\log J_c^{(\mathrm{jet})} = \int_s^{s/\bar{N}^2} \frac{\mathrm{d}q^2}{q^2}\, \alpha_s\left(q^2\right) \left(-\frac{C_c}{2\pi} \log\left(\frac{p_T^2 R^2}{s} \right) \right), \tag{6.8}$$

where $\bar{N} \equiv N\mathrm{e}^{\gamma_E}$ with the Euler constant γ_E, and where C_c denotes the color charge of parton c, $C_q = C_F$ for a quark and $C_g = C_A$ for a gluon. As expected, $J_c^{(\mathrm{jet})}$ is a function of R in this scheme.

The function $\Delta_{ab\to cd}^{(\mathrm{int})}(N, v)$ is obtained as a trace in color space over hard, soft, and anomalous dimension matrices [238]. All details have been given in [239] and need not be repeated here. The function contributes at NLL level and is the only function in the resummed expression that carries explicit dependence on v.

Finally, $\Delta_c^{(\mathrm{ng})}(N)$ in (7.10) contains the contributions from non-global logarithms. These were shown [243, 244] to arise when an observable is sensitive to radiation in only a part of phase space, as is the case for a jet defined by some jet "size" parameter R. Their resummation is highly non-trivial. Non-global logarithms for jet production first enter as a term $\propto [\log(z)/z]_+$ in $\omega_{ab}^{(2)}$. As discussed in [245], the non-global terms arise independently from the boundary of each individual (narrow) "observed" jet.

The appropriate second-order coefficient for our case of a single-inclusive jet cross section may therefore be directly obtained from [243, 245], adjusting the argument of the logarithm properly. We note that these considerations– and in fact the general structure of our resummed cross section– apply to the anti-k_t algorithm [245]. We finally also mention that the non-global component makes a rather small contribution (a few per cent) to our numerical NNLO results presented below. All in all, after performing the

Mellin-inverse to z-space, the two-loop expansion of the product $\Delta^{(\mathrm{int})}_{ab\to cd}(N,v)\,\Delta^{(\mathrm{ng})}_{c}(N)$ in equation (7.10) takes the form

$$\begin{aligned}\left(\frac{\alpha_s}{\pi}\right)^2 \Bigg[&\tilde{\omega}^{(0)}_{ab}(v)\left(\delta(z)+\frac{1}{2}\left(\frac{\alpha_s}{\pi}\right)^2 \mathcal{C}^{(\mathrm{ng})}_{c}\left(\frac{\log(z)}{z}\right)_+\right)\\ &+\frac{\alpha_s}{\pi}\left(\mathcal{T}_{ab\to cd}(v)\delta(z)+\mathcal{G}^{(1)}_{ab\to cd}(v)\left(\frac{1}{z}\right)_+\right)\\ &+\left(\frac{\alpha_s}{\pi}\right)^2 \mathcal{G}^{(2)}_{ab\to cd}(v)\left(\frac{\log(z)}{z}\right)_+\Bigg],\end{aligned} \tag{6.9}$$

with $\mathcal{C}^{(\mathrm{ng})}_{c} = -C_A C_c \pi^2/3$ for the coefficient of the non-global term. The coefficients $\mathcal{G}^{(1)}_{ab\to cd}(v)$ are predicted by the resummation formalism. The coefficients $\mathcal{T}_{ab\to cd}(v)$ may be derived by comparison to the explicit NLO results of [117] in the narrow-jet approximation. Along with the known resummation coefficients, knowledge of the $\mathcal{T}_{ab\to cd}(v)$ is sufficient for determining $\mathcal{G}^{(2)}_{ab\to cd}(v)$ [200, 246]. In this way, combining with the contributions from $\Delta_a, \Delta_b, J^{(\mathrm{jet})}_c, J^{(\mathrm{recoil})}_d$, we obtain full control over the terms $\propto (\log^3(z)/z)_+, (\log^2(z)/z)_+, (\log(z)/z)_+$ in $\omega^{(2)}_{ab}$.

6.3. Phenomenological results and discussion.

— Figure 6.2 shows results for the differential single-inclusive jet cross section at the LHC, at lowest order as well as for the NLO and NNLO threshold terms. Here we use the CTEQ6.6 [**cteq66**] parton distribution functions and scale $\mu = p_T$. The left part of Figure 6.3 displays the corresponding "K-factors", defined as ratios of higher-order cross sections over the leading-order one, while the right part of the figure is for $p\bar{p}$ collisions at Tevatron at $\sqrt{S} = 1.96$ TeV. Results are presented for various jet parameters R. The dotted lines show the NLO results of [117] which were obtained in the NJA for the anti-k_t algorithm. We note that these agree with the NLO ones by the "FastJet" code [242] (as shown in [240]) to better than 3%, even at $R = 0.7$. The dashed lines present the results for the NLO expansion of the threshold terms. It is evident that the latter provide a very faithful description of the full NLO results for much of the p_T ranges relevant at LHC and Tevatron. This holds true for each value of R, thanks to the fact that the threshold logarithms carry R-dependence in our approach, in contrast to that in [239, 240]. Finally, the solid lines display the approximate NNLO results. These show a striking further increase of the jet cross sections as compared to NLO, particularly so at high p_T where the threshold terms are expected to dominate.

Given the large size of the NNLO corrections observed in Fig. 6.3, it is of course crucial to verify that the predicted enhancements are realistic. Fortunately, recently a full NNLO calculation for jet production in the "gluon-only" channel was presented [236,

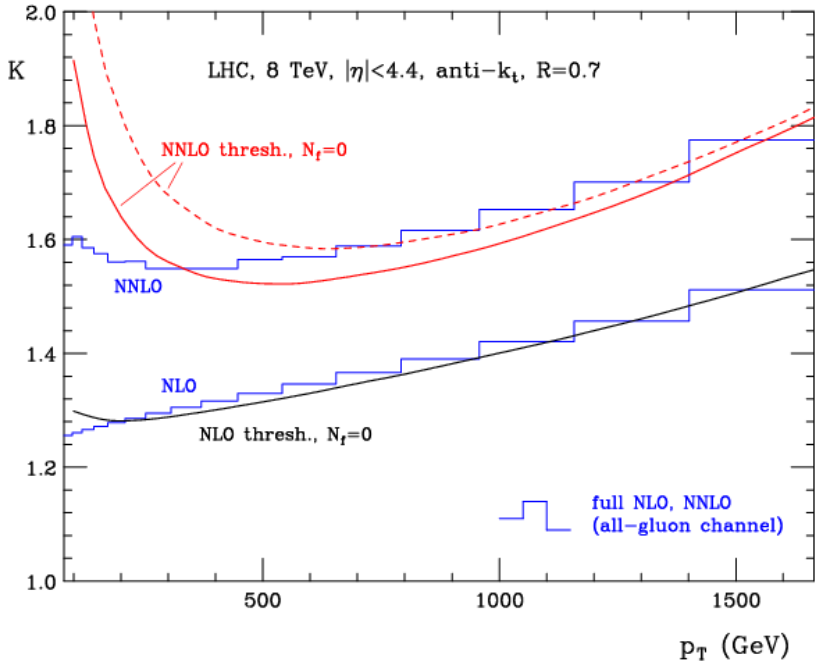

Figure 6.4.: K-factors for jet production in pp-collisions at the LHC at $\sqrt{S} = 8$ TeV in the "gluon-only" channel. The anti-k_t algorithm with $R = 0.7$ was used and the NNLO parton distributions of [32]. The histograms show the results of the recent full NNLO calculation [237] and its NLO counterpart, while the lines display the NLO and NNLO threshold terms.

237], corresponding to gg scattering and to setting the number of flavors $N_f = 0$ in the partonic matrix elements. It is straightforward to compute our threshold terms in this limit. The comparison is shown in Fig. 6.4. One can see that the large enhancement at high p_T predicted by the NNLO threshold terms is very nicely consistent with the full result. Judging from the comparison, the NNLO threshold terms become accurate at about $p_T = 400$ GeV for the chosen rapidity interval. Additional comparisons with the results of [237] show that this value is representative of rapidity intervals that contain the dominant region $\eta \approx 0$. One also finds that at very forward rapidities, $\eta \sim 4$, our results indicate substantial NNLO K-factors of order 5 or so at $p_T \sim 40$ GeV. This again appears to be consistent with the results shown in [237]. In this regime, the coefficients of the threshold logarithms become large, due to "small-x" t-channel gluon exchange contributions. It will be important for future work to address this region in more detail in order to derive reliable predictions for the forward jet cross section at the LHC. Such contributions may also be responsible in part for the rise of the K-factor toward lower p_T. This rise is more pronounced for the NNLO threshold terms, implying that subleading contributions become relevant here. Whether these are related to subleading logarithmic terms, or to terms that vanish at partonic threshold $z = 0$, will need to be studied in more detail. In order to shed light on terms of the latter type, the dashed line in Fig. 6.4 shows the NNLO threshold result found when using a different angular variable, $v' \equiv 1 + t/s = z + v(1 - z)$, in equation (6.1). Clearly, $v' = v + \mathcal{O}(z)$. The difference between the two NNLO threshold results indicates a typical uncertainty of the prediction obtained from threshold resummation.

Chapter 7.

Approximate NNLO Corrections to Longitudinally Polarized Hadronic Jet Production

7.1. Introduction

The production of high p_T single inclusive jets in longitudinally polarized proton beams opens various possibilities to answer interesting questions in spin physics and opens up an unique possibility to explore the spin structure of the nucleon [247]. Since the first successful runs of the Relativistic Heavy Ion Collider at the Brookhaven National Laboratories (BNL-RHIC) many interesting experimental results [248–251] were published. Also on the theory side significant progress has been achieved over the last decade. For reliable QCD predictions analytical calculations up to next-to-leading-order (NLO) are crucial and became available for different jet clustering algorithms [116, 252].

A main goal for the RHIC spin program was to access the gluon helicity distribution of the proton $\Delta g(x)$. It is a fundamental quantity that characterizes the inner spin structure of the nucleon. Its integral over all momentum fractions $\Delta G = \int_0^1 \mathrm{d}x\ \Delta g(x)$ may be interpreted as the gluon spin contribution to the proton spin. Therefore, ΔG contributes to the proton helicity sum rule

$$\frac{1}{2} = \frac{1}{2}\Delta\Sigma + \Delta G + L_q + L_g\ , \tag{7.1}$$

where L_q and L_g are the quark and gluon orbital angular momentum contributions and $\Delta\Sigma$ the quark and antiquark spin contributions. In particular, the quark and gluon helicity distributions are accessible in highly inelastic processes with polarized nucleons involved. Since the late 80's several experiments on polarized deep inelastic scattering showed that the quark contributions to the nucleons spin is relatively little $\Delta\Sigma \sim 0.25$

[247, 253]. Unfortunately, the sensitivity to Δg is very poor to lepton induced processes. Therefore, it was not possible to give good estimations for the gluon polarization from lepton hadron scattering experiments. A better probe for Δg are processes where all initial state particles in the hard part are color charged. That results in more gluon induced processes and therefore to a better sensitivity to their polarization. Besides the inclusive pion production data from BNL-RHIC [254–256] jet data [250, 251] are the important input for helicity dependent global PDF fits [133, 253, 257]. Recent DSSV analysis [133], including the 2009 RHIC jet data [250] lead to a non vanishing gluon polarization Δg of the nucleon. The analysis imply a polarization of gluons in the intermediate momentum scales accessible at RHIC. So far, the NLO predictions [116, 252] for inclusive single jet production, seem to be in good accordance with the experimental results for the asymmetry.

To this day, pQCD calculations for high p_T jet production in longitudinally polarized pp scattering are limited to NLO. For the unpolarized process approximate NNLO results are available [1, 239–241] and in the gluon only channel even the full NNLO result exists [236, 237]. Recently, an unpolarized full NNLO calculation for the leading color contribution has been published [258]. The approximate results mentioned above rely on the fact that the QCD perturbation series contains classes of logarithms, that dominate in certain regions of the phase space. Well known resummation techniques in QCD allow to determine the all order structure of these logarithms. Therefore, we can predict the dominant logarithms at threshold that arise at NNLO level. The logarithms arise near a partonic threshold where all the available energy is inside the observed jet and the recoiling one. In particular, the threshold is set for a vanishing invariant mass of the recoiling unobserved partonic system $s_4 \to 0$. At kth order in perturbation series logarithms of the form $\alpha_s^k \left[\log^m(z)/z\right]_+$ arise, where $z = s_4/s$ with $\sqrt{s}$ the initial state partonic center of mass energy and $0 \leq m \leq 2k-1$.

By using the resummed result to next-to-leading logarithm (NLL) it is possible to predict logarithms with, $m = 2k-1, 2k-2, 2k-3$. However, a resummed study in unpolarized scattering is only available for the rapidity integrated cross section [227]. For rapidity dependent cross sections, the resummation formalism complicates considerably. Therefore, studies that are differential in the rapidity of the observed jet are limited to fixed order expansions. In particular, we mention [1] (and chapter (6) in this thesis) where the observed jet produce beneath the rapidity, the correct jet size parameter R dependency. In this chapter we will derive approximate NNLO result for $\vec{p}\vec{p} \to \text{jet}X$ following closely the strategy of [1]. We determine the three leading logarithmic contributions $\propto (\log^3(z)/z)_+$,$(\log^2(z)/z)_+$, $(\log(z)/z)_+$ at NNLO and predict the spin asymmetry. The last contribution is possible to obtain, by matching analytically to existing NLO results [252]. Our results are obtained in the so called narrow jet approximation [116, 117], where only small jet size parameters R are considered. It has been showed, that this approximations hold up to relatively large jet size parameters $R \sim 0.7$.

7.2. Theoretical framework

The factorized cross section for high transverse momentum p_T single inclusive jet production with pseudorapidity η is given by

$$\begin{aligned}\frac{\mathrm{d}^2\Delta\sigma}{\mathrm{d}p_T\mathrm{d}\eta} &= \frac{1}{2}\left[\frac{\mathrm{d}\sigma^{++}}{\mathrm{d}p_T\,\mathrm{d}\eta} - \frac{\mathrm{d}\sigma^{+-}}{\mathrm{d}p_T\,\mathrm{d}\eta}\right] \\ &= \frac{2}{p_T}\sum_{ab}\int_0^{V(1-W)}\mathrm{d}z\int_{\frac{VW}{1-z}}^{1-\frac{1-V}{1-z}}\mathrm{d}v\, x_a\Delta f_a(x_a,\mu_f)\, x_b\Delta f_b(x_b,\mu_f) \\ &\quad\times\frac{\mathrm{d}\Delta\hat{\sigma}_{ab}}{\mathrm{d}v\mathrm{d}z}(v,z,p_T,\mu_r,\mu_f,R),\end{aligned} \tag{7.2}$$

where $V = 1 - x_T\mathrm{e}^{-\eta}/2$, $VW = x_T\mathrm{e}^{\eta}/2$, with $x_T = 2p_T/\sqrt{S}$ and the hadronic center-of-mass energy $\sqrt{S}$. The superscripts in the first equality denotes the helicities of the colliding polarized protons and $\Delta f_{a,b}$ denotes the polarized parton distribution functions evaluated at factorization scale μ_f and momentum fractions $x_a = VW/v(1-z)$ and $x_b = (1-V)/(1-v)(1-z)$. The sum in the second equality is over all contributing partonic processes $a + b \to \mathrm{jet} + X$ with their helicity dependent partonic cross section

$$\frac{\mathrm{d}\Delta\hat{\sigma}_{ab}}{\mathrm{d}v\mathrm{d}z} = \frac{1}{2}\left[\frac{\mathrm{d}\hat{\sigma}^{++}}{\mathrm{d}v\;\mathrm{d}z} - \frac{\mathrm{d}\hat{\sigma}^{+-}}{\mathrm{d}v\,\mathrm{d}z}\right]\,, \tag{7.3}$$

where the superscripts refer now to the partonic helicities. The polarized partonic cross sections are functions of the renormalization and factorization scales as well as the transverse momentum of the jet and two kinematical variables

$$v = \frac{u}{t+u}, \qquad z = \frac{s_4}{s}, \tag{7.4}$$

where $s = x_a x_b S$ is the partonic center-of-mass energy squared, $t = (p_a - p_J)^2$, $u = (p_b - p_J)^2$ and s_4 is the invariant mass squared of the "unobserved" partonic system recoiling against the jet. $p_{a,b}$ and p_J are the four momenta of the initial state partons a, b or the jet respectively. We mention, as indicated in (7.2) the partonic function is also dependent on the "jet size parameter" R, which is a measurement of the "size" of the jet which is defined by the jet algorithm. We mention that for our study we define the observed jet in the anti-k_t algorithm [121].

The partonic hard scattering may be calculated order by order in terms of the strong coupling α_s in QCD perturbation theory

$$\frac{s\mathrm{d}\Delta\hat{\sigma}_{ab}}{\mathrm{d}v\;\mathrm{d}z} = \left(\frac{\alpha_s}{\pi}\right)^2\left[\Delta\omega_{ab}^{(0)} + \frac{\alpha_s}{\pi}\Delta\omega_{ab}^{(1)} + \left(\frac{\alpha_s}{\pi}\right)^2\Delta\omega_{ab}^{(2)} + \mathcal{O}(\alpha_s^3)\right], \tag{7.5}$$

where $\Delta\omega_{ab}^{(k)} \equiv \Delta\omega_{ab}^{(k)}(s, v, z, p_T/\mu, R)$. We choose the renormalization scale and the factorization scale at equal values $\mu \equiv \mu_R = \mu_f$.

At leading order in perturbation theory the unobserved final state consists of only one massles parton. Therefore, we have

$$\Delta\omega_{ab}^{(0)}(v, z) \equiv \Delta\tilde{\omega}_{ab}^{(0)}(v)\delta(z). \tag{7.6}$$

It is important to mention, that $z = 0$ sets a threshold for the process to take place. The threshold phase space area is the origin of large logarithmic enhancements in our cross section. They arise as a finite remnant of the pole cancellation from soft or collinear parton configurations and are the dominant contributions in the threshold region. More precisely, the threshold terms have the following form

$$\alpha_s^k \Delta\omega_{ab}^{(k)} \sim \alpha_s^k \left(\frac{\log^m(z)}{z}\right)_+, \quad \text{with } 0 \leq m \leq 2k-1, \tag{7.7}$$

where we define the plus distribution as

$$\int_0^1 dz g(z)[f(z)]_+ \equiv \int_0^1 dz (g(z) - g(0)) f(z)\ . \tag{7.8}$$

As we mention before, the origin of these logarithmic enhancements rely in soft and/or collinear gluon emission diagrams. Resummation techniques [39, 40] predict the structure of these logarithms to all order in QCD perturbation theory. The knowledge of "towers" of logarithms with $m = 2k-1, 2k-2, \ldots$ allows us to determine the dominant threshold contributions at NNLO by expanding the resummed result to order α_s^3. There are various studies for unpolarized scattering that follow this strategy to determine NNLO corrections [1, 227, 239, 240].

Threshold resummation is achieved by transforming the hard scattering part by the mellin transformation in terms of the threshold variable z into its N-moments

$$\Delta\Omega_{ab}(v, N) \equiv \int_0^1 \mathrm{d}z (1-z)^{N-1} \frac{s \mathrm{d}\Delta\hat{\sigma}_{ab}}{\mathrm{d}v \mathrm{d}z}. \tag{7.9}$$

Threshold resummation in longitudinally polarized scattering, follows closely the strategy for the spin averaged case [1]. This is due to the fact that soft gluon emission is spin independent [259]. Therefore, we can write the resummed cross section as

$$\Delta\Omega_{ab}^{\rm res}(v,N,\alpha_s(\mu^2),\mu^2/s) =$$

$$\sum_{c,d}\mathcal{D}_a(N_a,\alpha_s(\mu^2),\mu^2/s)\,\mathcal{D}_b(N_b,\alpha_s(\mu^2),\mu^2/s)\,J_c^{(\rm jet)}(N,R,\alpha_s(\mu^2),\mu^2/s)$$
$$\times J_d^{(\rm recoil)}(N,\alpha_s(\mu^2),\mu^2/s)\Delta\mathcal{D}_{ab\to cd}^{(\rm int)}(N,v)\,\mathcal{D}_c^{(\rm ng)}(N), \tag{7.10}$$

where $N_a = vN$, $N_b = (1-v)N$ and the sum runs over the two final-state partons c,d in an underlying $ab\to cd$ subprocess where the observed jet is formed by parton c. The functions $\mathcal{D}_a$, $\mathcal{D}_b$, $J_d^{(\rm recoil)}$ and $J_c^{(\rm jet)}$ are exponentials well known from the spin averaged case [1]. Δ_a,Δ_b resum threshold logarithms arising from soft/collinear radiation off the incoming hard partons. Their expressions are very well known and may be found in the form we need them in, for example, [180]. Likewise, also the expression for gluon radiation off the "unobserved" recoiling parton d is standard and may be found there. Δ_a,Δ_b and $J_d^{(\rm recoil)}$ contain all the leading logarithmic pieces $\propto(\log^3(z)/z)_+,(\log^2(z)/z)_+$ in $\omega_{ab}^{(2)}$.

As was pointed out in [1] it is important to assume a massive jet at partonic threshold. For NLL accuracy we have for the observed jet

$$\log J_c^{(\rm jet)} = \int_s^{s/\bar N^2}\frac{{\rm d}q^2}{q^2}\,\alpha_s\left(q^2\right)\left(-\frac{C_c}{2\pi}\log\left(\frac{p_T^2R^2}{s}\right)\right), \tag{7.11}$$

where $\bar N\equiv N{\rm e}^{\gamma_E}$ with the Euler constant γ_E, and where C_c denotes the color charge of parton c, $C_q=C_F$ for a quark and $C_g=C_A$ for a gluon. The assumption that the jet is massive at threshold, is responsible for the R dependence in $J_c^{(\rm jet)}$.

The function $D_{ab\to cd}^{(\rm int)}(N,v)$ is obtained as a trace in color space over hard, soft, and anomalous dimension matrices [238].

$$D_{ab\to cd}^{(\rm int)}(N,v) = {\rm Tr}\Bigg[\Delta H(\alpha_s(\mu^2),v)\;\overline{\rm P}\exp\left\{\int_{p_T}^{p_T/N}\frac{{\rm d}\mu'}{\mu'}\Gamma^\dagger(\alpha_s(\mu'),v)\right\}$$
$$S(\alpha_s(p_T^2/N^2),v)\;{\rm P}\exp\left\{\int_{p_T}^{p_T/N}\frac{{\rm d}\mu'}{\mu'}\Gamma(\alpha_s(\mu'),v)\right\}\Bigg] \tag{7.12}$$

where the helicity dependence in $D_{ab\to cd}^{(\rm int)}(N,v)$ is given by the hard matrix $\Delta H(\alpha_s(\mu^2),v)$ that contains all the contributions associated with momenta of the order of the hard scale p_T. At NLL the hard matrices are needed to zeroth order in QCD perturbation theory and are given in [259]. The evolution between the hard scale of ΔH and the scale of the soft matrix $S(\alpha_s(p_T^2/N^2),v)$ is given by the soft anomalous dimension matrix $\Gamma(\alpha_s(\mu'))$ which is obtained by vertex corrections to eikonal diagrams. Therefore,

it is spin independent like the soft matrix itself.

Finally, $\Delta_c^{(\mathrm{ng})}(N)$ in (7.10) contains the contributions from non-global logarithms. These were shown [243, 244] to arise when an observable is sensitive to radiation in only a part of phase space, as is the case for a jet defined by some jet "size" parameter R. Since they arise at the boundaries of our final state jet definition, these logarithms are independent of the initial state partons spin. Their resummation is highly non-trivial. Non-global logarithms for jet production first enter as a term $\propto [\log(z)/z]_+$ in $\Delta\omega_{ab}^{(2)}$. As discussed in [245], the non-global terms arise independently from the boundary of each individual (narrow) "observed" jet. The appropriate second-order coefficient for our case of a single-inclusive jet cross section may therefore be directly obtained from [243, 245], adjusting the argument of the logarithm properly. We note that these considerations– and in fact the general structure of our resummed cross section– apply to the anti-k_t algorithm [245]. We finally also mention that the non-global component makes a rather small contribution (a few percent) to our numerical NNLO results presented below. All in all, after performing the Mellin-inverse to z-space, the two-loop expansion of the product $\Delta_{ab\to cd}^{(\mathrm{int})}(N,v)\,\Delta_c^{(\mathrm{ng})}(N)$ in equation (7.10) takes the form

$$\begin{aligned}\left(\frac{\alpha_s}{\pi}\right)^2 \Bigg[& \Delta\tilde{\omega}_{ab}^{(0)}(v)\left(\delta(z)+\frac{1}{2}\left(\frac{\alpha_s}{\pi}\right)^2 \mathcal{C}_c^{(\mathrm{ng})}\left(\frac{\log(z)}{z}\right)_+\right) \\ & + \frac{\alpha_s}{\pi}\left(\Delta\mathcal{T}_{ab\to cd}(v)\delta(z)+\Delta\mathcal{G}_{ab\to cd}^{(1)}(v)\left(\frac{1}{z}\right)_+\right) \\ & + \left(\frac{\alpha_s}{\pi}\right)^2 \Delta\mathcal{G}_{ab\to cd}^{(2)}(v)\left(\frac{\log(z)}{z}\right)_+\Bigg], \end{aligned} \tag{7.13}$$

with $\mathcal{C}_c^{(\mathrm{ng})} = -C_A C_c \pi^2/3$ for the coefficient of the non-global term. The coefficients $\Delta\mathcal{G}_{ab\to cd}^{(1)}(v)$ are predicted by the resummation formalism. The coefficients $\Delta\mathcal{T}_{ab\to cd}(v)$ may be derived by comparison to the explicit NLO results of [252] in the narrow-jet approximation. Along with the known resummation coefficients, knowledge of the $\Delta\mathcal{T}_{ab\to cd}(v)$ is sufficient for determining $\Delta\mathcal{G}_{ab\to cd}^{(2)}(v)$ [200, 246]. In this way, combining with the contributions from $\mathcal{D}_a$, $\mathcal{D}_b$, $J_d^{(\mathrm{recoil})}$ and $J_c^{(\mathrm{jet})}$, we obtain full control over the terms $\propto (\log^3(z)/z)_+$, $(\log^2(z)/z)_+$, $(\log(z)/z)_+$ in $\Delta\omega_{ab}^{(2)}$.

7.3. Phenomenological results and discussion

Figure (7.1) shows results for the differential polarized single jet inclusive cross sections at different perturbative orders. The dotted blue line is the full nlo prediction [117] within the small cone approximation compared to the threshold predictions for NLO (green dash dotted)- and NNLO (red dashed) lines. Here we use the DSSV-14 helicity dependent parton distribution from [133].

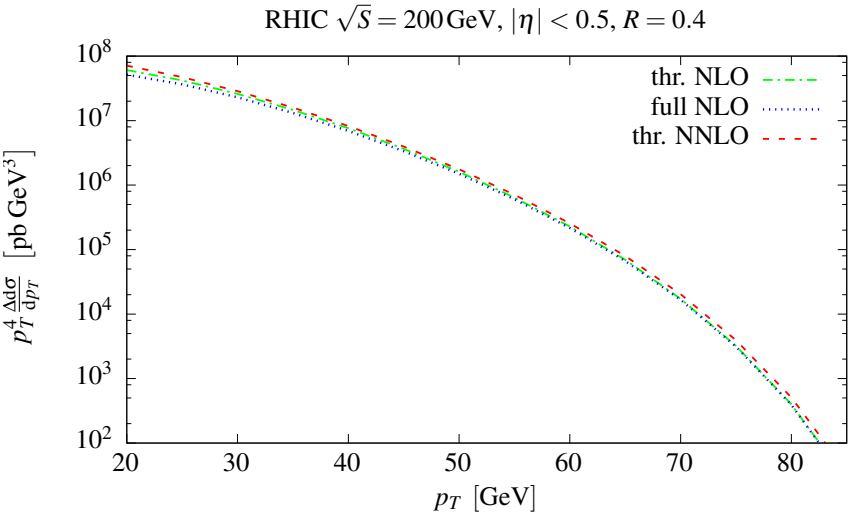

Figure 7.1.: Differential cross section for jet production in longitudinally polarized pp collisions at RHIC with center of mass energy $\sqrt{S} = 200$ GeV using the anti-k_t algorithm with $R = 0.4$.

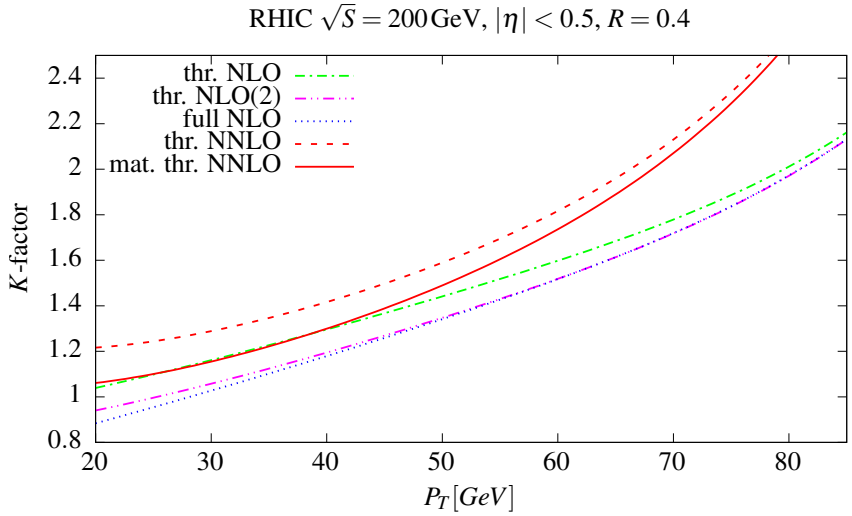

Figure 7.2.: K-factors at mid rapidity $|\eta| < 0.5$ for jet production in longitudinally polarized pp collisions at RHIC at $\sqrt{S} = 200$ GeV using the anti-k_t algorithm with $R = 0.4$.

Figure (7.2) displays K-factors, defined as the higher-order cross sections normalized by the leading-order one at RHIC. Results are presented for various cross sections

taking different parts of the perturbative order into account. The blue dotted line shows the full NLO result within the small cone approximation of [117]. This "full" result sets a benchmark for our approximate NLO results where we can verify the quality of our calculation. First we compare the "normal" threshold expansion (green dashed dotted line) with the full result. Here, "normal" means an one loop expansion of equation (7.10). Unfortunately, the threshold expansion for polarized scattering fits much poorer to the full result than in the unpolarized case (compare to figure (6.3)). For reliable QCD predictions at threshold it is not sufficient taking only the NLL-threshold logs into account. We can clearly identify terms $\propto \log(z)$ as an important contribution to the NLO cross section in this area of phase space. Unlike in unpolarized scattering these subleading terms are important at surprisingly large p_T, where they should be supressed by $\sim 1/N$. This behavior is supported by the fact that in some quark induced channels the polarized partonic function has sign changes. The magenta dashed dotted line, includes besides the threshold NLO prediction, the subleading $\log(z)$ contributions. This can be achieved by adding the terms $\sim \log(z)$ from the fixed order calculation [117], to the one loop expansion of the resummed result. We will call this prediction threshold NLO(2). We observe a very nice behavior of the NLO(2) calculation in a sence that we describe fairly well the full NLO result.

The full all order description of these subleading terms is highly non-trivial and we leave that for future research. In the present work, we achieve a proper treatment of these terms at least at NLO level, by matching numerically our threshold NNLO prediction (red dashed line) to the full NLO result

$$\Delta \mathrm{d}\sigma\Big|^{\mathrm{NNLO}}_{\mathrm{match.}} = \Delta \mathrm{d}\sigma\Big|^{\mathrm{NNLO}}_{\mathrm{thresh.}} - \Delta \mathrm{d}\sigma\Big|^{\mathrm{NLO}}_{\mathrm{thresh.}} + \Delta \mathrm{d}\sigma\Big|^{\mathrm{NLO}}_{\mathrm{full}} \,. \tag{7.14}$$

We present our final polarized matched threshold NNLO result as the red solid line. It shows a striking further increase of the jet cross sections as compared to NLO, particularly so at high p_T where the threshold terms are expected to dominate.

Figure (7.3) shows a comparison of the RHIC 2009 run STAR data with our calculation. We show the high p_T and central rapidity region where our approximate results give credible predictions for the double spin asymmetry

$$A_{LL} = \frac{\Delta \mathrm{d}\sigma/\mathrm{d}p_T}{\mathrm{d}\sigma/\mathrm{d}p_T} \,. \tag{7.15}$$

The denominator is calculated by using the results of [1] in conjunction with the MSTW unpolarized parton distributions of [32], where we also adopt the strong coupling for all our results including the polarized predictions. The matched NNLO result gives a further reduction of the double spin asymmetry compared to NLO. The difference between NLO and threshold NNLO increases for increasing p_T. In this large p_T region the subleading $\log(z)$ contributions vanish and the asymmetry is mainly dominated by threshold logarithms. If we compare to the high p_T tail of the STAR data, it is

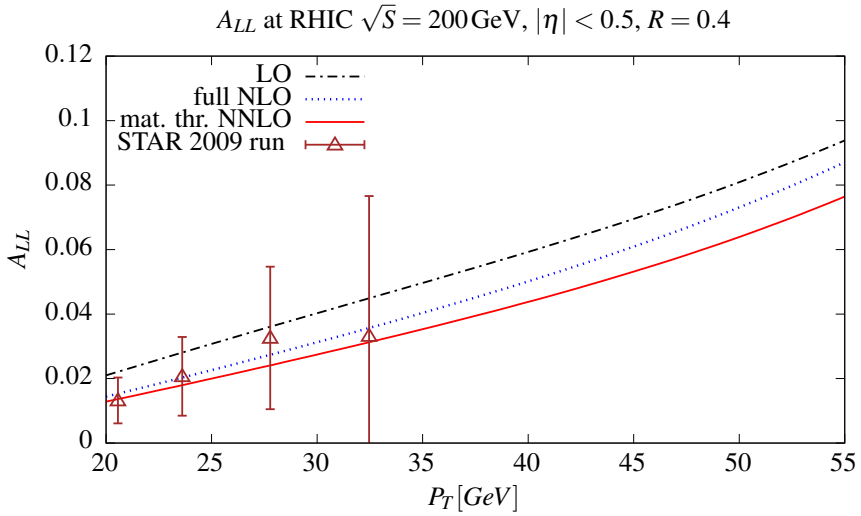

Figure 7.3.: A_{LL} at mid rapidity $|\eta| < 0.5$ for jet production in longitudinally polarized pp collisions at RHIC at $\sqrt{S} = 200$ GeV using the anti-k_t algorithm with $R = 0.4$. The 2009 STAR data is taken from [251].

still in a very well accordance with our new NNLO prediction. We mention that in further studies an implementation of $\log(z)$ terms at NNLO level is inevitable to get more precise results that can be the next step in terms of accuracy in the protons spin puzzle. The main goal of the present study is to determine a first approximation of the next order. An interesting result is that in the very high p_T region where our results should match very closely to the full result, the contribution to the asymmetry from NNLO seems of the order of NLO and even above. Therefore, data at larger p_T would be very interesting to compare with our results. In this threshold region NNLO or a proper all order treatment of the threshold logarithms seems to be unavoidable for reliable pQCD predictions. We mention that there is an other contribution that can effect this phase space area we have not include so far. An inclusion of the resummation of logarithms getting large with small R give rise to an additional maybe important contribution [260].

7.4. Conclusions

We have presented approximate higher order predictions for single-inclusive jet production in polarized hadronic scattering. Our results are a first step towards new accuracies in spin physics. We showed that formal subleading terms give significant contributions to the NLO cross section, even at relatively large p_T. By matching to the full NLO result, we can determine the general behavior and effects of the NNLO correction at

large p_t.

In future studies, we are going to investigate the all order treatment of terms of the type $\log(z)$ and how they can be determined at NNLO accuracy. As we have shown, these formally subleading terms give relevant contributions to the spin dependent analysis.

Appendix A.

NLO Coefficients for $lN \to hx$

Here we present the NLO coefficients defined in equations (2.23), (2.24), (2.25) for the different channels:

$q \to q$ **channel:**

$$
\begin{aligned}
A_0^{q\to q} &= \frac{1+v^2}{(1-v)^2}\left((3+2\ln(v))\ln\left(\frac{s(1-v)}{\mu^2}\right)+\ln^2(v)-8\right),\\
A_1^{q\to q} &= 8w\frac{1+v^2}{(1-v)^2},\\
B_1^{q\to q} &= 4w\frac{1-v(1-w)+v^2(1-w(1-w))}{(1-v)^2},\\
B_2^{q\to q} &= \frac{2w}{(1-v)^2(1-v(1-w))}\times\\
&\quad\Big[\big(1-2v(1-w)+v^2(1-2w+2w^2)\big)\times\\
&\quad\big(2-2v(1-w)+v^2(1-w)^2\big)\Big],\\
B_3^{q\to q} &= 4w\frac{1+v^2}{(1-v)^2}.
\end{aligned}
\tag{A.1}
$$

$$
\begin{aligned}
C_1^{q\to q} = \frac{1}{(1-v)^2(1-vw)(1-v(1-w))}\Big[&2-w-2v(1+4w)\\
&+v^2(2+9w-10w^2+w^3)-2v^3(1-w+w^2-4w^3)\\
&+v^4w(2-2w-7w^2+8w^3)
\end{aligned}
$$

$$
\begin{aligned}
&\quad -2v^5w^2(1-3w+4w^2-2w^3)\Big],\\
C_2^{q\to q} &= \frac{2(1+v^2(1+2w^2))}{(1-v)^2},\\
C_3^{q\to q} &= \frac{-2vw(3-2v(1-w)+v^2(1-2w+2w^2))}{(1-v)^2},\\
C_4^{q\to q} &= \frac{1}{(1-v)^2(1-vw)(1-v(1-w))}\Big[2-w-2v(1+2w)\\
&\quad +v^2(2+5w-6w^2+w^3)-2v^3(1-w+w^2-2w^3)\\
&\quad +v^4w(2-2w-3w^2+4w^3)\\
&\quad -2v^5w^2(1-3w+4w^2-2w^3)\Big],\\
C_5^{q\to q} &= \frac{1}{(1-v)^2(1-vw)(1-v(1-w))}\Big[2-w-2v(2-w)\\
&\quad +v^2(4-w-2w^2+w^3)-2v^3+v^4w(2-w^2)\\
&\quad -2v^5w^2(1-2w+2w^2-w^3)\Big].
\end{aligned}
\tag{A.2}
$$

$q \to g$ **channel:**

$$
\begin{aligned}
C_1^{q\to g} &= \frac{2vw(1+v^2(1-w)^2)}{(1-v)^2(1-v(1-w))^2}\\
&\quad \times(1-2v(1-w)+v^2(1-2w(1-w))),\\
C_2^{q\to g} &= \frac{vw(6-4vw+2v^2(1-2w(1-w)))}{(1-v)^2},\\
C_3^{q\to g} &= \frac{vw}{(1-v)^2(1-vw)^2(1-v(1-w))^2}\Big[3-2v(3+w)\\
&\quad +v^2(6+4w-w^2)-2v^3(3-3w+5w^2-2w^3)\\
&\quad +v^4(3-4w+5w^2-2w^3)\\
&\quad -2v^5w(2-6w+9w^2-7w^3+2w^4)\\
&\quad +2v^6(1-w)^2w^2(1-2w+2w^2)\Big],\\
C_4^{q\to g} &= \frac{vw}{(1-v)^2(1-vw)^2(1-v(1-w))^2}\Big[2-2v(5-3w)\\
&\quad +v^2(16-3w-11w^2)-v^3(10+15w-27w^2+2w^3)\\
&\quad +v^4(2+17w-23w^2+7w^3-3w^4)\\
&\quad -v^5w(5-5w-w^2+3w^3-2w^4)
\end{aligned}
$$

$$+2v^6(1-w)^2w^2(1-w+w^2)\Big]. \tag{A.3}$$

$g \to q$ channel:

$$\begin{aligned}
C_1^{g\to q} &= \frac{2(1+v(4vw^2-2w(1+v)+v))}{(1-v)^2},\\
C_2^{g\to q} &= \frac{1}{(1-v)^2(1-vw)^2}\Big[2(1-w+w^2)\\
&\quad -2vw(3-2w+2w^2)\\
&\quad +v^2(2-4w+11w^2-2w^3+2w^4)\\
&\quad -4v^3w(1-2w+3w^2)+3v^4w^2(1-2w+2w^2)\Big],\\
C_3^{g\to q} &= \frac{1}{(1-v)^2(1-vw)^2}\Big[1+4w-6w^2\\
&\quad -2v(1+3w+w^2-6w^3)+\\
&\quad v^2(1+9w+4w^2-8w^3-6w^4)\\
&\quad -v^3w(3+9w-4w^2-6w^3)\\
&\quad +v^4w^2(1+4w-4w^2)\Big].
\end{aligned} \tag{A.4}$$

Appendix B.

NLO Coefficients for Longitudinally Polarized $\vec{l}\vec{N} \to hX$

Here we present the NLO coefficients defined in equations (3.11), (3.13), (3.14) for the different channels:

$q \to q$ **channel:**

$$\Delta A_0^{q\to q} = \frac{1+v}{1-v}\left((3+2\ln(v))\ln\left(\frac{s(1-v)}{\mu^2}\right)+\ln^2(v)-8\right),$$

$$\Delta A_1^{q\to q} = 8w\frac{1-v(1-2w)}{1-v},$$

$$\Delta B_1^{q\to q} = 4w\frac{1+vw}{1-v},$$

$$\Delta B_2^{q\to q} = 4w\frac{1-v(1-2w)}{1-v},$$

$$\Delta B_3^{q\to q} = 4w\frac{1-v(1-2w)}{1-v},$$

$$\Delta C_1^{q\to q} = \frac{1}{(1-v)(1-v(1-w))}\Big[2-w+vw(9-w) \\ -v^2(2+2w-3w^2)-2v^3w(1-3w+2w^2)\Big],$$

$$\Delta C_2^{q\to q} = \frac{2(1+v)}{1-v},$$

$$\Delta C_3^{q\to q} = \frac{-2vw(1-v(1-2w))}{1-v},$$

$$
\begin{aligned}
\Delta C_4^{q\to q} &= \frac{2v^2 w(1-w)(1-v(1-2w))}{(1-v)(1-v(1-w))},\\
\Delta C_5^{q\to q} &= \frac{1}{(1-v)(1-v(1-w))}\Big[2-w+vw(5-w)\\
&\qquad -v^2(2-2w+w^2)-2v^3w(1-3w+2w^2)\Big],\\
\Delta C_6^{q\to q} &= \frac{(1-v)(1-w)(1+vw)}{1-v(1-w)}.
\end{aligned}
\tag{B.1}
$$

$q \to g$ channel:

$$
\begin{aligned}
\Delta C_1^{q\to g} &= \frac{2vw(1-v(1-2w))(1+v^2(1-w)^2)}{(1-v)(1-v(1-w))^2},\\
\Delta C_2^{q\to g} &= \frac{-2vw(1+v(1-2w))}{1-v},\\
\Delta C_3^{q\to g} &= \frac{vw}{(1-v)(1-vw)^2(1-v(1-w))^2}\Big[1-v(1-2w)\\
&\qquad +v^2(1-2w-3w^2)-v^3(1-7w^2+4w^3)\\
&\qquad +2v^4w(2-7w+7w^2-2w^3)\\
&\qquad -2v^5w^2(1-w)^2(1-2w)\Big],\\
\Delta C_4^{q\to g} &= \frac{vw}{(1-v)(1-vw)^2(1-v(1-w))^2}\Big[2-4v\\
&\qquad +v^2(4-13w+12w^2)-v^3(2-14w+13w^2)\\
&\qquad -v^4w(3-4w+3w^2-2w^3)+v^5w^2(1-w)^2\Big].
\end{aligned}
\tag{B.2}
$$

$g \to q$ channel:

$$
\begin{aligned}
\Delta C_1^{g\to q} &= \frac{-2(1+v(1-2w))}{1-v},\\
\Delta C_2^{g\to q} &= \frac{-1}{(1-v)(1-vw)^2}\Big[2-2w+2v(1-4w+2w^2)\\
&\qquad -v^2w(4-11w+2w^2)+3v^3w^2(1-2w)\Big],
\end{aligned}
$$

$$\Delta C_3^{g\to q} = \frac{1}{(1-v)(1-vw)^2}\Big[2(1-w)+2v(2-5w+2w^2) \\ -v^2w(7-12w+2w^2)+v^3w^2(7-8w)\Big]. \tag{B.3}$$

R-dependent coefficients for jet production:

$$\begin{aligned} A_0^{\text{jet}} &= \left(\frac{3}{2}+2\ln(v)\right)\ln\left(\frac{v(1-v)s}{\mu^2}R^2\right)+2\ln^2(v)-\frac{13}{2}+\frac{2}{3}\pi^2, \\ A_1^{\text{jet}} &= 4w, \\ B_1^{\text{jet}} &= 2w\,\ln\left(\frac{wv^3(1-v)s}{\mu^2}R^2\right), \\ C_1^{\text{jet}} &= \frac{vw}{1-v(1-w)}\times \\ &\quad \left[\frac{1+v(1-w)}{1-v(1-w)}\ln\left(\frac{w(1-w)^2v^3(1-v)s}{\mu^2}R^2\right)+1\right]. \end{aligned} \tag{B.4}$$

The explicit form of the coefficient A_0^{jet} depends on the jet algorithm. The coefficient A_0^{jet} in (B.4) is given for an anti-k_T algorithm [117].

Appendix C.

3-Particle Phase Space for Single Inclusive Kinematics

We adapt the notation from [261] for the $2 \to 3$ process

$$p_1 + p_2 \to p_3 + p_4 + k \tag{C.1}$$

where p_1 is the momentum of the observed particle. The three particle phase space is given by

$$\begin{aligned}(PS)_3 = \int \frac{\mathrm{d}^n p_3}{(2\pi)^{n-1}} \int \frac{\mathrm{d}^n p_4}{(2\pi)^{n-1}} \int \frac{\mathrm{d}^n k}{(2\pi)^{n-1}} (2\pi)^n \delta^n(p_1 + p_2 - p_3 - p_4 - k) \\ \times \delta(p_3^2)\, \delta(p_4^2)\, \delta(k^2)\end{aligned} \tag{C.2}$$

We decompose the phase space integral in two Lorentz invariant parts

$$\begin{aligned}(PS)_3 = \int \frac{1}{(2\pi)^{5-4\varepsilon}} \mathrm{d}s_2\, \mathrm{d}^n p_3\, \mathrm{d}^n p_{4k}\, \delta(p_3^2)\delta(p_{4k}^2 - s_2)\delta^n(p_1 + p_2 - p_3 - p_{4k}) \\ \times \mathrm{d}^n k\, \mathrm{d}^n p_4\, \delta(k^2)\delta(p_4^2)\delta^n(p_{4k} - p_4 - k)\ .\end{aligned} \tag{C.3}$$

The advantage of the decomposition above relies in the fact that we can evaluate the first and the second line independently in any frame. We start with the second line.

$$\begin{aligned}&\int \mathrm{d}^n k\, \mathrm{d}^n p_4\, \delta(k^2)\delta(p_4^2)\delta^n(p_{4k} - p_4 - k) \\ &\quad = \int \mathrm{d}^n k\, \delta(k^2)\delta((p_{4k} - k)^2) \\ &\quad = \int \mathrm{d}E_k\, \mathrm{d}^2 k_{||}\, \mathrm{d}^{n-3} k_\perp \delta(E_k^2 - k_{||}^2 - k_\perp^2)\delta((p_{4k} - k)^2)\end{aligned} \tag{C.4}$$

where in the first line we use the momentum conservation delta function and in the second line we decompose the unobserved momentum k into its longitudinal and perpendicular components. The simple structure of the delta function $\delta((p_{4k}-k)^2)$ is the reason why we decompose the phase space like in equation (C.3). Therefore, in equation (C.3) we are free to choose the rest frame of k and p_4. Then, the delta function is independent of the angles θ_1 and θ_2.

We can further decompose

$$\mathrm{d}^{n-3}k_\perp = \mathrm{d}k_\perp^2 \ (k_\perp^2)^{(\frac{n-5}{2})} \ \mathrm{d}\Omega_{n-3} \ . \tag{C.5}$$

We can integrate over $\mathrm{d}\Omega_{n-3}$ in a trivial way by using

$$\int \mathrm{d}\Omega_n = \frac{\pi^{n/2}}{\Gamma(\frac{n}{2})} \ , \tag{C.6}$$

then equation (C.4) can be written as

$$\begin{aligned} &\int \mathrm{d}E_k \ \mathrm{d}^2k_\parallel \ \mathrm{d}^{n-3}k_\perp \delta(E_k^2 - k_{||}^2 - k_\perp^2)\delta((p_{4k}-k)^2) \\ &\quad = \int \mathrm{d}E_k \ \mathrm{d}^2k_{||} \ \delta((p_{4k}-k)^2)(E_K^2 - K_{||}^2)^{(\frac{n-5}{2})} \ \frac{\pi^{(n-3)/2}}{\Gamma(\frac{n-3}{2})} \end{aligned} \tag{C.7}$$

By using

$$k_{||} = E_k(\cos\theta_1, \sin\theta_1\cos\theta_2), \tag{C.8}$$

we can rewrite

$$\begin{aligned} k_{||}^2 &= E_k^2(1-\sin^2\theta_1\sin^2\theta_2) \ , \\ d^2k_{||} &= E_k^2 \sin\theta_1 \sin\theta_2 \ \mathrm{d}\theta_1 \ \mathrm{d}\theta_2 \ , \end{aligned} \tag{C.9}$$

inserting in equation (C.7) we end up with

$$\begin{aligned} &\int \mathrm{d}^n k \ \mathrm{d}^n p_4 \ \delta(k^2)\delta(p_4^2)\delta^n(p_{4k}-p_4-k) \\ &\quad = \frac{\pi^{(n-3)/2}}{\Gamma(\frac{n-3}{2})} \int \mathrm{d}E_k \frac{1}{2\sqrt{s_2}} \delta\left(\frac{p_{4k}^2}{2\sqrt{s_2}} - E_k\right) E_k^{(n-3)} \\ &\qquad\qquad \times \int \mathrm{d}\theta_1 \mathrm{d}\theta_2 \sin^{n-3}\theta_1 \sin^{n-4}\theta_2 \\ &\quad = \frac{\pi^{(n-3)/2}}{\Gamma(\frac{n-3}{2})} \frac{1}{2\sqrt{s_2}} \left(\frac{p_{4k}^2}{2\sqrt{s_2}}\right)^{(n-3)} \int \mathrm{d}\theta_1 \mathrm{d}\theta_2 \sin^{n-3}\theta_1 \sin^{n-4}\theta_2 \end{aligned} \tag{C.10}$$

We now evaluate the firts line of (B.2)

$$\begin{aligned}
&\int \frac{1}{(2\pi)^{5-4\varepsilon}} \mathrm{d}s_2 \; \mathrm{d}^n p_3 \; \mathrm{d}^n p_{4k} \; \delta(p_3^2)\delta(p_{4k}^2 - s_2)\delta^n(p_1 + p_2 - p_3 - p_{4k}) \\
&= \frac{1}{(2\pi)^{5-4\varepsilon}} \int \mathrm{d}s_2 \; \mathrm{d}^n p_3 \; \delta(p_3^2)\delta((p_1 + p_2 - p_3)^2 - s_2) \\
&= \frac{1}{(2\pi)^{5-4\varepsilon}} \int \mathrm{d}s_2 \; \frac{\mathrm{d}^{n-1} p_3}{2E_{p1}} \; \delta(s + t + u - s_2) \\
&= \frac{1}{(2\pi)^{5-4\varepsilon}} \int \mathrm{d}s_2 \; \mathrm{d}p_{3,||} \; \mathrm{d}p_{3,\perp}^2 \; \mathrm{d}\Omega_{n-2} \; (p_{3,\perp}^2)^{(n-4)/2} \frac{1}{2E_{p1}} \; \delta(s + t + u - s_2) \\
&= \frac{1}{(2\pi)^{5-4\varepsilon}} \frac{\pi^{(n-2)/2}}{\Gamma(\frac{n-2}{2})} \int \mathrm{d}s_2 \; \mathrm{d}p_{3,||} \; \mathrm{d}p_{3,\perp}^2 \; (p_{3,\perp}^2)^{(n-4)/2} \frac{1}{2E_{p1}} \; \delta(s + t + u - s_2) \qquad \text{(C.11)}
\end{aligned}$$

We can write $p_{3,||}$ and $p_{3,\perp}$ as

$$\begin{aligned}
p_{3,||} &= \frac{t-u}{2\sqrt{s}} = \frac{\sqrt{s}}{2}(-1 + v + vw) \\
p_{3,\perp}^2 &= \frac{tu}{s} = s(1-v)vw \\
E_{p_3} &= -\frac{t+u}{2\sqrt{s}} = \frac{\sqrt{s}}{2}(1 - v + vw) \qquad \text{(C.12)}
\end{aligned}$$

We find the Jacobian $\frac{\partial(p_{3,||}, p_{3,\perp}^2)}{\partial(v,w)} = E_{p_3} vs$. Then we have for the first line in equation (B.2)

$$\begin{aligned}
&\int \frac{1}{(2\pi)^{5-4\varepsilon}} \mathrm{d}s_2 \; \mathrm{d}^n p_3 \; \mathrm{d}^n p_{4k} \; \delta(p_3^2)\delta(p_{4k}^2 - s_2)\delta^n(p_1 + p_2 - p_3 - p_{4k}) \\
&= \frac{1}{(2\pi)^{5-4\varepsilon}} \frac{\pi^{(n-2)/2}}{\Gamma(\frac{n-2}{2})} \int \mathrm{d}s_2 \; \mathrm{d}w \; \mathrm{d}v \; \frac{sv}{2}(s(1-v)vw)^{(n-4)/2} \; \delta(sv(1-w) - s_2) \; . \qquad \text{(C.13)}
\end{aligned}$$

Merge line one and line two from equation (C.3) we get

$$\begin{aligned}
(PS)_3 = \frac{1}{(2\pi)^{5-4\varepsilon}} &\frac{\pi^{(n-2)/2}}{\Gamma(\frac{n-2}{2})} \int \mathrm{d}s_2 \; \mathrm{d}w \; \mathrm{d}v \; \frac{sv}{2}(s(1-v)vw)^{(n-4)/2} \\
&\times \delta(sv(1-w) - s_2) \\
&\times \frac{\pi^{(n-3)/2}}{\Gamma(\frac{n-3}{2})} \frac{1}{2\sqrt{s_2}} \left(\frac{\sqrt{s_2}}{2}\right)^{(n-3)} \int \mathrm{d}\theta_1 \mathrm{d}\theta_2 \sin^{n-3}\theta_1 \sin^{n-4}\theta_2 \\
= \frac{s}{2^8 \pi^4 \Gamma(1-2\varepsilon)} &\left(\frac{4\pi}{s}\right)^{2\varepsilon} \int \mathrm{d}v \; \mathrm{d}w \; v((1-v)(1-w)w)^{-\varepsilon} v^{-2\varepsilon} \\
&\times \int \mathrm{d}\theta_1 \mathrm{d}\theta_2 \sin^{1-2\varepsilon}\theta_1 \sin^{-2\varepsilon}\theta_2 \qquad \text{(C.14)}
\end{aligned}$$

This result is in agreement with the results given in [115, 261].

Appendix D.

Angular Integration

For single inclusive phase space integration we have the angular integral (see Appendix C)

$$\int \mathrm{d}\theta_1 \mathrm{d}\theta_2 \sin^{1-2\varepsilon}\theta_1 \sin^{-2\varepsilon}\theta_2 \mathcal{M} \tag{D.1}$$

where θ_1 and θ_2 are the angles between the two unobserved final states and $\mathcal{M}$ the partonic matrix element which depends on these angles. We label the momenta of the partonic process in $n = 4 - 2\varepsilon$ dimensions as

$$p_1 + p_2 \to k_1 + k_2 + k_3 \ , \tag{D.2}$$

where k_1 is the observed particle. The $2 \to 3$ Mandelstam variables read

$$\begin{aligned} t_i &= (p_1 - k_i)^2 \ , \\ u_i &= (p_2 - k_i)^2 \ , \\ s_{ij} &= (k_i + k_j) \ ,^2 \\ s &= (p_1 + p_2)^2 \ . \end{aligned} \tag{D.3}$$

We work in the rest frame of the two unobserved particles. Thus we have,

$$\begin{aligned} k_2 &= k_2^0(1, ..., \sin\theta_1 \cos\theta_2, \cos\theta_1) \\ k_3 &= k_3^0(1, ..., -\sin\theta_1 \cos\theta_2, -\cos\theta_1) \end{aligned} \tag{D.4}$$

with $k_2^0 = k_3^0 = \frac{\sqrt{s_{23}}}{2}$. Since we already chose which momenta defines the rest frame we are still free to chose which momentum defines the z-axis. Therefore, three choices are useful where either p_1, p_2 or k_1 is in the direction of the z-axis.

Set 1: p_1 in z-direction

$$\begin{aligned} p_1 &= p_1^0(1, 0, ..., 0, 1) \\ p_2 &= p_2^0(1, 0, ..., -\sin\psi'', \cos\psi'') \\ k_1 &= k_1^0(1, 0, ..., -\sin\psi, \cos\psi) \end{aligned} \tag{D.5}$$

that leads to the following Mandelstam variables

$$\begin{aligned} s_{12} &= s_{12}^0(1 + \sin\psi \sin\theta_1 \cos\theta_2 - \cos\psi \cos\theta_1) \\ s_{13} &= s_{13}^0(1 - \sin\psi \sin\theta_1 \cos\theta_2 + \cos\psi \cos\theta_1) \\ t_2 &= t_2^0(1 - \cos\theta_1) \\ t_3 &= t_3^0(1 + \cos\theta_1) \\ u_2 &= u_2^0(1 + \sin\psi'' \sin\theta_1 \cos\theta_2 - \cos\psi'' \cos\theta_1) \\ u_3 &= u_3^0(1 - \sin\psi'' \sin\theta_1 \cos\theta_2 + \cos\psi'' \cos\theta_1) \ . \end{aligned} \tag{D.6}$$

Set 2: p_2 in z-direction

$$\begin{aligned} p_1 &= p_1^0(1, 0, ..., \sin\psi'', \cos\psi'') \\ p_2 &= p_2^0(1, 0, ..., 0, 1) \\ k_1 &= k_1^0(1, 0, ..., \sin\psi', \cos\psi') \end{aligned} \tag{D.7}$$

that leads to the following Mandelstam variables

$$\begin{aligned} s_{12} &= s_{12}^0(1 - \sin\psi' \sin\theta_1 \cos\theta_2 - \cos\psi' \cos\theta_1) \\ s_{13} &= s_{13}^0(1 + \sin\psi' \sin\theta_1 \cos\theta_2 + \cos\psi' \cos\theta_1) \\ t_2 &= t_2^0(1 - \sin\psi'' \sin\theta_1 \cos\theta_2 - \cos\psi'' \cos\theta_1) \\ t_3 &= t_3^0(1 + \sin\psi'' \sin\theta_1 \cos\theta_2 + \cos\psi'' \cos\theta_1) \\ u_2 &= u_2^0(1 - \cos\theta_1) \\ u_3 &= u_3^0(1 + \cos\theta_1) \ . \end{aligned} \tag{D.8}$$

Set 3: k_1 in z-direction

$$\begin{aligned} p_1 &= p_1^0(1, 0, ..., \sin\psi, \cos\psi) \\ p_2 &= p_2^0(1, 0, ..., -\sin\psi', \cos\psi') \\ k_1 &= k_1^0(1, 0, ..., 0, 1) \end{aligned} \tag{D.9}$$

that leads to the following Mandelstam variables

$$\begin{aligned}
s_{12} &= s_{12}^0(1-\cos\theta_1)\\
s_{13} &= s_{13}^0(1+\cos\theta_1)\\
t_2 &= t_2^0(1-\sin\psi\sin\theta_1\cos\theta_2-\cos\psi\cos\theta_1)\\
t_3 &= t_3^0(1+\sin\psi\sin\theta_1\cos\theta_2+\cos\psi\cos\theta_1)\\
u_2 &= u_2^0(1+\sin\psi'\sin\theta_1\cos\theta_2-\cos\psi'\cos\theta_1)\\
u_3 &= u_3^0(1-\sin\psi'\sin\theta_1\cos\theta_2+\cos\psi'\cos\theta_1)\ .
\end{aligned} \tag{D.10}$$

We used

$$s_{12}^0 = s_{13}^0 \equiv \frac{s(1-v+vw)}{2}\ ,\ \ t_2^0 = t_3^0 \equiv -\frac{sv}{2}\ ,\ \ u_2^0 = u_3^0 \equiv -\frac{s(1-vw)}{2}\ , \tag{D.11}$$

and

$$\begin{aligned}
\cos\psi &= 1-\frac{2(1-v)(1-w)}{1-v+vw}\\
\cos\psi' &= 1-\frac{2v^2w(1-w)}{(1-vw)(1-v+vw)}\\
\cos\psi'' &= 1-\frac{2(1-w)}{1-vw}
\end{aligned} \tag{D.12}$$

More details and derivation can be found in [131, 261, 262]. It turns out that by using relations among Mandelstam variables, that $\mathcal{M}$ can be simplified in a such way that each term contains at highest two Mandelstam variables which are dependent on the angles θ_1 and θ_2. Therefore, we can choose one of the sets introduced in this appendix for each of these terms and we always end up with an angular integral of the form

$$\Omega_{ij} \equiv \int_0^\pi \mathrm{d}\theta_1 \int_0^\pi \mathrm{d}\theta_2\ \frac{\sin^{1-2\varepsilon}\theta_1\sin^{-2\varepsilon}\theta_2}{(1-\cos\theta_1)^i(1-\cos\theta_1\cos\chi-\sin\theta_1\cos\theta_2\sin\chi)^j} \tag{D.13}$$

where χ is one of the anngles ψ, ψ' and ψ''. This integral has a general result [112, 131, 261]

$$\Omega_{ij} = 2\pi\frac{\Gamma(1-2\varepsilon)}{\Gamma(1-\varepsilon)^2}2^{-i-j}\ B\left(1-\varepsilon-i, 1-\varepsilon-j\right)\ {}_2F_1(i,j,1-\varepsilon,\cos^2\frac{\chi}{2})\ . \tag{D.14}$$

Note Ω_{ij} is symmetric under the interchange of i and j and B is the beta function and ${}_2F_1$ is the hypergeometric function.

Appendix E.

New Integral for Twist-3 Calculation

Using the notation given in appendix C "group 2" in [112], we need one additional integral given by:

$$\begin{aligned}
&\bar{I}^{(3,1)}_{n=4-2\varepsilon} \\
&= \frac{\pi}{a^3(A+B)}\Bigg[\left(B^2(A+B)^2-(A-5B)(A+B)\frac{C^2}{2}+\frac{3}{2}C^4\right) \\
&\quad\times\left(-\frac{1}{\varepsilon}+\log\left(\frac{(A+B)^2}{A^2-B^2-C^2}\right)\right)\frac{1}{(A+B)^4} \\
&\quad-\frac{(A+B)^3(A+5B)+2(A+B)(A+11B)C^2+16C^4}{4(A+B)^4}\Bigg]
\end{aligned} \tag{E.1}$$

Appendix F.

The Normalization of the Soft Function

The soft matrix S_{LI} in the resumed cross section in moment space, equation (7.10), is computed as described in Ref. [177, 178]. Its all-orders form is most conveniently exhibited in moment space, as the ratio of the moments of a fully eikonal cross section $\hat{\sigma}_{LI}^{ab\to cd}$ and four factorized jets, two to absorb the factorizing collinear singularities of the incoming parton lines, and two to absorb the collinear singularities of outgoing lines:

$$\begin{aligned}&\Big(S_{ab\to cd}\left(\alpha_s(\hat{m}/\bar{N}),\Delta\eta\right)\Big)_{LI}\\&\quad=\frac{\hat{\sigma}_{LI}^{ab\to cd}\left(\frac{\hat{m}}{N\mu_R},\Delta\eta,\alpha_s(\mu_R),\varepsilon\right)}{\prod_{i=a,b}\tilde{j}_{\rm in}^{(i)}\left(\frac{\hat{m}}{N\mu_R},\alpha_s(\mu_R),\varepsilon\right)\prod_{j=c,d}\tilde{j}_{out}^{(j)}\left(\frac{\hat{m}}{N\mu_R},\alpha_s(\mu_R),\varepsilon\right)}\,.\end{aligned}\tag{F.1}$$

As described in Refs. [40, 177, 178], these "in" and "out" jets, $\tilde{j}_{in}$ and $\tilde{j}_{out}$, respectively are defined to match the collinear singularities and radiation phase space in the partonic threshold limit.

The explicit calculation of $(S_{ab\to cd})_{LI}$ at one loop as given here is equivalent to the procedure described in Sec. 5.3.3. The functions on the right of (F.1), as defined in

detail below, are normalized and expanded according to

$$\begin{aligned}
\hat{\sigma}_{LI}^{ab\to cd}\left(\frac{\hat{m}}{N\mu_R},\Delta\eta,\alpha_s(\mu_R),\varepsilon\right) &= (S^{(0)}_{ab\to cd})_{LI} \;+\; \frac{\alpha_s(\mu_R)}{\pi}\,\hat{\sigma}_{LI}^{ab\to cd\,(1)} \\
&\quad + \mathcal{O}(\alpha_s(\mu_R)^2)\,, \\
\tilde{j}^{(i)}_{\rm in}\left(\frac{\hat{m}}{N\mu_R},\alpha_s(\mu_R),\varepsilon\right) &= 1 \;+\; \frac{\alpha_s(\mu_R)}{\pi}\,\tilde{j}^{(i,1)}_{\rm in} \;+\; \mathcal{O}(\alpha_s(\mu_R)^2)\,, \\
\tilde{j}^{(j)}_{\rm out}\left(\frac{\hat{m}}{N\mu_R},\alpha_s(\mu_R),\varepsilon\right) &= 1 \;+\; \frac{\alpha_s(\mu_R)}{\pi}\,\tilde{j}^{(j,1)}_{\rm out} \;+\; \mathcal{O}(\alpha_s(\mu_R)^2)\,,
\end{aligned} \tag{F.2}$$

where $S^{(0)}$ is the tree-level soft matrix, defined as in equation (5.52). The first-order expansion of the soft matrix is thus,

$$\left(S^{(1)}_{ab\to cd}\right)_{LI} = \hat{\sigma}_{LI}^{ab\to cd\,(1)} \;-\; (S^{(0)}_{ab\to cd})_{LI}\left[\sum_{i=a,b}\tilde{j}^{(i,1)}_{\rm in} \;+\; \sum_{j=c,d}\tilde{j}^{(j,1)}_{\rm out}\right]. \tag{F.3}$$

At any loop order, the collinear singularities of the eikonal cross section $\hat{\sigma}_{LI}$ match those of properly-defined incoming and outgoing jet functions. At one loop, this will result in a finite soft function by simple cancellation in equation (F.3), as seen in Sec. 5.3.3. That is, division by the regularized jet functions plays the role of the collinear factorization of the soft function. It also provides finite, factorizing corrections to the soft function, which depend on the definitions of the jets functions. Here we use jet functions defined directly from the eikonal resummations of Drell-Yan and double inclusive cross sections [188]. The choices, defined below, match collinear singularities of the eikonal cross section, and have the advantage of being Lorentz and gauge invariant. They differ from those made in Refs. [40, 177, 178] by finite terms, but the collinear structure is identical. When restricted to the amplitude level, this is the same formalism that was implemented in Refs. [222–225, 231].

To make the connection to the calculation of the soft function in chapter 5 explicit, we recall that eikonal diagrams are generated by path-ordered exponentials with constant velocities β, which we represent as

$$\Phi^{(f)}_{\beta}(\lambda_2,\lambda_1;x) = P\exp\left(-ig\int_{\lambda_1}^{\lambda_2} d\eta\;\beta\cdot A^{(f)}(\eta\beta+x)\right), \tag{F.4}$$

where superscript f represents the color representation of the parton to which this "Wilson line" corresponds. In terms of these path-ordered exponentials, we define products corresponding to scattering, pair annihilation and pair creation. For the case of $2\to 2$ scattering, the ends of two incoming and two outgoing Wilson lines are coupled

locally by a constant color tensor $\mathcal{C}_I$,

$$w_I^{(ab\to cd)}(x)_{\{j\}} = \sum_{\{i\}} \Phi^{(d)}_{\beta_d}(\infty,0;x)_{j_d,i_d}\ \Phi^{(c)}_{\beta_c}(\infty,0;x)_{j_c,i_c} \times \left(\mathcal{C}_I^{(ab\to cd)}\right)_{i_d i_c, i_b i_a} \Phi^{(a)}_{\beta_a}(0,-\infty;x)_{i_a,j_a}\Phi^{(b)}_{\beta_b}(0,-\infty;x)_{i_b,j_b}\,. \tag{F.5}$$

For pair annihilation, two lines in conjugate representations that come from the infinite past are joined by a color singlet tensor, that is, a simple Kronecker delta,

$$w_0^{(a\bar{a})}(x)_{\{j\}} = \sum_{\{i\}} (\delta)_{i_a,i_{\bar{a}}}\ \Phi^{(\bar{a})}_{\beta_{\bar{a}}}(0,-\infty;x)_{i_{\bar{a}},j_{\bar{a}}}\Phi^{(a)}_{\beta_a}(0,-\infty;x)_{i_a,j_a}\,, \tag{F.6}$$

and similarly for pair creation, using color-conjugate lines that emerge from a point, and extend into the infinite future,

$$\hat{w}_0^{(a\bar{a})}(x)_{\{j\}} = \sum_{\{i\}} \Phi^{(\bar{a})}_{\beta_{\bar{a}}}(\infty,0;x)_{i_{\bar{a}},j_{\bar{a}}}\Phi^{(a)}_{\beta_a}(\infty,0;x)_{i_a,j_a}\ (\delta)_{i_a,i_{\bar{a}}}\ . \tag{F.7}$$

In terms of these operators, the eikonal cross section is defined by

$$\begin{aligned}
&\hat{\sigma}_{LI}^{ab\to cd}\left(\frac{\hat{m}}{N\mu_R},\Delta\eta,\alpha_s(\mu_R),\varepsilon\right)\\
&= \int_0^1 d\tau\ \tau^{N-1}\ \int\frac{dy^0}{2\pi}\ e^{i\tau\hat{m}y^0}\\
&\quad\times \mathrm{Tr}_{\{j\}}\ \langle 0|\,\bar{T}\left(w_L^{(ab\to cd)\dagger}\left((y^0,\vec{0})\right)_{\{j\}}\right)\ T\left(w_I^{(ab\to cd)}(0)_{\{j\}}\right)|0\rangle\\
&= \int_0^1 d\tau\ \tau^{N-1}\ \sum_{\xi}\ \delta(\tau\hat{m}-p_\xi^0)\\
&\quad\times \mathrm{Tr}_{\{j\}}\ \langle 0|\,\bar{T}\left(w_L^{(ab\to cd)\dagger}(0)_{\{j\}}\right)|\xi\rangle\,\langle\xi|T\left(w_I^{(ab\to cd)}(0)_{\{j\}}\right)|0\rangle\,,
\end{aligned} \tag{F.8}$$

where T represents time ordering, $\bar{T}$ anti-time ordering, and p_ξ^0 is the energy of state $|\xi\rangle$. The in jet is defined *in* terms of its square in moment space as

$$\begin{aligned}
\left(\tilde{j}_{\rm in}^{(a)}\left(\frac{\hat{m}}{N\mu_R},\alpha_s(\mu_R),\varepsilon\right)\right)^2 &= \int_0^1 d\tau\ \tau^{N-1}\ \sum_{\xi}\ \delta(\tau\hat{m}-p_\xi^0)\\
&\quad\times \mathrm{Tr}_{\{j\}}\ \langle 0|\,\bar{T}\left(w_0^{(a\bar{a})\dagger}(0)_{\{j\}}\right)|\xi\rangle\,\langle\xi|T\left(w_0^{(a\bar{a})}(0)_{\{j\}}\right)|0\rangle\,.
\end{aligned} \tag{F.9}$$

With this choice, $\left(\tilde{j}_{\rm in}^{(a)}\right)^2$ is exactly the eikonal Drell-Yan cross section. It was computed to two loops in Ref. [263]. The out jet is defined by the same integrals but with the

pair of incoming Wilson lines of the operator $w_0(x)$ replaced by the outgoing pair in $\hat{w}_0(x)$, corresponding to double inclusive annihilation [211]:

$$\left(\tilde{j}^{(c)}_{out}\left(\frac{\hat{m}}{N\mu_R},\alpha_s(\mu_R),\varepsilon\right)\right)^2 \;=\; \int_0^1 d\tau\;\tau^{N-1}\;\sum_{\xi}\;\delta(\tau\hat{m}-p_\xi^0) \\ \times\;\mathrm{Tr}_{\{j\}}\;\langle 0|\,\bar{T}\left(\hat{w}_0^{(c\bar{c})\dagger}(0)_{\{j\}}\right)|\xi\rangle\,\langle\xi|T\left(\hat{w}_0^{(c\bar{c})}(0)_{\{j\}}\right)|0\rangle\,. \tag{F.10}$$

It is easy to confirm explicitly in Ref. [263] that the calculation of this quantity depends only on the inner products $\beta_a\cdot\beta_{\bar{a}}$ so that the full two-loop calculation and renormalization of this operator is the same for outgoing as for incoming eikonal jets.

The resummation of logarithms of N in this cross section leads precisely to the functions $\ln\Delta_i^N$ in equation (5.25), which summarize factoring NNLL dependence on the moment variable N, as confirmed recently in Ref. [264]. We note, however, that in the NNLL exponentiation as implemented into the expression for the functions Δ_i^N in equation (5.20), the Drell-Yan soft function is treated as an overall prefactor evaluated at the hard scale $\hat{m}$, rather than at $\hat{m}/N$. Logarithms at NNLL that are associated with this shift are already incorporated into the exponent by use of the relation [264]

$$S(\alpha_s(\hat{m}/N))\;=\;S(\alpha_s(\hat{m}))\exp\left[-\int_{\hat{m}/N}^{\hat{m}}\frac{d\mu}{\mu}\frac{\partial\ln S(\alpha_s(\mu))}{\partial\mu}\right]. \tag{F.11}$$

To match logarithms associated with these factors consistently we include in our definition of Δ_i^N in equation (5.20) an extra factor of $R_i=1-(3\alpha_s/4\pi)A_i^{(1)}\zeta(2)$, equation (5.24), to account for our definitions of the in- and out-jet functions in terms of Drell-Yan and double inclusive cross sections. The combined factors for all four jet functions match the π^2 contribution in (5.87), which in turn arises from the explicit π^2 terms in the integrals $dI_{ij}/d\hat{\tau}$ in (5.83).

Bibliography

[1] D. de Florian, P. Hinderer, A. Mukherjee, F. Ringer, and W. Vogelsang, "Approximate Next-to-Next-to-Leading Order Corrections to Hadronic Jet Production", Physical Review Letters **112**, 082001 (2014) 10.1103/PhysRevLett.112.082001.

[2] P. Hinderer, F. Ringer, G. F. Sterman, and W. Vogelsang, "Toward NNLL threshold resummation for hadron pair production in hadronic collisions", Physical Review D **91**, 014016 (2015) 10.1103/PhysRevD.91.014016, arXiv:1411.3149.

[3] P. Hinderer, M. Schlegel, and W. Vogelsang, "Single-inclusive production of hadrons and jets in lepton-nucleon scattering at NLO", Physical Review D **92**, 014001 (2015) 10.1103/PhysRevD.92.014001.

[4] P. Hinderer, M. Schlegel, and W. Vogelsang, "Double-Longitudinal Spin Asymmetry in Single-Inclusive Lepton Scattering at NLO", Phys. Rev. **D96**, 014002 (2017) 10.1103/PhysRevD.96.014002, arXiv:1703.10872 [hep-ph].

[5] Y. Koike, P. Hinderer, and W. Vogelsang, "NLO Correction to Single Spin Asymmetry in $lp^{\uparrow} \to hX$", in preparation.

[6] M. Schlegel, P. Hinderer, and W. Vogelsang, "NLO K-factors for Single-Inclusive Leptoproduction of Hadrons", (2015), arXiv:1510.07421.

[7] P. Hinderer, F. Ringer, G. F. Sterman, and W. Vogelsang, "Toward NNLL Resummation for Hadron Production in Hadronic Collisions", (2015), arXiv:1510.08037.

[8] H. Fritzsch, M. Gell-Mann, and H. Leutwyler, "Advantages of the color octet gluon picture", Physics Letters B **47**, 365–368 (1973) 10.1016/0370-2693(73)90625-4.

[9] H. Fritzsch and M. Gell-Mann, "Current algebra: Quarks and what else?", Proceedings, 16th International Conference on High-Energy Physics, ICHEP, Batavia, Illinois, 6-13 Sep 1972 **C720906V2**, 135–165 (1972).

[10] D. J. Gross and F. Wilczek, "Asymptotically free gauge theories. II", Physical Review D **9**, 980–993 (1974) 10.1103/PhysRevD.9.980.

[11] H. D. Politzer, "Reliable Perturbative Results for Strong Interactions?", Physical Review Letters **30**, 1346–1349 (1973) 10.1103/PhysRevLett.30.1346.

[12] E. Abers and B. Lee, "Gauge theories", Physics Reports **9**, 1–2 (1973) 10.1016/0370-1573(73)90027-6.

[13] L. Faddeev and V. Popov, "Feynman diagrams for the Yang-Mills field", Physics Letters B **25**, 29–30 (1967) 10.1016/0370-2693(67)90067-6.

[14] J. Polchinski, "Renormalization and effective lagrangians", Nuclear Physics B **231**, 269–295 (1984) 10.1016/0550-3213(84)90287-6.

[15] S. Weinberg, "New Approach to the Renormalization Group", Physical Review D **8**, 3497–3509 (1973) 10.1103/PhysRevD.8.3497.

[16] O. Tarasov, A. Vladimirov, and A. Zharkov, "The gell-mann-low function of QCD in the three-loop approximation", Physics Letters B **93**, 429–432 (1980) 10.1016/0370-2693(80)90358-5.

[17] S. A. Larin and J. A. M. Vermaseren, "The three-loop QCD β-function and anomalous dimensions", (1993) 10.1016/0370-2693(93)91441-O, arXiv:9302208 [hep-ph].

[18] S. Bethke, "The 2009 world average of α_s", The European Physical Journal C **64**, 689–703 (2009) 10.1140/epjc/s10052-009-1173-1, arXiv:0908.1135.

[19] S. Bethke, "World Summary of α_s", Nuclear Physics B - Proceedings Supplements **234**, 229–234 (2013) 10.1016/j.nuclphysbps.2012.12.020.

[20] R. Ellis, B. Webber, and W. Stirling, "QCD and collider physics", Camb. Monogr. Part. Phys. Nucl. Phys. Cosmol. **8**, 1–435 (1996).

[21] T. Kinoshita, "Mass Singularities of Feynman Amplitudes", Journal of Mathematical Physics **3**, 650 (1962) 10.1063/1.1724268.

[22] T. D. Lee and M. Nauenberg, "Degenerate Systems and Mass Singularities", Physical Review **133**, B1549–B1562 (1964) 10.1103/PhysRev.133.B1549.

[23] D. E. Soper, "Basics of QCD Perturbation Theory", (1997), arXiv:9702203 [hep-ph].

[24] Z. Kunszt and D. E. Soper, "Calculation of jet cross-sections in hadron collisions at order alpha-s**3", Phys.Rev. **D46**, 192–221 (1992) 10.1103/PhysRevD.46.192.

[25] J. C. Collins, D. E. Soper, and G. Sterman, "Factorization of Hard Processes in QCD", (2004), arXiv:0409313 [hep-ph].

[26] Y.-Q. Ma and J.-W. Qiu, "Extracting Parton Distribution Functions from Lattice QCD Calculations", (2014), arXiv:1404.6860.

[27] X. Ji, "Parton Physics on Euclidean Lattice", (2013) 10.1103/PhysRevLett.110.262002, arXiv:1305.1539.

[28] R. P. (P. Feynman, *Photon-hadron interactions* (Addison-Wesley Pub. Co., Advanced Book Program, 1998), p. 282.

[29] J. C. (C. Collins, *Renormalization : an introduction to renormalization, the renormalization group, and the operator-product expansion* (Cambridge University Press, 1985), p. 380.

[30] G. Altarelli and G. Parisi, "Asymptotic freedom in parton language", Nuclear Physics B **126**, 298–318 (1977) 10.1016/0550-3213(77)90384-4.

[31] W. K. Tung et al., "Heavy Quark Mass Effects in Deep Inelastic Scattering and Global QCD Analysis", (2006) 10.1088/1126-6708/2007/02/053, arXiv:0611254 [hep-ph].

[32] A. D. Martin, W. J. Stirling, R. S. Thorne, and G. Watt, "Parton distributions for the LHC", (2009) 10.1140/epjc/s10052-009-1072-5, arXiv:0901.0002.

[33] T. N. The NNPDF Collaboration et al., "Parton distributions for the LHC Run II", (2014) 10.1007/JHEP04(2015)040, arXiv:1410.8849.

[34] J. C. Collins and D. E. Soper, "Parton distribution and decay functions", Nuclear Physics B **194**, 445–492 (1982) 10.1016/0550-3213(82)90021-9.

[35] A. Vogt, S. Moch, and J. Vermaseren, "The Three-Loop Splitting Functions in QCD", (2004), arXiv:0407321 [hep-ph].

[36] S. Moch, J. A. M. Vermaseren, and A. Vogt, "The Three-Loop Splitting Functions in QCD: The Helicity-Dependent Case", (2014) 10.1016/j.nuclphysb.2014.10.016, arXiv:1409.5131.

[37] A. Vogt, "Efficient evolution of unpolarized and polarized parton distributions with QCD-PEGASUS", (2004) 10.1016/j.cpc.2005.03.103, arXiv:0408244 [hep-ph].

[38] G. Altarelli, R. Ellis, and G. Martinelli, "Large perturbative corrections to the Drell-Yan process in QCD", Nuclear Physics B **157**, 461–497 (1979) 10.1016/0550-3213(79)90116-0.

[39] G. Sterman, "Summation of large corrections to short-distance hadronic cross sections", Nuclear Physics B **281**, 310–364 (1987) 10.1016/0550-3213(87)90258-6.

[40] N. Kidonakis and G. Sterman, "Resummation for QCD Hard Scattering", (1997) 10.1016/S0550-3213(97)00506-3, arXiv:9705234 [hep-ph].

[41] A. Vogt, "Next-to-next-to-leading logarithmic threshold resummation for deep-inelastic scattering and the Drell-Yan process", (2000) 10.1016/S0370-2693(00)01344-7, arXiv:0010146 [hep-ph].

[42] S. Catani, M. L. Mangano, P. Nason, and L. Trentadue, "The Resummation of Soft Gluon in Hadronic Collisions", (1996) 10.1016/0550-3213(96)00399-9, arXiv:9604351 [hep-ph].

[43] S. Catani, L. Trentadue, G. Turnock, and B. Webber, "Resummation of large logarithms in event shape distributions", Nuclear Physics B **407**, 3–42 (1993) 10.1016/0550-3213(93)90271-P.

[44] H. Contopanagos, E. Laenen, and G. Sterman, "Sudakov factorization and resummation", Nuclear Physics B **484**, 303–327 (1997) 10.1016/S0550-3213(96)00567-6.

[45] T. E. The E155 Collaboration and P. L. A. et Al, "Inclusive Hadron Photoproduction from Longitudinally Polarized Protons and Deuterons", (1999) 10.1016/S0370-2693(99)00589-4, arXiv:9902412 [hep-ph].

[46] T. H. The HERMES Collaboration et al., "Transverse target single-spin asymmetry in inclusive electroproduction of charged pions and kaons", (2013), arXiv:1310.5070.

[47] C. Van Hulse and C. V. Hulse, "Recent HERMES results from inclusive and semi-inclusive hadron production", EPJ Web of Conferences **85**, edited by U. D'Alesio and F. Murgia, 02020 (2015) 10.1051/epjconf/20158502020.

[48] K. Allada et al., "Single Spin Asymmetries of Inclusive Hadrons Produced in Electron Scattering from a Transversely Polarized ^{3}He Target", (2013) 10.1103/PhysRevC.89.042201, arXiv:1311.1866.

[49] Y. Koike, "Single Transverse Spin Asymmetry in $p^\uparrow p \to \pi X$ and $ep^\uparrow \to \pi X$", Nuclear Physics A **721**, C364–C367 (2003) 10.1016/S0375-9474(03)01070-4.

[50] Y. Koike, "Single Transverse-Spin Asymmetry in $pp^\uparrow \to \pi X$ and $ep^\uparrow \to \pi X$", (2002) 10.1063/1.1607176, arXiv:0210396 [hep-ph].

[51] Z.-B. Kang, A. Metz, J.-W. Qiu, and J. Zhou, "Exploring the structure of the proton through polarization observables in $lp \to \mathrm{jet}X$", (2011) 10.1103/PhysRevD.84.034046, arXiv:1106.3514.

[52] L. Gamberg, Z.-B. Kang, A. Metz, D. Pitonyak, and A. Prokudin, "Left-right spin asymmetry in $\ell N^\uparrow \to hX$", (2014) 10.1103/PhysRevD.90.074012, arXiv:1407.5078.

[53] M. Anselmino et al., "Single spin asymmetries in $lp^\uparrow \to hX$ processes: a test of factorization", (2009) 10.1103/PhysRevD.81.034007, arXiv:0911.1744.

[54] M. Anselmino, M. Boglione, J. Hansson, and F. Murgia, "Predictions for single spin asymmetries in $lp^\uparrow \to \pi X$ and $\gamma p^\uparrow \to \pi X$", (1999) 10.1007/s100520050714, arXiv:9906418 [hep-ph].

[55] M. Anselmino et al., "Single Spin Asymmetries in $lp^\uparrow \to hX$ processes and TMD factorisation", (2014), arXiv:1404.6465.

[56] M. Klasen, "Theory of hard photoproduction", (2002) 10.1103/RevModPhys.74.1221, arXiv:0206169 [hep-ph].

[57] C. A. Aidala, S. D. Bass, D. Hasch, and G. K. Mallot, "The Spin Structure of the Nucleon", (2012) 10.1103/RevModPhys.85.655, arXiv:1209.2803.

[58] N. Christ and T. D. Lee, "Possible Tests of C st and T st Invariances in $l^\pm + N \to l^\pm + \Gamma$ and $A \to Bee$", Physical Review **143**, 1310–1321 (1966) 10.1103/PhysRev.143.1310.

[59] M. Schlegel, "A partonic description of the transverse target single-spin asymmetry in inclusive DIS", (2012) 10.1103/PhysRevD.87.034006, arXiv:1211.3579.

[60] A. Metz et al., "Single-spin asymmetries in inclusive deep inelastic scattering and multiparton correlations in the nucleon", (2012) 10.1103/PhysRevD.86.094039, arXiv:1209.3138.

[61] A. Afanasev, M. Strikman, and C. Weiss, "Transverse target spin asymmetry in inclusive DIS with two-photon exchange", (2007) 10.1103/PhysRevD.77.014028, arXiv:0709.0901.

[62] A. Metz, M. Schlegel, and K. Goeke, "Transverse single spin asymmetries in inclusive deep-inelastic scattering", (2006) 10.1016/j.physletb.2006.11.009, arXiv:0610112 [hep-ph].

[63] K. Kanazawa, A. Metz, D. Pitonyak, and M. Schlegel, "Longitudinal-transverse double-spin asymmetries in single-inclusive leptoproduction of hadrons", (2014) 10.1016/j.physletb.2015.02.005, arXiv:1411.6459.

[64] K. Kanazawa, A. Metz, D. Pitonyak, and M. Schlegel, "Single-spin asymmetries in the leptoproduction of transversely polarized Λ hyperons", (2015) 10.1016/j.physletb.2015.04.011, arXiv:1503.02003.

[65] J. Qiu and G. Sterman, "Single transverse spin asymmetries in direct photon production", Nuclear Physics B **378**, 52–78 (1992).

[66] J. Qiu and G. Sterman, "Single transverse spin asymmetries", Physical Review Letters **67**, 2264–2267 (1991) 10.1103/PhysRevLett.67.2264.

[67] J. Qiu and G. Sterman, "Single transverse-spin asymmetries in hadronic pion production", Physical Review D **59**, 014004 (1998) 10.1103/PhysRevD.59.014004, arXiv:9806356 [hep-ph].

[68] Y. Kanazawa and Y. Koike, "Chiral-Odd Contribution to Single-Transverse Spin Asymmetry in Hadronic Pion Production", (2000) 10.1016/S0370-2693(00)00261-6, arXiv:0001021 [hep-ph].

[69] C. Kouvaris, J.-W. Qiu, W. Vogelsang, and F. Yuan, "Single transverse-spin asymmetry in high transverse momentum pion production in pp collisions", (2006) 10.1103/PhysRevD.74.114013, arXiv:0609238 [hep-ph].

[70] Z. Kang, F. Yuan, and J. Zhou, "Twist-three Fragmentation Function Contribution to the Single Spin Asymmetry in pp Collisions", (2010) 10.1016/j.physletb.2010.07.003, arXiv:1002.0399.

[71] K. Kanazawa and Y. Koike, "A phenomenological study of single transverse-spin asymmetry for inclusive light-hadron productions at RHIC", (2011) 10.1103/PhysRevD.83.114024, arXiv:1104.0117.

[72] H. Beppu, K. Kanazawa, Y. Koike, and S. Yoshida, "Three-gluon contribution to the single spin asymmetry for light hadron production in pp collision", (2013) 10.1103/PhysRevD.89.034029, arXiv:1312.6862.

[73] A. Metz and D. Pitonyak, "Fragmentation contribution to the transverse single-spin asymmetry in proton-proton collisions", (2012) 10.1016/j.physletb.2013.05.043, arXiv:1212.5037.

[74] K. Kanazawa and Y. Koike, "Contribution of twist-3 fragmentation function to single transverse-spin asymmetry in semi-inclusive deep inelastic scattering", (2013) 10.1103/PhysRevD.88.074022, arXiv:1309.1215.

[75] F. Yuan and J. Zhou, "Collins Fragmentation and the Single Transverse Spin Asymmetry", (2009) 10.1103/PhysRevLett.103.052001, arXiv:0903.4680.

[76] K. Kanazawa, Y. Koike, A. Metz, and D. Pitonyak, "Towards an explanation of transverse single-spin asymmetries in proton-proton collisions: the role of fragmentation in collinear factorization", (2014) 10.1103/PhysRevD.89.111501, arXiv:1404.1033.

[77] M. Anselmino, M. Boglione, and F. Murgia, "Phenomenology of single spin asymmetries in $p^{\uparrow}p \to \pi X$", (1999) 10.1103/PhysRevD.60.054027, arXiv:9901442 [hep-ph].

[78] M. Anselmino, M. Boglione, and F. Murgia, "Single spin asymmetry for $p^{\uparrow}p \to \pi X$ in perturbative QCD", (1995) 10.1016/0370-2693(95)01168-P, arXiv:9503290 [hep-ph].

[79] U. D'Alesio and F. Murgia, "Parton intrinsic motion in inclusive particle production: unpolarized cross sections, single spin asymmetries and the Sivers effect", (2004) 10.1103/PhysRevD.70.074009, arXiv:0408092 [hep-ph].

[80] M. Anselmino et al., "Sivers effect and the single spin asymmetry A_N in $p^{\uparrow}p \to hX$ processes", Physical Review D **88**, 054023 (2013) 10.1103/PhysRevD.88.054023.

[81] W. Vogelsang and F. Yuan, "Next-to-leading Order Calculation of the Single Transverse Spin Asymmetry in the Drell-Yan Process", (2009) 10.1103/PhysRevD.79.094010, arXiv:0904.0410.

[82] L.-Y. Dai, Z.-B. Kang, A. Prokudin, and I. Vitev, "Next-to-leading order transverse momentum-weighted Sivers asymmetry in semi-inclusive deep inelastic scattering: the role of the three-gluon correlator", (2014) 10.1103/PhysRevD.92.114024, arXiv:1409.5851.

[83] Z.-B. Kang, I. Vitev, and H. Xing, "Transverse momentum-weighted Sivers asymmetry in semi-inclusive deep inelastic scattering at next-to-leading order", (2012) 10.1103/PhysRevD.87.034024, arXiv:1212.1221.

[84] D. Bödeker, "QCD corrections to inclusive jet photoproduction via direct photons", Zeitschrift für Physik C Particles and Fields **59**, 501–510 (1993) 10.1007/BF01498632.

[85] D. Bödeker, "Jet photoproduction at HERA in next-to-leading-order QCD", Physics Letters B **292**, 164–168 (1992) 10.1016/0370-2693(92)90625-E.

[86] L. E. Gordon, "Next-to-leading-order corrections to inclusive hadron photoproduction", Physical Review D **50**, 6753–6774 (1994) 10.1103/PhysRevD.50.6753.

[87] L. Gordon and J. Storrow, "The single jet inclusive cross section at HERA in next-to-leading order QCD", Physics Letters B **291**, 320–324 (1992) 10.1016/0370-2693(92)91052-B.

[88] P. Aurenche, R. Baier, A. Douiri, M. Fontannaz, and D. Schiff, "Scheme invariant higher order QCD predictions for large pT photoproduction reactions", Nuclear Physics B **286**, 553–591 (1987) 10.1016/0550-3213(87)90453-6.

[89] M. Klasen and G. Kramer, "Inclusive Two-Jet Production at HERA: Direct and Resolved Cross Sections in Next-to-Leading Order QCD", (1996), arXiv:9611450 [hep-ph].

[90] M. Klasen and G. Kramer, "Inclusive Dijet Production at HERA: Direct Photon Cross Sections in Next-To-Leading Order QCD", (1995) 10.1007/s002880050229, arXiv:9511405 [hep-ph].

[91] M. Klasen and G. Kramer, "Dijet Cross Sections at $O(\alpha\alpha_s^2)$ in Photon-Proton Collisions", (1995) 10.1016/0370-2693(95)01352-0, arXiv:9508337 [hep-ph].

[92] D. Bödeker, G. Kramer, and S. G. Salesch, "Inclusive jet production at HERA: Next-to-leading order QCD corrections to the resolved and direct photon contribution", Zeitschrift für Physik C Particles and Fields **63**, 471–476 (1994) 10.1007/BF01580327.

[93] G. Kramer and S. G. Salesch, "Single jet photoproduction at HERA in next-to-leading order QCD", Zeitschrift für Physik C Particles and Fields **61**, 277–283 (1994) 10.1007/BF01413105.

[94] B. W. Harris and J. F. Owens, "Jet photoproduction and the structure of the photon", (1997) 10.1103/PhysRevD.57.5555, arXiv:9712299 [hep-ph].

[95] B. W. Harris and J. F. Owens, "Photoproduction of jets at HERA in next-to-leading order QCD", (1997) 10.1103/PhysRevD.56.4007, arXiv:9704324 [hep-ph].

[96] D. de Florian and W. Vogelsang, "Next-to-leading order QCD corrections to inclusive-hadron photoproduction in polarized lepton-proton collisions", (1997) 10.1103/PhysRevD.57.4376, arXiv:9712273 [hep-ph].

[97] D. de Florian and S. Frixione, "Jet cross sections in polarized photon-hadron collisions", (1999) 10.1016/S0370-2693(99)00544-4, arXiv:9904320 [hep-ph].

[98] S. Frixione and G. Ridolfi, "Jet photoproduction at HERA", (1997) 10.1016/S0550-3213(97)00575-0, arXiv:9707345 [hep-ph].

[99] B. Jager, "Photoproduction of single inclusive jets at future ep colliders in next-to-leading order QCD", (2008) 10.1103/PhysRevD.78.034017, arXiv:0807.0066.

[100] B. Jager, M. Stratmann, and W. Vogelsang, "Longitudinally Polarized Photoproduction of Inclusive Hadrons at Fixed-Target Experiments", (2005) 10.1140/epjc/s2005-02380-0, arXiv:0505157 [hep-ph].

[101] B. Jager, M. Stratmann, and W. Vogelsang, "Longitudinally Polarized Photoproduction of Inclusive Hadrons Beyond the Leading Order", (2003) 10.1103/PhysRevD.68.114018, arXiv:0309051 [hep-ph].

[102] Z.-B. Kang, X. Liu, S. Mantry, and J.-W. Qiu, "Probing nuclear dynamics in jet production with a global event shape", (2013) 10.1103/PhysRevD.88.074020, arXiv:1303.3063.

[103] Z.-B. Kang, X. Liu, and S. Mantry, "The 1-Jettiness DIS event shape: NNLL + NLO results", (2013) 10.1103/PhysRevD.90.014041, arXiv:1312.0301.

[104] E. J. Williams, "Nature of the High Energy Particles of Penetrating Radiation and Status of Ionization and Radiation Formulae", Physical Review **45**, 729–730 (1934) 10.1103/PhysRev.45.729.

[105] C. F. v. Weizsäcker, "Ausstrahlung bei Stössen sehr schneller Elektronen", Zeitschrift für Physik **88**, 612–625 (1934) 10.1007/BF01333110.

[106] A. C. Bawa et al., "Validity of the equivalent photon approximation in high-energy electron-proton collisions", Journal of Physics G: Nuclear and Particle Physics **15**, 004 (1989) 10.1088/0954-3899/15/9/004.

[107] S. Frixione, M. L. Mangano, P. Nason, and G. Ridolfi, "Improving the Weizsäcker-Williams Approximation in Electron-Proton Collisions", (1993) 10.1016/0370-2693(93)90823-Z, arXiv:9310350 [hep-ph].

[108] A. Afanasev, C. E. Carlson, and C. Wahlquist, "Measuring Polarized Gluon and Quark Distributions with Meson Photoproduction", (1997) 10.1103/PhysRevD.58.054007, arXiv:9706522 [hep-ph].

[109] A. Afanasev, C. E. Carlson, and C. Wahlquist, "Probing Polarized Parton Distributions with Meson Photoproduction", (1997) 10.1016/S0370-2693(97)00219-0, arXiv:9701215 [hep-ph].

[110] A. Afanasev, C. E. Carlson, and C. Wahlquist, "Soft Contributions to Hard Pion Photoproduction", (1999) 10.1103/PhysRevD.61.034014, arXiv:9903493 [hep-ph].

[111] W. Van Neerven, "Dimensional regularization of mass and infrared singularities in two-loop on-shell vertex functions", Nuclear Physics B **268**, 453–488 (1986) 10.1016/0550-3213(86)90165-3.

[112] W. Beenakker, H. Kuijf, W. van Neerven, and J. Smith, "QCD corrections to heavy-quark production in $p\bar{p}$ collisions", Physical Review D **40**, 54–82 (1989) 10.1103/PhysRevD.40.54.

[113] L. E. Gordon and W. Vogelsang, "Polarized and unpolarized isolated prompt photon production beyond the leading order", Physical Review D **50**, 1901–1916 (1994) 10.1103/PhysRevD.50.1901.

[114] J. C. Collins, *Foundations of perturbative QCD* (Cambridge University Press, Cambridge., 2011).

[115] M. Stratmann and W. Vogelsang, "Next-to-leading order QCD corrections to high-p T pion production in longitudinally polarized pp collisions", (2002), arXiv:0211007v1 [arXiv:hep-ph].

[116] B. Jager, M. Stratmann, and W. Vogelsang, "Single-Inclusive Jet Production in Polarized pp Collisions at $O(\alpha_s^3)$", (2004) 10.1103/PhysRevD.70.034010, arXiv:0404057 [hep-ph].

[117] A. Mukherjee and W. Vogelsang, "Jet production in (un)polarized pp collisions: dependence on jet algorithm", (2012) 10.1103/PhysRevD.86.094009, arXiv:1209.1785.

[118] T. Kaufmann, A. Mukherjee, and W. Vogelsang, "Next-to-leading Order Calculation for Jets Defined by a Maximized Jet Function", (2014) 10.1103/PhysRevD.91.034001, arXiv:1412.0298.

[119] D. de Florian, R. Sassot, M. Epele, R. J. Hernandez-Pinto, and M. Stratmann, "Parton-to-Pion Fragmentation Reloaded", (2014) 10.1103/PhysRevD.91.014035, arXiv:1410.6027.

[120] A. Accardi et al., "Electron Ion Collider: The Next QCD Frontier - Understanding the glue that binds us all", (2012), arXiv:1212.1701.

[121] M. Cacciari, G. P. Salam, and G. Soyez, "The anti $-k_t$ jet clustering algorithm", (2008) 10.1088/1126-6708/2008/04/063, arXiv:0802.1189.

[122] D. de Florian, M. Pfeuffer, A. Schafer, and W. Vogelsang, "Soft-gluon Resummation for High-pT Inclusive-Hadron Production at COMPASS", (2013) 10.1103/PhysRevD.88.014024, arXiv:1305.6468.

[123] M. Gluck, E. Reya, and M. Stratmann, "Probing the Parton Densities of Virtual Photons at ep Colliders", (1996) 10.1103/PhysRevD.54.5515, arXiv:9605297 [hep-ph].

[124] A. Airapetian et al., "Leading-order determination of the gluon polarization from high-p T hadron electroproduction", Journal of High Energy Physics **2010**, 130 (2010) 10.1007/JHEP08(2010)130.

[125] K. Kanazawa, Y. Koike, A. Metz, D. Pitonyak, and M. Schlegel, "Operator Constraints for Twist-3 Functions and Lorentz Invariance Properties of Twist-3 Observables", (2015) 10.1103/PhysRevD.93.054024, arXiv:1512.07233.

[126] G. Abelof, R. Boughezal, X. Liu, and F. Petriello, "Single-inclusive jet production in electron-nucleon collisions through next-to-next-to-leading order in perturbative QCD", (2016) 10.1016/j.physletb.2016.10.022, arXiv:1607.04921.

[127] D. De Florian, M. Pfeuffer, A. Schäfer, and W. Vogelsang, "Soft-gluon resummation for high-pT inclusive-hadron production at COMPASS", Physical Review D - Particles, Fields, Gravitation and Cosmology **88** (2013) 10.1103/PhysRevD.88.014024, arXiv:1305.6468.

[128] C. Uebler, A. Schäfer, and W. Vogelsang, "Threshold Resummation for Polarized High-p_T Hadron Production at COMPASS", Physical Review D **92**, 094029 (2015) 10.1103/PhysRevD.92.094029, arXiv:1510.01058.

[129] G. 't Hooft and M. Veltman, "Regularization and renormalization of gauge fields", Nuclear Physics B **44**, 189–213 (1972) 10.1016/0550-3213(72)90279-9.

[130] P. Breitenlohner and D. Maison, "Dimensional renormalization and the action principle", Communications in Mathematical Physics **52**, 11–38 (1977) 10.1007/BF01609069.

[131] L. G. and W.VOGELSANG, "Polarized and unpolarized prompt photon production beyond the leading order", PHYSICAL REVIEW D VOLUME 48, NUMBER 7 **48** (1993).

[132] M. Stratmann, A. Weber, and W. Vogelsang, "Spin-dependent nonsinglet structure functions in next-to-leading order", Physical Review D **53**, 138–149 (1996) 10.1103/PhysRevD.53.138.

[133] D. De Florian, R. Sassot, M. Stratmann, and W. Vogelsang, "Evidence for polarization of gluons in the proton", Physical Review Letters **113** (2014) 10.1103/PhysRevLett.113.012001, arXiv:1404.4293.

[134] D. de Florian, R. Sassot, and M. Stratmann, "Global analysis of fragmentation functions for pions and kaons and their uncertainties", (2007) 10.1103/PhysRevD.75.114010, arXiv:0703242 [hep-ph].

[135] C. Adolph et al., "Longitudinal double spin asymmetries in single hadron quasi-real photoproduction at high pT", Physics Letters B **753**, 573–579 (2016) 10.1016/j.physletb.2015.12.035.

[136] K. Allada et al., "Single Spin Asymmetries of Inclusive Hadrons Produced in Electron Scattering from a Transversely Polarized He-3 Target", 1–6 (2014), arXiv:arXiv:1311.1866v2.

[137] D. Adams et al., "Analyzing power in inclusive π^+ and π^- production at high x_F with a 200 GeV polarized proton beam", Physics Letters B **264**, 462–466 (1991) 10.1016/0370-2693(91)90378-4.

[138] D. Adams et al., "Comparison of spin asymmetries and cross sections in $\pi 0$ production by 200 GeV polarized antiprotons and protons", Physics Letters B **261**, 201–206 (1991) 10.1016/0370-2693(91)91351-U.

[139] J. Adams et al., "Cross Sections and Transverse Single-Spin Asymmetries in Forward Neutral-Pion Production from Proton Collisions at s = 200 GeV", Physical Review Letters **92**, 171801 (2004) 10.1103/PhysRevLett.92.171801.

[140] K. Krueger et al., "Large analyzing power in inclusive $\pi^{\pm}$ production at high x_F with a 22-GeV/c polarized proton beam", Physics Letters B **459**, 412–416 (1999) 10.1016/S0370-2693(99)00677-2.

[141] C. A. Aidala, "Measurement of the Transverse Single-Spin Asymmetry for Mid-rapidity Production of Neutral Pions in Polarized $p + p$ Collisions at 200 GeV Center-of-Mass Energy", (2006), arXiv:0601009 [hep-ex].

[142] C. A. Gagliardi and f. t. S. Collaboration, "Transverse Spin Studies with STAR at RHIC", (2006), arXiv:0607003 [hep-ex].

[143] P. PHENIX Collaboration and S. S. Adler, "Measurement of Transverse Single-Spin Asymmetries for Mid-rapidity Production of Neutral Pions and Charged Hadrons in Polarized p+p Collisions at $\sqrt{s} = 200$ GeV", (2005) 10.1103/PhysRevLett.95.202001, arXiv:0507073 [hep-ex].

[144] F. Videbaek and f. t. B. Collaboration, "Single Spin Asymmetries in the BRAHMS Experiment", (2005) 10.1063/1.2122205, arXiv:0508015 [nucl-ex].

[145] K. Heller, O. Overseth, G. Bunce, F. Dydak, and H. Taureg, "Λ 0 hyperon polarization in inclusive production by 24 GeV protons on platinum", Physics Letters B **68**, 480–482 (1977) 10.1016/0370-2693(77)90476-2.

[146] G. Bunce et al., "Λ 0 Hyperon Polarization in Inclusive Production by 300-GeV Protons on Beryllium", Physical Review Letters **36**, 1113–1116 (1976) 10.1103/PhysRevLett.36.1113.

[147] G. L. Kane, J. Pumplin, and W. Repko, "Transverse Quark Polarization in Large-p T Reactions, Jets, and Leptoproduction: A Test of Quantum Chromodynamics", Physical Review Letters **41**, 1689–1692 (1978) 10.1103/PhysRevLett.41.1689.

[148] A. Efremov and O. Teryaev, "On Spin Effects in Quantum Chromodynamics", Sov.J.Nucl.Phys. **36**, 242–246 (1981).

[149] A. Efremov and O. Teryaev, "QCD asymmetry and polarized hadron structure function measurement", Physics Letters B **150**, 383–386 (1985) 10.1016/0370-2693(85)90999-2.

[150] A. Efremov and O. Teryaev, "ON HIGH P(T) VECTOR MESONS SPIN ALIGNMENT", Sov.J.Nucl.Phys. **36**, 557 (1981).

[151] J. Qiu and G. Sterman, "Power corrections in hadronic scattering (II). Factorization", Nuclear Physics B **353**, 137–164 (1991) 10.1016/0550-3213(91)90504-Q.

[152] H. Eguchi, Y. Koike, and K. Tanaka, "Single transverse spin asymmetry for semi-inclusive deep inelastic scattering", AIP Conference Proceedings **915**, 529–532 (2007) 10.1063/1.2750836, arXiv:0611382 [hep-ph].

[153] Z.-B. Kang, I. Vitev, and H. Xing, "Transverse momentum-weighted Sivers asymmetry in semi-inclusive deep inelastic scattering at next-to-leading order", 1–11 (2012) 10.1103/PhysRevD.87.034024, arXiv:1212.1221.

[154] S. Yoshida, "New pole contribution to $P_{h\perp}$ -weighted single-transverse spin asymmetry in semi-inclusive deep inelastic scattering", Physical Review D **93**, 054048 (2016) 10.1103/PhysRevD.93.054048.

[155] H. Eguchi, Y. Koike, and K. Tanaka, "Twist-3 Formalism for Single Transverse Spin Asymmetry Reexamined: Semi-Inclusive Deep Inelastic Scattering", (2006) 10.1016/j.nuclphysb.2006.11.016, arXiv:0610314 [hep-ph].

[156] R. Jaffe and X. Ji, "Chiral-odd parton distributions and Drell-Yan processes", Nuclear Physics B **375**, 527–560 (1992) 10.1016/0550-3213(92)90110-W.

[157] H. Eguchi, Y. Koike, and K. Tanaka, "Single Transverse Spin Asymmetry for Large-p_T Pion Production in Semi-Inclusive Deep Inelastic Scattering", (2006) 10.1016/j.nuclphysb.2006.05.036, arXiv:0604003 [hep-ph].

[158] Y. Koike and K. Tanaka, "Master Formula for Twist-3 Soft-Gluon-Pole Mechanism to Single Transverse-Spin Asymmetry", (2006) 10.1016/j.physletb.2007.01.04410.1016/j.physletb.2008.09.026, arXiv:0612117 [hep-ph].

[159] Y. Koike and K. Tanaka, "Universal structure of twist-3 soft-gluon-pole cross sections for single transverse-spin asymmetry", Physical Review D - Particles, Fields, Gravitation and Cosmology **76**, 1–5 (2007) 10.1103/PhysRevD.76.011502, arXiv:0703169 [hep-ph].

[160] K. Kanazawa, Y. Koike, A. Metz, and D. Pitonyak, "Transverse single-spin asymmetries in $p^{\uparrow}p \to \gamma X$ from quark-gluon-quark correlations in the proton", (2014) 10.1103/PhysRevD.91.014013, arXiv:1410.3448.

[161] C. Kouvaris, J.-w. Qiu, W. Vogelsang, and F. Yuan, "Single transverse-spin asymmetry in high transverse momentum pion production in pp collisions", 1–32 (2008), arXiv:0609238v1 [arXiv:hep-ph].

[162] Z.-B. Kang and J.-W. Qiu, "QCD evolution of naive-time-reversal-odd quark-gluon correlation functions", (2012) 10.1142/S2010194512009154, arXiv:1210.4103.

[163] W. Vogelsang, F. Yuan, N. S. Division, and L. Berkeley, "Next-to-leading Order Calculation of the Single Transverse Spin Asymmetry in the Drell-Yan Process", 1–19 (2009), arXiv:arXiv:0904.0410v2.

[164] Z.-b. Kang and J.-w. Qiu, "Evolution of twist-3 multi-parton correlation functions relevant to single transverse-spin asymmetry", 1–28 (2013), arXiv:arXiv:0811.3101v2.

[165] V. M. Braun, A. N. Manashov, and B. Pirnay, "Scale dependence of twist-three contributions to single spin asymmetries", (2009) 10.1103/PhysRevD.80.114002, arXiv:0909.3410.

[166] J. P. Ma and Q. Wang, "Scale Dependence of Twist-3 Quark-Gluon Operators for Single Spin Asymmetries", (2012) 10.1016/j.physletb.2012.07.036, arXiv:1205.0611.

[167] S. Yoshida, "New pole contribution to $P_{h\perp}$ -weighted single-transverse spin asymmetry in semi-inclusive deep inelastic scattering", Physical Review D **93**, 054048 (2016) 10.1103/PhysRevD.93.054048.

[168] S. Catani and L. Trentadue, "Resummation of the QCD perturbative series for hard processes", Nuclear Physics B **327**, 323–352 (1989) 10.1016/0550-3213(89)90273-3.

[169] S. Catani and L. Trentadue, "Comment of QCD exponentiation at large x", Nuclear Physics B **353**, 183–IN2 (1991) 10.1016/0550-3213(91)90506-S.

[170] R. Bonciani, S. Catani, M. L. Mangano, and P. Nason, "Sudakov resummation of multiparton QCD cross sections", (2003) 10.1016/j.physletb.2003.09.068, arXiv:0307035 [hep-ph].

[171] S. Catani, D. de Florian, M. Grazzini, and P. Nason, "Soft-gluon resummation for Higgs boson production at hadron colliders", Journal of High Energy Physics **2003**, 028–028 (2003) 10.1088/1126-6708/2003/07/028.

[172] V. Ahrens, T. Becher, M. Neubert, and L. L. Yang, "Renormalization-group improved prediction for Higgs production at hadron colliders", The European Physical Journal C **62**, 333–353 (2009) 10.1140/epjc/s10052-009-1030-2.

[173] V. Ahrens, T. Becher, M. Neubert, and L. L. Yang, "Updated predictions for Higgs production at the Tevatron and the LHC", Physics Letters B **698**, 271–274 (2011) 10.1016/j.physletb.2010.12.072.

[174] M. Bonvini and S. Marzani, "Resummed Higgs cross section at N3LL", (2014) 10.1007/JHEP09(2014)007, arXiv:1405.3654.

[175] S. Catani, L. Cieri, D. de Florian, G. Ferrera, and M. Grazzini, "Threshold resummation at N3LL accuracy and soft-virtual cross sections at N3LO", Nuclear Physics B **888**, 75–91 (2014) 10.1016/j.nuclphysb.2014.09.012.

[176] C. Anastasiou et al., "Higgs boson gluon-fusion production at threshold in N3LO QCD", (2014) 10.1016/j.physletb.2014.08.067, arXiv:1403.4616.

[177] N. Kidonakis, G. Oderda, and G. Sterman, "Threshold Resummation for Dijet Cross Sections", (1998) 10.1016/S0550-3213(98)00243-0, arXiv:9801268 [hep-ph].

[178] N. Kidonakis, G. Oderda, and G. Sterman, "Threshold resummation for dijet cross sections", Nuclear Physics B **525**, 299–332 (1998) 10.1016/S0550-3213(98)00243-0.

[179] N. Kidonakis and J. F. Owens, "Effects of Higher-Order Threshold Corrections in High-E_T Jet Production", (2000) 10.1103/PhysRevD.63.054019, arXiv:0007268 [hep-ph].

[180] S. Catani, M. Grazzini, and A. Torre, "Soft-gluon resummation for single-particle inclusive hadroproduction at high transverse momentum", (2013), arXiv:1305.3870.

[181] N. Kidonakis and R. Vogt, "The theoretical top quark cross section at the Tevatron and the LHC", (2008) 10.1103/PhysRevD.78.074005, arXiv:0805.3844.

[182] N. Kidonakis, "NNNLO soft-gluon corrections for the top-quark p_T and rapidity distributions", (2014) 10.1103/PhysRevD.91.031501, arXiv:1411.2633.

[183] N. Kidonakis, "NNNLO soft-gluon corrections for the top-antitop pair production cross section", (2014) 10.1103/PhysRevD.90.014006, arXiv:1405.7046.

[184] N. Kidonakis, "Next-to-next-to-leading soft-gluon corrections for the top quark cross section and transverse momentum distribution", (2010) 10.1103/PhysRevD.82.114030, arXiv:1009.4935.

[185] M. Beneke, Y. Kiyo, and K. Schuller, "Third-order correction to top-quark pair production near threshold I. Effective theory set-up and matching coefficients", (2013), arXiv:1312.4791.

[186] M. Beneke, P. Falgari, S. Klein, and C. Schwinn, "Hadronic top-quark pair production with NNLL threshold resummation", (2011) 10.1016/j.nuclphysb.2011.10.021, arXiv:1109.1536.

[187] M. Beneke, P. Falgari, and C. Schwinn, "Soft radiation in heavy-particle pair production: all-order colour structure and two-loop anomalous dimension", (2009) 10.1016/j.nuclphysb.2009.11.004, arXiv:0907.1443.

[188] M. Czakon, A. Mitov, and G. Sterman, "Threshold Resummation for Top-Pair Hadroproduction to Next-to-Next-to-Leading Log", (2009) 10.1103/PhysRevD.80.074017, arXiv:0907.1790.

[189] L. L. Yang, C. S. Li, J. Gao, and J. Wang, "NNLL momentum-space threshold resummation in direct top quark production at the LHC", (2014) 10.1007/JHEP12(2014)123, arXiv:1409.6959.

[190] V. Ahrens, A. Ferroglia, M. Neubert, B. D. Pecjak, and L. L. Yang, "RG-improved single-particle inclusive cross sections and forward-backward asymmetry in $t\bar{t}$ production at hadron colliders", (2011) 10.1007/JHEP09(2011)070, arXiv:1103.0550.

[191] V. Ahrens, A. Ferroglia, M. Neubert, B. D. Pecjak, and L. L. Yang, "Renormalization-Group Improved Predictions for Top-Quark Pair Production at Hadron Colliders", (2010) 10.1007/JHEP09(2010)097, arXiv:1003.5827.

[192] N. Kidonakis, "Two-loop soft anomalous dimensions for single top quark associated production with a W- or H-", (2010) 10.1103/PhysRevD.82.054018, arXiv:1005.4451.

[193] N. Kidonakis, "NNLL resummation for s-channel single top quark production", (2010) 10.1103/PhysRevD.81.054028, arXiv:1001.5034.

[194] N. Kidonakis, "Next-to-next-to-leading-order collinear and soft gluon corrections for t-channel single top quark production", (2011) 10.1103/PhysRevD.83.091503, arXiv:1103.2792.

[195] N. Kidonakis, "Next-to-next-to-leading-order collinear and soft gluon corrections for t-channel single top quark production", (2011) 10.1103/PhysRevD.83.091503, arXiv:1103.2792.

[196] M. Beneke, P. Falgari, and C. Schwinn, "Threshold resummation for pair production of coloured heavy (s)particles at hadron colliders", (2010) 10.1016/j.nuclphysb.2010.09.009, arXiv:1007.5414.

[197] W. Beenakker et al., "Towards NNLL resummation: hard matching coefficients for squark and gluino hadroproduction", (2013) 10.1007/JHEP10(2013)120, arXiv:1304.6354.

[198] W. Beenakker et al., "NNLL resummation for squark and gluino production at the LHC", (2014) 10.1007/JHEP12(2014)023, arXiv:1404.3134.

[199] A. Broggio, A. Ferroglia, B. D. Pecjak, and Z. Zhang, "NNLO hard functions in massless QCD", (2014) 10.1007/JHEP12(2014)005, arXiv:1409.5294.

[200] L. G. Almeida, G. Sterman, and W. Vogelsang, "Threshold Resummation for Di-hadron Production in Hadronic Collisions", (2009) 10.1103/PhysRevD.80.074016, arXiv:0907.1234.

[201] C. De Marzo et al., "Measurement of the production of high-mass $\gamma\,\gamma$, $\pi^0\,\pi^0$, and $\gamma\,\pi^0$ pairs in pp collisions at 300 GeV/ c", Physical Review D **42**, 748–758 (1990) 10.1103/PhysRevD.42.748.

[202] H. B. White et al., "Massive hadron pair production by 800 GeV/ c protons on nuclear targets", Physical Review D **48**, 3996–4006 (1993) 10.1103/PhysRevD.48.3996.

[203] H. B. White, *A Study of angular dependence in parton-parton scattering from massive hadron pair production*, 1991.

[204] M. Begel, "Production of high mass pairs of direct photons and neutral mesons in a Tevatron fixed target experiment", PhD thesis (PhD Thesis Univ. of Rochester, 1999).

[205] A. Angelis et al., "Determination of the angular and energy dependence of hard constituent scattering from $\pi 0$ pair events at the CERN intersecting storage rings", Nuclear Physics B **209**, 284–300 (1982) 10.1016/0550-3213(82)90256-5.

[206] Z. Kunszt, A. Signer, and Z. Trócsányi, "One-loop helicity amplitudes for all $2 \to 2$ processes in QCD and N=1 supersymmetric Yang-Mills theory", (1993) 10.1016/0550-3213(94)90456-1, arXiv:9305239 [hep-ph].

[207] Z. Bern and D. A. Kosower, "Efficient calculation of one-loop QCD amplitudes", Physical Review Letters **66**, 1669–1672 (1991) 10.1103/PhysRevLett.66.1669.

[208] Z. Bern and D. A. Kosower, "The computation of loop amplitudes in gauge theories", Nuclear Physics B **379**, 451–561 (1992) 10.1016/0550-3213(92)90134-W.

[209] R. Kelley and M. D. Schwartz, "1-loop matching and NNLL resummation for all partonic 2 to 2 processes in QCD", (2010) 10.1103/PhysRevD.83.045022, arXiv:1008.2759.

[210] M. Cacciari and S. Catani, "Soft-Gluon Resummation for the Fragmentation of Light and Heavy Quarks at Large x", (2001) 10.1016/S0550-3213(01)00469-2, arXiv:0107138 [hep-ph].

[211] G. Sterman and W. Vogelsang, "Crossed Threshold Resummation", (2006) 10.1103/PhysRevD.74.114002, arXiv:0606211 [hep-ph].

[212] S. Moch, J. A. M. Vermaseren, and A. Vogt, "Higher-Order Corrections in Threshold Resummation", (2005) 10.1016/j.nuclphysb.2005.08.005, arXiv:0506288 [hep-ph].

[213] J. Kodaira and L. Trentadue, "Summing soft emission in QCD", Physics Letters B **112**, 66–70 (1982) 10.1016/0370-2693(82)90907-8.

[214] J. Kodaira and L. Trentadue, "Single logarithm effects in electron-positron annihilation", Physics Letters B **123**, 335–338 (1983) 10.1016/0370-2693(83)91213-3.

[215] S. Catani, E. D'Emilio, and L. Trentadue, "The gluon form factor to higher orders: Gluon-gluon annihilation at small Qt", Physics Letters B **211**, 335–342 (1988) 10.1016/0370-2693(88)90912-4.

[216] S. Moch, J. A. M. Vermaseren, and A. Vogt, "The Three-Loop Splitting Functions in QCD: The Non-Singlet Case", (2004) 10.1016/j.nuclphysb.2004.03.030, arXiv:0403192 [hep-ph].

[217] S. Catani, D. de Florian, and M. Grazzini, *Higgs production in hadron collisions: soft and virtual QCD corrections at NNLO*, 2001, 10.1088/1126-6708/2001/05/025, arXiv:0102227 [hep-ph].

[218] R. V. Harlander and W. B. Kilgore, *Soft and virtual corrections to pp -¿ H + X at NNLO*, 2001, 10.1103/physrevd.64.013015, arXiv:0102241 [hep-ph].

[219] E. Laenen and L. Magnea, "Threshold resummation for electroweak annihilation from DIS data", (2005) 10.1016/j.physletb.2005.10.038, arXiv:0508284 [hep-ph].

[220] T. O. Eynck, E. Laenen, and L. Magnea, "Exponentiation of the Drell-Yan cross section near partonic threshold in the DIS and MSbar schemes", (2003) 10.1088/1126-6708/2003/06/057, arXiv:0305179 [hep-ph].

[221] M. Sjodahl, "Color structure for soft gluon resummation - a general recipe", (2009) 10.1088/1126-6708/2009/09/087, arXiv:0906.1121.

[222] S. M. Aybat, L. J. Dixon, and G. Sterman, "The Two-loop Anomalous Dimension Matrix for Soft Gluon Exchange", (2006) 10.1103/PhysRevLett.97.072001, arXiv:0606254 [hep-ph].

[223] S. M. Aybat, L. J. Dixon, and G. Sterman, "The Two-loop Soft Anomalous Dimension Matrix and Resummation at Next-to-next-to Leading Pole", (2006) 10.1103/PhysRevD.74.074004, arXiv:0607309 [hep-ph].

[224] T. Becher and M. Neubert, "On the Structure of Infrared Singularities of Gauge-Theory Amplitudes", (2009) 10.1088/1126-6708/2009/06/081, arXiv:0903.1126.

[225] E. Gardi and L. Magnea, "Factorization constraints for soft anomalous dimensions in QCD scattering amplitudes", (2009) 10.1088/1126-6708/2009/03/079, arXiv:0901.1091.

[226] D. de Florian and W. Vogelsang, "Threshold Resummation for the Inclusive-Hadron Cross-Section in pp Collisions", (2005) 10.1103/PhysRevD.71.114004, arXiv:0501258 [hep-ph].

[227] D. de Florian and W. Vogelsang, "Resummed Cross Section for Jet Production at Hadron Colliders", (2007) 10.1103/PhysRevD.76.074031, arXiv:0704.1677.

[228] E. Laenen, G. Sterman, and W. Vogelsang, "Recoil and Threshold Corrections in Short-distance Cross Sections", (2000) 10.1103/PhysRevD.63.114018, arXiv:0010080 [hep-ph].

[229] A. Kulesza, G. Sterman, and W. Vogelsang, "Joint resummation in electroweak boson production", (2002) 10.1103/PhysRevD.66.014011, arXiv:0202251 [hep-ph].

[230] E. W. N. Glover, "Progress in NNLO calculations for scattering processes", (2002) 10.1016/S0920-5632(03)80133-0, arXiv:0211412 [hep-ph].

[231] G. Sterman and M. E. Tejeda-Yeomans, "Multi-loop Amplitudes and Resummation", (2002) 10.1016/S0370-2693(02)03100-3, arXiv:0210130 [hep-ph].

[232] S. Catani, "The Singular Behaviour of QCD Amplitudes at Two-loop Order", (1998) 10.1016/S0370-2693(98)00332-3, arXiv:9802439 [hep-ph].

[233] J. F. Owens, "A Next-to-Leading-Order Study of Dihadron Production", (2001) 10.1103/PhysRevD.65.034011, arXiv:0110036 [hep-ph].

[234] C. Meyer, for the ATLAS, and C. Collaborations, "Results on QCD jet production at ATLAS and CMS", (2013), arXiv:1310.2946.

[235] C. Mesropian, "Latest Jets Results from the Tevatron", (2011), arXiv:1106.3119.

[236] A. G.-D. Ridder, T. Gehrmann, E. W. N. Glover, and J. Pires, "Second order QCD corrections to jet production at hadron colliders: the all-gluon contribution", (2013) 10.1103/PhysRevLett.110.162003, arXiv:1301.7310.

[237] J. Currie, A. G.-D. Ridder, E. W. N. Glover, and J. Pires, "NNLO QCD corrections to jet production at hadron colliders from gluon scattering", (2013) 10.1007/JHEP01(2014)110, arXiv:1310.3993.

[238] N. Kidonakis, G. Oderda, and G. F. Sterman, "Threshold resummation for dijet cross-sections", Nucl.Phys. **B525**, 299–332 (1998) 10.1016/S0550-3213(98)00243-0, arXiv:hep-ph/9801268 [hep-ph].

[239] N. Kidonakis and J. Owens, "Effects of higher-order threshold corrections in high-ET jet production", Physical Review D **63**, 054019 (2001) 10.1103/PhysRevD.63.054019.

[240] M. C. Kumar and S.-O. Moch, "Phenomenology of threshold corrections for inclusive jet production at hadron colliders", (2013) 10.1016/j.physletb.2014.01.034, arXiv:1309.5311.

[241] M. Klasen, G. Kramer, and M. Michael, "NNLO contributions to jet photoproduction and determination of α_s", (2013), arXiv:1310.1724.

[242] M. Cacciari, G. P. Salam, and G. Soyez, "FastJet user manual", (2011) 10.1140/epjc/s10052-012-1896-2, arXiv:1111.6097.

[243] M. Dasgupta and G. P. Salam, "Resummation of non-global QCD observables", (2001) 10.1016/s0370-2693(01)00725-0, arXiv:0104277 [hep-ph].

[244] A. Banfi and M. Dasgupta, "Dijet rates with symmetric E_t cuts", (2003) 10.1088/1126-6708/2004/01/027, arXiv:0312108 [hep-ph].

[245] A. Banfi, M. Dasgupta, K. Khelifa-Kerfa, and S. Marzani, "Non-global logarithms and jet algorithms in high-pT jet shapes", (2010) 10.1007/JHEP08(2010)064, arXiv:1004.3483.

[246] N. Kidonakis, E. Laenen, S. Moch, and R. Vogt, "Sudakov Resummation and Finite Order Expansions of Heavy Quark Hadroproduction Cross Sections", (2001) 10.1103/PhysRevD.64.114001, arXiv:0105041 [hep-ph].

[247] C. A. Aidala, S. D. Bass, D. Hasch, and G. K. Mallot, "The Spin Structure of the Nucleon", (2012) 10.1103/RevModPhys.85.655, arXiv:1209.2803.

[248] S. STAR Collaboration, "Longitudinal double-spin asymmetry for inclusive jet production in p+p collisions at sqrt(s)=200 GeV", (2007) 10.1103/PhysRevLett.100.232003, arXiv:0710.2048.

[249] The STAR Collaboration, "Longitudinal and transverse spin asymmetries for inclusive jet production at mid-rapidity in polarized p+p collisions at sqrts=200 GeV", (2012), arXiv:1205.2735.

[250] P. Djawotho, "Gluon polarization and jet production at STAR", Journal of Physics: Conference Series **295**, 012061 (2011) 10.1088/1742-6596/295/1/012061.

[251] L. Adamczyk et al., "Precision Measurement of the Longitudinal Double-Spin Asymmetry for Inclusive Jet Production in Polarized Proton Collisions at s = 200 GeV", Physical Review Letters **115**, 092002 (2015) 10.1103/PhysRevLett.115.092002.

[252] A. Mukherjee and W. Vogelsang, "Jet production in (un)polarized pp collisions: dependence on jet algorithm", 11 (2012), arXiv:1209.1785.

[253] D. De Florian, R. Sassot, M. Stratmann, and W. Vogelsang, "Extraction of spin-dependent parton densities and their uncertainties", Physical Review D - Particles, Fields, Gravitation and Cosmology **80**, 1–25 (2009) 10.1103/PhysRevD.80.034030, arXiv:0904.3821.

[254] A. Adare, "Inclusive double-helicity asymmetries in neutral pion and eta meson production in $p + p$ collisions at $\sqrt{s} = 200$ GeV", (2014) 10.1103/PhysRevD.90.012007, arXiv:1402.6296.

[255] P. PHENIX Collaboration and A. Adare, "The gluon spin contribution to the proton spin from the double helicity asymmetry in inclusive π^0 production in polarized p+p collisions at $\sqrt{s} = 200$ GeV", (2008) 10.1103/PhysRevLett.103.012003, arXiv:0810.0694.

[256] P. PHENIX Collaboration and A. Adare, "Inclusive cross section and double helicity asymmetry for π^0 production in p+p collisions at $\sqrt{s} = 62.4$ GeV", (2008) 10.1103/PhysRevD.79.012003, arXiv:0810.0701.

[257] T. N. The NNPDF Collaboration et al., "Unbiased determination of polarized parton distributions and their uncertainties", (2013), arXiv:1303.7236.

[258] J. Currie, E. W. N. Glover, and J. Pires, "NNLO QCD predictions for single jet inclusive production at the LHC", (2016), arXiv:1611.01460.

[259] D. de Florian, W. Vogelsang, and F. Wagner, "Single-inclusive hadron production in polarized pp scattering at next-to-leading logarithmic accuracy", Physical Review D **76**, 94021 (2007) 10.1103/PhysRevD.76.094021, arXiv:arXiv:0708.3060v3.

[260] Z.-B. Kang, F. Ringer, and I. Vitev, "Inclusive production of small radius jets in heavy-ion collisions", (2017), arXiv:1701.05839.

[261] H. E. Haber and I. Hinchliffe, "Large Corrections to High p_T Hadron-Hadron Scattering in QCD", **73**, 397–421 (1980).

[262] D. W. Duke and J. F. Owens, "Quantum-chromodynamic corrections to deep-inelastic Compton scattering", Physical Review D **26**, 1600–1609 (1982) 10.1103/PhysRevD.26.1600.

[263] A. V. Belitsky, "Two-loop renormalization of Wilson loop for Drell-Yan production", (1998) 10.1016/S0370-2693(98)01249-0, arXiv:9808389 [hep-ph].

[264] G. Sterman and M. Zeng, "Quantifying Comparisons of Threshold Resummations", (2013) 10.1007/JHEP05(2014)132, arXiv:1312.5397.

Acknowledgements

I wish to acknowledge and thank those people who contributed to this thesis.

First of all and foremost I would like to express my special appreciation and thanks to my advisor Prof. Dr. Werner Vogelsang. I am very thankful for the opportunity to write my PhD thesis in his working group. I am very grateful for his continuous support, motivation, the many helpful discussions and for giving me many extremely interesting research projects.

Moreover I would like to thank Prof. Dr. Thomas Gutsche for helpful discussions, many advices and for providing the second appraisal of the thesis.

I want to express my gratitude to Prof. Dr. Yuji Koike. I am very thankful for giving me the opportunity to come to Niigata, for his support, advice, helpful discussions and the deep insight into twist-3 calculations. I very much enjoyed the hospitality in Japan.

"Föl toonk" to my office mate Martin Lambertsen for the very nice atmosphere and many helpful discussions on physics, advices on LaTeX issues and many interesting debates on more or less everything.

I would like to thank Dr. Felix Ringer, for the successful projects together and the nice time we had in Tübingen and also in Los Alamos. Dr. Marc Schlegel for many helpful discussions and the time we spend on the projects. Dr. Shinsuke Yoshida for the hospitality in Japan and useful discussions.

Furthermore, I would like to thank other collaborators on projects During my PhD which are Dr. Daniel de Florian, Prof. Dr. Asmita Mukherjee and Prof. Dr. George Sterman.

I am thankful to thank Umberto D'Alesio, Leandro Almeida, Aude Gehrmann-De Ridder,Yoshitaka Hatta, Michael Klasen, Meduri Kumar, Sven Moch, Andreas Metz, Marco Stratmann and Ilmo Sung for helpful discussions.

I would like to thank the entire theoretical physics group in Tübingen for the nice atmo-

sphere. Special thanks to the current and former members of our research group which are Daniele Anderle, Ingrid Estiry, Felix Hekhorn, Ilkka Helenius, Tom Kaufmann, Dr. Valery Lyubovitskij, Pit Burgbacher, Julius Steiglechner, Rouven Veigel, Marina Walt and Sabine Werner. I am also grateful to the theoretical physics group in Niigata/Japan for the hospitality during my stay.

I would like to thank Lukas Salfelder for the time we had between Stuttgart and Tübingen.

Many thanks to Andreas Schäfer for the invitation to Regensburg.

Furthermore, I would like to thank the Japan Society for the Promotion of Science for the Short Term JSPS Fellowship and the invitation to Japan.

Finally, I would like to thank my family for the continuous support.